Photochemistry of Chlorinated and Brominated Diaryl Ether Environmental Contaminants

by

Sierra Rayne
B.Sc., Okanagan University College, 2000

A Dissertation Submitted in Partial Fulfillment of the
Requirements for the Degree of

DOCTOR OF PHILOSOPHY

in the Department of Chemistry

We accept this thesis as conforming to the required standard

© Sierra Rayne, 2005
University of Victoria

All rights reserved. This dissertation may not be reproduced in whole or in part, by photocopying or other means, without the permission of the author.

Supervisor: Dr. Peter C. Wan

ABSTRACT

There is a need to better understand the fate of natural and anthropogenic organic materials being released into terrestrial, aquatic, and atmospheric systems. For halogenated aromatic compounds, environmental degradation via biological pathways is generally ineffective. Hence, abiotic methods of transformation – including photolysis – often play a significant role in the overall environmental fate of these compounds. Among the various potential halogenated aromatic compounds for study, those with a diaryl ether nucleus have been found to be of particular utility in industry, and are known to be the stable products of a wide range of natural and anthropogenic processes. The present work describes photochemical investigations on two representative classes of diaryl ether contaminants – (1) chlorinated dibenzo[1,4]dioxins and representative model analogs, and (2) brominated diphenyl ethers .

In order to better understand the underlying photochemistry of chlorinated dibenzo[1,4]dioxins, photochemical studies on a range of model halogenated, alkoxy, and alkyl dibenzo[1,4]dioxins have been performed in aqueous and organic solutions. The compounds were found to undergo a photochemically initiated aryl-ether bond homolysis that yields reactive 2-spiro-6'-cyclohexa-2',4'-dien-1'-one and subsequent 2,2'-biphenylquinone intermediates. Under steady-state irradiation, the 2,2'-biphenylquinones were observed to participate in excited state hydrogen abstraction from the organic solvent to give corresponding 2,2'-dihydroxybiphenyls. In the absence of continued irradiation, 2,2'-biphenylquinones with electron donating substituents thermally

rearrange to corresponding oxepino[2,3-b]benzofurans, whereas the unsubstituted 2,2'-biphenylquinone and its derivatives with electron withdrawing groups thermally rearrange to corresponding 1-hydroxydibenzofurans. The findings represent a possible general photochemically initiated mechanism for the degradation of dibenzo[1,4]dioxins, including the highly toxic chlorinated derivatives, that may shed insight into their fate in natural systems and potential mechanisms for toxicological action.

The photochemistry of model brominated diphenyl ethers has been investigated in organic and aqueous solution. These findings suggest that *para* brominated diphenyl ethers with 1 or 2 bromine substituents will likely undergo exclusive photochemically induced aryl-bromine bond homolysis in aqueous or organic solvents, followed by hydrogen abstraction from organic solvents or similar impurities in natural aquatic systems. No evidence of photochemical aryl-ether bond cleavage was observed with the model *para* substituted mono- and di-brominated diphenyl ethers. In contrast, the observed formation of brominated dibenzofurans and 2-hydroxybiphenyls from the photolysis of a model hexabrominated diphenyl ether suggests that brominated diphenyl ethers with >6 bromine substituents will undergo both photochemically induced aryl-ether and aryl-bromine bond homolysis in organic solvents. When the brominated diphenyl ether starting material has a bromine substituent in the *ortho* position relative to the ether linkage, the findings demonstrate that photochemical aryl-bond homolysis can lead to the production of brominated dibenzofurans.

Supervisor: Dr. P.C. Wan, (Department of Chemistry)

TABLE OF CONTENTS

LIST OF TABLES

LIST OF FIGURES

LIST OF SCHEMES

LIST OF IMPORTANT ABBREVIATIONS

EDG	Electron Donating Group
EWG	Electron Withdrawing Group
GC	Gas Chromatography
HOMO	Highest Occupied Molecular Orbital
HRGC	High Resolution Gas Chromatography
HRMS	High Resolution Mass Spectrometry
LFER	Linear Free Energy Relationship
LFP	Laser Flash Photolysis
LRMS	Low Resolution Mass Spectrometry
LUMO	Lowest Unoccupied Molecular Orbital
NMR	Nuclear Magnetic Resonance
UV-Vis	Ultraviolet-Visible
YAG	Yttrium Aluminum Garnet

LIST OF STRUCTURES

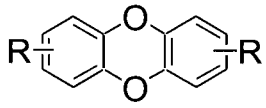

1

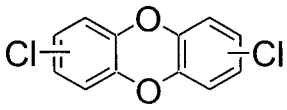

ΣCl=1-8

2

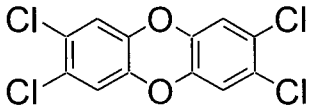

3

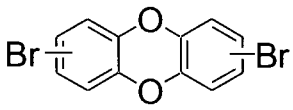

ΣBr=1-8

4

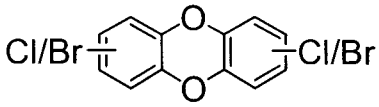

ΣCl+Br=1-8

5

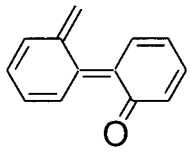

6

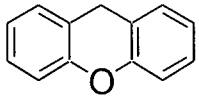

7

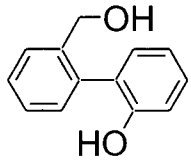

8

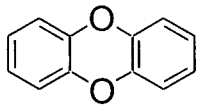

9

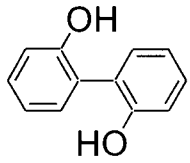

10

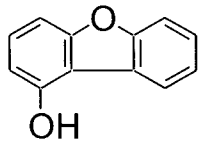

11

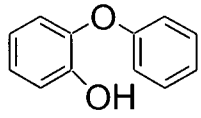

12

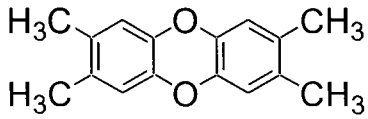

13

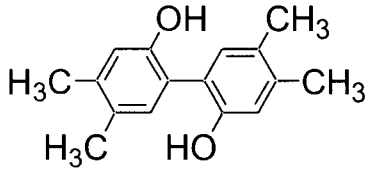

14

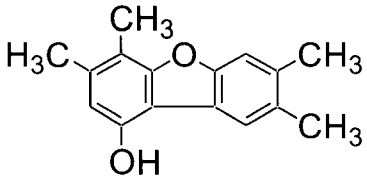

15

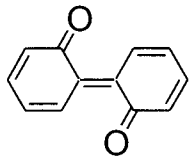

16

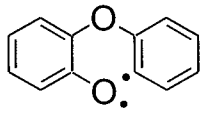

17

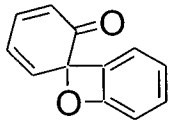

18

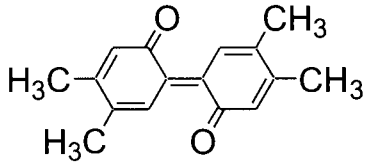

19

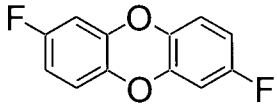

20

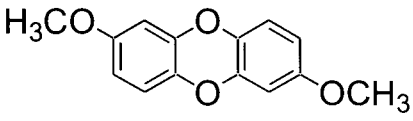

21

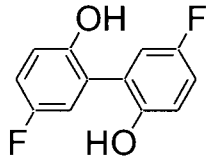

22

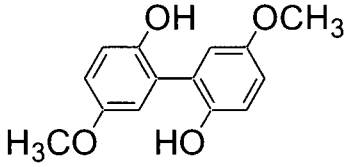

23

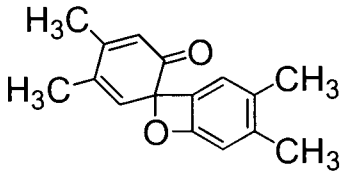

24

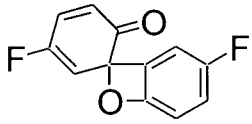

25

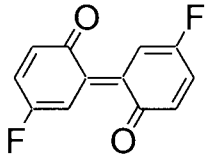

26

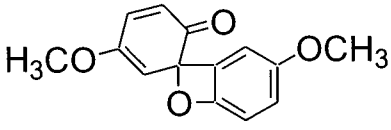

27

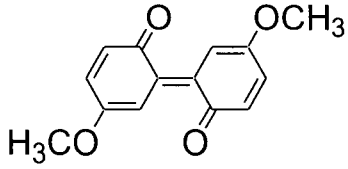

28

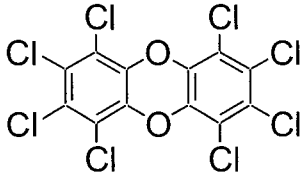

29

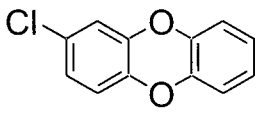

30

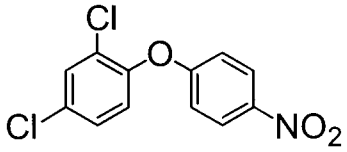

31

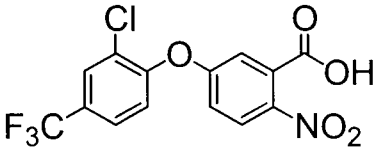

32

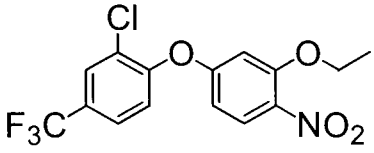

33

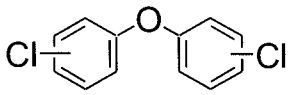

ΣCl=1-10

34

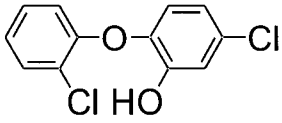

35

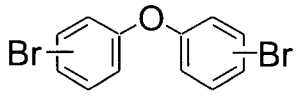

ΣBr=1-10

36

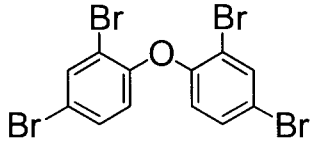

37

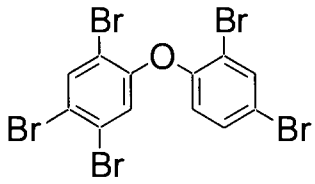

38

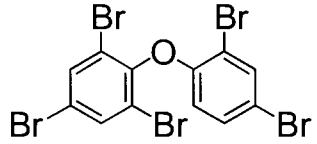

39

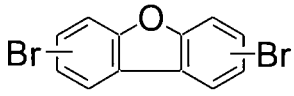

ΣBr=1-8

40

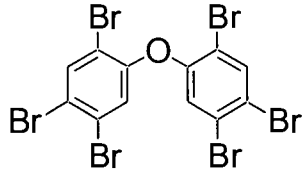

41

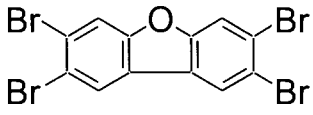

42

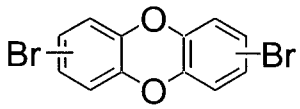

43

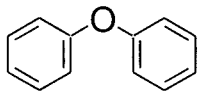

44

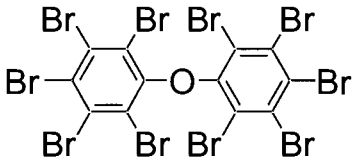

45

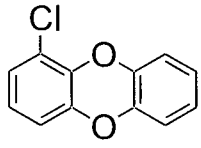

46

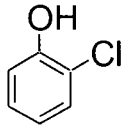

47

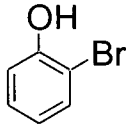

48

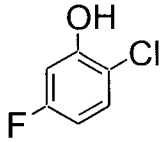

49

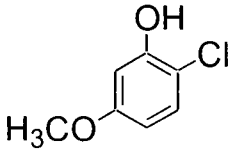

50

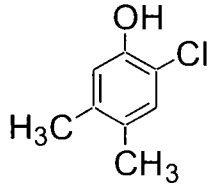

51

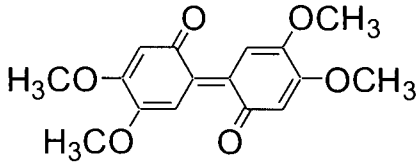

52

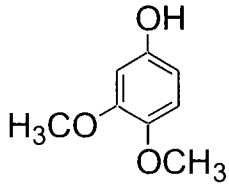

53

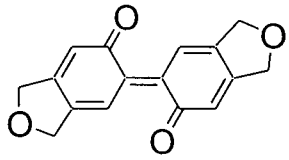

54

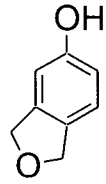

55

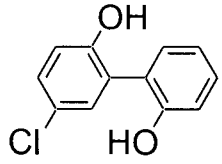

56

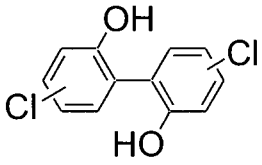

ΣCl=1

57

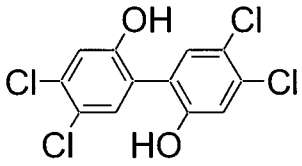

58

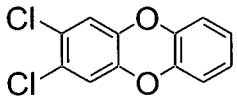

59

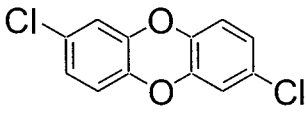

60

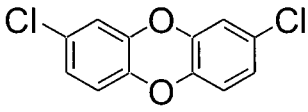

61

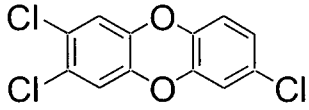

62

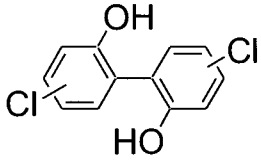

ΣCl=2

63

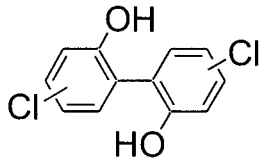

ΣCl=3

64

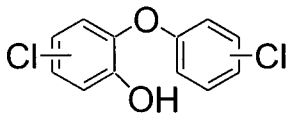

ΣCl=1

65

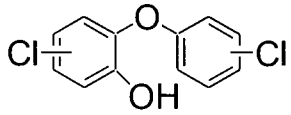

ΣCl=2

66

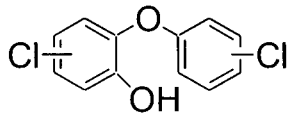

ΣCl=3

67

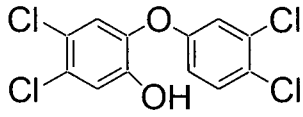

68

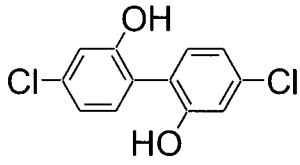

69

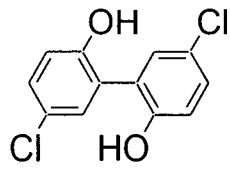

70

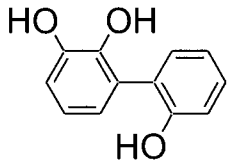

71

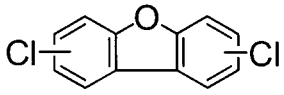

ΣCl=1-8

72

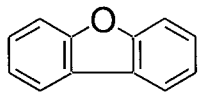

73

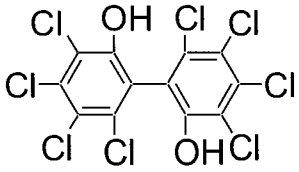

74

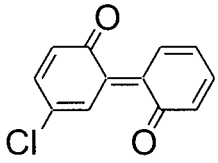

75

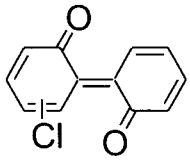

ΣCl=1

76

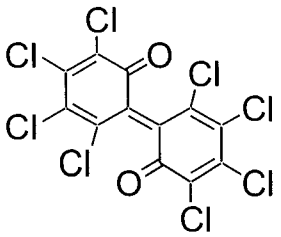

77

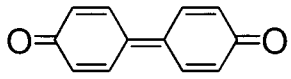

78

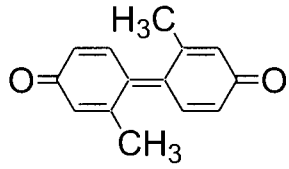

79

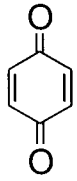

80

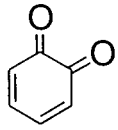

81

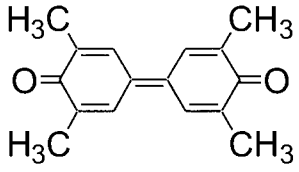

82

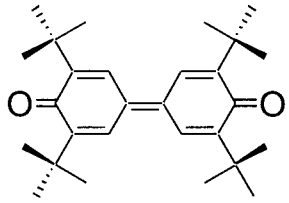

83

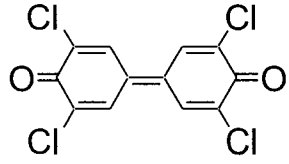

84

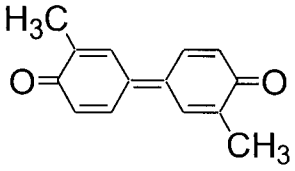

85

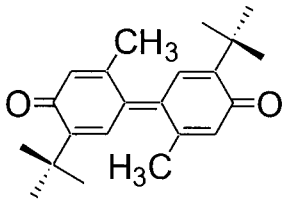

86

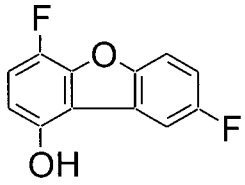

87

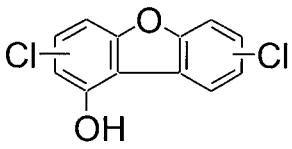

ΣCl=1

88

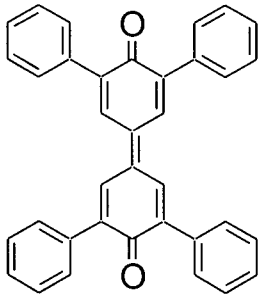

89

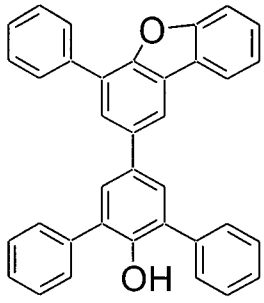

90

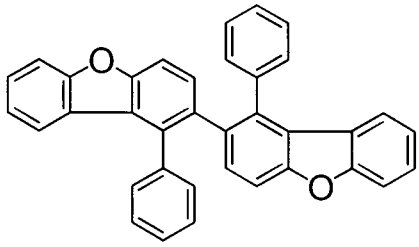

91

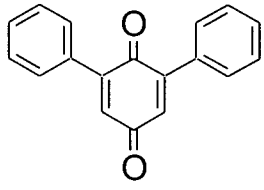

92

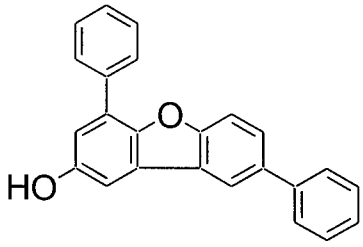

93

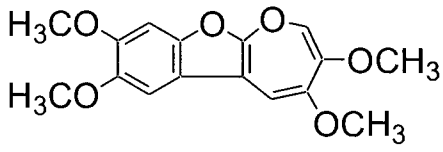

94

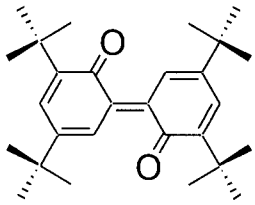

95

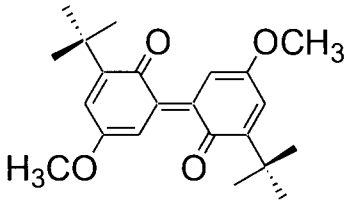

96

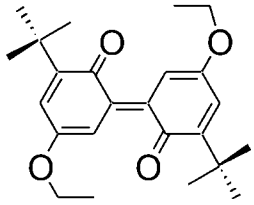

97

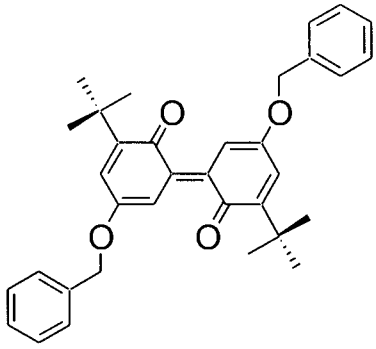

98

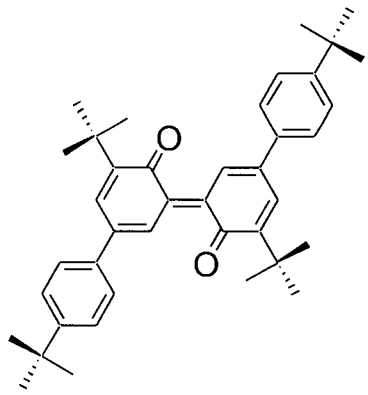

99

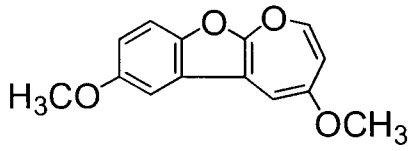

100

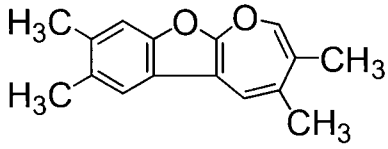

101

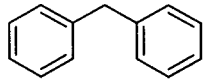

102

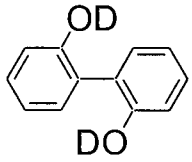

103

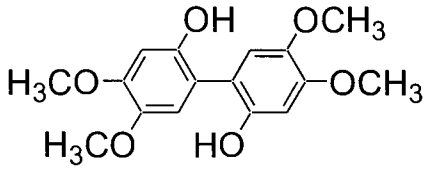

104

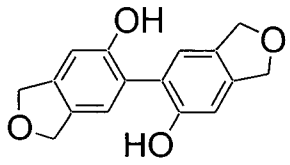

105

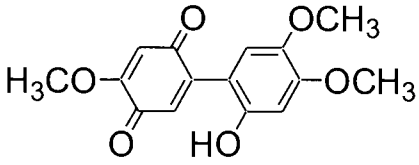

106

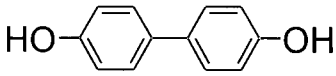

107

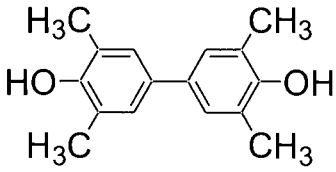

108

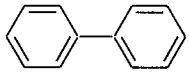

109

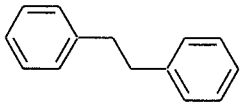

110

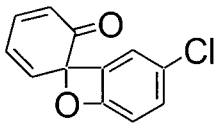

or

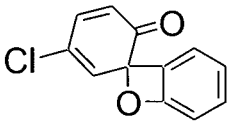

111

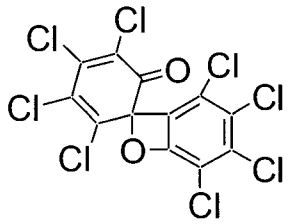

112

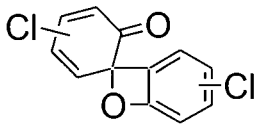

ΣCl=1

113

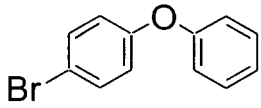

114

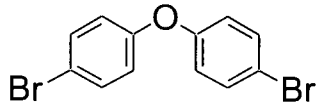

115

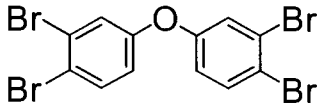

116

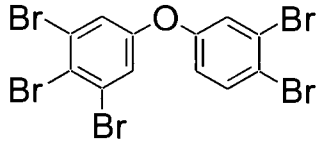

117

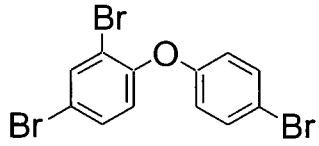

118

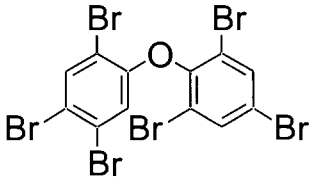

119

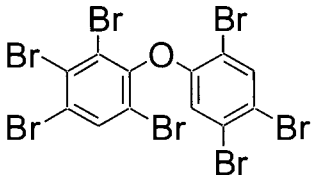

120

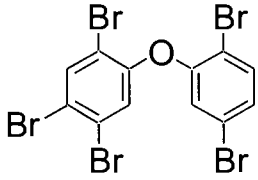

121

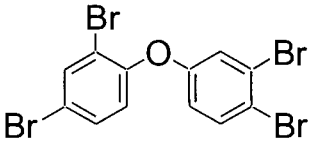

122

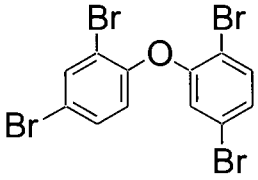

123

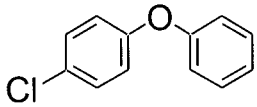

124

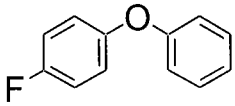

125

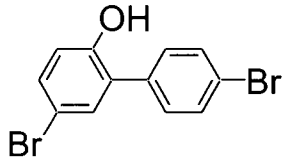

126

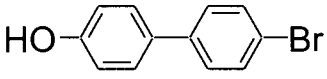

127

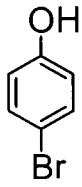

128

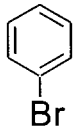

129

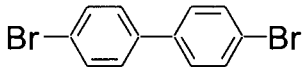

130

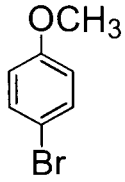

131

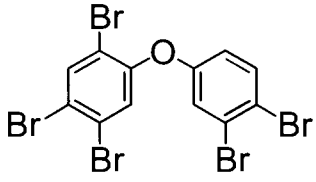

132

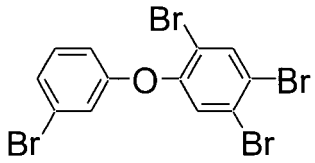

133

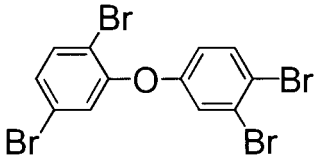

134

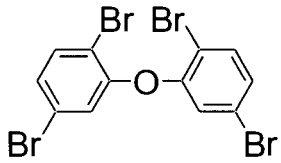

135

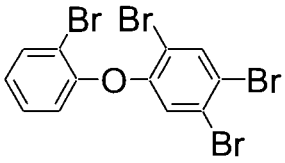

136

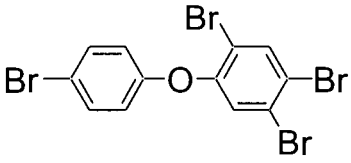

137

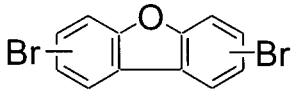

ΣBr=5

138

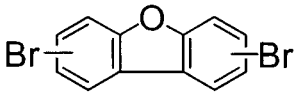

ΣBr=4

139

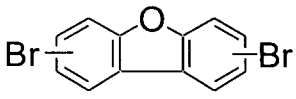

ΣBr=3

140

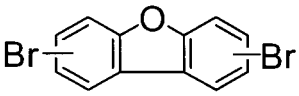

ΣBr=2

141

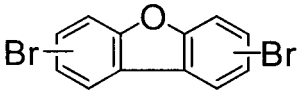

ΣBr=1

142

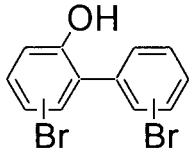

ΣBr=4

143

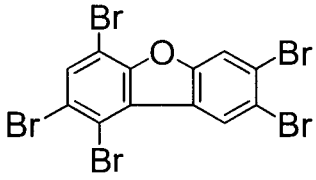

144

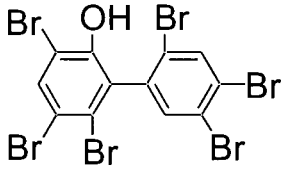

145

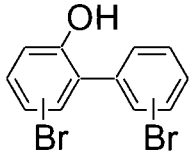

ΣBr=5

146

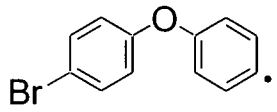

147

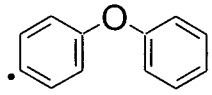

148

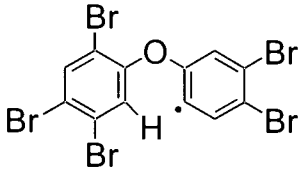

149

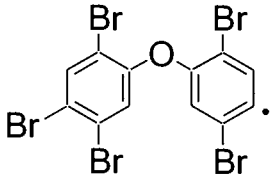

150

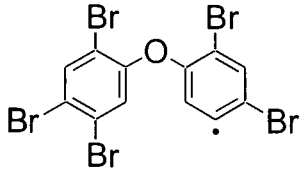

151

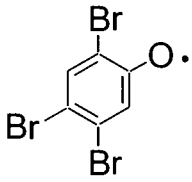

152

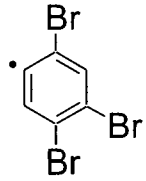

153

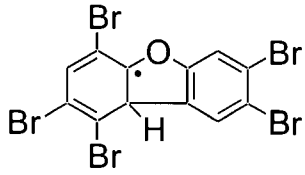

154

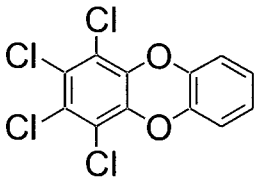

155

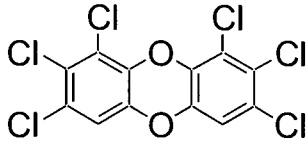

156

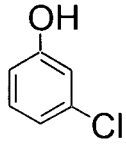

157

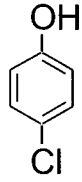

158

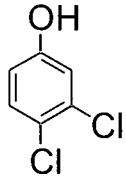

159

CHAPTER 1 - INTRODUCTION

1.1 Fundamentals of Environmental Photochemistry

Absorption of light energy (quanta) by organic compounds may lead to the occurrence of photophysical or photochemical events. Photophysical processes include the emission of radiant energy as light or heat. In comparison, photochemical processes give new compounds through transformations such as isomerization, bond cleavage, rearrangement, or intermolecular chemical reactions. In the environment, photochemical reactions are known to occur in the gas phase (e.g, troposphere, stratosphere), aqueous phase (e.g., atmospheric aerosols or droplets, surface waters, land-water interfaces), and in the solid phase (e.g., soil and mineral surfaces, exterior of plants). When the fate of organic compounds in natural systems are investigated, each of these possibilities must be considered. For some compounds the contribution of photolysis is not significant, while in other cases, photochemistry plays a dominant role in their environmental fate.

The starting event for any photochemical reaction is the absorption of a photon by a molecule. Following absorption of a photon, the molecule is converted to an electronically excited state having a new electronic configuration with a greater potential energy than the ground state. For a photon to be absorbed, the molecule must have an absorption band in the UV-visible spectrum that includes the wavelength of the photon. Since photons from sunlight have a minimum wavelength of 290 nm at the earth's surface due to the screening effects of the atmosphere, organic molecules must absorb light above 290 nm to participate in environmental photochemical reactions. Of note, the

lowest energy for electronic excitation of an organic molecule is around 800 nm, requiring light in the red/infrared (>760 nm) portion of the spectrum. However, most compounds of environmental relevance do not have absorption spectra that extend out into, and past, the visible region (400-760 nm). Thus, the majority of environmental photochemistry studies focus on molecules whose absorption spectrum is limited to the UV range (290-400 nm).

Excited states are electronically distinct from ground states. Thus, it is not unusual that excited states display different chemistry compared to ground state reactions. The unique molecular orbital interactions available to the highest occupied molecular orbitals (HOMO) of excited singlet and triplet states allow reaction pathways that would be unfavorable in the ground state to proceed readily via the excited state. It is also important to note that photochemically induced reactions may involve multistep mechanisms where only a single step involved the absorption of a photon. In general terms, photochemical reactions are insensitive to the ambient temperature, but in a strict sense, this only applies to the photon absorbing step and the subsequent rapid internal rearrangements of the excited state (e.g., bond cleavage). The kinetics of the ensuing thermal reactions that give rise to the isolated stable primary photoproduct may be very dependent on temperature.

It is a law of photochemistry that only light absorbed by a molecule can result in a photochemical reaction. The absorbing molecule can, after formation, transfer some of its energy or its structure (e.g., an electron) to a non-absorbing species (termed indirect

photolysis). However, many environmentally relevant reactions involve direct photolysis. Direct photolysis leads to photochemical reactions resulting from direct absorption of solar quanta by the reacting species. Such direct reactions are less kinetically complex and easier to model than indirect photochemical processes, especially if the absorption spectrum of the starting material is known. Yet many other compounds are transparent to solar radiation, and must react indirectly if they are to participate in photochemical reactions.

Following absorption of a photon, organic photochemical reactions are generally initiated via covalent bond cleavage. Covalent bond cleavage in excited state organic molecules may proceed by either homolytic or heterolytic pathways. Excited state bond homolysis involves an equal distribution of electrons that previously formed the bond between the resulting molecular fragments, which generally yields two radical species that may recombine to yield no net photochemical reaction, or may go on to react via intra- or inter-molecular pathways to give new compounds as photoproducts (eq. (1.1). In comparison, heterolytic cleavage involves the resulting unequal distribution of electrons previously forming the covalent bond following excited state bond cleavage (eq. (1.2). Cation-anion pairs are generally formed following heterolytic cleavage, and the location of the charges depends on the electron affinities of the resulting fragments. As with the products from a photochemically induced homolytic reaction, the molecular fragments resulting from photochemical bond heterolysis may either recombine to yield no net photochemistry, or may react via intra- or inter-molecular pathways to give new products.

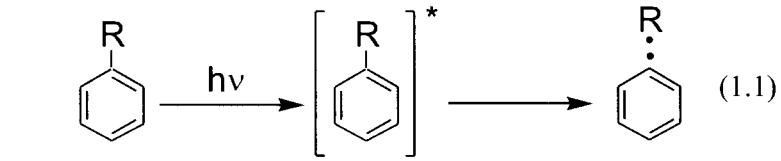

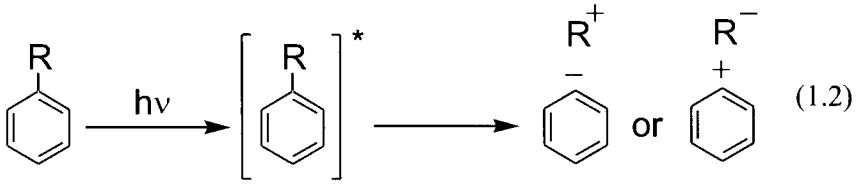

1.2 Dibenzo[1,4]dioxins

1.2.1 General

Dibenzo[1,4]dioxins ("dioxins") (**1**) are a well-known class of compounds largely due to the high acute toxicity of their chlorinated members (**2**) (*1-3*). For example, 2,3,7,8-tetrachlorodibenzo[1,4]dioxin (**3**) is widely regarded as one of the most problematic (and researched) compounds in the environment, with lethal doses in various mammals approaching 1 μg/kg body weight, environmental half-lives on the order of several years to decades depending on the matrix, and bioconcentration factors exceeding 100,000 (*1,4*). Hence, the environmental fate of chlorinated dibenzo[1,4]dioxins is of interest, owing both to this high acute toxicity, as well as evidence suggesting their role in endocrine disruption (*5*). Work over the past two decades suggests chlorinated dibenzo[1,4]dioxin emissions into the environment increased after 1940, reaching a peak in the 1960s and 1970s, and then declined up to the present date (*6*). However, their persistence and ubiquity in both biota and sediments at low ng/kg levels (*7-9*) with higher levels observed in waterways near industrial or populated regions is of concern and warrants further research into their environmental fate.

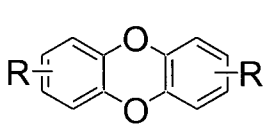

1

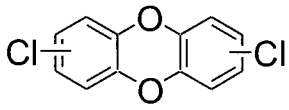

ΣCl=1-8

2

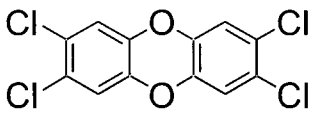

3

Dioxins are not produced intentionally. Instead, these compounds generally result as byproducts from a wide range of anthropogenic combustion and chlorination processes (*10-14*), leading to their ubiquitous nature in the environment (*1,2*). There is some debate on the relative magnitudes of anthropogenic versus natural sources of dioxins, but there appears to be a consensus that anthropogenic sources are dominant (*12,13*). Numerous efforts have been made over the past several decades to both determine and quantify the sources and exposure risks from dioxins in natural and engineered systems. However, still relatively little is known about the environmental and toxicological fate of these compounds, and whether there may be either hitherto unknown risks from potential degradation products or presently unexploited treatment technologies that could reduce releases of these compounds into the environment.

1.2.2 Photochemistry

In general, the research into dibenzo[1,4]dioxin photochemistry has focussed primarily on the chlorinated dibenzo[1,4]dioxins (**2**). These photochemical studies have historically (*15-27*) – and even recently (*28*) – also been directed only at starting material photodegradation or photochemically induced dechlorination processes, thereby limiting the scope and potential applicability of the work. Of course, many different permutations

of substituted dibenzo[1,4]dioxins can exist, and at present there is knowledge of the brominated (**4**) and mixed chlorinated/brominated (**5**) derivatives residing in humans and environmental matrices (*29-34*). Indeed, some recent reports have suggested that the brominated derivatives may be even more toxic than their chlorinated counterparts (*35*). This previous work implies that, in addition to more thorough photochemical studies on the chlorinated and brominated derivatives, there is also a need to both synthesize and examine the properties of additional types of substituted dibenzo[1,4]dioxins having common organic functional groups such as alkyl, alkoxy, and other halogenated moieties. Furthermore, most environmentally relevant members of the chlorinated and brominated dibenzo[1,4]dioxin series are simply too toxic to subject to standard milligram to gram-scale laboratory- or field-based organic photochemical mechanistic and product studies. Thus, other derivatives containing substituents with a range of steric and electronic influences on the dibenzo[1,4]dioxin nucleus are best used as models for, and probes into, the underlying mechanistic details that govern the general solution-phase photochemistry for this important class of chemicals.

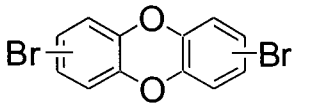

ΣBr=1-8

4

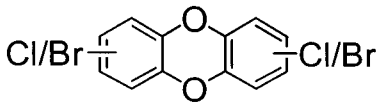

ΣCl+Br=1-8

5

In addition, the low solubility of dibenzo[1,4]dioxins in dominantly aqueous systems largely restricts the potential scope of mechanistic and product studies in this solvent. In natural systems, dibenzo[1,4]dioxins – because of their hydrophobic nature – preferentially reside in other hydrophobic environments, which are generally near other accumulations of organic molecules. In living systems, dibenzo[1,4]dioxins tend to

accumulate and reside in lipidic regions such as the outer skin and in organs such as the liver/pancreas. In aquatic systems, these compounds tend to associate strongly with dissolved organic carbon (DOC) in the water column and with particulate organic carbon (POC) in benthic or suspended sediments, or also reside within the thin organic microlayer that exists on the surface of water bodies (*36*). Photochemical studies in organic solvents, rather than being "environmentally irrelevant", can therefore often be thought of as good models for organic carbon environments in biotic and abiotic systems. Thus, purely aqueous solvent systems are not always the best models for a more complete understanding into the environmental photochemistry of dibenzo[1,4]dioxins (and other contaminant classes). Rather, laboratory studies in both aqueous and organic solvents, and in combinations thereof, typically provide complementary datasets from which to make a more informed assessment into the environmental fate of dibenzo[1,4]dioxins.

In particular, photochemical processes are often quite different in aqueous versus organic solvent systems – and both environments are relevant in more fully elucidating the potential range of mechanistic pathways and photoproducts that may exist in the natural world. In general, solvent characteristics have the potential to influence both the initial mechanistic details (e.g., mode/location of bond cleavage) following absorption of a photon (i.e., through enthalpic and entropic effects such as charge stabilization or destabilization and/or solvent cage reordering), as well as the identity of potential photoproducts that can be isolated from subsequent reactions of photochemically generated intermediates. For example, polar solvent systems may preferentially stabilize a greater charge distribution in both the excited state and in the initially formed product.

As well, in aqueous systems with very dilute starting material concentrations and little dissolved or particulate organic carbon, any radical intermediates formed via photochemical processes will generally not react with water (i.e., hydrogen abstraction from water is typically energetically unfavorable for ground state organic radicals), but instead will have a greater opportunity to participate in novel – and photochemically induced – thermal intramolecular rearrangements. Correspondingly, in reactive organic solvents – generally those with relatively weak carbon-hydrogen σ-bonds (e.g., 2-propanol, hexane) – photochemically generated organic radicals may be more prone to participate in the competing pathway of hydrogen abstraction from the solvent rather than undergo a (perhaps) less energetically favorable intramolecular rearrangement. Consequently, photochemical studies of hydrophobic materials such as dibenzo[1,4]dioxins (and diphenyl ethers as described below) should be undertaken in a variety of solvent systems (if possible) using a range of starting materials in order to better define the range of photolytic processes and products available in different environmental matrices.

The initial stimulus for more detailed explorations into the field of dibenzo[1,4]dioxin photochemistry began in the early 1990s after related studies on the photochemical generation of quinone methides (e.g., **6**) from a variety of substrates including xanthene (**7**) and dibenzo[b,d]pyran (**8**) (Scheme 1.1) (*37,38*).

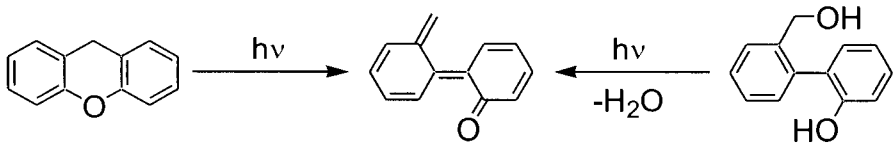

7 **6** **8**

Scheme 1.1

The similar structure of dibenzo[1,4]dioxin (**9**) to these other systems, as well as early reports suggesting the production of 2,2'-dihydroxybiphenyl (**10**) from the photolysis of **9** (eq. (1.3) (*16,39*) led to conjecture as to the possible existence of mechanistically interesting, and enviromentally and toxicologically relevant, pathways in the photochemistry of this important class of compounds.

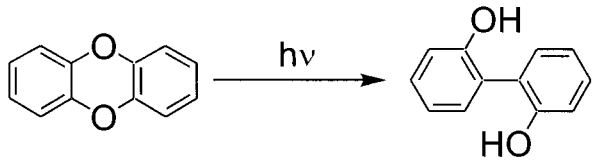

(1.3)

9 **10**

Subsequent work then demonstrated that in aqueous (CH_3CN:H_2O) and organic solutions (CH_3CN, THF, 1,4-dioxane, 2-propanol, and methanol), irradiation of **9** gives **10** as the major primary photoproduct in >60% yield, with 1-hydroxydibenzofuran (**11**; ca. 0-40% yield – only formed in aprotic solvents) and 2-phenoxyphenol (**12**; ca. 1% yield) as minor photoproducts (Scheme 1.2) (*40*).

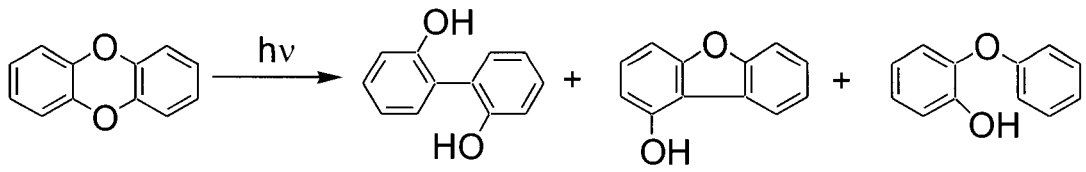

9 **10** **11** **12**

Scheme 1.2

In addition, the 2,3,7,8-methyl derivative (**13**) gave the corresponding 4,4',5,5'-tetramethyl-2,2'-bisphenol (**14**) as a major product upon irradiation in THF (eq. (1.4). Of note is that production of 3,4,7,8-tetramethyl-1-hydroxybenzofuran (**15**) was not observed during photolysis of **13** (*40*). These findings also corrected earlier reports suggesting **10** was a secondary photoproduct of 2-phenoxyphenol (**12**) (eq. (1.5) (*16,39*), which was thought at the time to be the primary photoproduct from **9**. As well, introductory photochemical mechanistic probes on **9** by time-resolved UV-Vis spectoscopy found that short irradiation times (ca. 30 s) of **9** in acetonitrile produced a highly colored solution ($\lambda_{max(500\text{-}700\ nm)}$ at ca. 530 nm) that subsequently decayed over the course of several minutes back to a largely colorless mixture. At the time, using product studies showing the formation of **10**, it was postulated that the colored solution might arise through the novel photochemical generation of 2,2'-biphenylquinone (**16**), which was subsequently reduced to give **10** in the final photoproduct mixture (Scheme 1.3) .

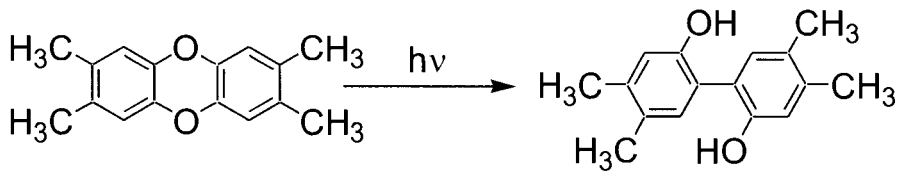

(1.4)

13 **14**

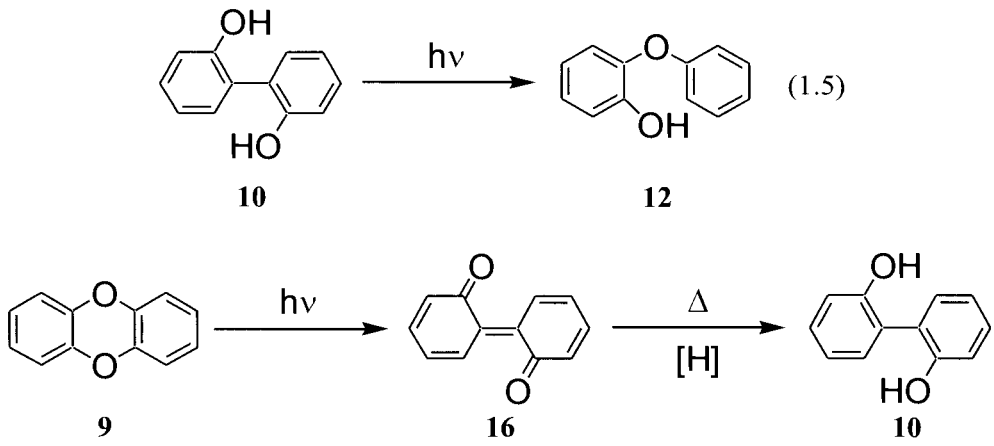

Scheme 1.3

With this preliminary mechanistic information, and when coupled to the product studies showing preferential formation of **10** as the major photoproduct from **9**, the following mechanism was proposed for the photolysis of **9** (Scheme 1.4) (*40*).

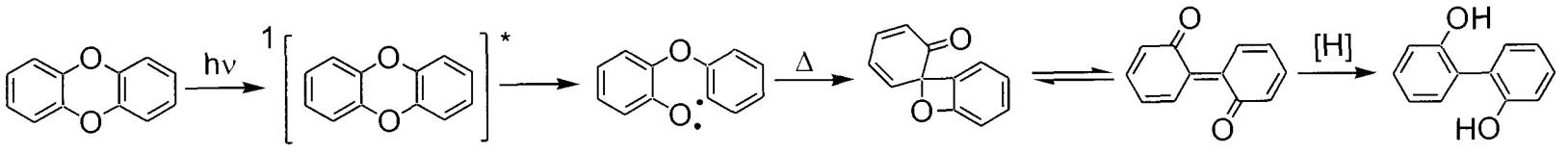

9 **17** **18** **16** **10**

Scheme 1.4

Following the initial photochemically induced homolytic aryl-ether bond cleavage in **9** via the singlet excited state to give the diradical species **17**, intramolecular *ipso* attack gives the spiroketone compound 2-spiro-6'-cyclohexa-2',4'-dien-1'-one (**18**), which subsequently undergoes thermally allowed 2+2 electrocyclic ring opening to yield 2,2'-biphenylquinone (**16**) that is then reduced to the final isolated 2,2'-bisphenol product (**10**). However, at the time there was no direct evidence for the formation of the spiroketone species (**18**), or as to the mode of reduction for 2,2'-biphenylquinone (**16**) (i.e., thermal or photochemical). In addition, the studies on the 2,3,7,8-tetramethyldibenzo[1,4]dioxin (**13**) were incomplete, and the potential for a corresponding tetramethyl-2,2'-biphenylquinone (**19**) to be photogenerated from this starting material had not been investigated.

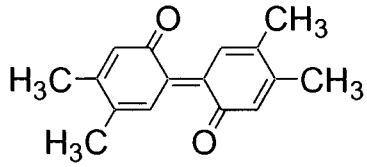

19

More recent work involved the synthesis of several new members of the dibenzo[1,4]dioxin family, and a preliminary examination of their photoproducts and potential transient species (*41*). The novel photochemistry of both the 2,7-difluorodibenzo[1,4]dioxin (**20**) and 2,7-dimethoxydibenzo[1,4]dioxin (**21**) were investigated. Corresponding photochemical formation of the respective difluorinated (**22**) and dimethoxylated (**23**) 2,2'-dihydroxybiphenyls as major photoproducts was observed (eqs. (1.6 and (1.7).

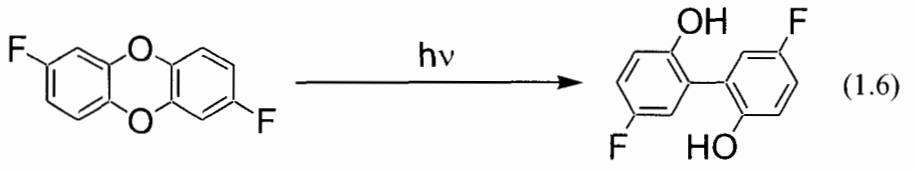

(1.6)

20 **22**

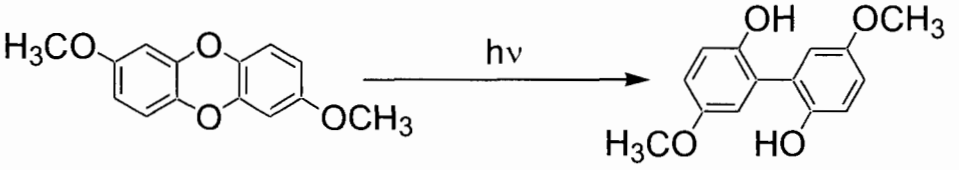

(1.7)

21 **23**

Preliminary UV-Vis studies (analogous to that performed on the parent dibenzo[1,4]dioxin system) on **13**, **20**, and **21**, as well as preliminary laser flash photolysis (LFP) work, showed the photochemical formation of the corresponding 2,2'-biphenylquinones (with characteristic spectra observable both via supra-second conventional UV-Vis techniques, as well as sub-second LFP methods). These findings resulted in an extension of the known photochemistry for **9** to these novel derivatives (Scheme 1.5, Scheme 1.6, and Scheme 1.7).

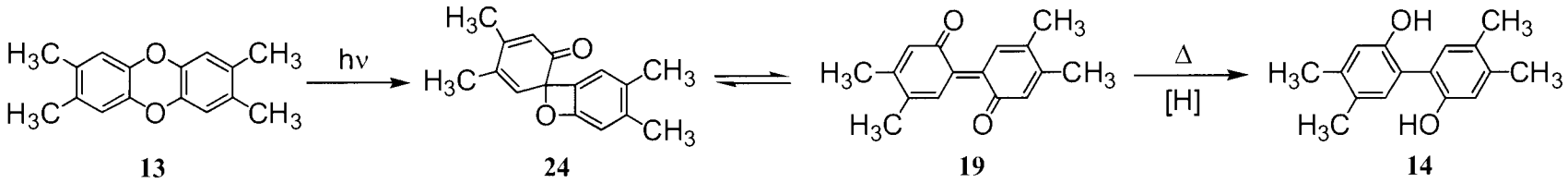

13 **24** **19** **14**

Scheme 1.5

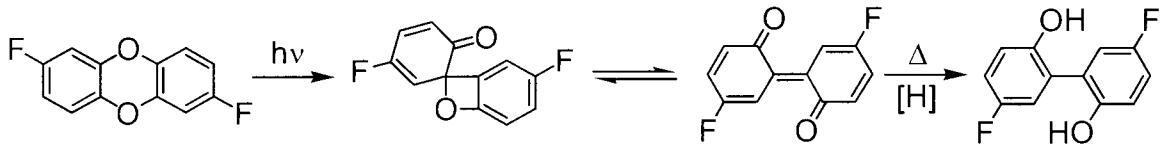

20 **25** **26** **22**

Scheme 1.6

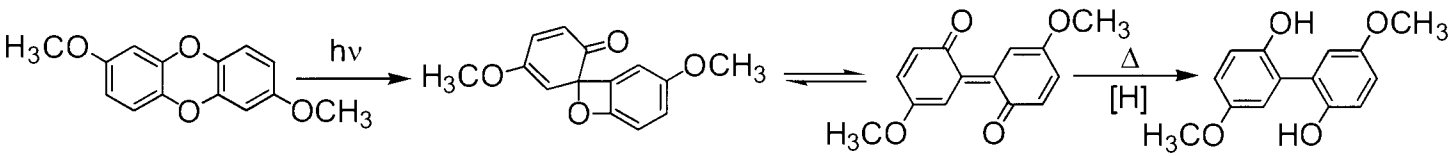

21 **27** **28** **23**

Scheme 1.7

Of note was the observed regioselectivity of photochemically induced homolytic bond cleavage observed for **20** and **21**. In general, dibenzo[1,4]dioxins substituted in the 2,7-positions (as with **20** and **21**), have two different points of bond cleavage to yield the corresponding 2,2'-biphenylquinones – and ultimately to give the isolated 2,2'-dihydroxybiphenyls (Scheme 1.8). Note that in Scheme 1.8, the 2,7-functional groups (R_1 and R_2, respectively) are equivalent moieties to illustrate the regioselective nature of the photochemical aryl-ether bond cleavage. Where R1 and R2 are not equivalent moieties, substituent effects will also been important in determining the regioselectivity of photochemical aryl-ether bond cleavage. To date, no studies have considered the regioselective nature of the photochemical aryl-ether bond cleavage in dibenzo[1,4]dioxins where the aryl rings contain different substituent identities.

For both **20** and **21**, the corresponding substituents (fluoro and methoxy moieties, respectively) were found to be located exclusively in the *para* position relative to the hydroxy groups in the isolated 2,2'-dihydroxybiphenyls. These results suggested that pathway (a) was dominant, with negligible contribution from pathway (b) (*41*). The results for **20** and **21** are consistent with the well-known regioselective excited state "*meta* effect" in organic photochemistry (*42*), whereby the *meta*-positions on aryl chromophores are activated – and thus result in preferential photochemistry at these locations versus the *ortho* and *para* positions. Hence, in a photochemical competition between pathways (a) and (b), pathway (a) would be expected to dominate because it offers the preferential homolytic cleavage of a bond *meta* to another functional group, versus pathway (b), which involves the less preferred homolytic cleavage of a bond *para*

to another functional group. For the 2,7-substituted dibenzo[1,4]dioxins, there is also another aryl-ether linkage *ortho* to the aryl-ether bond that is broken. However, this relationship is the case for both pathways (a) and (b). Thus, it is the relative position(s) of other substituent(s) on the aromatic nucleus that determines which location of bond cleavage dominates.

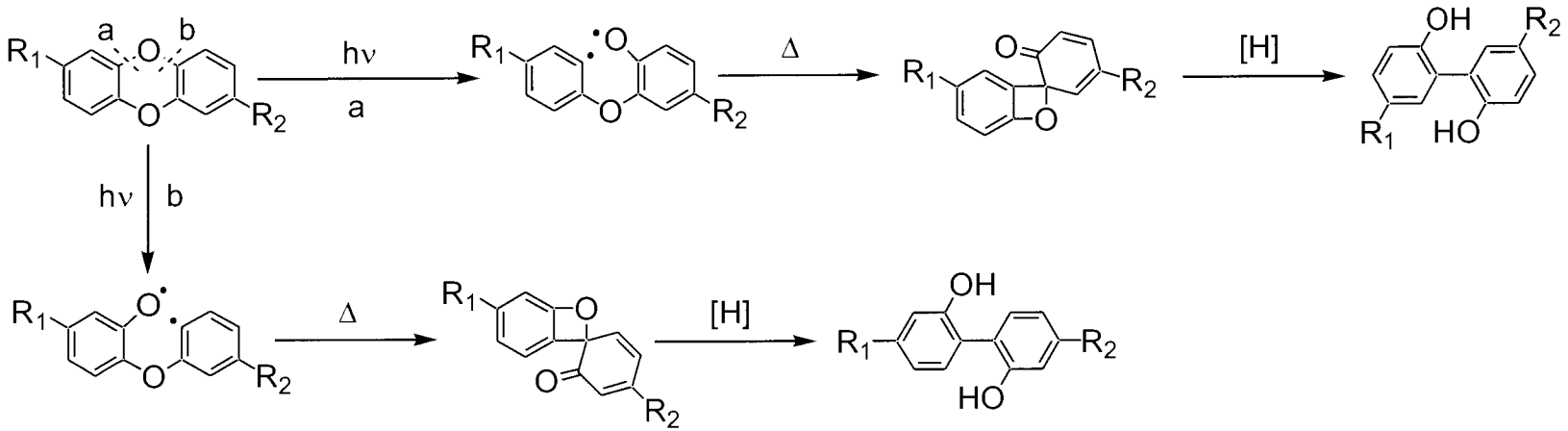

Scheme 1.8

For the chlorinated derivatives (**2**), despite having their photochemistry investigated for a longer period (>30 y) than the non-chlorinated analogues, little mechanistic insights – and even identification of the major photoproduct(s) in aqueous or organic solvents – were available. Overall, photochemical decomposition quantum yields for chlorinated dibenzo[1,4]dioxins had been reported to decrease with increasing level of chlorination (*43-45*). As well, chlorinated dibenzo[1,4]dioxins substituted at the 2,3,7,8 positions (see Figure 1.1 for the literature convention dibenzo[1,4]dioxin numbering system) were observed to be more photochemically stable than the non-2,3,7,8-substituted congeners (*46-48*). Relationships between the ground-state electronic and photochemical properties of chlorinated dibenzo[1,4]dioxins had also been observed. For example, increasing quantum yields for the photochemical loss of chlorinated dibenzo[1,4]dioxin starting material was found to be inversely related to the largest positive charge on a Cl atom, the molecular dipole moment, and the energies of the lowest unoccupied molecular orbital (LUMO), HOMO, and the HOMO-LUMO gap (*49,50*). Yet despite the efforts for a better physico-chemical understanding of chlorinated dibenzo[1,4]dioxin photoreactivity, the major photoproducts had yet to be identified.

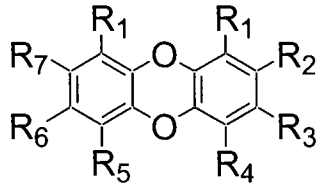

Figure 1.1. Literature convention numbering system for substituted dibenzo[1,4]dioxins.

More recent experiments with the octachlorodibenzo[1,4]dioxin (**29**) suggested either a short-lived triplet or both singlet and triplet states may be involved in homolytic

photodechlorination (*51*), but again the photochemical mass balance was not achieved and knowledge of the major photoproduct for even one of the chlorinated dibenzo[1,4]dioxins remained elusive. With its pre-eminence as the most toxic of the dibenzo[1,4]dioxins, numerous studies had also sought to achieve a quantitative photochemical mass balance for **3** on photolysis in either organic (*52-56*) or aqueous solvents (*25,48,56*); however, typically <20-30% of the mass balance was able to be accounted for. These studies collectively suggested reductive dechlorination was only a minor photolytic pathway for **3**, even in organic solvents where – as discussed above – the photodechlorination process would be expected to be favored over analogous experiments in aqueous solution (*17*). In comparison to other tetrachlorinated congeners, **3** is known to have the most rapid photodegradation rate in solution but the slowest in the solid state (*23*). Interestingly, one study found a linear relationship between the photolysis rates and toxicity of various 2,3,7,8-substituted chlorinated dibenzo[1,4]dioxins. It was suggested that the photolytic mechanism may have a related intermediate to the biological end point, such that a common molecular electronic requirement must be met (*57*).

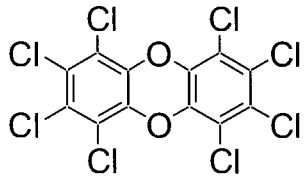

29

Having been unable to identify the major photoproduct(s) in organic and aqueous solutions, thoughts turned to mechanistic explanations for the observed minor photodechlorination pathway. Both photochemically generated carbocation intermediates via either aryl-chlorine bond homolysis followed by single electron transfer (SET) to the

chlorine atom or via heterolytic aryl-chlorine bond cleavage were proposed for chlorinated dibenzo[1,4]dioxins (Scheme 1.9 using 2-chlorodibenzo[1,4]dioxin (**30**) as an example). It was thought that such a carbocation intermediate would be stabilized in the 2,3,7,8 (lateral) positions and destabilized in the 1,4,6,9 positions, thereby explaining the more rapid photolysis rates of 2,3,7,8 substituted congeners versus other the other members of the chlorinated dibenzo[1,4]dioxins (*58*). On the basis of work with **29** (*51*), however, it appeared more likely that photochemically induced aryl-chlorine bond homolysis followed by hydrogen atom abstraction from the solvent was the operative mechanism to explain photodechlorination, rather than either the heterolytic cleavage or the homolytic cleavage followed by electron transfer pathways for which there was no experimental evidence and little theoretical support. In retrospect, simple photochemical studies with a nucleophilic solvent (e.g., CH_3OH, H_2O) would have more clearly demonstrated the potential for an aryl cation intermediate. Had the aryl cation been a significant mechanistic contributor to the observed overall photochemistry, the nucleophilic solvent should have reacted with the aryl cation to yield isolable products (Scheme 1.9). Most importantly, however, there remained no conclusive study identifying and reliably quantitating the major photoproduct for a chlorinated dibenzo[1,4]dioxin, and no understanding as to what potential mechanism may be operative in order to explain the low yields for photodechlorination.

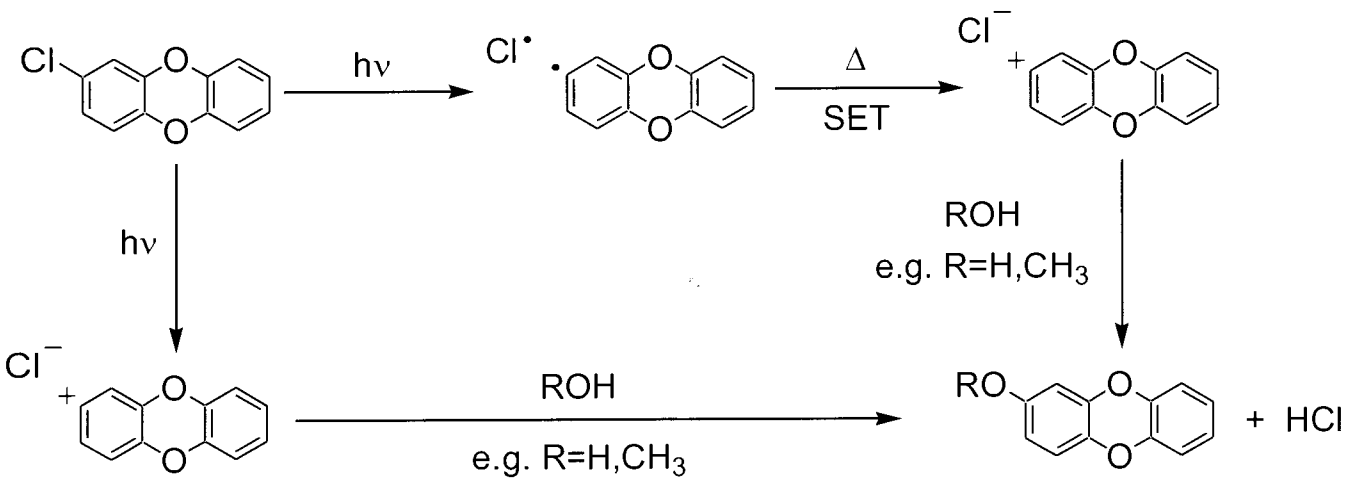

Scheme 1.9

1.3 Brominated Diphenyl Ethers

1.3.1 General

The diphenyl ether nucleus has been widely employed in the anthropogenic construction of environmentally-relevant compounds. For example, there are many examples of diphenyl ether based pesticides (e.g., nitrofen (**31**), acifluorfen (**32**), oxyfluorfen (**33**)), heat transfer fluids (e.g., chlorinated diphenyl ethers (**34**)), and antimicrobials (e.g., triclosan (**35**)). Since the 1970s, brominated diphenyl ethers (**36**) have come into widespread industrial use as flame retardants in a variety of technical mixtures (tetra-, penta-, octa-, and deca-brominated) applied to plastics, textiles, and foams used in both commercial and residential settings, at concentrations up to 30% by weight (*59-61*). Subsequent use and disposal of products containing brominated diphenyl ethers has resulted in widespread environmental contamination (see for example ref. (*59-62*)), and mounting bioaccumulatory and toxicological concerns over these compounds have led to several recent usage bans and voluntary production stoppages in Europe and North America (*63-67*).

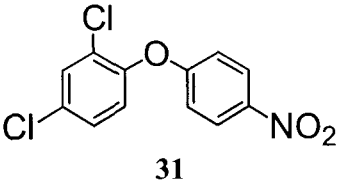

31

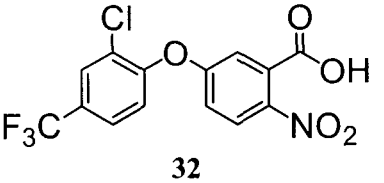

32

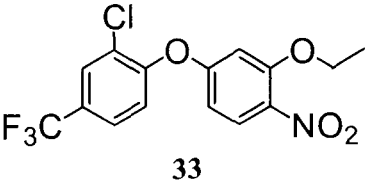

33

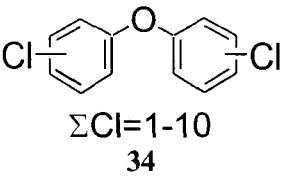

34

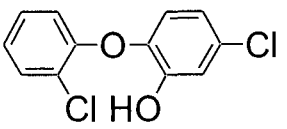

35

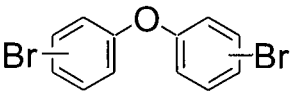

36

The brominated diphenyl ethers are the first class of halogenated diaryl compounds to cause widespread environmental concern since chlorinated biphenyls, chlorinated dibenzo[1,4]dioxins and dibenzofurans, and dichlorodiphenyltrichloroethane (DDT) were discovered in environmental samples during the 1940s through 1960s. Although other halogenated diaryl compounds have been observed in the environment over the last half-century (e.g., chlorinated diphenyl ethers, chlorinated naphthalenes, brominated biphenyls, brominated dibenzo[1,4]dioxins and dibenzofurans, and mixed halogenated dibenzo[1,4]dioxins and dibenzofurans), the concentrations and toxicological importance of these compounds are generally much less than the chlorinated biphenyls and chlorinated dibenzo[1,4]dioxins and furans. Only the brominated diphenyl ethers have recently been found at high concentrations, and are now well known to have levels reaching up into the mg/kg range for many environmental matrices such as marine mammals, sediments, and sewage residuals (*61,68-70*), and that in some cases approach or even exceed that of chlorinated biphenyls and DDT (*61,63,71-73*).

While the acute toxicity of brominated diphenyl ethers is thought to be low relative to chlorinated dibenzo[1,4]dioxins and dibenzofurans and the non-*ortho* substituted chlorinated biphenyls (*61*), the chronic effects may result in endocrine disruption and immunosuppression, among others (*60,61,74*). Furthermore, the limited

toxicological data available for only the most prevalent individual brominated diphenyl ether congeners in environmental samples (e.g., **37**, **38**, and **39**) (*60,61*), and the demonstrated experience with the widely differing acute toxicities of individual chlorinated dibenzo[1,4]dioxin, dibenzofuran, and biphenyl congeners (toxic equivalent factor (TEF) range of >6 orders of magnitude) illustrates the need to better understand the environmental fate of this emerging contaminant class.

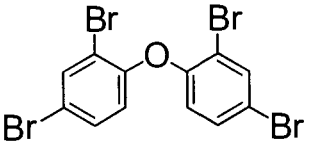

37

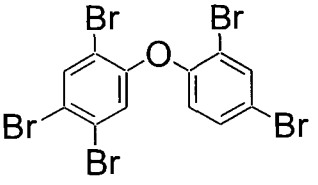

38

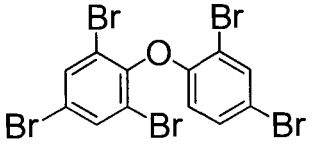

39

However, despite fairly extensive research into the environmental levels and patterns of brominated diphenyl ethers, relatively little is known regarding their environmental fate (*61,63,75*). The use of bromine rather than chlorine in industrial products is partly to enhance their environmental degradation due to the weaker aryl-bromine bond. For flame retardants, the presence of bromine is primarily because the weak carbon-bromine bond yields bromine atoms which interupt the free radical chain reactions in fires. Thus, there has been much speculation as to whether the dominant brominated diphenyl ether congeners typically observed in environmental samples (e.g., **37**, **38**, and **39**) arise from *in situ* or *in vivo* debromination of higher brominated congeners (i.e., hexa- through deca-brominated congeners), or whether they represent historical contamination from the use of tetra-brominated technical mixtures in the 1970s

(*76*). As well, brominated diphenyl ethers offer the potential to transform into brominated dibenzofurans (**40**) through, for example, loss of two opposing *ortho* substituents (e.g., from **41** in eq. (1.8). Given how recent toxicological work suggests the 2,3,7,8-tetrabrominated dibenzofuran congener (**42**) may be more acutely toxic than the well-known 2,3,7,8-tetrachlorodibenzo[1,4]dioxin (**3**) (*35*), there is much interest in the potential environmental transformations (including photolysis) that may lead to production of **42**. Furthermore, possible cleavage of the aryl-ether bond could result in formation of brominated phenols, benzenes, biphenyls, and hydroxybiphenyls, which may themselves be of environmental concern and/or may act as precursor materials for the thermal formation of brominated dibenzo[1,4]dioxins (**43**) and dibenzofurans under combustion conditions (*61,77,78*).

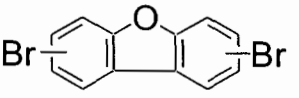

ΣBr=1-8

40

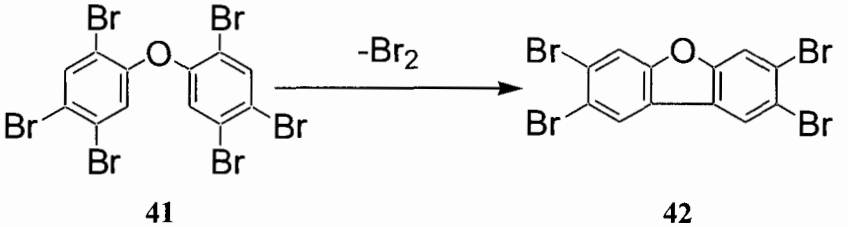

(1.8)

41 **42**

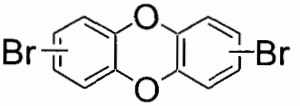

ΣBr=1-8

43

1.3.2 Photochemistry

While little is currently known about the environmental photochemistry of the brominated diphenyl ethers, a substantial body of knowledge exists regarding the photochemistry of diphenyl ethers in general. It is within this field of research that the environmental fate of brominated diphenyl ethers must be contextualized and integrated. In general, the parent diphenyl ether (**44**) and a wide range of its substituted derivatives may undergo three general types of photochemically induced homolytic bond cleavage reactions that preserve a diaryl system (Scheme 1.10): (1) photo-Fries rearrangement to yield *ortho* and *para* substituted hydroxybiphenyls; (2) radical-induced cyclization to dibenzofurans where a labile group is present *ortho* to the aryl-ether linkage; and (3) either loss or reaction at other functional groups present on the aryl system (*79*).

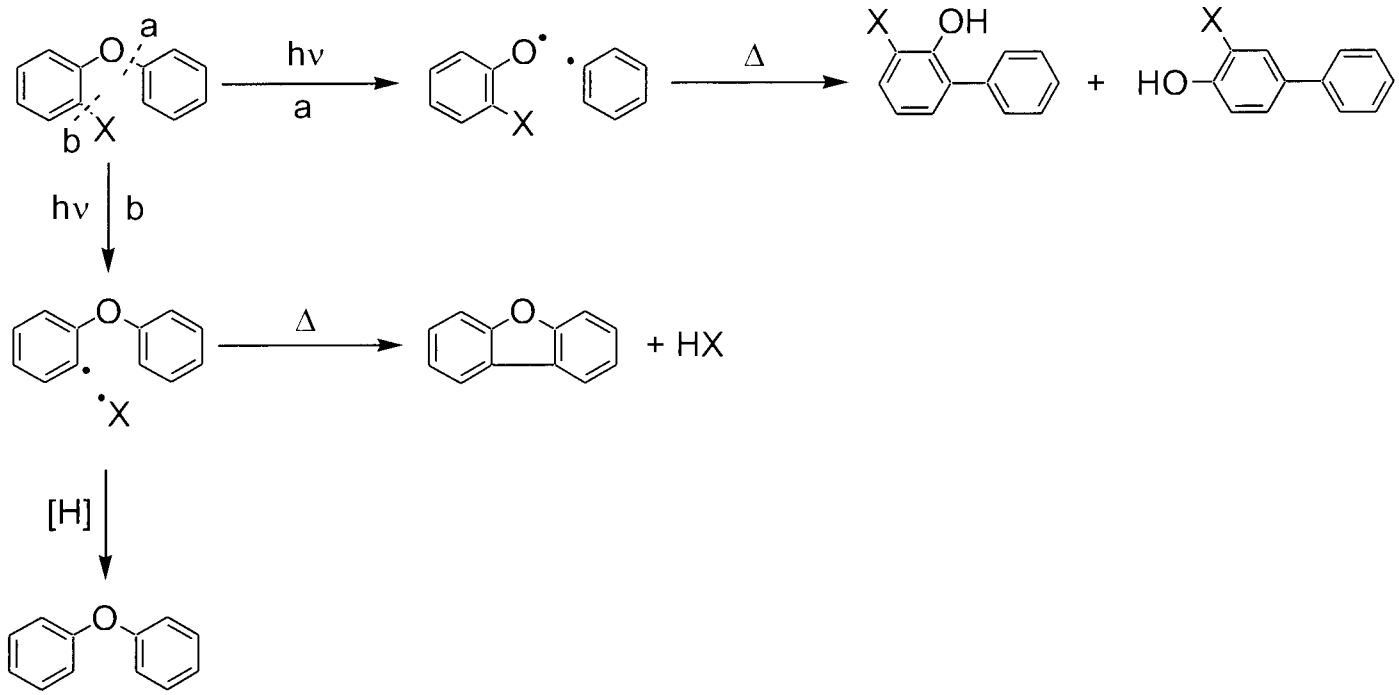

Scheme 1.10

In organic solvents, or where organic impurities are present in solution, the radical cleavage products from Scheme 1.10 may also abstract hydrogen atoms from the surrounding medium to yield phenolic and benzene products (e.g., eq. (1.9).

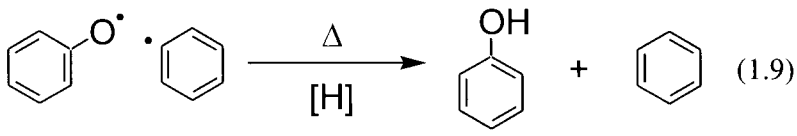

(1.9)

An alternative photodegradation pathway for diphenyl ethers is heterolytic aryl ether bond cleavage. Where the heterolytic cleavage yields a phenolate ion and an aryl cation, in protic solvents the resulting phenolate ion may be protonated and the resulting cation undergo nucleophilic attack by the solvent to yield a phenol and a –OR substituted benzene (e.g., eq. (1.10). If the solvent is water (where ROH=HOH), the overall process yields two phenolic molecules. Generally, because of the high electronegativity of the oxygen atom, heterolytic cleavage would not result in a oxygen cation and aryl anion (such a process has not been reported).

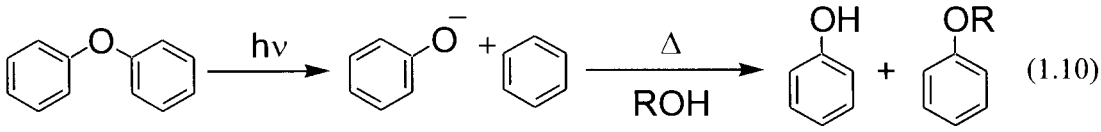

(1.10)

Despite the previous photochemical work with a variety of diphenyl ether derivatives that demonstrates the wide photolytic reactivity of this compound class, to date all studies on the photochemistry of brominated diphenyl ethers have both focussed on the higher brominated derivatives (e.g., those with >6 bromine substituents; typically with decabromodiphenyl ether (**45**) as the starting material) and have concentrated almost

entirely on the rate of loss of starting material and the photochemically induced debromination products (*80-84*). The general lack of comprehensive photoproduct studies and/or attempts to complete photochemical mass balances, as well as high concentrations and/or use of exclusively organic solvents, necessitates continuing efforts in this area in an effort to better understand the environmental fate of brominated diphenyl ethers.

1.4 Proposed Research

Halogenated dibenzo[1,4]dioxins are well-known environmental contaminants due to their characteristics of high acute toxicity, propensity to bioaccumulate and biomagnify, and potential to engage in long-range transport to formerly pristine regions. However, very little is known regarding the fate of these compounds in natural systems. In particular, abiotic processes – such as photodegradation, reduction/oxidation, and hydrolysis – are difficult to probe because the high toxicity of certain members of this compound class prevents the use of conventional laboratory experiments for complete kinetic and product studies. Thus, models are often needed for compounds that are difficult to work with using traditional techniques. In the case of dibenzo[1,4]dioxins, while limited photochemical studies can be performed on the halogenated derivatives (particularly the highly toxic chlorinated and brominated members), other functional groups can be placed on the dibenzo[1,4]dioxin nucleus in an attempt to develop predictive models based on underlying electronic and steric molecular properties. The intent in using such surrogates lies in the belief that the compound to be modeled (e.g., 2,3,7,8-tetrachlorodibenzo[1,4]dioxin (**3**)) does not have substituent effects that are so

unique as to fall outside the generally predictive trend for a range of other substituents that may be placed on the common molecular framework.

The focus of the present investigations will be to investigate whether the most environmentally relevant mono-, tetra-, and octa-chlorinated dibenzo[1,4]dioxins participate in similar photochemical processes as related alkyl, alkoxy, and fluorinated members of this compound class. While previous work has shown that the parent dibenzo[1,4]dioxin system (**9**) and its 2,3,7,8-tetramethyl (**13**), 2,7-difluoro (**20**), and 2,7-dimethoxy (**21**) derivatives give the corresponding 2,2'-dihydroxybiphenyl based photoproducts when irradiated, suggesting that the halogenated derivatives may yield analogous products when photolyzed under artificial or natural conditions, extending this apparently general photochemical reaction to the more environmentally relevant chlorinated derivatives requires confirmation and calibration with selected models. To date, no photoproduct studies on the related chlorinated dibenzo[1,4]dioxin systems have been able to account for greater than 20-30% of the photochemical mass balance, even in organic solvents that should favor photoreductive dechlorination mechanisms. The current work seeks to investigate the photoproduct distributions of representative members of the chlorinated dibenzo[1,4]dioxin series in an attempt to complete photochemical mass balances for these environmentally important compounds.

These models will contain chlorine moieties at various positions such as to confirm, refute, extend, or modify the hypothesis that all dibenzo[1,4]dioxins – regardless of substitution pattern and type – yield 2,2'-dihydroxybiphenyls as their major

photoproducts. However, the high toxicity of the chlorinated dibenzo[1,4]dioxins (and their having only a single substituent type) prevents the use of more traditional kinetic and product studies using classic physical-organic methods to perform investigations into the underlying governance of excited and ground-state molecular reactivity. Hence, the present work aims to synthesize and acquire a more complete range of dibenzo[1,4]dioxins in order to perform more detailed photochemical studies on this compound class, examining the fundamental molecular and environmental properties that help determine the nature and distribution of photoproducts and the reactivity of any intermediates. In particular, there is an especial interest in elucidating the mechanistic details underlying the photochemical generation and subsequent reactivity of the novel 2,2'-biphenylquinone intermediates for which preliminary studies have been undertaken on selected members of the dibenzo[1,4]dioxin series. Earlier studies had suggested the potential for thermal hydrogen abstraction from organic solvents, but the variability in the reported results suggests that there may be other controls on the thermal, and possibly photochemical, reactivity of these previously unknown compounds. At present, a greater understanding of the 2,2'-biphenylquinone reactivity remains a key component towards elucidating the complete photochemical and thermal mechanisms by which dibenzo[1,4]dioxins are transformed into 2,2'-dihydroxybiphenyls.

An additional halogenated diaryl ether contaminant class for which little is known regarding their environmental fate is the brominated diphenyl ethers. Previous photochemical work on these compounds had focussed exclusively on the decabrominated derivative, for which only the loss of starting material and subsequent

yield of debromination products had been reported. While these prior studies had attempted to follow the sequential photochemical conversion of the decabrominated starting material to the lower brominated derivatives, decreasing photochemical mass balances (with up to 70-80% unaccounted for) with increasing loss of starting material suggested that non-photodebromination pathways were the dominant contribution to the overall observed photochemistry of compounds with >4 bromine substituents.

Therefore, the current study sought to use three representative members of the brominated diphenyl ethers – congeners that are among the most widely reported in environmental samples, containing one, two, and six bromine substituents, respectively – in order to investigate whether the number of substituents could potentially govern the nature and distribution of the resulting photoproduct profiles. It was also thought that other well-known photochemical processes previously reported for various diphenyl ethers (e.g., photo-Fries rearrangements) could help to explain the incomplete mass balance and better integrate the photochemistry of brominated diphenyl ethers with their parent compound class. Furthermore, with recent reports suggesting the potential thermal and photochemical conversion of brominated diphenyl ethers into the more acutely toxic brominated dibenzofurans, comprehensive photoproduct studies on such representative members of this important class of flame retardants may highlight new potential environmental contaminants whose ambient concentrations and patterns may warrant future attention.

CHAPTER 2 - PHOTOCHEMISTRY OF DIBENZO[1,4]DIOXINS

2.1 Materials

The chlorinated dibenzo[1,4]dioxins **3**, **29**, **30**, and **46** were commercially available at high purity (>98-99%) and were used as received.

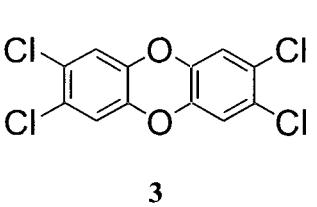

3

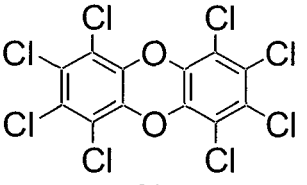

29

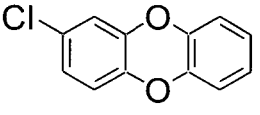

30

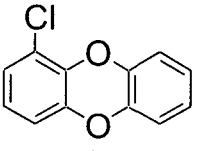

46

The parent dibenzo[1,4]dioxin (**9**) was synthesized via separate base-assisted Ullman ether couplings of 2-chlorophenol (**47**; eq. (2.1) and 2-bromophenol (**48**; eq. (2.2). A moderately higher yield was obtained via the **48** coupling route (30%) versus that of the **47** coupling route (20%).

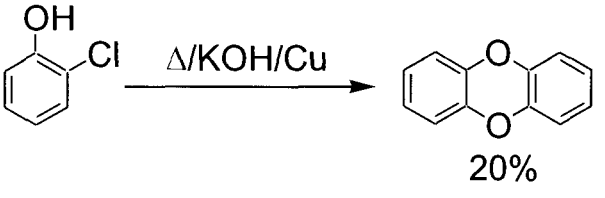

(2.1)

47 **9**

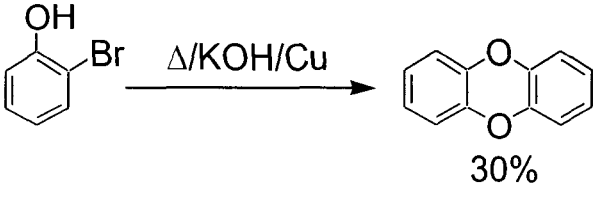

(2.2)

48 **9**

The 2,7-difluoro (**20**), 2,7-dimethoxy (**21**), and 2,3,7,8-tetramethyl dibenzo[1,4]dioxin derivatives were also synthesized via base-assisted Ullman ether couplings of the appropriate chlorophenol precursors (eqs. (2.3, (2.4, and (2.5).

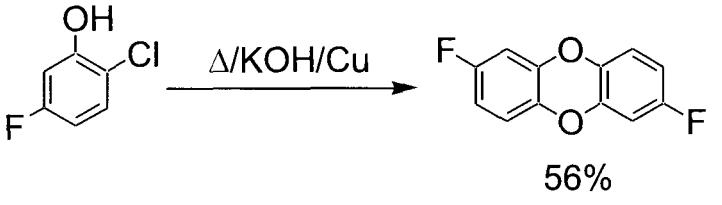

(2.3)

56%

49 **20**

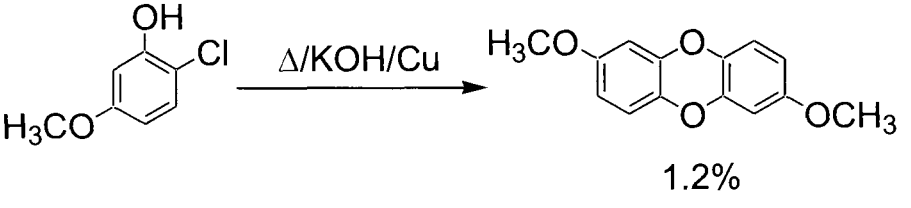

(2.4)

1.2%

50 **21**

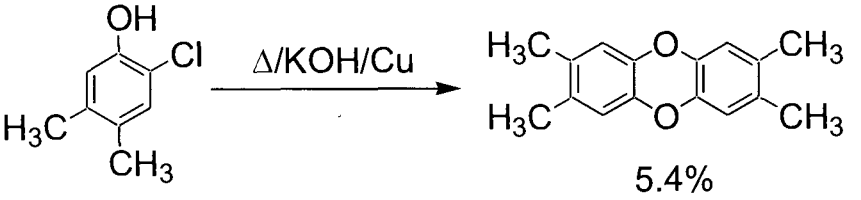

(2.5)

5.4%

51 **13**

Two 2,2'-biphenylquinones were also synthesized via the base assisted potassium ferricyanide oxidation and dimerization of the corresponding phenol precursors. 4,4',5,5'-Tetramethoxy-2,2'-biphenylquinone (**52**) was obtained in modest yield through oxidation of 3,4-dimethoxyphenol (**53**) (eq. (2.6) (*85*).

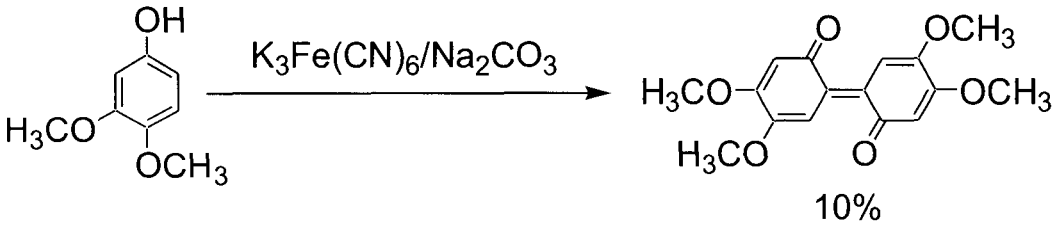

(2.6)

53 **52**

4,5,4'5'-Bismethylenedioxy-2,2'-biphenylquinone (**54**) was obtained in good yield through oxidation of 3,4-bismethylenedioxyphenol (**55**) (eq. (2.7) (*86*).

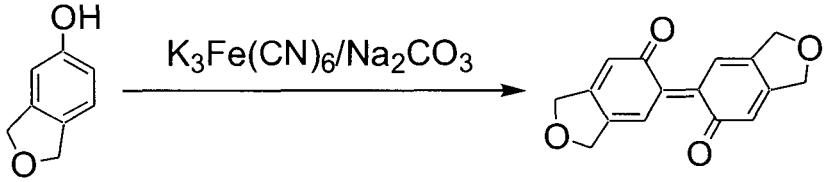

(2.7)

55 **54**

2.2 Photoproduct Studies

In dry CH_3CN, photolysis of **9** (10^{-3} M, 300 nm, CH_3CN, 60 min) yields 2,2'-dihydroxybiphenyl (**10**) as the major photoproduct in 70% yield at ca. 60% conversion of starting material (Scheme 2.1). Product studies for **9** were also performed in CH_3CN:H_2O (1:1 v/v, 10^{-3} M, 300 nm, 30 min) at pH values of 1, 7, and 12. Previous work had shown the presence of uncharacterizable highly-colored material (at up to ca. 30-40% yields) from the photolysis of **9** in dry CH_3CN (*40*), and hence the ca. 70% yield of **10** in dry CH_3CN. As discussed below in more mechanistic detail, the highly-colored material may arise from the thermal coupling (dimerization and/or polymerization) of a reactive 2,2'-biphenylquinone (**16**) observed upon irradiation of **9**.

Water as a cosolvent (at 1:1 v/v with CH_3CN) was found to significantly reduce the formation of these dimeric and/or polymeric products, such that >95% of the mass balance could be accounted for as **10** (at ca. 70% conversion of **9**), or as unreacted starting material. These results were consistent with previous work performed on **9** that showed the presence of water as a cosolvent resulted in a significantly higher yield of **10** compared to photolyses performed in acetonitrile (*41*). In addition, the presence of water increased the rate of conversion, with 67% conversion of **9** to after 30 min irradiation in 1:1 CH_3CN:H_2O at pH 7 compared to 60 min irradiation required for a similar conversion in dry CH_3CN. No acid or base catalysis was observed during the photolysis of **9** at pH 1 or 12, with these pH values giving similar conversions (70% and 62%, respectively) to that at pH 7.

Photoproduct studies for **9** were also performed in a variety of protic and aprotic organic solvents (10^{-3} M, 300 nm, 60 min) to examine the influence of solvent properties on product yields and distributions. Distinct differences were observed in yields of **10** during photolyses of **9** in protic and aprotic organic solvents. In protic organic solvents (1-butanol, *t*-butanol, ethanol, methanol, and 2-propanol), >95% of the mass balance could be accounted for as either **10** or unreacted **9** with >90% yields of **10**, and similar conversions after 30 min irradiation (ca. 60-82%) to that observed in 1:1 CH_3CN:H_2O over the pH range from 1 to 12. By comparison, photolysis in aprotic organic solvents (benzene, cyclohexane, diethyl ether, ethyl acetate, hexane, and toluene) showed significantly lower conversions (ca. 20-41%) and yields (33-68%) of **10** even after 60 min irradiation, with yields reaching what was observed upon photolysis in dry CH_3CN

(ca. 70%). The possible reasons for an enhanced photochemical production of **10** in protic solvents is discussed in more detail below.

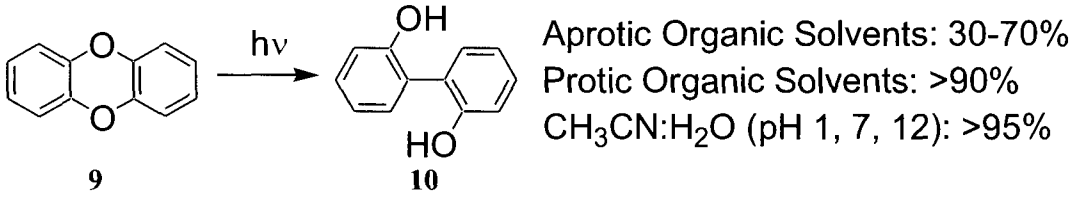

9 **10**

Scheme 2.1

Subsequent photoproduct studies were then performed on the various commercially obtained and synthesized dibenzo[1,4]dioxin derivatives. Photolysis (10^{-3} M, 300 nm, CH_3CN, 20 to 45 min) of **13** (eq. (2.8), **20** (eq. (2.9), **21** (eq. (2.10), and **30** (eq. (2.11) also gave the corresponding 2,2'-dihydroxybiphenyls as major products in ca. 50-70% yields at ca. 40-70% conversion of starting material, with ca. 20-40% yields of uncharacterizable material. Previous work had shown the production of these 2,2'-dihydroxybiphenyls from the photolysis of **13**, **20**, and **21** (*41*). As discussed above, the regioselectivity of the initial photochemically induced homolytic aryl-ether bond cleavage in **13**, **20**, and **21** has been previously reported (*41*), and now the regioselective trend can be extended to **30**, which yields the chlorine substituent in the isolated photoproduct (**56**) at the *para* position relative to the hydroxy group. However, because of the asymmetry of **30**, the location of initial photochemical bond homolysis cannot be determined. Due to the high toxicity of **3**, thereby necessitating study in trace quantities of starting material and specialized analytical techniques, its product studies are described separately in more detail below.

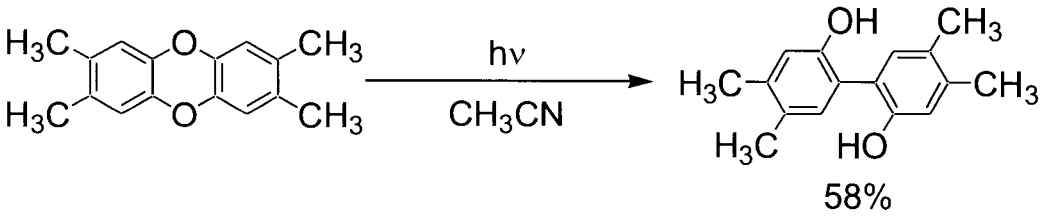

58% (2.8)

13 **14**

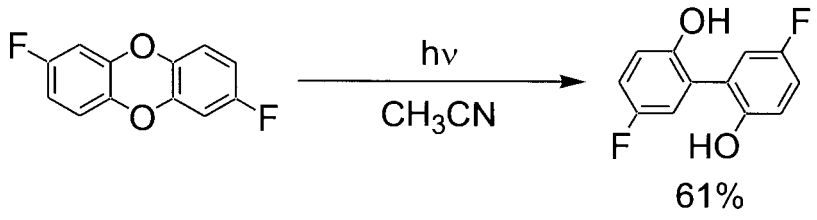

61% (2.9)

20 **22**

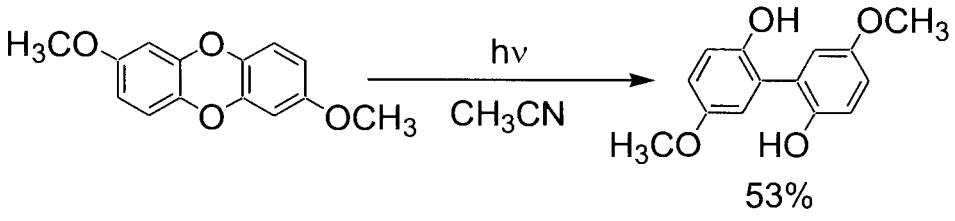

53% (2.10)

21 **23**

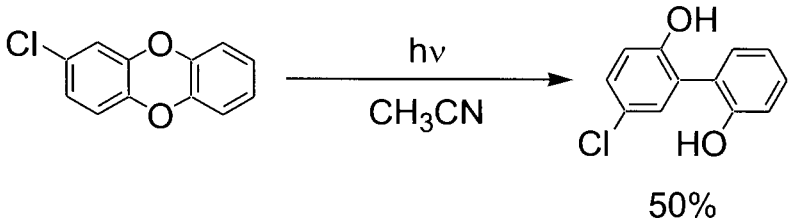

50% (2.11)

30 **56**

Of note is the lack of chlorinated 2,2'-dihydroxybiphenyl photoproduct able to be isolated following photolysis of **46** (10^{-3} M, 300 nm, CH_3CN, 30 min). The reaction was followed by UV-Vis spectroscopy by monitoring the decrease in absorbance of starting material at λ_{max}=299 nm until ca. 40% of starting material was reacted, but upon workup, only **10** was isolated in 37% yield. As discussed below, both LFP and UV-Vis studies

suggested initial aryl-oxygen bond cleavage is a minor photochemical pathway (although present) for **46**, which should give a monochloro-2,2'-dihydroxybiphenyl (**57**) as a product. However, work described below on the photochemistry of 2,3,7,8-tetrachlorodibenzo[1,4]dioxin (**3**) and reported elsewhere (*48,87*) suggests efficient photochemical dechlorination of chlorinated 2,2'-dihydroxybiphenyls takes place such that any photochemically formed monochloro-2,2'-dihydroxybiphenyl would rapidly photodechlorinate *in situ* to yield only **10** in the resulting product mixture, as was observed (Scheme 2.2).

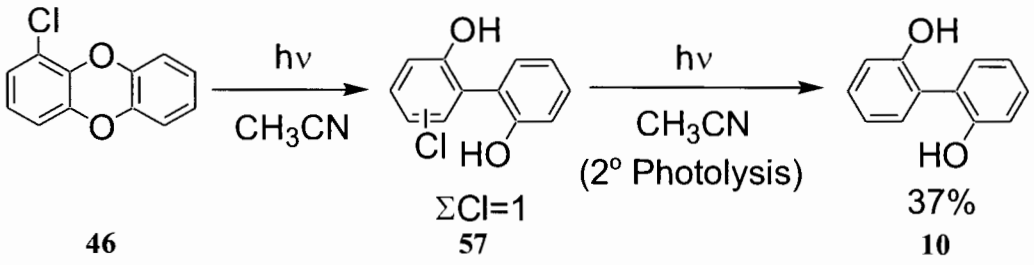

46 **57** **10**

Scheme 2.2

Similarly, while **56** was isolated in ca. 50% yield from the photolysis of **30**, an equal quantity of its dechlorinated counterpart **10** was also obtained (Scheme 2.3).

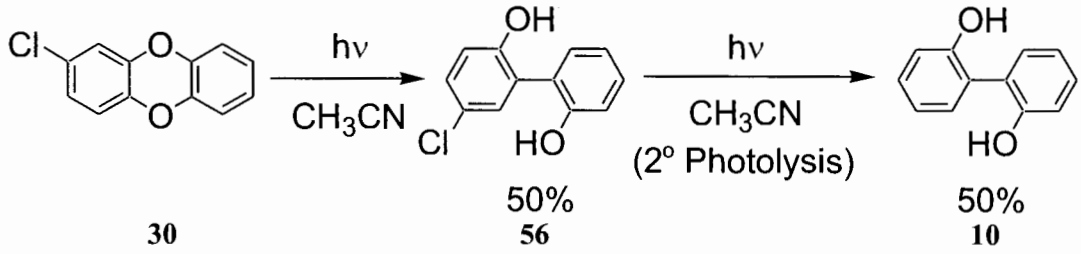

30 **56** **10**

Scheme 2.3

The comparative reactivities of **46** and **30** demonstrate the influence of monochloro substitution pattern on the relative contributions of aryl-oxygen and aryl-chlorine bond cleavage. The photochemical work presented here on these compounds in

dry CH_3CN suggests preferential aryl-chlorine bond cleavage the 1-position is substituted, compared to preferential aryl-ether bond cleavage where the 2-position is substituted.

In H_2O/CH_3CN (19:1 v/v; 1.8×10^{-9} M starting material), the major primary photoproduct of **3** is 4,4',5,5'-tetrachloro-2,2'-dihydroxybiphenyl (**58**) (eq. (2.12). Absolute quantities of the starting material and individual photoproducts, along with percent recoveries of the recovery standards and methods for correcting absolute analyte quantities to observed standard recoveries, are presented and discussed in Section 4.3.1.2.1. While nonextractable photoproducts as measured by ^{14}C activity have previously been reported for **3** in distilled water (*46,88*), the present study was able to account for 92-99% of the starting material and photoproducts extractable by CH_2Cl_2 over the course of the 60 min irradiation period. The improvement in mass balance over previous studies may be partly a result of acidifying the solutions to pH 2 after irradiation and then extracting. The presence of several electron-withdrawing Cl substituents on phenolic compounds such as **58** may result in a pK_a sufficiently low to result in near complete dissociation in neutral aqueous solutions (ca. pH 7). Dissociation of a phenolic compound would render it non-extractable in organic solvents such as dichloromethane (CH_2Cl_2). Working at low starting material concentrations (1.75×10^{-12} M) may also assist in preventing photochemically induced polymerization of **3**.

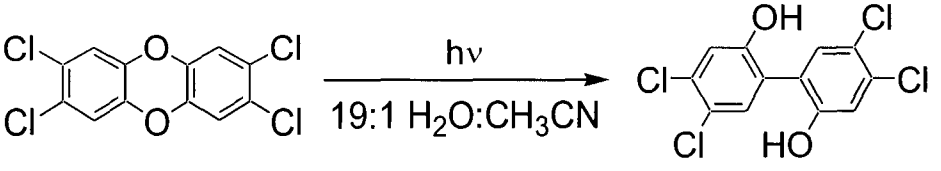

3 **58** (2.12)

In addition to the finding of **58** as the major photoproduct, HRGC-HRMS analytical methods facilitated the identification and quantitation of the following three groups of photoproducts (in addition to monitoring the fraction of **3** during the course of the photolysis): (1) sequential photodechlorination products of **3** (i.e., **9** and mono-, di-, and tri-chlorinated dibenzo[1,4]dioxins – **30**, **59**, **60**, **61**, and **62**); (2) **10** and mono- through tri-chlorinated 2,2'-dihydroxybiphenyls (**57**, **63**, and **64**; arising either by sequential photodechlorination of **58**, or by conversion of photodechlorinated starting material); and (3) **12** and mono- through tetra-chlorinated 2-phenoxyphenols (**65**, **66**, **67**, and **68**; arising from aryl-oxygen bond homolysis of **3** or any of the members of class (1) above).

The majority of starting material (>50%) is converted to **58** over the course of the photolysis, and this compound subsequently sequentially reductively photodechlorinates to **64**, **63**, **57**, and ultimately **10** (Scheme 2.4 and Figure 2.1). **58** (in methylated form) arising from the irradiation of **3** in isooctane has been tentatively identified in a previous report (*87*); however, an authentic standard was not available for definitive identification, nor was there a rational mechanism proposed for its formation. This previous work found that the proposed **58** product made up <10% of converted starting material in the organic solvent, far less than the value presented here for a primarily aqueous system. Lower conversion of **3** to **58** in organic solvents is expected, as a better hydrogen "donating" solvent (e.g., isooctane) will tend to favor formation of **68** following photochemically induced homolytic aryl-ether bond cleavage, rather than an intramolecular rearrangement to **58** (Scheme 2.5). In comparison to other organic

solvents, CH_3CN is a poor hydrogen donor and is not expected to significantly alter the aqueous nature of the system. While no **64** was observed during the irradiation period, two isomers of **63** were observed after 5 min photolysis and reached peak levels at 30 min. One isomer of **63** was formed in preference to the other (11% vs. <1% contribution after 30 min), but the lack of authentic standards precluded identification. Significant quantities of an isomer of **57** were present during all photolyses and accumulated to a peak contribution of 38% after 45 min irradiation.

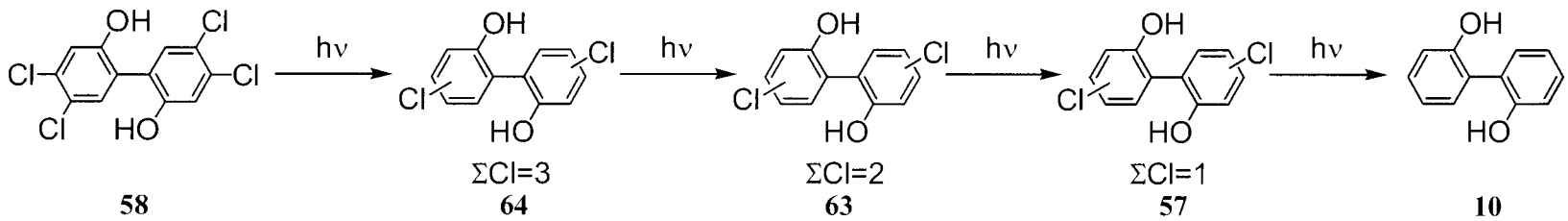

58 **64** **63** **57** **10**

Scheme 2.4

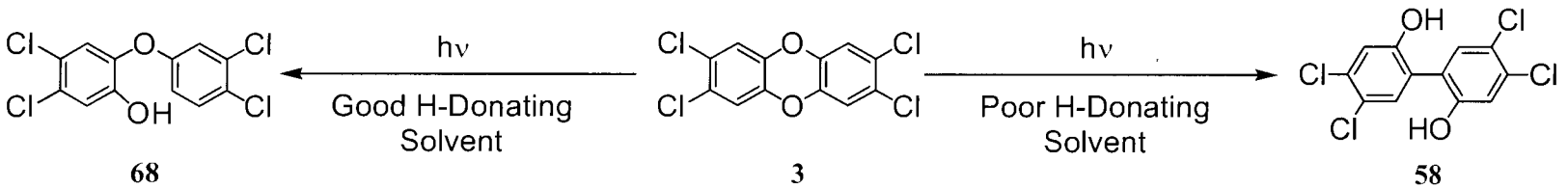

68 **3** **58**

Scheme 2.5

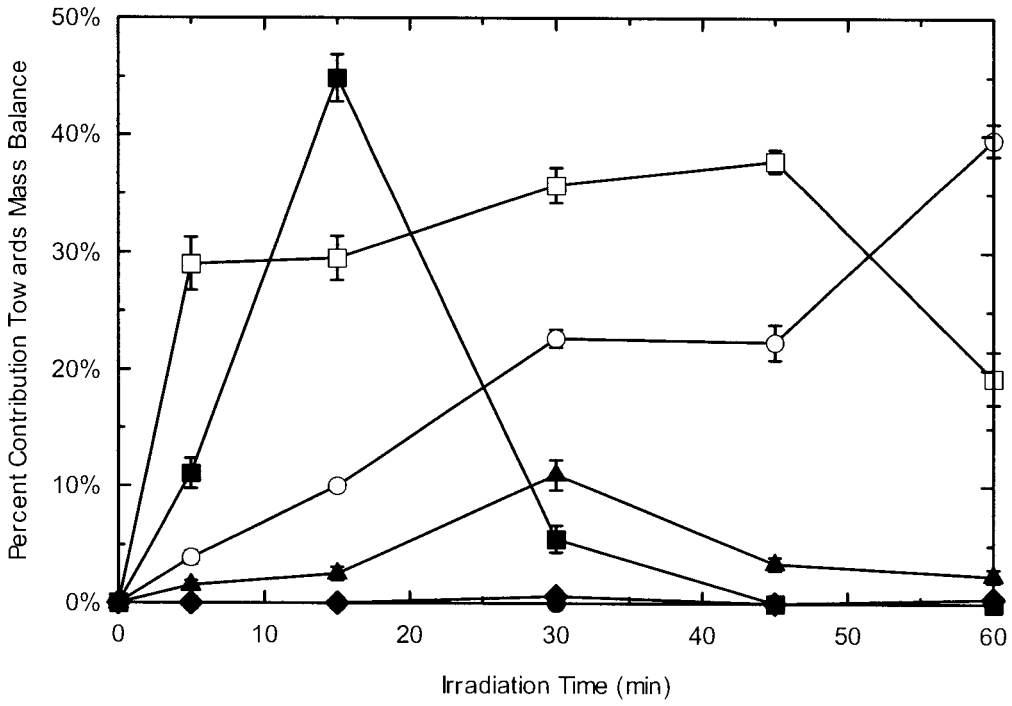

Figure 2.1. Contributions of the individual 2,2'-dihydroxybiphenyl photoproducts towards the overall photochemical mass balance for **3** over a 60 min irradiation period in 19:1 (v/v) H_2O:CH_3CN: **10** (○), **57** (□), **63** (isomer 1) (◆), **63** (isomer 2) (▲), **64** (●), and **58** (■). Error bars show the range of duplicate photolyses where available.

The significant quantity of **57** observed after 5 min irradation (29% of the starting material mass balance) precedes the peak for **58** and suggests a corresponding conversion of photodechlorinated dibenzo[1,4]dioxins to the corresponding chlorinated 2,2'-dihydroxybiphenyls (eq. (2.13). The molecular specifics of this process are unclear, as clearly several photochemical pathways are available – starting with **3** – in order to form **57**. Conversion of **60** to **69** has been previously reported (*87*) (eq. (2.14), supporting the current findings of potential secondary, tertiary, and quaternary photochemistry that contributes to the running mass balance of chlorinated 2,2'-dihydroxybiphenyls. However, given the general trend in location of aryl-ether bond homolysis when the

dibenzo[1,4]dioxin nucleus is substituted the 2- and/or 2,7-positions (e.g., **20**, **21**, and **30**; see above), and the lack of analytical standard for **69** in this previous report, it may be more likely that **60** photochemically rearranges to **70** (eq. (2.15). This also suggests that the primary dechlorination pathway to **62** may be more significant than first thought on the basis of observed photodechlorination products, and possibly accounting for ca. 30% conversion of starting material. Hence, several photodechlorination steps (taking place either from chlorinated 2,2'-dihydroxybiphenyls or chlorinated dibenzo[1,4]dioxins) and one photochemically induced intramolecular rearrangement step (from a chlorinated dibenzo[1,4]dioxin to a chlorinated 2,2'-dihydroxybiphenyl) would need to proceed more rapidly than the rearrangement step for **3** to **58** in order for the monochloro-2,2'-dihydroxybiphenyl contribution to exceed the contribution of **58** prior to the peak contribution of **58**.

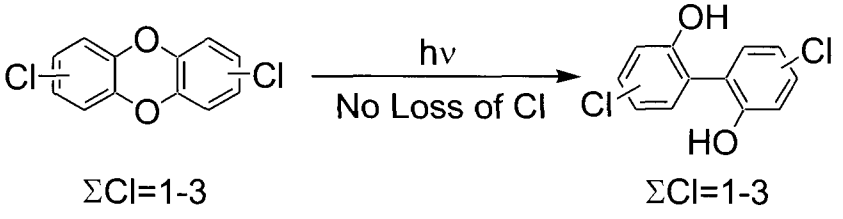

ΣCl=1-3 ΣCl=1-3 (2.13)

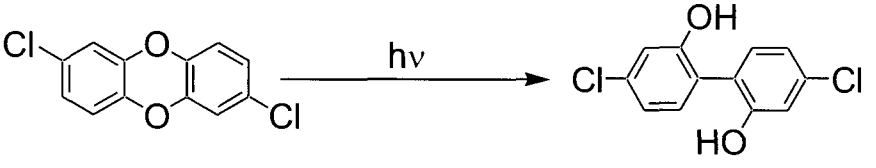

60 **69** (2.14)

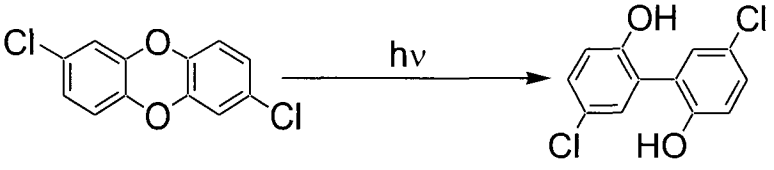

60 **70** (2.15)

In support of this potential explanation, increasing quantum yields for photodechlorination have been previously shown to correlate with decreasing level of substrate chlorination for chlorinated dibenzo[1,4]dioxins (*56*). This increased photodechlorination efficiency with decreasing chlorine substitution may help explain such findings. These results are also consistent with the observation that the majority of converted starting material generally resides throughout the photolysis as either the tetrachlorinated primary photoproducts **58** and **68**, or as the unsubstituted quaternary photoproducts **9**, **10**, and **12**. Hence, build-up of photodechlorinated products in any of the three major photochemical pathways is prevented by their more rapid photolysis than the corresponding primary photoproducts.

Minor primary photoproducts include **68** and **62**, which at no point contribute greater than 5% and 2% of the photochemical mass balance, respectively. As mentioned above, the photodechlorination pathway may contribute more than the presence of observable products indicates, possibly up to 30% conversion. The lack of observable dechlorinated dibenzo[1,4]dioxins is consistent with previous studies in aqueous and organic solvents showing they contributed <20% towards the photochemical mass balance (*25,55*). Previous work has also shown that quantum yields for the photodechlorination of the primary (i.e., trichloro), secondary (i.e., dichloro), and tertiary (i.e., monoichloro) chlorinated dibenzo[1,4]dioxin photoproducts arising from the photolysis of **3** are up to four times higher than the overall quantum yield for disappearance of starting material.

Combined with the comparative molar absorptivities, the rate of photolysis of **62** is generally thought to be approximately three times more rapid than **3** (*56*). Hence, an accumulation of photodechlorination products was not observed or expected. Preferential aryl-chlorine bond homolysis of chlorinated dibenzo[1,4]dioxins has been previously examined by both product studies and computational methods (*89,90*). The results presented here are consistent with these previous reports in that only **60** and **61** were observed as photodechlorination products of **62** (Figure 2.2), with levels of **59** remaining below method detection limits for the course of the photolysis (eq. (2.16). Because of the low yields of **60** and **61**, the major dichlorinated isomer could not be determined, although previous studies suggest **60** is predicted to dominate (*89,90*). No **30** is observed at any time while **9** begins to contribute to the photochemical mass balance after 30 min (3%), with its yield not changing substantially over the ensuing 30 min of irradiation.

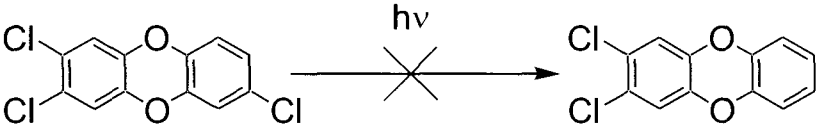

62 **59** (2.16)

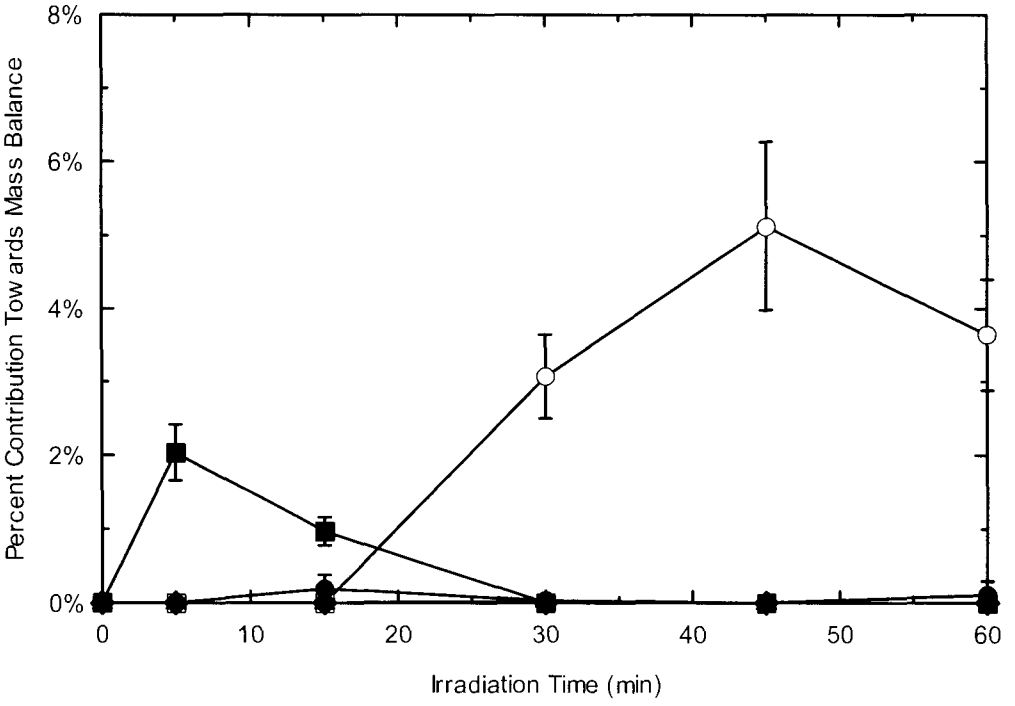

Figure 2.2. Contributions of the individual dechlorination photoproducts towards the overall photochemical mass balance for **3** over a 60 min irradiation period in 19:1 (v/v) H_2O:CH_3CN: **9** (○), **30** (□), **59** (◆), **115** (▲), **61** (●), and **62** (■). Error bars show the range of duplicate photolyses where available.

The relatively low yield of **68** (5%) from **3** is analogous to previous reports for the parent dibenzo[1,4]dioxin system, which displays <10% conversion to **12** (*40*), and is comparable to the previous findings showing ca. 10% yield of **68** from the irradiation of **3** in hexane (*54*) (Figure 2.3). Such findings are consistent with the 19:1 (v/v) H_2O:CH_3CN solvent system being a poorer hydrogen donor than organic solvents (e.g., hexane). The more reactive organic solvents would tend to promote rapid hydrogen abstraction following the initial photochemically induced homolytic aryl-ether bond cleavage in **3**, rather than promote an intramolecular rearrangement to **58** (as per Scheme 2.5 above). Conversion of **3** to **68** peaks after 5 min irradiation (5%), and then declines with no

mono- and trichloro-2-phenoxyphenols observed over the remaining photolysis period. One dichloro-2-phenoxyphenol isomer (**66**) is seen at low yield (1%) after 15 min, but subsequent conversion of photodechlorinated 2-phenoxyphenols appears more rapid than the production of **68**. Hence, there is no build-up of **65**, **66**, or **67**. As with the 2,2'-dihydroxybiphenyl and dibenzo[1,4]dioxin classes, the yield of the parent 2-phenoxyphenol (**12**) increases after first appearing at 30 min (9%) to a maximum after 60 min (16%).

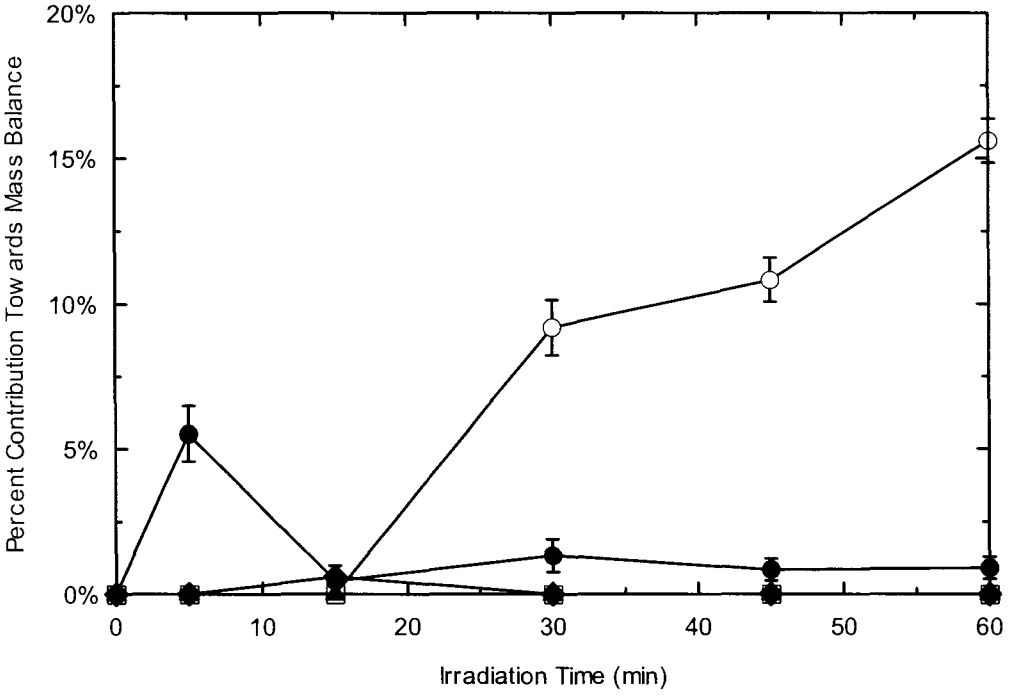

Figure 2.3. Contributions of the individual 2-phenoxyphenol photoproducts towards the overall photochemical mass balance for **3** over a 60 min irradiation period in 19:1 (v/v) H_2O:CH_3CN: **12** (○), **65** (◆), **66** (▲), **67** (■), and **68** (●). Error bars show the range of duplicate photolyses where available.

These results are summarized in Figure 2.4, which shows the relative contributions of each photoproduct class towards the overall mass balance at each

irradiation time. 2,2'-Dihydroxybiphenyls dominate the photoproduct distribution and account for up to 87% mass balance after 15 min, whereas the summation of 2-phenoxyphenols and photodechlorinated dibenzo[1,4]dioxins each account for <20% mass balance at all times. On the basis of the observed photoproduct profiles, the relative importance of each of the three major photochemical pathways for **3** in 19:1 H_2O:CH_3CN (v/v) were assigned as follows: (1) ca. 55% primary aryl-ether bond homolysis followed by intramolecular rearrangement to give **58**; (2) ca. 30% primary aryl-chlorine bond homolysis followed by hydrogen abstraction from the organic cosolvent to give **62**; and (3) ca. 15% primary aryl-ether bond homolysis followed by hydrogen abstraction from the organic cosolvent to give **68**.

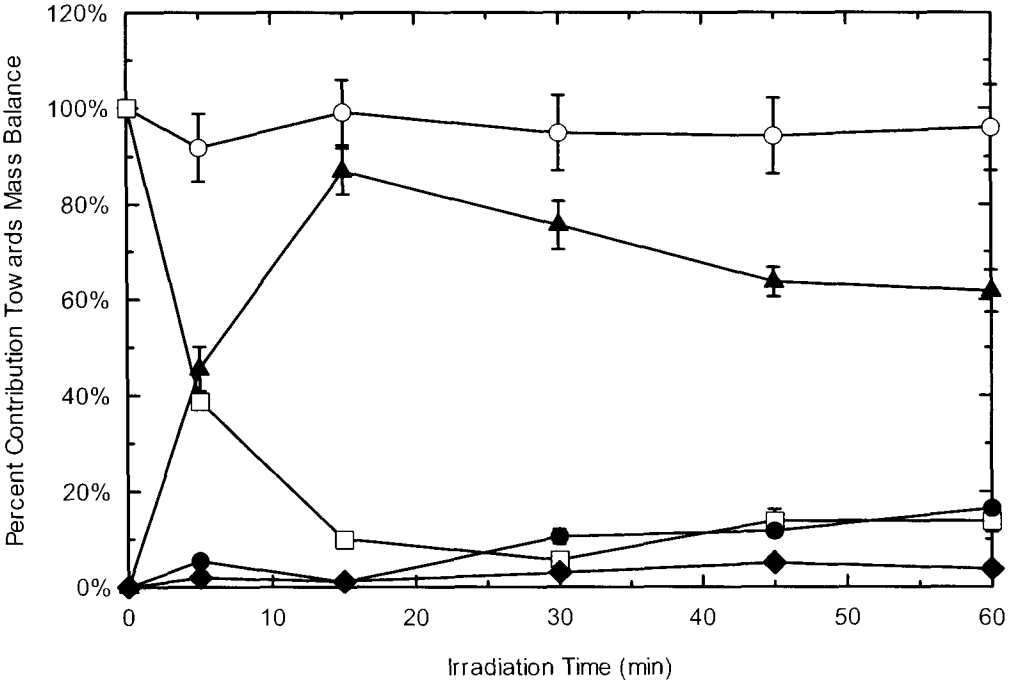

Figure 2.4. Solution mass balance (○) and contributions of unreacted starting material (□), the sum of photodechlorination photoproducts (◆), the sum of 2,2-dihydroxybiphenyl photoproducts (▲), and the sum of 2-phenoxyphenol photoproducts (●) towards the overall photochemical mass balance for **3** over a 60 min irradiation period in 19:1 (v/v) H_2O:CH_3CN. Error bars show the range of duplicate photolyses where available.

The pseudo first order rate constant (k) for the disappearance of **3** was calculated to be $1.55\pm0.13\times10^{-3}$ s^{-1} (τ=10.7±0.9 min; R^2=0.90), which provides an estimated half-life ($t_{½}$) of 7.4 min under the present experimental conditions.

Previous studies have also shown that **12** cannot convert to **10** (*40*), and hence, the 2,2-dihydroxybiphenyl and 2-phenoxyphenol pathways are not connected (eq. (2.17). Although photochemical ring closure of chlorinated 2-phenoxyphenols to chlorinated

dibenzo[1,4]dioxins has been observed and is thought to occur from the triplet state (*91*) (e.g., eq. (2.18), this requires *ortho* chlorine substituents on one of the phenyl systems. Such a geometry is not expected in the present studies. Thus, in the case of **3** photochemistry, the photolytic conversions of chlorinated dibenzo[1,4]dioxins to the corresponding chlorinated 2-phenoxyphenols are not reversible (e.g., Scheme 2.6).

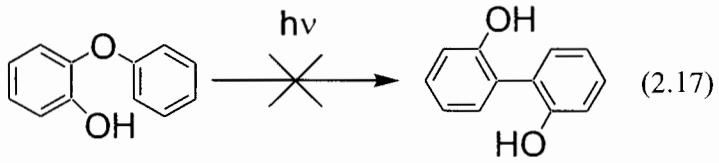

(2.17)

12 **10**

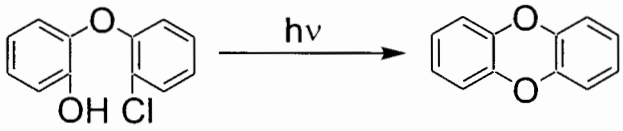

(2.18)

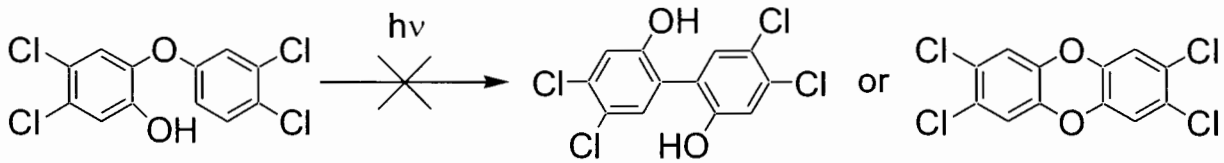

68 **58** **3**

Scheme 2.6

When attempting to complete a photochemical mass balance involving primary through quaternary photoproducts of **3**, of note is the potential for photochemical aryl-ether bond cleavage of the chlorinated 2-phenoxyphenols. This process has been previously reported, leading to the formation of chlorinated phenols, catechols, and benzenes, and is thought to take place from the singlet state (*91*). In the present work, products arising from photochemical aryl-oxygen bond homolysis in the chlorinated 2-phenoxyphenols were not considered as their GC retention time under the instrumental

conditions in use (and with toluene as the solvent) would have made them difficult to identify and quantitate. However, the nearly complete mass balance for all photochemical extracts suggests this pathway is not a major contributor to the overall photochemistry. As well, the photochemical conversion of **10** to 2,2',3-trihydroxybiphenyl (**71**) was not observed (eq. (2.19), although it had been suggested in irradiations of lake water (*48*). However, the potential photochemical conversion of **10** to **71** was not actively investigated.

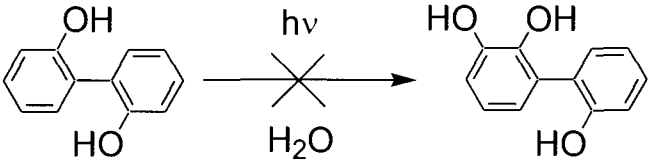

10 **71** (2.19)

In comparison to the photolysis described above in 19:1 (v/v) H_2O:CH_3CN, photodegradation of **3** (1.8×10^{-9} M) in 100% water during a 60 min irradiation period was more rapid than in 19:119:1 H_2O:CH_3CN (v/v) (Table 2.1 and Table 2.2). A higher relative contribution of 2,2-dihydroxybiphenyl photoproducts, and a lower relative contribution of photodechlorination products, was also observed when **3** was photolyzed in 100% water versus 19:1 H_2O:CH_3CN (v/v). These findings are consistent with previous studies involving the related compound class, chlorinated dibenzofurans (**72**), that reported reduced photodechlorination rates in polar, hydroxylic solvents such as water (*25,47*), which is expected because hydrogen abstraction from H_2O is generally not possible by ground state carbon-based radicals. Studies on the parent dibenzo[1,4]dioxin system (**9**) also show an enhancement of starting material degradation by water (*40*). For

the parent dibenzo[1,4]dioxin system, water also appears to increase the yield of 2,2'-dihydroxybiphenyl photoproduction.

Some studies have also suggested the conversion of dibenzofuran (**73**) to **10** at 300 nm in natural waters (*48*). This result could not be reproduced in the present study when **73** was irradiated in 1:1 (v/v) H_2O:CH_3CN. The preliminary investigation by preparatory photolysis showed no photochemical conversion of **73** after up to 2 h irradiation at 254 nm in a Rayonet RPR 100 photochemical reactor with 16 lamps as followed by ^1H NMR (eq. (2.20). In contrast to the observations from the present work, and those in the literature for chlorinated dibenzofurans, chlorinated dibenzo[1,4]dioxin photolysis rates have generally been reported to be higher in organic solvents (*25,92*) with the presence of sodium borohydride ($NaBH_4$) enhancing the rate to an even greater extent (*93*). However, the observed rate increase for dibenzo[1,4]dioxin photolysis (both for **9** and **3**) during the present study with an increasing water content is consistent with the proposed general dibenzo[1,4]dioxin photochemical mechanism discussed below.

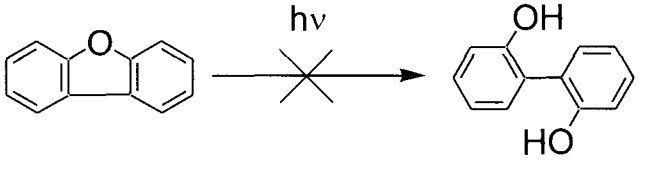

(2.20)

73 **10**

Table 2.1. Contributions of the individual 2,2'-dihydroxybiphenyl, dibenzo[1,4]dioxin, and 2-phenoxyphenol analytes towards the photochemical mass balance of **3** in H_2O after 60 min irradiation.

	Percent Contribution Towards Mass Balance
10	70.5±3.6%
57	8.3±1.7%
63 (Isomer 1)	0.2±0.2%
63 (Isomer 2)	0.3±0.2%
64	0.8%±0.3%
58	nd[a]
9	1.3±0.6%
30	nd
59	nd
60	nd
61	nd
62	nd
3	4.0±0.6%
12	7.4±0.4%
65	nd
66	0.3±0.3%
67	nd
68	1.0±0.4%
Total	94.1±8.4%

[a] "nd" defined as analyte concentration below method detection limit.

Table 2.2. Contributions of the major photoproduct classes towards the photochemical mass balance of **3** after 60 min irradiation in 19:1 (v/v) H_2O:CH_3CN and H_2O.

	19:1 (v/v) H_2O:CH_3CN	H_2O
Unreacted Starting Material	13.8±0.7%	3.9±0.2%
2,2'-Dihydroxybiphenyls	61.8±3.3%	80.2±4.2%
2-Phenoxyphenols	16.5±0.9%	8.7±0.5%
Dechlorination Photoproducts	3.8±0.2%	1.3±0.1%

For each of the photochemical product studies on the various individual dibenzo[1,4]dioxins with the exception of **3**, replicate photolyses were performed while continuously purging the solutions with oxygen or nitrogen. Oxygen is a known triplet quencher, and where oxygen is sparged through a solution during irradiation, triplet reactions are typically prevented. Short-lived triplet states (τ<1 ns) may escape quenching by oxygen and thus go on to participate in triplet reactions. For all dibenzo[1,4]dioxin photochemical studies where identical trials were performed under nitrogen or oxygen purging, no difference in percent conversion of starting material, photoproduct yields, or photoproduct distributions was observed. The results suggest that dibenzo[1,4]dioxin photochemistry was occurring via the singlet state, and that triplet state reactions were not significant contributors to the observed photochemistry. The results are consistent with previous work on **9**, **13**, **20**, and **21**, which also did not observe evidence of an active triplet state in the resulting photochemistry (*40,41*). In addition, photochemical studies on **9** (E_T=290-330 kJ/mol) using acetone (E_T=330-340 kJ/mol) as a triplet sensitizer also did not result in any observable triplet reactions (*40*). Weak fluorescence for **9** and **13** prevented further probing of singlet state reactivity, and also

supports facile aryl-ether cleavage from S_1 (*40*). Previous work with **29** suggests that both states are reactive in the photodechlorination reactions, but no investigations of aryl-ether cleavage were performed (*51*). Because of the increase in spin-orbit coupling, all chlorinated dibenzo[1,4]dioxins are expected to have shorter singlet and triplet state lifetimes than the parent system.

As **3** has the highest toxic equivalence factor (TEF; defined as 1.0 for this congener) of all chlorinated dibenzo[1,4]dioxin congeners for which this rating scheme has been developed, the photochemical conversion of **3** to other chlorinated dibenzo[1,4]dioxins can only decrease the ΣTEF of a solution. Note that the TEFs of chlorinated dibenzo[1,4]dioxins having <4 chlorine substituents are defined as zero (*94*). Chlorinated 2,2'-dihydroxybiphenyls, which may also arise through polychlorinated biphenyl metabolism, have been identified in humans and wildlife (*95,96*). While some chlorinated 2,2'-dihydroxybiphenyls are readily excreted, bioaccumulation of some congeners may be related to their high binding affinity for the serum thyroid hormone binding protein transthyretin (TTR) (*97,98*). In addition, chlorinated 2,2'-dihydroxybiphenyls may exert endocrine disrupting abilities (*99,100*), with some congeners having up to 10 times the binding affinity for TTR relative to the endogenous and major blood thyroid hormone, thyroxine (*101*). However, the structure of chlorinated 2,2'-dihydroxybiphenyls is an important determinant of their biological effects. Those congeners with *ortho* hydroxy groups (i.e., the 2,2'-dihydroxybiphenyls) are significantly less disruptive to biological systems than congeners with *meta* and *para* hydroxy functions (*102*). Because only *ortho* hydroxylated biphenyls can be produced

photochemically from chlorinated dibenzo[1,4]dioxins, the photodegradation of chlorinated dibenzo[1,4]dioxins will not produce the most potent of the endocrine disrupting chlorinated dihydroxybiphenyls. Chlorinated 2-phenoxyphenols have also been shown to have deleterious biological effects such as mutagenicity (*103*) and toxicity (albeit at threshold concentrations much lower than that of **3**) (*104*). Overall, it appears as though the aqueous photolysis of **3**, resulting in the production of chlorinated 2,2'-dihydroxybiphenyls and 2-phenoxyphenols, will produce a solution of lower acute toxicity but one with potential chronic endocrine disrupting and mutagenic effects.

While a product study was not undertaken on **29** because of the potential for formation of highly toxic dechlorination products (e.g., **3**), recent work performed elsewhere suggests that highly chlorinated 2,2'-dihydroxybiphenyls may be the dominant photoproducts (in up to 80% yields with <20% as dechlorination) for this compound (*105*), suggesting that octachloro-2,2'-dihydroxybiphenyl (**74**) may be the major primary photoproduct of **29** (eq. (2.21). This finding would be consistent with the findings presented below on the relative contributions of aryl-oxygen and aryl-chlorine bond cleavage for **3**.

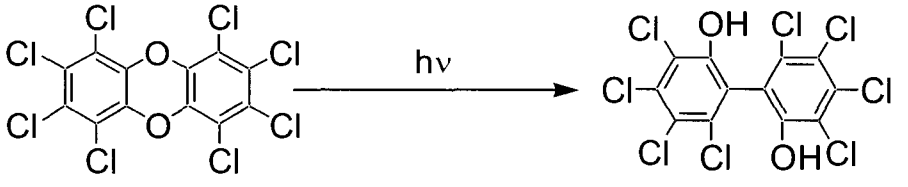

29 **74** (2.21)

2.3 UV-Vis Studies

While previous work on **9** suggested the formation of a thermally unstable 2,2'-biphenylquinone (**16**) following short irradiation periods (ca. 30 s) of starting material (*40,41*), the present work sought to confirm these findings and examine in greater detail both the kinetics and potential thermal and photochemical products resulting from the decay of **16**. In addition, although a previous report (*41*) had shown the formation of analogous 2,2'-biphenylquinones from **13**, **20**, and **21**, the kinetics of their thermal decays – and the potential thermal and photochemical products arising from their observed reactivity – had only been explored in preliminary detail. It was the objective of the present work to gain a more complete understanding of the 2,2'-biphenylquinone generation and subsequent reactivity from **9**, **13**, **20**, and **21**, as well as to examine the potential formation of these unique transient compounds from **29**, **30**, and **46**, which had not been previously studied.

After a short irradiation period under dilute conditions (6×10^{-5} M; 15 s; 300 nm) in dry CH_3CN, characteristic 2,2'-biphenylquinone absorption spectra (containing a λ_{max} in the visible region between 500 and 700 nm; $\lambda_{max(500\text{-}700\ nm)}$) were observed at the suprasecond timescale for **9**, **13**, **20**, **21**, and **30**. Following the short irradiation of **9** in dry CH_3CN, a species with a $\lambda_{max(500\text{-}700\ nm)}$=522 nm was observed that subsequently decayed thermally over the course of several minutes (Figure 2.5). The identity of this transient compound has been previously assigned (*40,41*) as **16** (eq. (2.22).

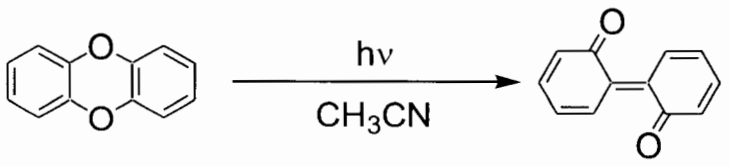

(2.22)

9 **16**

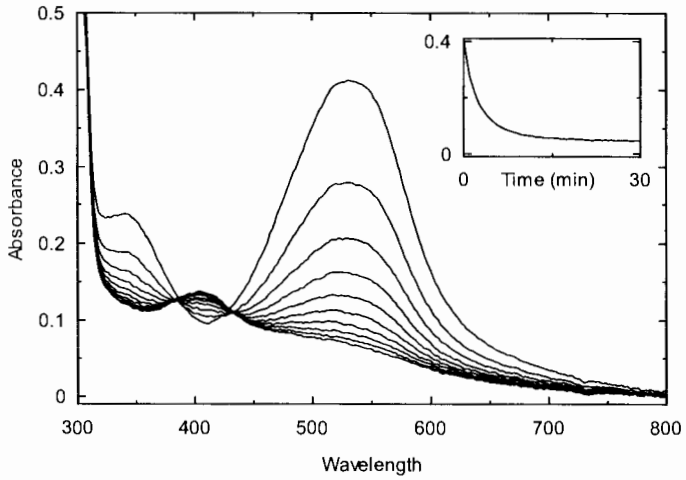

Figure 2.5. UV-Vis spectra taken at 60 s intervals following photogeneration of **16** in dry CH_3CN. Inset shows transient decay traces taken at 10 s intervals at the λ_{max}=522 nm of the 2,2'-biphenylquinone. The intensity of the absorption band at λ_{max}=522 decreased continuously over the monitoring period.

Following the short irradiation of **30** in dry CH_3CN, a species with a $\lambda_{max(500\text{-}700\ nm)}$=548 nm was observed that subsequently decayed thermally over the course of several minutes (Figure 2.6). The UV-Vis spectrum of this transient has not been previously reported, and its identity (based on the product studies described above) is assigned as **75** (eq. (2.23).

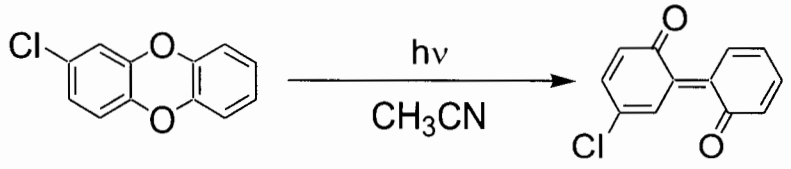

(2.23)

30 **75**

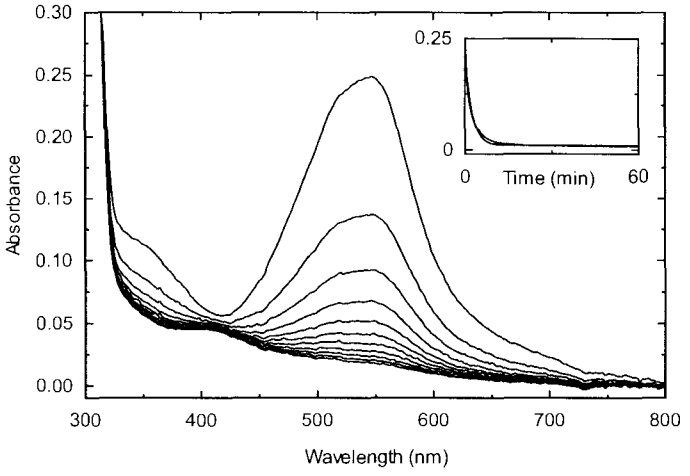

Figure 2.6. UV-Vis spectra taken at 60 s intervals following photogeneration of **75** in dry CH_3CN. Inset shows transient decay traces taken at 10 s intervals at the λ_{max}=548 nm of the 2,2'-biphenylquinone. The intensity of the absorption band at λ_{max}=548 decreased continuously over the monitoring period.

Following the short irradiation of **20** in dry CH_3CN, a species with a $\lambda_{max(500\text{-}700\ nm)}$=530 nm was observed that subsequently decayed thermally over the course of several minutes (Figure 2.7). The identity of this transient compound has been previously assigned (*41*) as **26** (eq. (2.24).

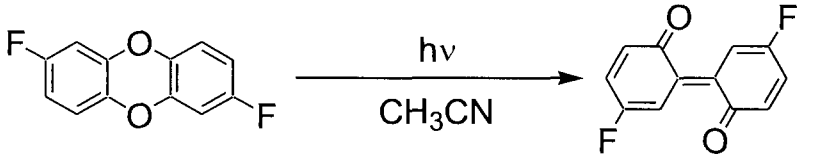

20 **26** (2.24)

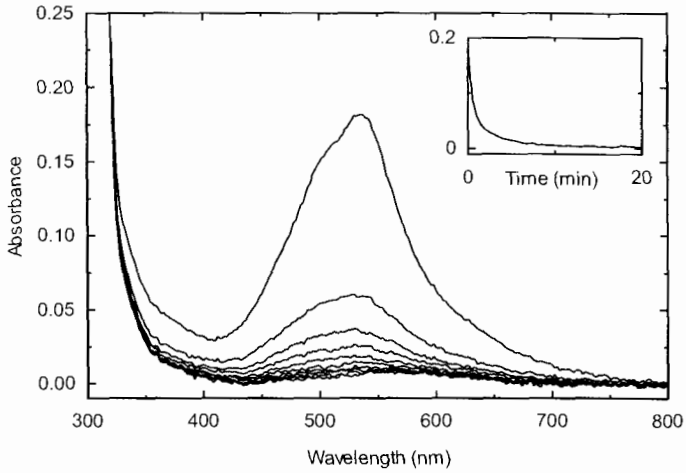

Figure 2.7. UV-Vis spectra taken at 60 s intervals following photogeneration of **26** in dry CH_3CN. Inset shows transient decay traces taken at 10 s intervals at the λ_{max}=530 nm of the 2,2'-biphenylquinone. The intensity of the absorption band at λ_{max}=530 decreased continuously over the monitoring period.

Following the short irradiation of **21** in dry CH_3CN, a species with a $\lambda_{max(500\text{-}700\ nm)}$=607 nm was observed that subsequently decayed thermally over the course of several minutes (Figure 2.8). The identity of this transient compound has been previously assigned (*41*) as **28** (eq. (2.25).

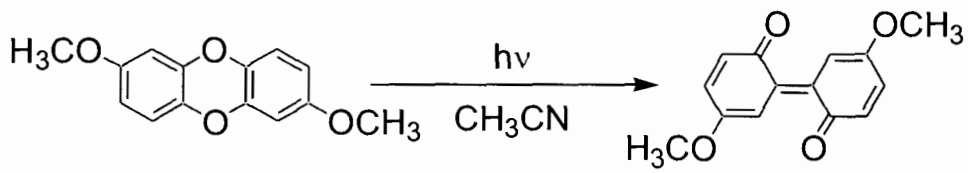

21 **28** (2.25)

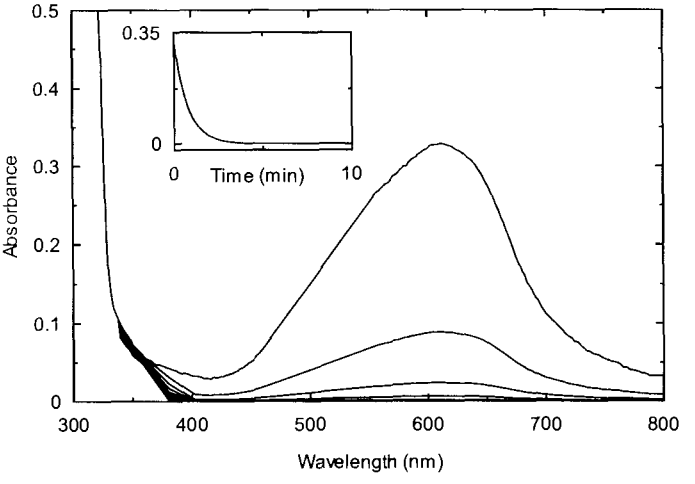

Figure 2.8. UV-Vis spectra taken at 60 s intervals following photogeneration of **28** in dry CH_3CN. Inset shows transient decay traces taken at 10 s intervals at the λ_{max}=607 nm of the 2,2'-biphenylquinone. The intensity of the absorption band at λ_{max}=607 decreased continuously over the monitoring period.

Following the short irradiation of **13** in dry CH_3CN, a species with a $\lambda_{max(500\text{-}700\ nm)}$=566 nm was observed that subsequently decayed thermally over the course of several minutes (Figure 2.9). The identity of this transient compound has been previously assigned (*41*) as **19** (eq. (2.26).

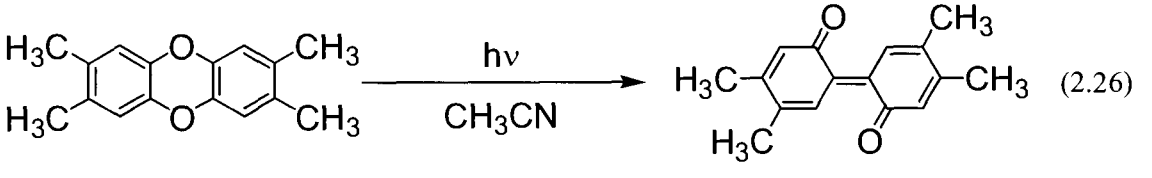

(2.26)

13 **19**

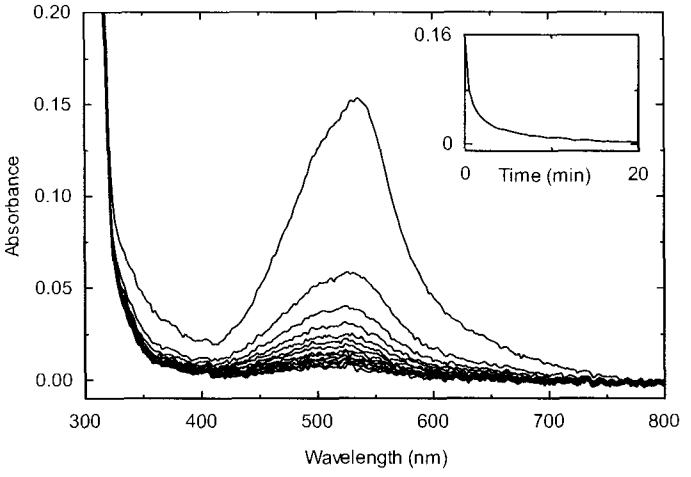

Figure 2.9. UV-Vis spectra taken at 60 s intervals following photogeneration of **19** in dry CH_3CN. Inset shows transient decay traces taken at 10 s intervals at the λ_{max}=566 nm of the 2,2'-biphenylquinone. The intensity of the absorption band at λ_{max}=566 decreased continuously over the monitoring period.

While conventional supra-second UV-Vis spectra of the corresponding 2,2'-biphenylquinones from **46** (eq. (2.27) and **29** (eq. (2.28) could not be obtained, nanosecond-scale laser-flash photolysis (LFP) studies with transient UV-Vis absorption indicate that both compounds are formed. The LFP spectra of these compounds are presented in Section 2.6.

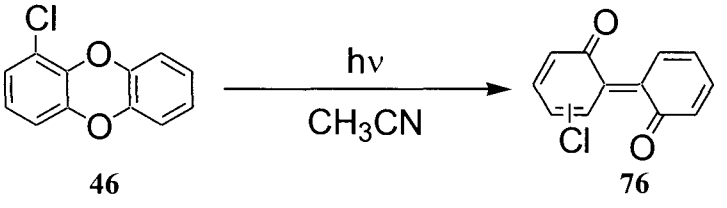

46 **76** (2.27)

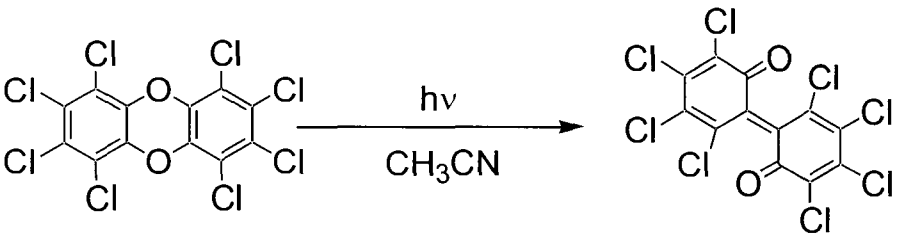

(2.28)

29 **77**

To help understand the underlying molecular properties governing the absorption characteristics of these transient compounds, potential relationships between the well-known Hammett constants widely used in physical-organic chemistry and the wavelength of maximum absorption in the visible region ($\lambda_{max(500\text{-}700\ nm)}$) for the 2,2'-biphenylquinones were investigated.

The $\lambda_{max(500\text{-}700\ nm)}$ of the photogenerated 2,2'-biphenylquinones was found to depend on both the identity and position of substituents, where $\lambda_{max(500\text{-}700\ nm)}$ varies with the sum of Hammett σ^+ values for the substituents (Figure 2.10). The Hammett equation is a linear free-energy relationship (LFER), often represented in the forms $\ln(K/K_o)=\rho\sigma$ or $\ln(k/k_o)$, where – for a given reaction – K and k are the equibrium or rate constants, respectively, of a substituted derivative, and K_o and k_o are the equibrium or rate constants, respectively, of the unsubstituted parent system. The logarithmic relationship between free energies of reaction ($\Delta G=-RT\times\ln K$) and free energies of activation ($\Delta G^{\ddagger}=-RT\times\ln k$) results in a linear relationship between the $\rho\sigma$ values in the Hammett equation and the energies of reaction and activation (*106*). The λ_{max} of a compound is a measure of the energy required to move a molecule from its ground state into an excited state, and is inversely proportional to energy (i.e., $E=hc/\lambda$). Thus, correlations between the energy of

maximum absorption and Hammett substituent constants represent a LFER, and as such, the relationships between λ_{max} and $\Sigma\sigma$ may be treated using the Hammett approach.

To construct the Hammett plot, σ^+ and σ values were taken from ref. (*106*). As noted in ref (*106*), σ^+ values for some meta substituents have been determined, but they do not differ appreciably from σ meta values. Thus, σ_m was used in place of σ^+_m for the plot shown in Figure 2.10. The substituent positions relative to the "reaction center" were determined with regard to the ketone group on each ring of the 2,2'-biphenylquinone. For example, **26** was treated as having two fluorine atoms (σ^+_p=-0.07) in the *para* position, and thus its $\Sigma\sigma^+$ value is -0.14. Values of the Hammett constants used for constructing Figure 2.10, as well as those values used in Hammett relationships discussed elsewhere in this work, are given in Table 2.3.

Table 2.3. Hammett constants used in the current work.

Functional Group	σ_m	σ_p	σ^+_p
H	0	0	0
Cl	0.37	0.23	0.11
F	0.34	0.06	-0.07
OCH_3	0.12	-0.27	-0.78
CH_3	-0.07	-0.17	-0.31

Thus, the $\Sigma\sigma^+$ and $\Sigma\sigma$ values for each of the 2,2'-biphenylquinones investigated as to the relationships between $\Sigma\sigma^+$ and $\Sigma\sigma$ versus the $\lambda_{max(500\text{-}700\ nm)}$ are given in Table 2.4.

Table 2.4. $\Sigma\sigma^+$ and $\Sigma\sigma$ values for the 2,2'-biphenylquinones used in constructing Figure 2.10 and Figure 2.11.

Compound	$\Sigma\sigma^+$	$\Sigma\sigma$
16	0	0
19	-0.76	-0.48
26	-0.14	0.12
28	-1.56	-0.54
75	0.11	0.23

Both electron donating and withdrawing substituents increase $\lambda_{max(500\text{-}700\ nm)}$ of the 2,2'-biphenylquinone, and the better correlation with σ^+ versus σ (see Figure 2.11 for a plot of $\lambda_{max(500\text{-}700\ nm)}$ versus $\Sigma\sigma$) suggests extensive resonance interaction governing the

value of the $\lambda_{max(500\text{-}700\ nm)}$. Note that in Figure 2.10, only two points are available with a $\Sigma\sigma^{+}\geq 0$ and a discussion of the potential linearity of the relationship between $\lambda_{max(500\text{-}700\ nm)}$ and $\Sigma\sigma^{+}$ cannot be made over this range. This strong resonance contribution contributing to the $\lambda_{max(500\text{-}700\ nm)}$ of such a highly conjugated system is not unexpected given the well-known "particle-in-a-box" approach to calculating $\lambda_{max(500\text{-}700\ nm)}$ as a function of number of conjugated π-bonds (*107*). In the present case, the structural "backbone" is constant across the 2,2'-biphenylquinone series, and the electronic character of the substituents appears to be influencing the degree of resonance interaction and thereby controlling $\lambda_{max(500\text{-}700\ nm)}$.

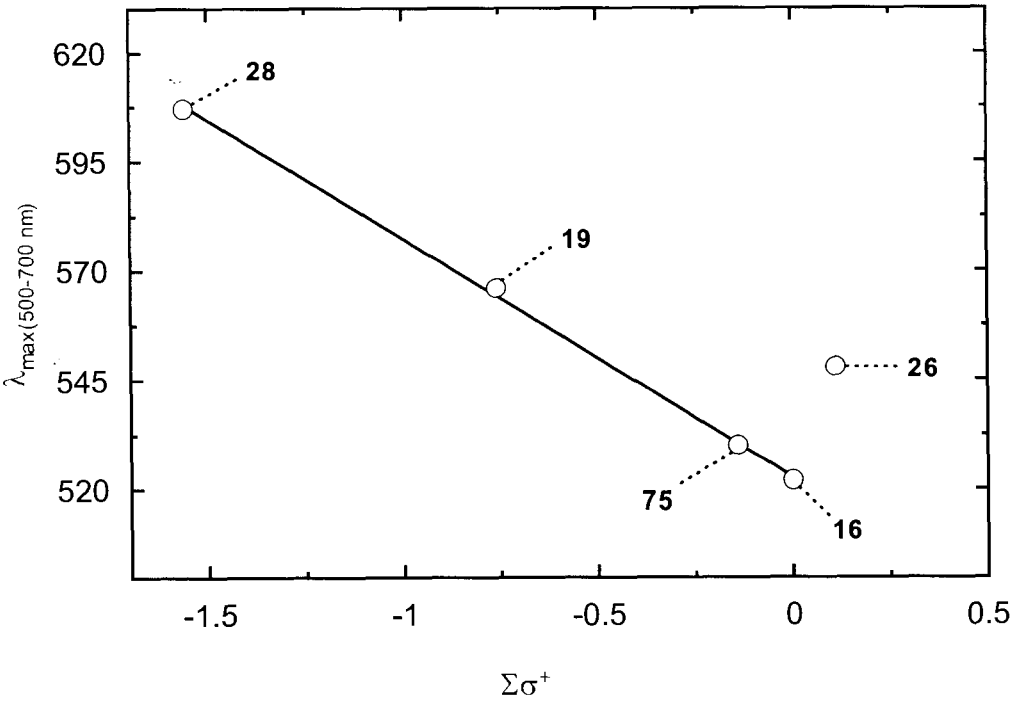

Figure 2.10. Hammett plot with the dependence of $\lambda_{max(500\text{-}700\ nm)}$ for **16**, **19**, **26**, **28**, and **75** on $\Sigma\sigma^{+}$ of the substituents. A regression line of the form $\lambda_{max}=-55\times\Sigma\sigma^{+}+523$ with a $R^2=0.9990$ is shown over the range from $-1.56\leq\Sigma\sigma^{+}\leq 0$. Only two points with $\Sigma\sigma^{+}\geq 0$ were available, and thus, a regression analysis could not be performed over this range.

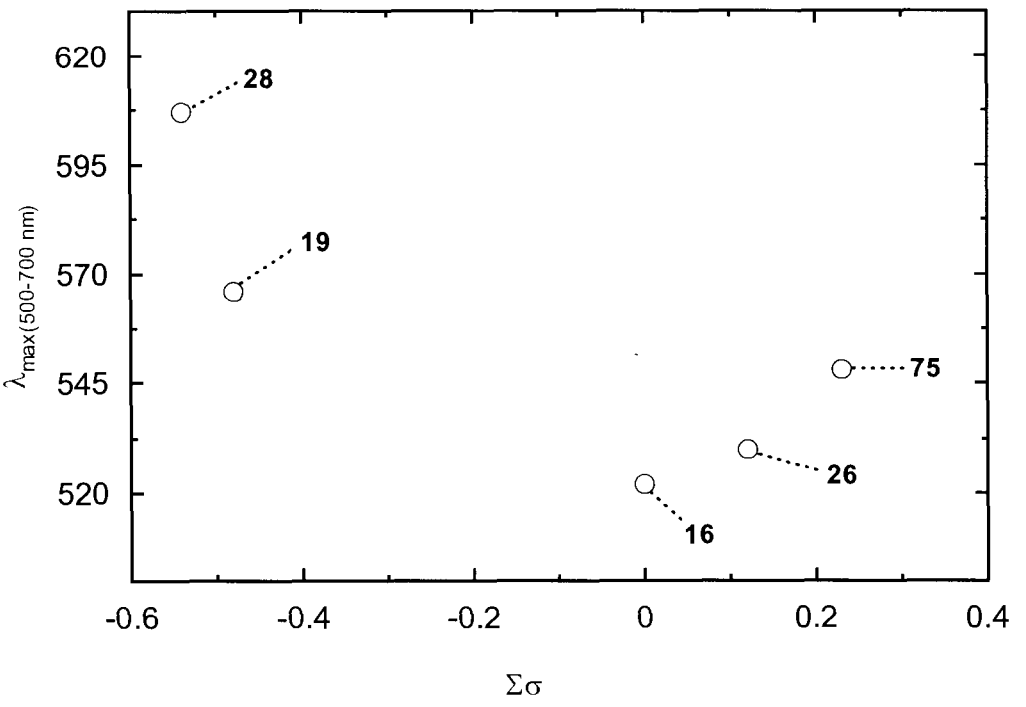

Figure 2.11. Hammett plot with the dependence of $\lambda_{max(500\text{-}700\ nm)}$ for **16**, **19**, **26**, **28**, and **75** on Σσ of the substituents.

Evidence for such charge separation in the UV-visible spectra of 2,2'-biphenylquinones has been previously suggested based on the observed effect solvents of differing dielectric constants have on $\lambda_{max(500\text{-}700\ nm)}$ (*108*). Similar effects on the absorption spectra of the related 4,4'-biphenylquinone (**78**) system and its derivatives have been reported, with – for example – the addition of two *ortho*-CH_3 groups (**79**) yielding an increase in λ_{max} for the visible region of ca. 10 nm from 399 to 409 nm (*109*). In addition, the *ortho* configuration of a quinone is known to increase the $\lambda_{max(500\text{-}700\ nm)}$ substantially (likely by extending the maximum potential length of conjugation), and for the parent benzoquinone systems, an increase in the λ_{max} for the visible region of ca. 120 nm is observed in moving from the 1,4- (*para*; **80**) to 1,2- (*ortho*; **81**) configurations

(*109*). Based on the present study, a similar ca. 120 nm increase in the λ_{max} for the visible region is observed in moving from **78** to **16** (ca. 400 to 520 nm).

While not considered by previous authors, a similar relationship appears to hold between the λ_{max} in the visible region and $\Sigma\sigma^+$ for the 4,4'-biphenylquinones. For example, the data of Detroit and Hart on **78** and its 3,3',5,5'-substituted tetramethyl (**82**), tetra-t-butyl (**83**), and tetrachloro (**84**) derivatives in ethanol yields slopes of -18 nm and +75 nm for $\Sigma\sigma^+\leq 0$ and $\Sigma\sigma^+\geq 0$, respectively (*110*). The weaker fit (R^2=0.86) for $\Sigma\sigma^+\leq 0$ is likely due to the difficulty in applying a σ^+ value to a *t*-butyl group *ortho* to the ketone because of strong steric influences not originally accounted for when this parameter was developed. Likewise, the data of Bourdon and Calvin on **78** and its 3,3'-dimethyl (**85**) and 2,2'-dimethyl-5,5'-di-*t*-butyl (**86**) derivatives in benzene (*109*) yields a good fit (R^2=0.997) between the λ_{max} in the visible region and $\Sigma\sigma^+$ with a slope of –63 nm for $\Sigma\sigma^+\leq 0$. These results are comparable to the observed slope of -55 nm for $\Sigma\sigma^+\leq 0$ for the photogenerated 2,2'-biphenylquinones shown in Figure 2.10.

Such quantitative predictive tools for the λ_{max} in the visible region based on Hammett substituent constants are, in many cases, a satisfactory complement to the well-known Woodward rules for estimating the λ_{max} in the visible region of conjugated carbonyl compounds (*111,112*) because they incorporate both substituent identity and position on the conjugated system for a potentially wider range of functional groups. The Woodward rules predict a $\lambda_{max(500\text{-}700\ nm)}$ of 525 nm for **16**, close to the observed value of 522 nm, if the system is modeled as two six-membered ring parent enones (2×215 nm)

with three double-bonds extending the conjugation (3×30 nm) and an exocyclic double bond (5 nm). However, **19**, **28**, and **75** are predicted to have $\lambda_{max(500\text{-}700\ nm)}$ of 585, 559, and 537 nm, respectively, using the Woodward rules, differing from the respective observed $\lambda_{max(500\text{-}700\ nm)}$ values of 566, 607, and 548 nm. The discrepancies in the substituted 2,2'-biphenylquinone $\lambda_{max(500\text{-}700\ nm)}$ values likely arise from the lack of incorporating significant substituent resonance contributions in the Woodward values (i.e., a CH_3 group in the γ-position to the carbonyl has an additive constant of 18 nm, greater than the value for a OCH_3 group [17 nm] in the same position).

2.4 Thermal Reactivity of the 2,2'-Biphenylquinones

Following their photochemical generation in dry CH_3CN, **16**, **19**, **26**, **28**, and **75** were observed to decay thermally via a pseudo first order process with lifetimes ($\tau=1/k$) on the order of 0.6-2.4 min ($k=7.09\pm0.14\times10^{-3}$ to $2.86\pm0.01\times10^{-2}$ s^{-1}) depending on compound and solvent identity (see Table 2.6 below). The thermal decay of **77** was found to occur within the timescale of the LFP system with a lifetime of ca. 55 ms ($k=1.8\times10^{4}$ s^{-1}), whereas **76** (although observable by nanosecond LFP) could not be generated on a scale sufficent to reliably observe its decay by conventional UV-Vis instrumentation. The rate constants for these thermal processes (and for the thermal reaction of 4,4',5,5'-tetramethoxy-2,2'-biphenylquinone in dry CH_3CN (**52**; $k=1.3\times10^{-2}$ s^{-1}, which was synthesized independently as described below) are correlated with the sum of Hammett substituent constants present on one of the rings of the 2,2'-biphenylquinone (Figure 2.12). The Hammett plot reveals a pair of lines intersecting at $\Sigma\sigma=0$ with ρ-values of -4.9 and 21.3, respectively, suggesting two alternate mechanistic paths for the

2,2'-biphenylquinone thermal decays depending on whether the substituent has electron withdrawing or donating properties.

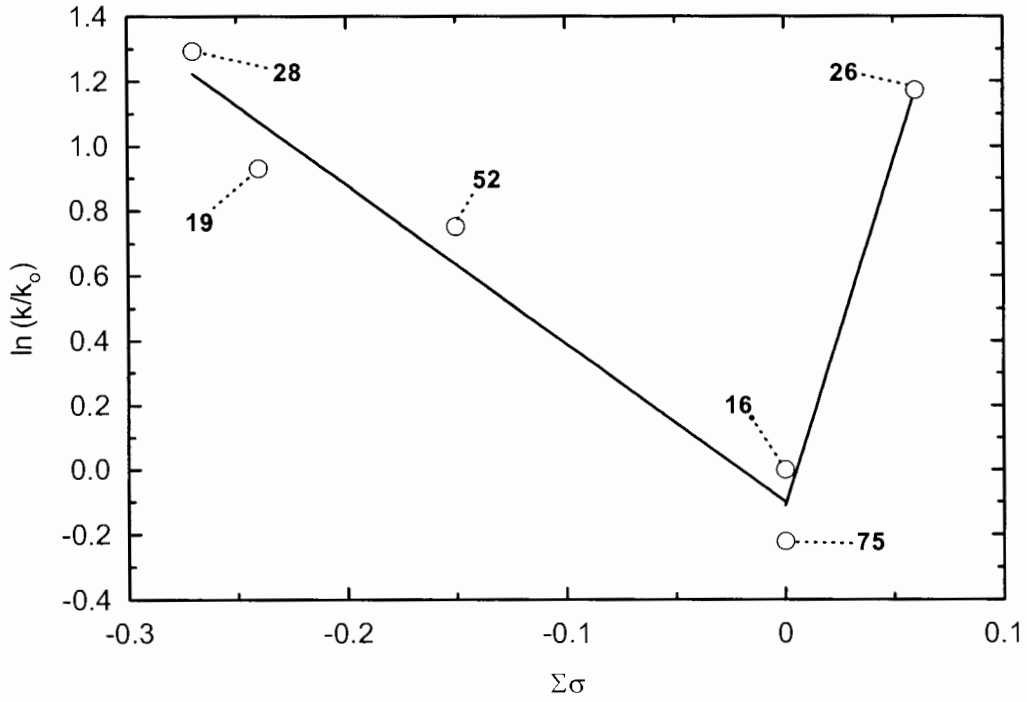

Figure 2.12. Hammett plot showing the dependence of the rate of thermal decays for **16**, **19**, **26**, **28**, **52**, and **75** on the $\Sigma\sigma$ of the substituents on one of the biphenylquinone rings. Two linear regression lines of the following form are shown: (1) $\ln(k/k_o)=-4.9\Sigma\sigma-0.1$ with an $R^2=0.981$ over the range from $-0.27\leq\Sigma\sigma\leq0$; and (2) $\ln(k/k_o)=21.4\Sigma\sigma-0.1$ with an $R^2=0.989$ over the range from $0\leq\Sigma\sigma\leq0.97$.

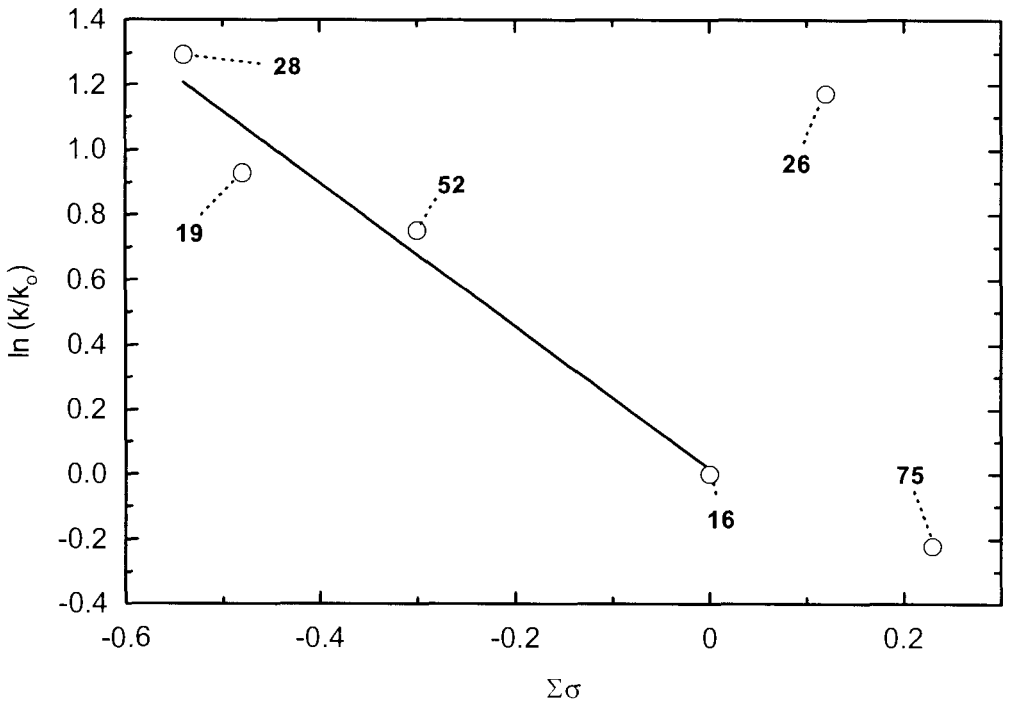

Figure 2.13. Hammett plot showing the dependence of the rate of thermal decays for **16**, **19**, **26**, **28**, **52**, and **75** on the $\Sigma\sigma$ of the substituents on both of the biphenylquinone rings. A linear regression line of the following form is shown over the range from $-0.54 \leq \Sigma\sigma \leq 0$: $\ln(k/k_o) = -2.2\Sigma\sigma + 0.017$ with an $R^2 = 0.962$.

The Hammett plots shown in Figure 2.12 and Figure 2.13 were constructed as follows. For Figure 2.12, the σ values given in Table 2.3 were used to calculate $\Sigma\sigma$ values for each of the 2,2'-biphenylquinones on one of the rings. The ketone moiety was treated as the reaction center, with a 5,5' substitution pattern (e.g., **26**). Substituents in the 4, 4', 6, and 6' positions (e.g., as on **19**) were treated as *meta* groups for the purpose of the Hammett analysis. The monochlorinated 2,2'-biphenylquinone **76** could not be used in the Hammett analysis as photoproduct studies for this compound were not able to successfully isolate a monochlorinated 2,2-dihydroxybiphenyl. Thus, the chlorine location on **76** is not known. For all 2,2'-biphenylquinones with the exception of **75**,

both rings contain equivalent substitution patterns. For **75**, a better correlation was observed where the ring without a chlorine substituent was used in the modeling process, suggesting the unsubstituted ring in **75**. For Figure 2.13, the ketone moieties were both treated as the reaction centers in the same manner as described for Figure 2.12, and the σ values for all substituents on the 2,2'-biphenylquinone ring were summed according to this aprroach. The resulting Σσ values for each of the 2,2'-biphenylquinones used to construct Figure 2.12 and Figure 2.13 are given in Table 2.5.

Table 2.5. Σσ values for the 2,2'-biphenylquinones used in constructing Figure 2.12 and Figure 2.13.

Compound	Σσ (Figure 2.12)	Σσ (Figure 2.13)
16	0	0
19	-0.24	-0.48
26	0.06	0.12
28	-0.27	-0.54
52	-0.15	-0.30
75	0	0.23

To help understand the potential thermal products from the photogenerated 2,2'-biphenylquinones, the time-resolved thermal decay of **16** was followed by liquid chromatography (LC) methods. In concert with the decrease in concentration of **16** was observed the concomitant formation of 1-hydroxybenzofuran (**11**) (eq. (2.29).

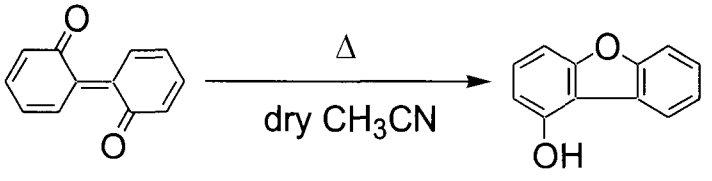

(2.29)

16 **11**

For **26** and **75**, authentic standards of the corresponding 1-hydroxybenzofurans were not available for analysis by LC in the same manner as for **16**. In addition, the low steady-state concentrations of **26** and **75** able to be generated via photochemical means (without subsequent photochemical hydrogen abstraction from the organic solvent by **26** and **75** to yield the corresponding 2,2'-dihydroxybiphenyls) prevent the isolation and structural elucidation of any photogenerated 1-hydroxydibenzofurans from **26** and **75**. However, based on the observed thermal formation of **11** from **16**, the Hammett plot shown in Figure 2.12 which suggests a similar mechanism for the thermal decay of 2,2'-biphenylquinones with electron withdrawing groups (e.g., **26**, **75**, and the parent **16**), as well as studies into the different thermal reactivity of 2,2'-biphenylquinones with electron donating substituents (see below), **26** (eq. (2.30) and **75** (eq. (2.31) are also expected to rearrange into the corresponding 1-hydroxybenzofurans.

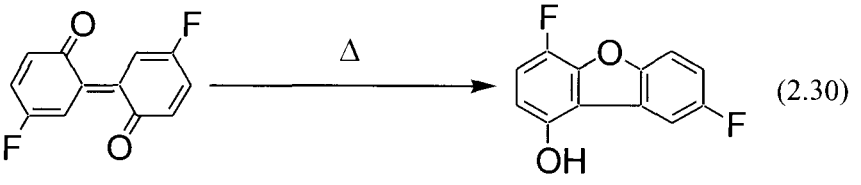

(2.30)

26 **87**

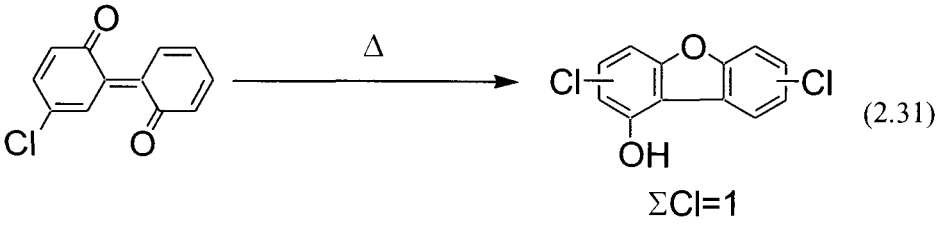

(2.31)

75 **88**

As support for these findings, previous work on both 2,2'- and 4,4'-biphenylquinones (*113*) has shown thermal rearrangements to the corresponding

benzofurans. For example, upon thermolysis 3,3',5,5'-tetraphenyl-4,4'-biphenylquinone (**89**) yields 2-(3,5-diphenyl-4-hydroxyphenyl)-4-phenyldibenzofuran (**90**) and bis(4-phenyl-3-dibenzofuran) (**91**) (*113*) by intramolecular rearrangements analogous to what is proposed above for the photogenerated 2,2'-biphenylquinones. Conversely, in the steady state photolysis of **9** in aprotic solvents (e.g., dry CH_3CN), **11** has been shown to be formed as a significant product (up to 40% yield depending on the solvent) and thought to be via exclusive secondary photochemistry of **16** (*40*). Other groups have also reported the photochemical rearrangements of related quinones to hydroxydibenzofurans, such as the conversion of 2,6-diphenyl-1,4-benzoquinone (**92**) to 2-hydroxy-3-phenyldibenzofuran (**93**) (*114*). Thus, because secondary photochemistry of the 2,2'-biphenylquinones cannot be ruled out as a contribution to the formation of 1-hydroxybenzofurans during the photolysis of dibenzo[1,4]dioxins, both thermal and photochemical pathways may be sufficiently active to help explain the presence of a 1-hydroxybenzofuran in the final photoproduct mixture from irradiation of either the parent dibenzo[1,4]dioxin, or derivatives having electron donating groups.

By comparison, to model the potential thermochemistry of the photogenerated 2,2'-biphenylquinones with electron donating substituents (**19** and **28**) – for which the Hammett plot suggested an mechanism different from 1-hydroxybenzofuran production – 4,4'5,5'-tetramethoxy-2,2'-biphenylquinone (**52**) was synthesized as described above. In contrast to the other photogenerated 2,2'-biphenylquinones, this compound can be stably isolated in the solid form, likely only because of its near insolubility (evident by the clear solution above an excess of solid state **52**) in all of the less polar organic solvents (e.g.,

benzene, hexane, toluene). By comparison, photogenerated 2,2'-biphenylquinones **16**, **19**, **26**, **28**, and **75** are at least sufficiently soluble in these less polar organic solvents to give absorbance values of 0.2-0.5 or greater at the $\lambda_{max(500\text{-}700\ nm)}$. However, **52** is fairly soluble in polar organic solvents (e.g., CH_3CN), and in such solutions **52** (10^{-3} M, dry CH_3CN) rapidly rearranges to the corresponding oxepino[2,3-b]dibenzofuran (**94**) via a first-order process with a lifetime of ca. 1.3 min ($k=1.3\times10^{-2}\ s^{-1}$) (eq. (2.32).

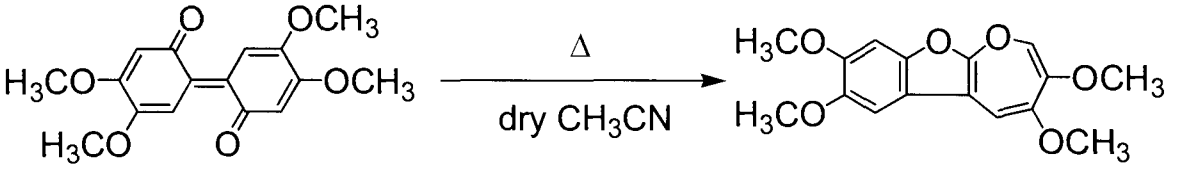

(2.32)

52 **94**

These findings are consistent with work on other 2,2'-biphenylquinones with electron donating groups, which are also known to thermally rearrange into oxepino[2,3-b]benzofurans, such as for the 3,3'5,5'-tetra-*t*-butyl (**95**) (*115-117*), 3,3'-di-*t*-butyl-5,5'-dimethoxy (**96**), 3,3'-di-*t*-butyl-5,5'-diethoxy (**97**), 3,3'-di-*t*-butyl-5,5'-dibenzyloxy (**98**), and 3,3'-di-*t*-butyl-5,5'-di(4-t-butylphenyl)- (**99**) derivatives (*117*) via a mechanism involving the *syn* configuration of the 2,2'-biphenylquinone (Scheme 2.7; where R is an electron donating group *para* to one of the ketone groups) (*118*). For **28** and **19**, authentic standards of the corresponding oxepino[2,3-b]benzofurans were not available for analysis. In addition, the low steady-state concentrations of **28** and **19** able to be generated via photochemical means (without subsequent photochemical hydrogen abstraction from the organic solvent by **28** and **19** to yield the corresponding 2,2'-dihydroxybiphenyls) prevent the isolation and structural elucidation of any photogenerated 1-hydroxydibenzofurans from **28** and **19**. However, based on the

observed thermal formation of **94** from **52**, the Hammett plot shown in Figure 2.12, the historic literature precedents in this area of study, and the present investigations into the different thermal reactivity of 2,2'-biphenylquinones with electron withdrawing substituents (see above), **28** (eq. (2.33) and **19** (eq. (2.34) are expected to rearrange thermally into the corresponding oxepino[2,3-b]benzofurans.

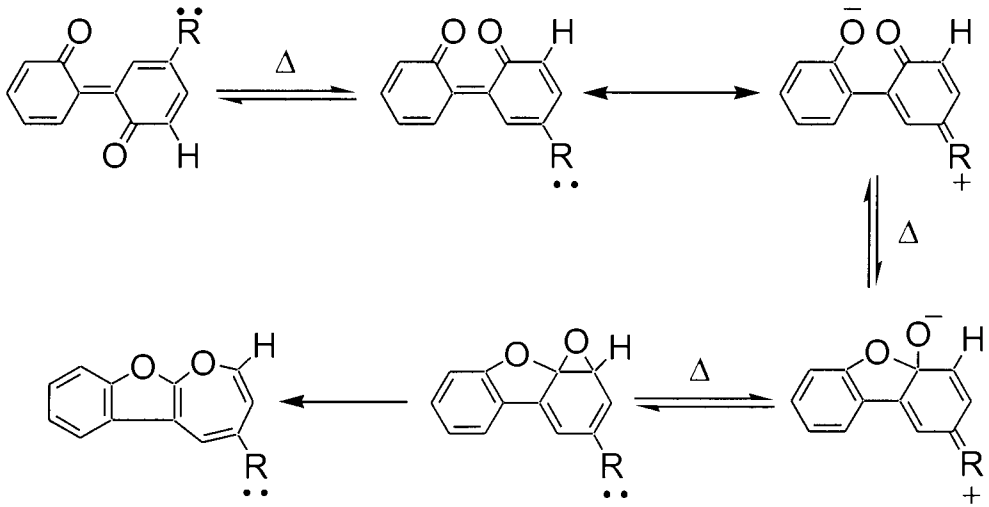

Scheme 2.7

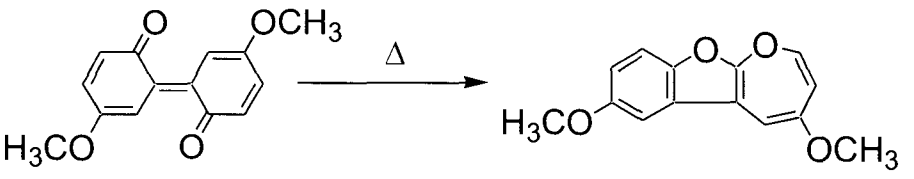

(2.33)

28 **100**

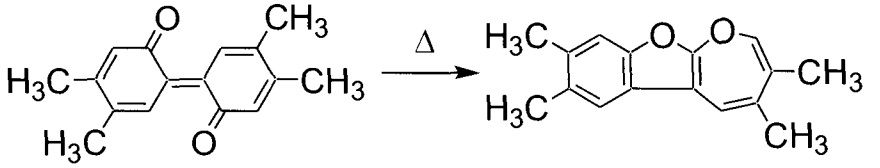

(2.34)

19 **101**

Following preliminary observations showing **16** had a shorter lifetime in nonpolar versus polar aprotic organic solvents, a more quantitative relationship between solvent properties and the rate of rearrangement from **16** to **11** was undertaken. In general, nonpolar aprotic organic solvents appear to have a strong positive influence on the rate of conversion of **16** to **11**, such that rate constants for this thermal process increase by almost an order of magnitude in moving from diethyl ether with a dielectric constant ($\varepsilon/\varepsilon_o$; obtained from ref. (*124*)) of 4.0 ($k=7.14\times10^{-3}$ s^{-1}) to cyclohexane with $\varepsilon/\varepsilon_o=2.0$ ($k=5.31\times10^{-2}$ s^{-1}) (Figure 2.14). In aprotic organic solvents with $\varepsilon/\varepsilon_o>4$, there is no observable influence on the reaction rate. The underlying rationale behind this trend is governed by the influence of solvent polarity on the height of activation barrier between **16** and **11**. Polar solvents would stabilize the starting material (**16**) more than the less polar product (**11**), decreasing the overall driving force for reaction. In addition, if the transition complex between **16** and **11** is also less positively influenced by increasing solvent polarity than **16**, then the activation barrier for the conversion of **16** to **11** would

increase in moving to a more polar solvent. The lower rate constant for conversion of **16** to **11** in more polar solvents in consistent with this rationalization.

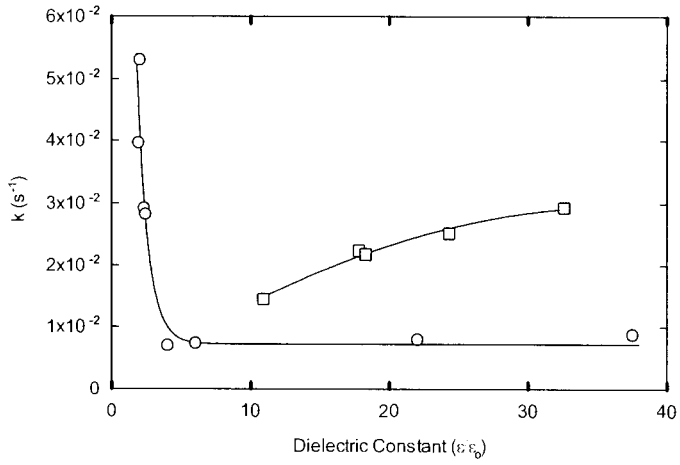

Figure 2.14. Dependence of the thermal decay of **16** on the solvent dielectric constant in aprotic (○) and protic (□) organic solvents.

In protic organic solvents the opposite trend was observed, with an increase in thermal reaction rate with increasing $\varepsilon/\varepsilon_o$, rather than the absence of an observable effect in aprotic solvents of similar polarity. The likely explanation for this change in reactivity is evident when the rate is examined as a function of solvent pK_a (obtained from ref. (*124*)). Here there is a strong negative trend that suggests general acid catalysis by the protic solvents in the conversion of **16** to **11** (Figure 2.15).

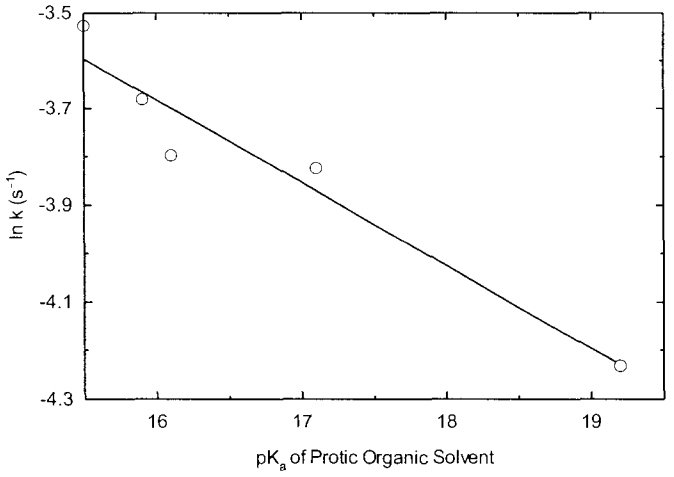

Figure 2.15. Dependence of the thermal decay of **16** on the pK_a of the protic organic solvent.

For both sets of organic solvents (aprotic and protic), no correlations between the rate of thermal decay and solvent ionization potential or viscosity were observed, suggesting the absence of hydrogen abstraction from the solvent and intermolecular reactions not involving the solvent, respectively. Previous work has established that hydrogen abstraction/hydride transfer from the solvent to quinones is influenced by the solvent's ionization potential (*119,120*), and in the absence of other significant effects, intermolecular reactions not involving the solvent should be inhibited as solvent viscosity increases due to a reduction in the diffusion controlled rate constant. The absence of a second order component to the thermal decay of **16** also suggests no significant contribution from intermolecular reactions not involving the solvent.

The Arrhenius equation is a means of relating the temperature dependence of observed reaction rate constant (k_{obs}) to the experimental activation energy (E_a) and the pre-exponential factor (A) via the following equation (eq. (2.35),

$$k_{obs}=A\times\exp(E_a/RT) \quad (2.35)$$

where R is the gas constant (8.3145 J/K·mol) and T is the temperature in kelvins. Where k_{obs} is obtained over a range of temperatures, the natural logarithm of k_{obs} can be plotted against the inverse of the absolute temperature (an Arrhenius plot). A linear regression fit against the data yields the following equation (eq. (2.36), from which the activation energy and pre-exponential factor can be calculated from the slope of the graph and the y-intercept, respectively:

$$\ln k_{obs}=\ln A\times -E_a/R(1/T) \quad (2.36)$$

An Arrhenius plot on the thermal decay of **16** (Figure 2.16) provided an activation energy of 25.8±10.8 kJ/mol (±95% confidence interval) and a pre-exponential constant of 221 s^{-1}. The large error in the estimate for the y-intercept (5.4±4.3), and the logarithmic y-axis indicates a high uncertainty in the value of A, the pre-exponential constant (from 3 to 16,300 s^{-1} based on the 95% confidence interval limits for ln A ranging from 1.1 to 9.7). This high level of uncertainty prevents a detailed analysis of the potential entropy of activation ($\Delta S^{\ddagger}$). The low activation barrier suggests a concerted electrocyclic or radical process without σ-bond cleavage in the initial ring closing.

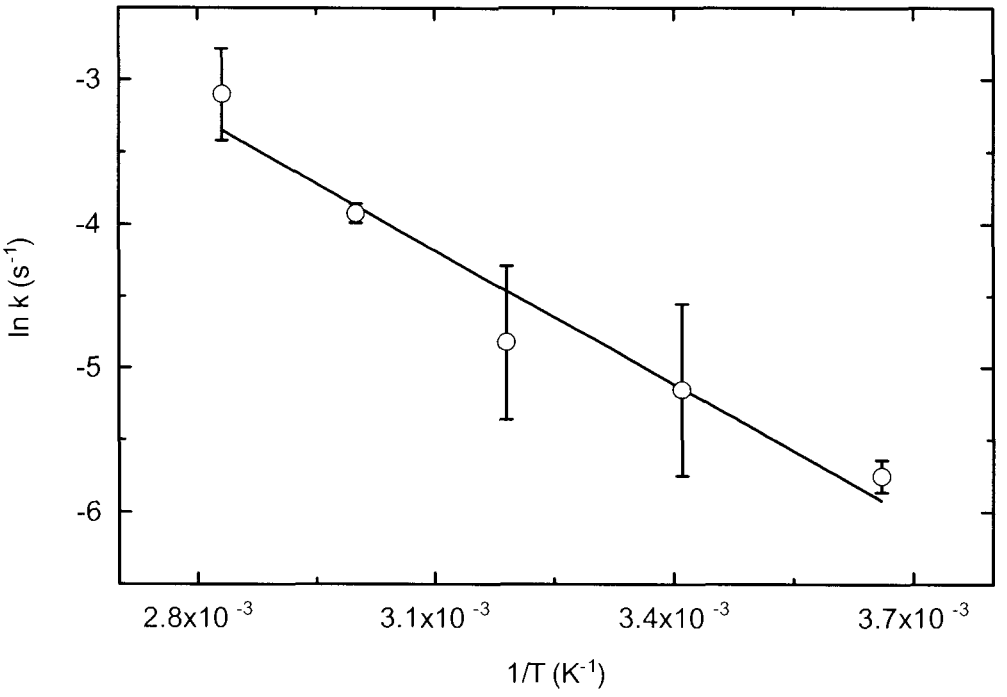

Figure 2.16. Arrhenius plot for the thermal decay of **16** into **11** in CH_3CN as measured by monitoring the intensity of absorption at the $\lambda_{max(500\text{-}700\ nm)}$ of **16** using UV-vis spectroscopy. Error bars are 95% confidence intervals about the mean. A regression equation of the form ln k=-3100±1300×(1/T)+5.4±4.3 with a R^2=0.94 is shown.

As a further probe into the mechanistic details of photogenerated 2,2'-biphenylquinone thermochemistry, kinetic isotope effect analyses were undertaken in acetonitrile (Table 2.6), benzene (Table 2.7), and toluene (Table 2.8). Based on these results, and the thermal product and solvent studies discussed above, there is no evidence that the 2,2'-biphenylquinones can abstract hydrogen from a typical solvent C-H bond. Previous work has shown these compounds can be used to oxidize phenols to dimeric products (*121-123*), presumably by initial hydrogen abstraction from the phenolic O-H (D^o_{298}=361.9 kJ/mol in hydroxybenzene (*124*)). In contrast, the bond strength of even a labile solvent C-H (e.g., D^o_{298}=381 kJ/mol for the 3° C-H in 2-propanol or 375.7 kJ/mol

for the benzylic C-H in toluene (*124*)) still resides ca. 15-20 kJ/mol above that for a phenolic bond. While a previous report has suggested thermal hydrogen abstraction by 3,3',5,5'-tetra-*t*-butyl-4,4'-diphenylquinone (**83**) from the methine C-H in diphenylmethane (**102**) (*125*), it is of note that this C-H bond is particularly labile (D^{o}_{298}=340.6 kJ/mol (*124*)) and that the reaction took place at elevated temperatures (1 h reflux at 260°C). The absence of solvent isotope effects significantly different from unity for the thermal decay of photogenerated 2,2'-biphenylquinones in CH_3CN, benzene, and toluene also suggests the absence of solvent oxidation as a relevant decay pathway (especially when Figure 2.14 shows a significantly more rapid decay of **16** in benzene versus diethyl ether).

Table 2.6. Rate constants (in s^{-1}) and deuterium isotope effects for the first-order thermal decays of **16**, **19**, **26**, **28**, and **75** in acetonitrile (k_H) and acetonitrile-d_3 (k_D). Error bars are the range of duplicate trials.

	k_H	k_D	k_H/k_D
16	$8.87\pm0.21\times10^{-3}$	$7.08\pm0.11\times10^{-3}$	1.25±0.05
19	$2.25\pm0.07\times10^{-2}$	$2.30\pm0.02\times10^{-2}$	0.98±0.04
26	$2.86\pm0.01\times10^{-2}$	$2.91\pm0.05\times10^{-2}$	0.98±0.02
28	$2.18\pm0.12\times10^{-2}$	$2.04\pm0.07\times10^{-2}$	1.07±0.10
75	$7.09\pm0.14\times10^{-3}$	$6.13\pm0.37\times10^{-3}$	1.16±0.07

Table 2.7. Rate constants (in s^{-1}) and deuterium isotope effects for the first-order thermal decays of **16**, **19**, **26**, **28**, and **75** in benzene (k_H) and benzene-d_6 (k_D). Error bars are the range of duplicate trials.

	k_H	k_D	k_H/k_D
16	$2.93\pm0.10\times10^{-2}$	$2.32\pm0.14\times10^{-2}$	1.26±0.10
19	$6.93\pm0.40\times10^{-3}$	$6.60\pm0.62\times10^{-3}$	1.05±0.15
26	$2.40\pm0.07\times10^{-2}$	$2.37\pm0.09\times10^{-2}$	1.01±0.07
28	$7.34\pm0.11\times10^{-2}$	$6.87\pm0.15\times10^{-2}$	1.07±0.04
75	$2.34\pm0.04\times10^{-2}$	$2.19\pm0.02\times10^{-2}$	1.07±0.03

Table 2.8. Rate constants (in s^{-1}) and deuterium isotope effects for the first-order thermal decays of **16**, **19**, **26**, **28**, and **75** in toluene (k_H) and toluene-d_8 (k_D). Error bars are the range of duplicate trials.

	k_H	k_D	k_H/k_D
16	$2.83\pm0.14\times10^{-2}$	$2.38\pm0.12\times10^{-2}$	1.19±0.12
19	$6.99\pm0.05\times10^{-3}$	$6.74\pm0.09\times10^{-3}$	1.04±0.03
26	$2.07\pm0.03\times10^{-2}$	$2.05\pm0.08\times10^{-2}$	1.01±0.05
28	$6.67\pm0.14\times10^{-2}$	$6.13\pm0.10\times10^{-2}$	1.09±0.04
75	$2.10\pm0.12\times10^{-2}$	$1.81\pm0.05\times10^{-2}$	1.16±0.10

Slight isotope effects appear evident in a few cases (i.e., k_H/k_D ca. 1.2 to 1.3), and this is likely due to a minor contribution from the thermal reaction between a photogenerated 2,2'-biphenylquinone and its corresponding photogenerated 2,2'-dihydroxybiphenyl. Although irradiation periods used to generate the 2,2'-biphenylquinones were short (ca. 15 s), this length of time is still sufficient for a portion

of the photogenerated 2,2'-biphenylquinone to undergo excited state hydrogen abstraction from the solvent to give the corresponding 2,2'-dihydroxybiphenyl. Evidence for the completion of this process is given by LC analyses at these timescales that showed formation of ca. 1-2% conversion of **16** to **10** after 15-30 s irradiation. In addition, a previous report on steady state irradiation product studies of **9** in CD_3CN giving exclusive formation of 2,2'-dihydroxybiphenyl-*O,O'-d*$_2$ (**103**) in high conversion shows the potential for 2,2'-biphenylquinone to photochemically abstract hydrogen from an organic solvent (*40*).

As mentioned above, time resolved LC analyses following 30 s irradiation of **9** and subsequent generation and decay of **16** did not show any increase in contribution from **10**, further demonstrating that reduction of the 2,2'-biphenylquinones is likely only by photochemical means. It was also observed that addition of ca. 100-fold excess of **10** to a solution of photogenerated **16** immediately quenched the 2,2'-biphenylquinone's UV-visible spectrum. This reaction between the photogenerated 2,2'-biphenylquinones and their corresponding 2,2'-dihydroxybiphenyls would likely show a significant isotope effect. Previous reports on isotope effects from the hydrogen abstraction/hydride transfer reactions of other quinones show values exceeding the primary isotope effect theoretical limit of 7 (k_H/k_D from ca. 4-14) (*119,120*). Thus, even the minor thermal side reaction of a photogenerated 2,2'-biphenylquinone with its corresponding photogenerated 2,2'-dihydroxybiphenyl would be expected to yield small overall isotope effects where the dominant decay pathways to oxepino[2,3-b]benzofurans and 1-hydroxybenzofurans (for

$\Sigma\sigma<0$ and ≥ 0, respectively) – which are not expected to exhibit isotope effects at the 2,2'-biphenylquinone's $\lambda_{max(500\text{-}700\ nm)}$ – are included in the kinetic analysis.

2.5 Photochemical Reactivity of the 2,2'-Biphenylquinones

With the working hypothesis of 2,2'-biphenylquinone photoreduction that yields 2,2'-dihydroxybiphenyls as the major final photoproduct of dibenzo[1,4]dioxins, a "stable" model system was needed on which to test this mechanism. Because of the low steady state concentrations of the photogenerated 2,2'-biphenylquinones under continuing irradiation, their photochemistry is difficult to study independently. Thus, to model the potential photochemistry of the photogenerated 2,2'-biphenylquinones, 4,5,4'5'-bismethylenedioxy-2,2'-biphenylquinone (**54**) was synthesized and used in concert with **52** for the investigations.

Upon photolysis, both **52** (eq. (2.37) and **54** (eq. (2.38) (10^{-4} M, 300 nm, CH_3CN, 1 and 15 min, respectively) gave the corresponding 2,2'-dihydroxybiphenyls in yields of 4% and 13%, respectively.

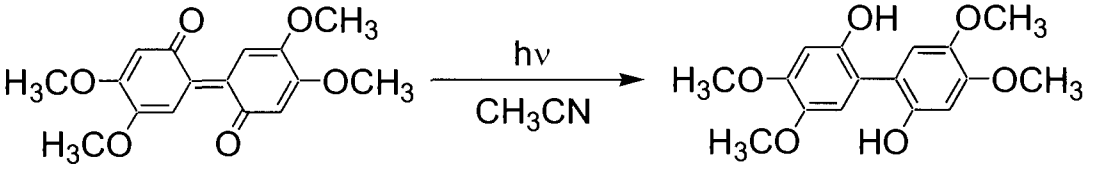

(2.37)

52 **104** 13%

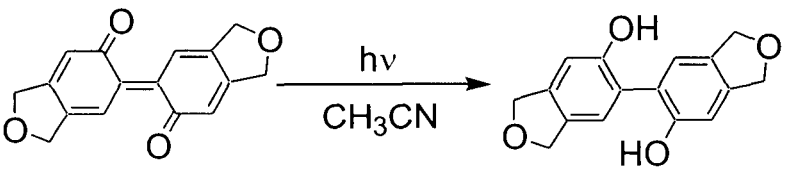

(2.38)

13%

54 **105**

The photochemistry of **54** has not been previously examined, while a prior report on the irradiation of **52** in $CHCl_3$ showed formation of 2-(2-hydroxy-4,5-dimethoxyphenyl)-5-methoxy-1,4-benzoquinone (**106**). Demethylation of **52** during photolysis was suggested to occur via acid-catalyzed hydrolysis in the presence of photochemically generated hydrochloric acid, with the other ring photochemically reduced by excited state hydrogen abstraction from the solvent (*118*). Using these models, it appears likely that the 2,2'-dihydroxybiphenyls observed following the steady state irradiation of dibenzo[1,4]dioxins arise via excited state hydrogen abstraction from the organic solvent by the 2,2'-biphenylquinone intermediates. Further support for this pathway also comes from the known photochemistry of the parent 4,4'-biphenylquinone (**78**) and its 3,3',5,5'-tetramethyl derivative (**82**), which both give the corresponding 2,2'-dihydroxybiphenyls (**107** and **108**, respectively) upon irradiation (*126-128*).

The multiplicity of the 2,2'-biphenylquinone reduction is likely via the singlet state. Replicate photolyses of **52** and **54** in dry CH_3CN under nitrogen and argon purging showed no significant difference in product yields, suggesting a singlet state reaction. In addition, the replicate photolyses of the dibenzo[1,4]dioxins did not show a difference in 2,2'-dihydroxybiphenyl yields under nitrogen or oxygen purging. With the likelihood that the final isolated 2,2'-dihydroxybiphenyl products arise via secondary dibenzo[1,4]dioxin

photochemistry (i.e., primary photochemistry of the intermediate 2,2'-biphenylquinones), it appears that both the intial photochemical aryl-ether bond cleavage of the dibenzo[1,4]dioxin starting material, as well as the photochemical hydrogen abstraction of the intermediate 2,2'-biphenylquinone, proceed by way of the singlet excited states.

Photochemical hydrogen abstraction from benzene has also been reported for **82**, giving **108** and **109** (through dimerization of two phenyl radicals) as photoproducts (*126*). Similar production of **109** and **110** from the steady state irradiation of **9** was observed in benzene (Scheme 2.8) and toluene (Scheme 2.9), respectively. Together with the previous report showing that steady-state irradiation of **9** in CD_3CN gives exclusive formation of **103** (*40*), it appears photochemical hydrogen abstraction from the solvent is the dominant formation process of **10** from **16**. These observations of a photochemical reduction pathway for 2,2'-biphenylquinones to yield the corresponding 2,2'-dihydroxybiphenyls, combined with recent work suggesting the existence of a proton mediated photoreduction pathways for 1,4-benzoquinones (*129,130*), may help explain the observed higher yields and cleaner reactions for the photochemical formation of **10** from **9** in protic solvents.

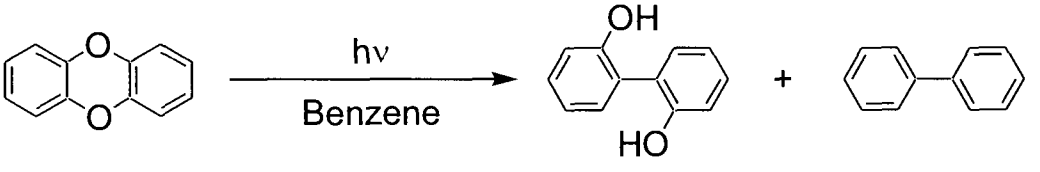

9 **10** (33%) **109** (15%)

Scheme 2.8

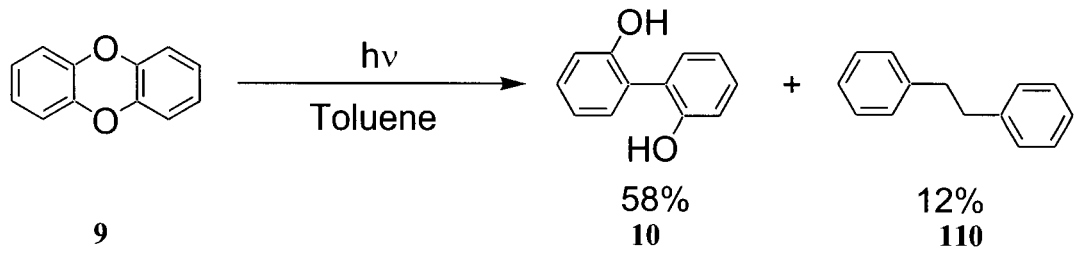

Scheme 2.9

2.6 Laser Flash Photolysis

To investigate the mechanistic details of 2,2'-biphenylquinone formation, LFP studies were undertaken on **9**, **13**, **20**, **21**, **46**, **30**, and **29**. For all systems, the photochemically initiated formation of the corresponding 2,2'-biphenylquinones discussed above (where their decays were followed by conventional suprasecond UV-Vis spectroscopic methods) could be observed by transient absorption spectroscopy. The high acute toxicity of **3** prevents any mechanistic investigations in order to help explain its observed photochemistry. With the exception of **46** and **29**, for which the LFP experiments showed only weak signals (ΔOD at $\lambda_{max(500\text{-}700\ nm)}$ of ca. 10^{-3}-10^{-4}) and poor quality spectra for the growth of the 2,2'-biphenylquinone, transient absorption spectra in dry CH_3CN revealed the same characteristic spectra also observed by UV-visible spectroscopy (Figure 2.17, Figure 2.18, Figure 2.19, Figure 2.20, and Figure 2.21).

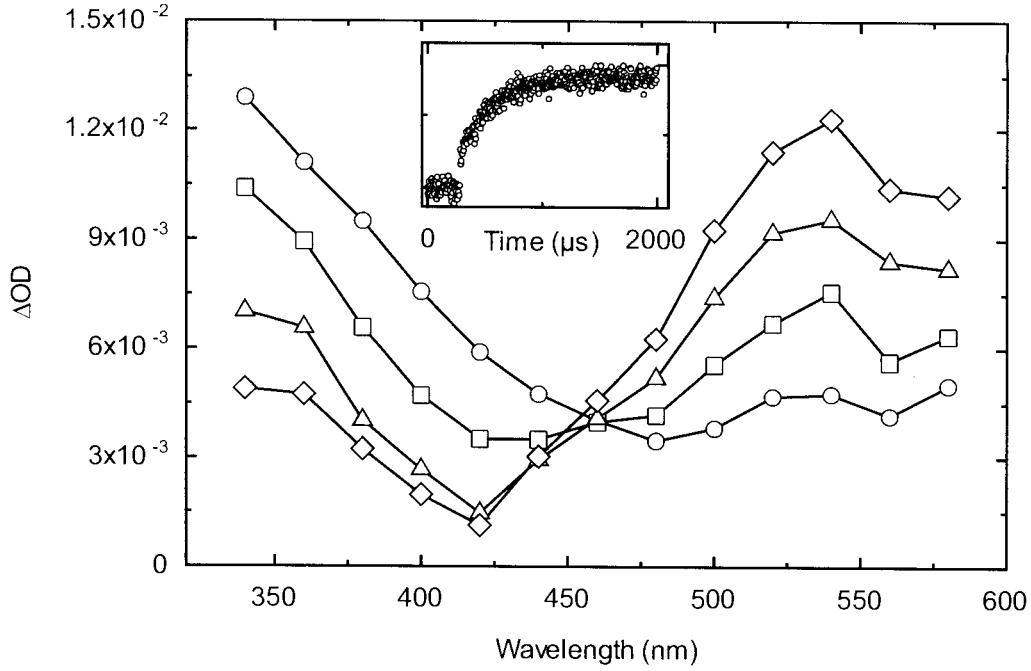

Figure 2.17. Transient absorption spectra obtained via LFP for the generation of **16**. Inset shows signal growth at the $\lambda_{max(540\ nm)}$ of the 2,2'-biphenylquinone. Points in the spectra are shown at 152 μs (○), 340 μs (□), 525 μs (Δ), and 1543 μs (◇) after the laser pulse, respectively.

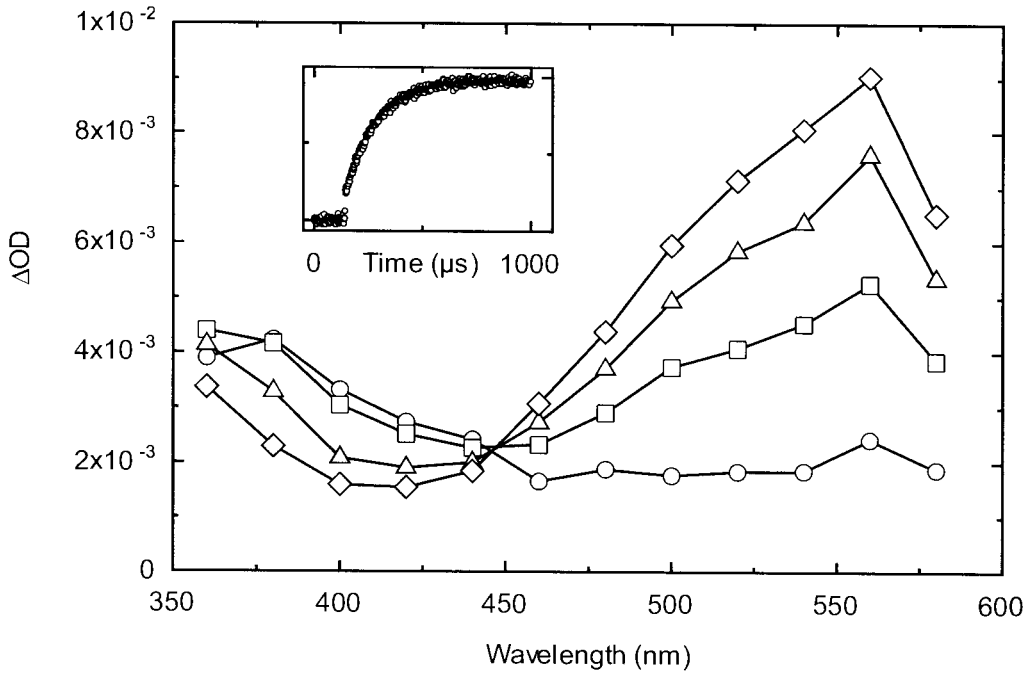

Figure 2.18. Transient absorption spectra obtained via LFP for the generation of **75**. Inset shows signal growth at the $\lambda_{max(560\ nm)}$ of the 2,2'-biphenylquinone. Points in the spectra are shown at 87 μs (○), 311 μs (□), 485 μs (Δ), and 996 μs (◇) after the laser pulse, respectively.

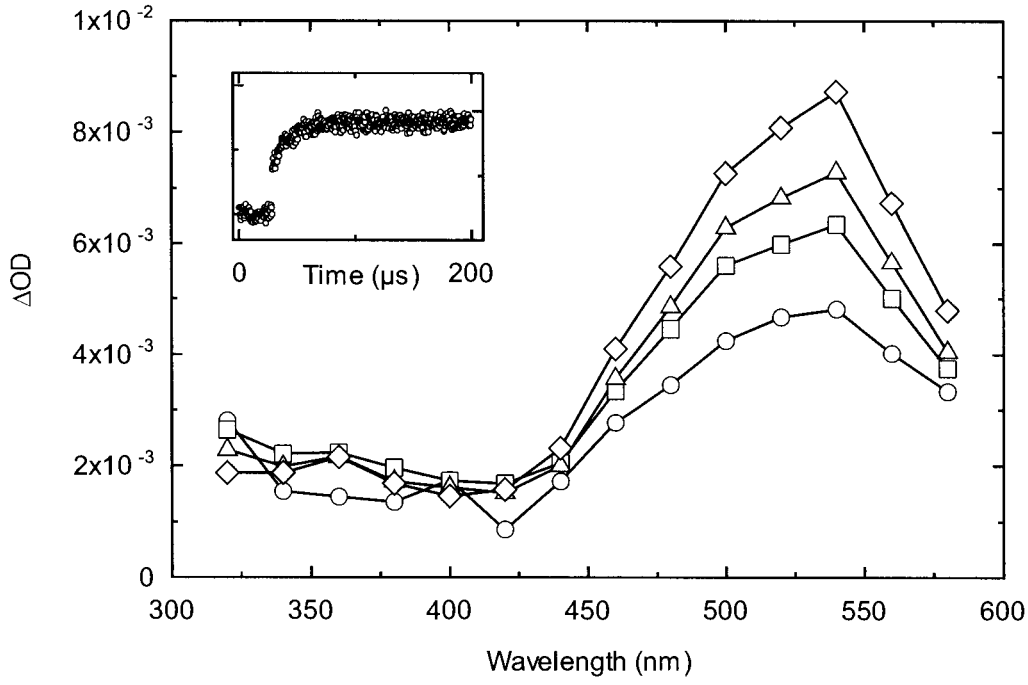

Figure 2.19. Transient absorption spectra obtained via LFP for the generation of **26**. Inset shows signal growth at the $\lambda_{max(540\ nm)}$ of the 2,2'-biphenylquinone. Points in the spectra are shown at 11 μs (○), 35 μs (□), 58 μs (Δ), and 108 μs (◇) after the laser pulse, respectively.

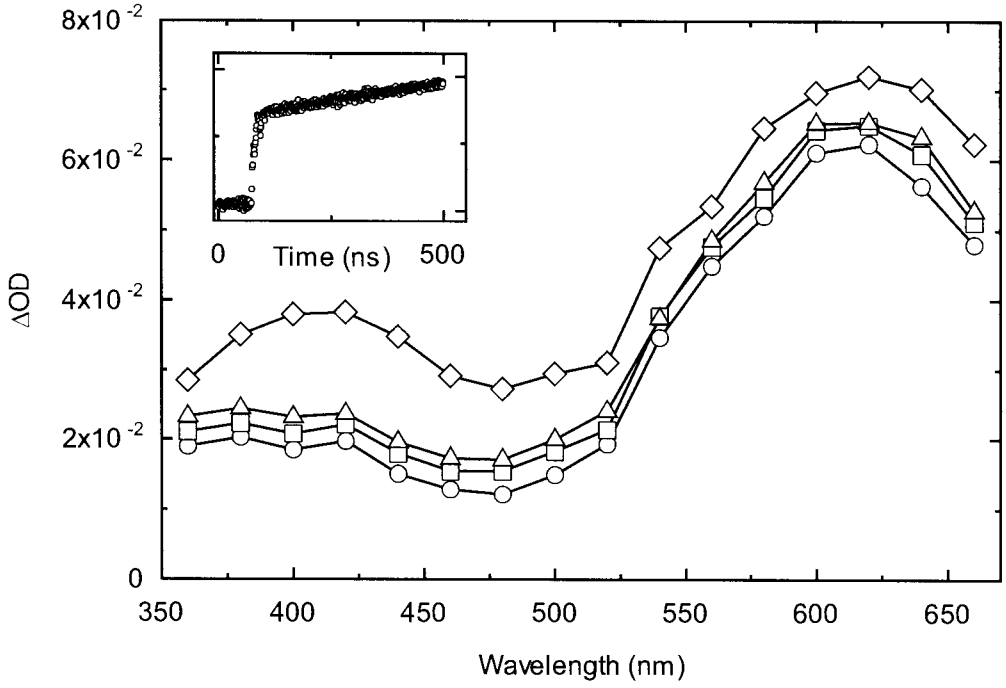

Figure 2.20. Transient absorption spectra obtained via LFP for the generation of **28**. Inset shows signal growth at the $\lambda_{max(620\ nm)}$ of the 2,2'-biphenylquinone. Points in the spectra are shown at 63 ns (○), 114 ns (□), 183 ns (△), and 264 ns (◇) after the laser pulse, respectively.

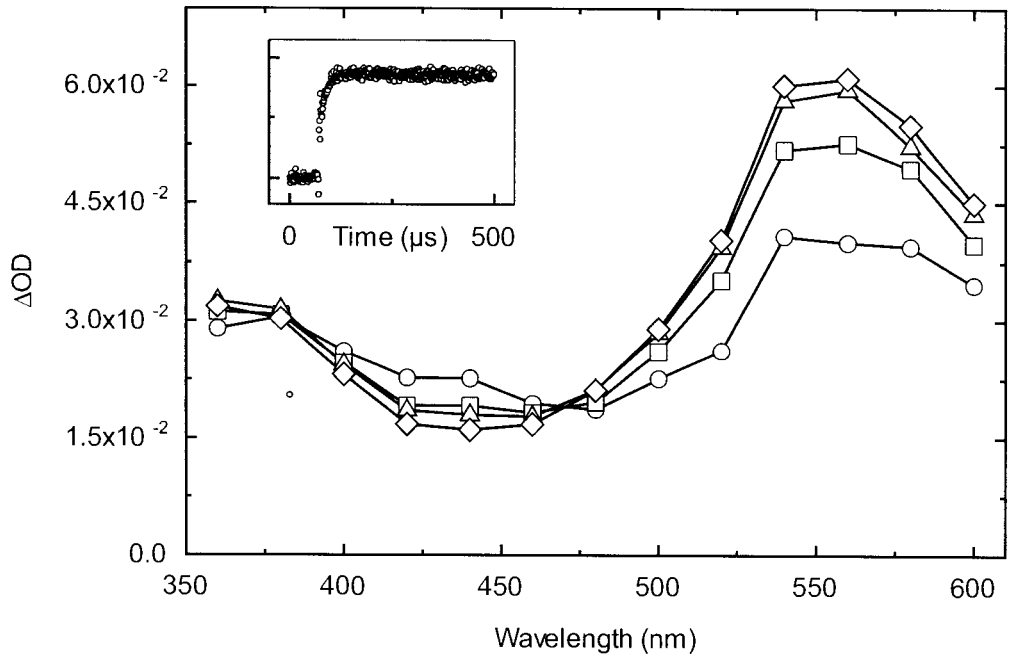

Figure 2.21. Transient absorption spectra obtained via LFP for the generation of **19**. Inset shows signal growth at the $\lambda_{max(560\ nm)}$ of the 2,2'-biphenylquinone. Points in the spectra are shown at 74 μs (○), 87 μs (□), 104 μs (Δ), and 190 μs (◇) after the laser pulse, respectively.

For 2,2'-biphenylquinones **16** (Figure 2.17), **75** (Figure 2.18), and **19** (Figure 2.21), growth of the absorbance at the $\lambda_{max(500\text{-}700\ nm)}$ (pseudo first-order rate constants, $k=4.9\times10^3\ s^{-1}$, $6.8\times10^3\ s^{-1}$, and $7.2\times10^4\ s^{-1}$, respectively) occurred concomittment with decay of an absorption band observed over the range from ca. 340-460 nm (pseudo first-order rate constants, $k=5.4\times10^3\ s^{-1}$, $6.2\times10^3\ s^{-1}$, and $6.8\times10^4\ s^{-1}$, respectively). The absorption band at ca. 340-460 nm that decays in concert with 2,2'-biphenylquinone growth is tentatively assigned to 2-spiro-6'-cyclohexa-2',4'-dien-1'-ones **18** (eq. (2.39), **111** (eq. (2.40), and **24** (eq. (2.41), and is discussed in greater mechanistic detail below.

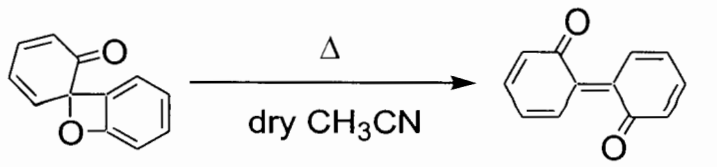

(2.39)

18 **16**

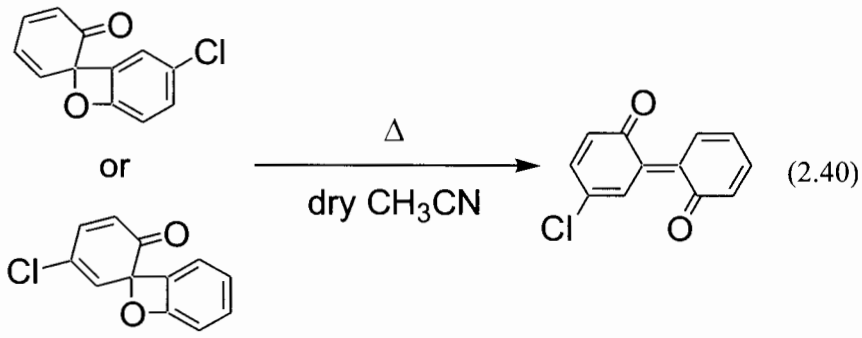

(2.40)

111 **75**

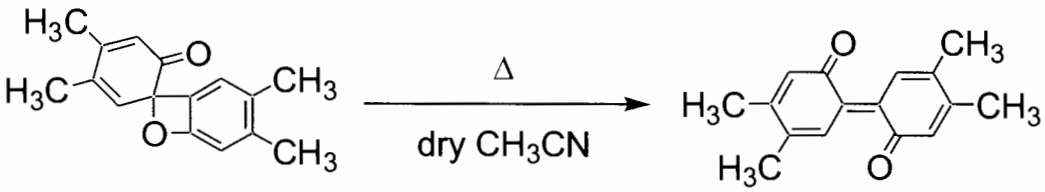

(2.41)

24 **19**

For 2,2'-biphenylquinones **26** (eq. (2.42) and **28** (eq. (2.43), the decay of the corresponding 2-spiro-6'-cyclohexa-2',4'-dien-1'-one absorbance bands for **25** and **27** was not observed. This may be due to the effect of the relative magnitudes of molar extinction coefficients for the 2,2'-biphenylquinones (ε_{DPQ}) and 2-spiro-6'-cyclohexa-2',4'-dien-1'-ones (ε_{SP}) in this wavelength range. The 2,2'-biphenylquinones are thought to have a $\pi \rightarrow \pi^*$ transition in this range (*131*) and where $\varepsilon_{DPQ} \approx \varepsilon_{SP}$ (**26**/**25**) or where $\varepsilon_{DPQ} > \varepsilon_{SP}$ (**28**/**27**), the decay of the 2-spiro-6'-cyclohexa-2',4'-dien-1'-one from ca. 340-460 nm will be overshadowed by the growth of the 2,2'-biphenylquinones over these wavelengths.

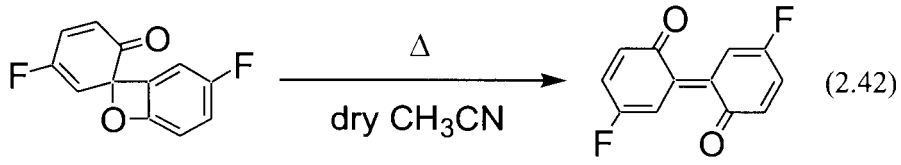

(2.42)

25 **26**

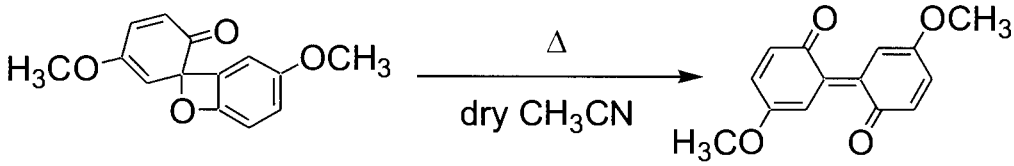

(2.43)

27 **28**

Although poor quality spectra were obtained, LFP also showed the formation of **77** via octachloro-2-spiro-6'-cyclohexa-2',4'-dien-1'-one (**112**) (eq. (2.44 and Figure 2.22), as well as the monochloro-2,2'-biphenylquinone of unknown configuration (**76**) via the monochloro-2-spiro-6'-cyclohexa-2',4'-dien-1'-one (**113**) using **46** as starting material (eq. (2.45 and Figure 2.23). Previous LFP studies on these two chlorinated dibenzo[1,4]dioxins had not been performed.

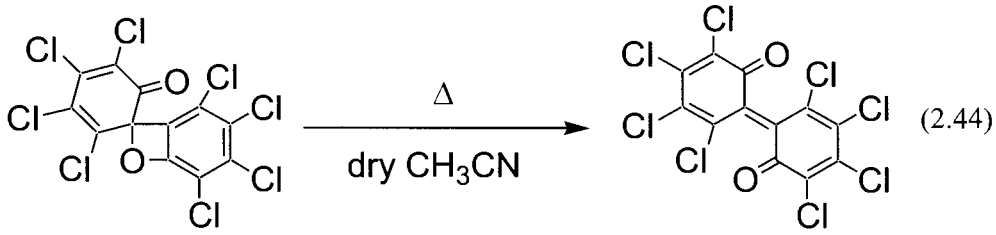

(2.44)

112 **77**

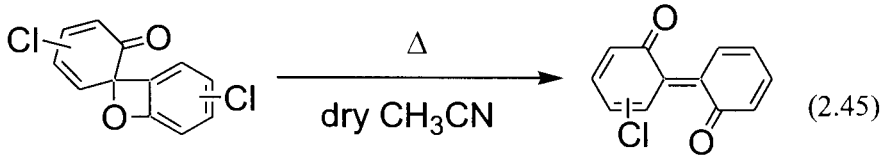

(2.45)

ΣCl=1 ΣCl=1

113 **76**

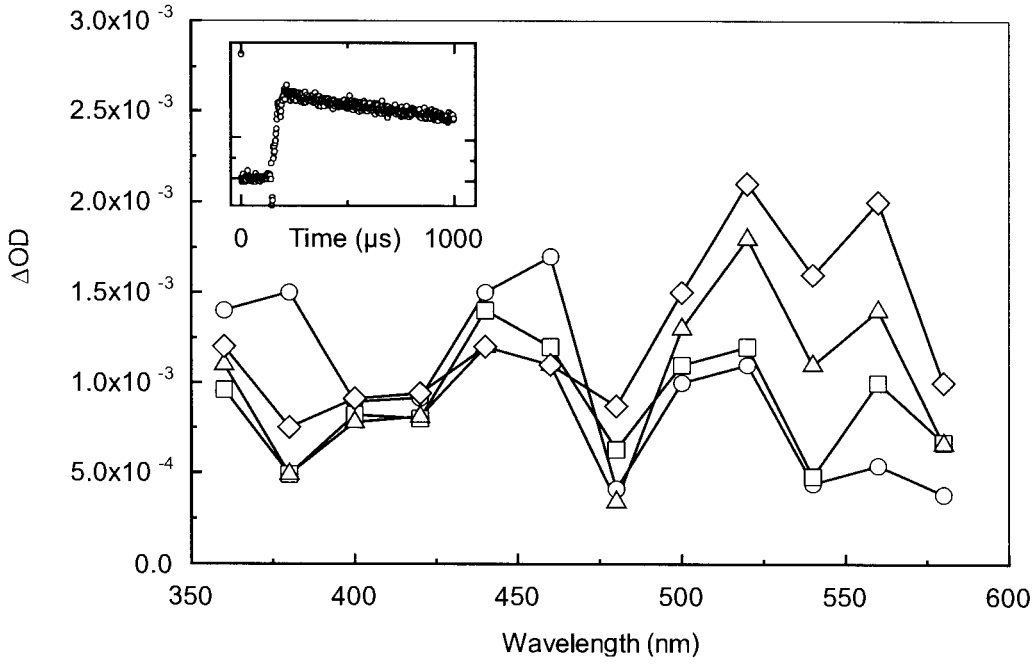

Figure 2.22. Transient absorption spectra obtained via LFP for the generation of **77**. Inset shows signal growth at the $\lambda_{max(560\ nm)}$ of the 2,2'-biphenylquinone. Points in the spectra are shown at 62 μs (○), 84 μs (□), 105 μs (△), and 116 μs (◇) after the laser pulse, respectively.

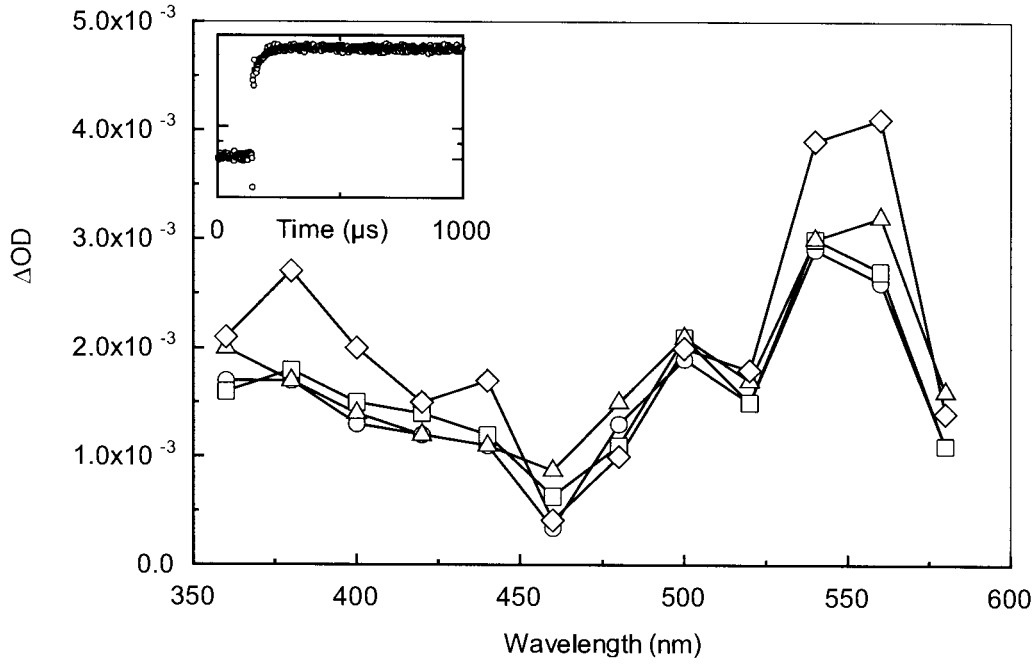

Figure 2.23. Transient absorption spectra obtained via LFP for the generation of **76**. Inset shows signal growth at the $\lambda_{max(560\ nm)}$ of the 2,2'-biphenylquinone. Points in the spectra are shown at 89 μs (○), 96 μs (□), 114 μs (Δ), and 211 μs (◇) after the laser pulse, respectively.

For all LFP studies, replicate experiments were performed under nitrogen and oxygen purging of the solution. No differences in the intensity or location of the 2,2'-biphenylquinone absorption bands were observed between nitrogen and oxygen purging. In addition, the rate constants for 2,2'-biphenylquinone generation were not different when the solution was purged with either nitrogen or oxygen. The results further suggest, along with the similar photoproduct study results under nitrogen and oxygen purging, that the primary photochemical aryl-ether cleavage in dibenzo[1,4]dioxins occurs via the singlet state.

A wide range of rate constants for the rearrangement of various 2-spiro-6'-cyclohexa-2',4'-dien-1'-ones to the corresponding 2,2'-biphenylquinones was observed, and these could be modeled used the Swain-Lupton approach. Unsuccessful attempts were made to model the rate of this rearrangement using Hammett constants; however, it is likely that the unknown relationships between reaction center and substitution pattern on each ring of a 2-spiro-6'-cyclohexa-2',4'-dien-1'-one were the cause of these difficulties. Hence, the Swain-Lupton approach appears suitable for making quantitative models of this rearrangement since the substituent constants do not depend on their relationship to the reaction center.

Although σ values are widely used to correlate rates and equilibria, these substituent constants are not sufficient for the correlation of all rates and equilibria even where steric effects are absent. The failure for σ values to correlate with all rates and equilibria likely arises because the overall substituent effect (σ) has both polar and resonance contributions, and the relatively contribution of these components depends on the nature of the reaction. Swain and Lupton initially proposed a solution to these issues based on the assumption that the σ constant of any substituent in any reaction can be expressed by the following equation (eq. (2.46),

$$\sigma = fF + rR \qquad (2.46)$$

where F and R are polar and resonance constants, respectively, difference for each substituent but constant for an individual substituent over all reactions. The factors f and r are empirical sensitivities or weighting factors independent of substituent but dependent on, and different for, each reaction. The LFER than becomes as shown in eq. (2.47,

$$\ln(k/k_o) \text{ or } \ln(K/K_o)=\rho\sigma=\rho fF+\rho rR \qquad (2.47)$$

where F and R values can be obtained from the literature for a particular functional group, and *f* and *r* can then be calculated by performing a correlation for a number of different substituents against a series of the correponding relative reaction rate constants (*106*).

For the various substiuents on the suite of 2-spiro-6'-cyclohexa-2',4'-dien-1'-ones under study, the F and R values used in the modeling approach were taken from ref. (*106*) and are given in Table 2.9. For each of 2-spiro-6'-cyclohexa-2',4'-dien-1'-ones 18, 24, 25, 27, 111, 112, and 113, the sum of the F and R values on the molecule is given in Table 2.10, along with the absolute and relative pseudo first-order rate constants for the conversions into the corresponding 2,2'-biphenylquinones. The ΣF and ΣR were then subjected to multiple linear regression against the ln(k/ko) values (using the rate constant for the parent 2-spiro-6'-cyclohexa-2',4'-dien-1'-one **18** as k_o). A regression equation of the form $\ln(k/k_o)=fF+rR$ was obtained with f=-0.50 and r=-3.12, with a R^2=0.9986. Plotting the observed and predicted rate constants against each other indicates good predictive ability over a range of up to 10 orders of magnitude (Figure 2.24).

Table 2.9. F and R values for the 2-spiro-6'-cyclohexa-2',4'-dien-1'-ones used in the Swain-Lupton modeling approach.

Substituent	F	R
H	0	0
F	0.74	-0.60
CH_3	0.01	-0.41
OCH_3	0.54	1.68
Cl	0.72	-0.24

Table 2.10. Sum of the field (F) and resonance (R) substituent constants and absolute and relative pseudo first-order rate constants for the rearrangement of **18**, **24**, **25**, **27**, **111**, **112**, and **113** into the corresponding 2,2'-biphenylquinones used in the Swain-Lupton modeling approach.

Compound	**ΣF**	**ΣR**	**k** (s^{-1})	**ln(k/k$_0$)**
18	0	0	4.90×10^{3}	0
24	0.04	-0.82	7.20×10^{4}	2.68
25	1.48	-1.20	8.30×10^{4}	2.83
27	1.08	-3.36	9.80×10^{7}	9.90
111	0.72	-0.24	6.80×10^{3}	0.33
112	5.76	-0.96	5.47×10^{4}	0.11
113	0.72	-0.24	6.11×10^{3}	0.22

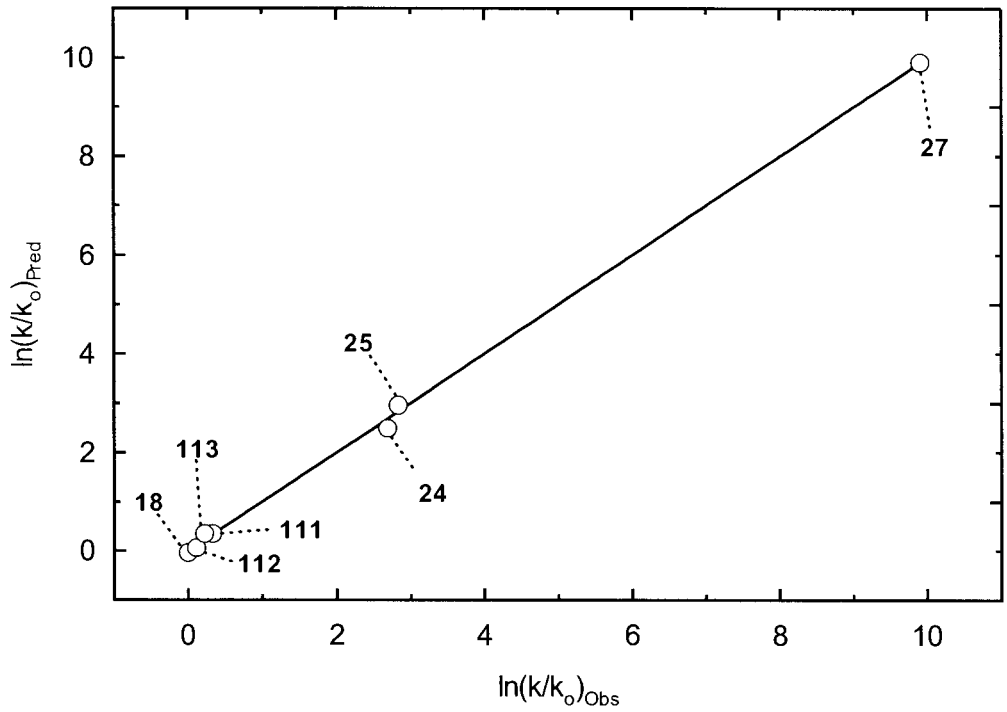

Figure 2.24. Observed and predicted relative rate constants (k) for the rearrangements of **18**, **24**, **25**, **27**, **111**, **112**, and **113** into the corresponding 2,2'-biphenylquinones using the Swain-Lupton modeling approach. A regression equation of the form $\ln(k/k_o)_{Prcd}=m\times\ln(k/k_o)_{Obs}+b$ where m=0.9990, b=0.0022, and R^2=0.9995 is shown. The high R^2-value, slope (m) near unity, and y-intercept (b) near zero indicate a satisfactory fit between the observed and predicted relative rate constants.

The regression constants of f=-0.50 and r=-3.12 show that substituent resonance effects are significantly greater than the field (inductive) effects, and that a relatively large positive charge accrues at the reaction center in the transition state to be stabilized by resonance donation on either one or both rings. Thermally allowed 2+2 electrocyclic ring opening in oxetane function of the 2-spiro-6'-cyclohexa-2',4'-dien-1'-one can give rise to a transition state where the ether oxygen carries either a δ^+ or δ^- charge. The higher electronegativity of the oxygen compared to the ring carbons would perhaps mitigate

against the oxygen carrying a δ^+ charge, although the non-specific substitution requirements in the Swain-Lupton approach do not allow us to rule out this possibility.

It has been previously shown that the presence of $NaBH_4$ increases the rate and yield of photochemical conversion of **9** to **10** (*40*), although it was not clear at that time whether this may be through thermal reduction of **16** or **18**. In the presence of freshly prepared 0.1 M $NaBH_4$ in 3:1 CH_3CN:CH_3OH v/v, formation of **16** was still observed by LFP with no diminution in absorbance and with a growth lifetime of 75 μs, and a pseudo-first order decay rate constant of ca. 143 s^{-1} (τ~7 ms). This subsequent decay of **16** on the scale of the LFP, is not observed for **16** in the absence of $NaBH_4$. The observation of a thermal decay of **16** within the timeframe of the LFP system (<1 μs) in the presence of $NaBH_4$ is consistent with previous studies showing the UV-Vis spectrum of **16** (taken within 1-2 s following 15-30 s irradiation of **9**) could not be observed with $NaBH_4$ in solution , but yet **10** was still observed as the major photoproduct following photolysis (*40*). These results suggest direct thermal reduction of 2,2'-biphenylquinones by hydride as the source of 2,2'-dihydroxybiphenyls when solutions of dibenzo[1,4]dioxins are irradiated in the presence of such reducing agents.

The activation parameters of the 2-spiro-6'-cyclohexa-2',4'-dien-1'-one to corresponding 2,2'-biphenylquinone rearrangement were also determined by LFP by way of Arrhenius plots for **18** (Figure 2.25), **24** (Figure 2.26), **111** (Figure 2.27), and **25** (Figure 2.28). The activation energies and pre-exponential factors for these reactions are summarized in Table 2.11. The activation parameters for the rearrangement of **27**→**28** could not be reliably determined as at temperatures greater than 25°C, the reaction occurs

within the temporal detection limit of the LFP system (<10-20 ns). As noted above, very weak LFP signals for the rearrangements of **112** and **113** into the corresponding 2,2'-biphenylquinones were obtained at 20°C, and signal degradation and high variability at other temperatures prevented the determination of activation parameters for these other two systems. Note that for each of the compounds subjected to an Arrhenius plot using LFP, the large errors in the estimates for the y-intercepts, coupled with the logarithmic scale of the y-axes, resulted in high uncertainties for the value of A (the pre-exponential constant). This high level of uncertainty prevents a detailed analysis of the potential entropy of activation ($\Delta S^{\ddagger}$). The low activation energies are consistent with a lack of carbon-carbon σ-bond cleavage for the process (Table 2.11).

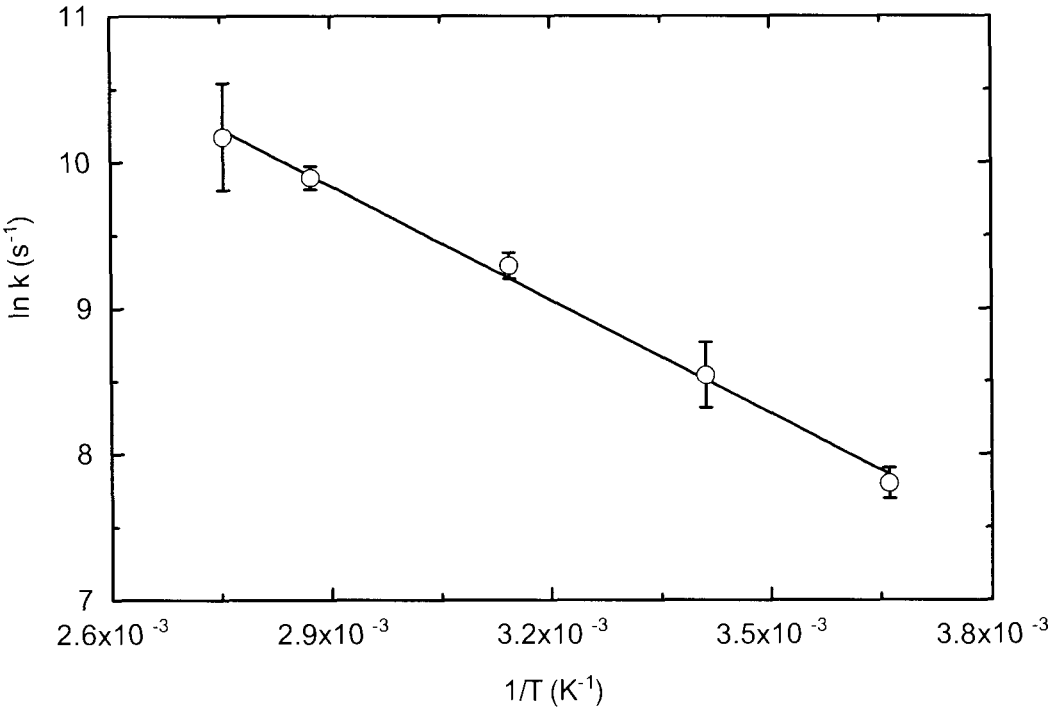

Figure 2.25. Arrhenius plot for the thermal rearrangement of **18** into **16** in dry CH_3CN using nanosecond LFP with transient UV-vis spectroscopy. Error bars are 95% confidence intervals about the mean. A regression equation of the form ln $k=-2610\pm300\times(1/T)+17.4\pm1.0$ with a $R^2=0.9981$ is shown.

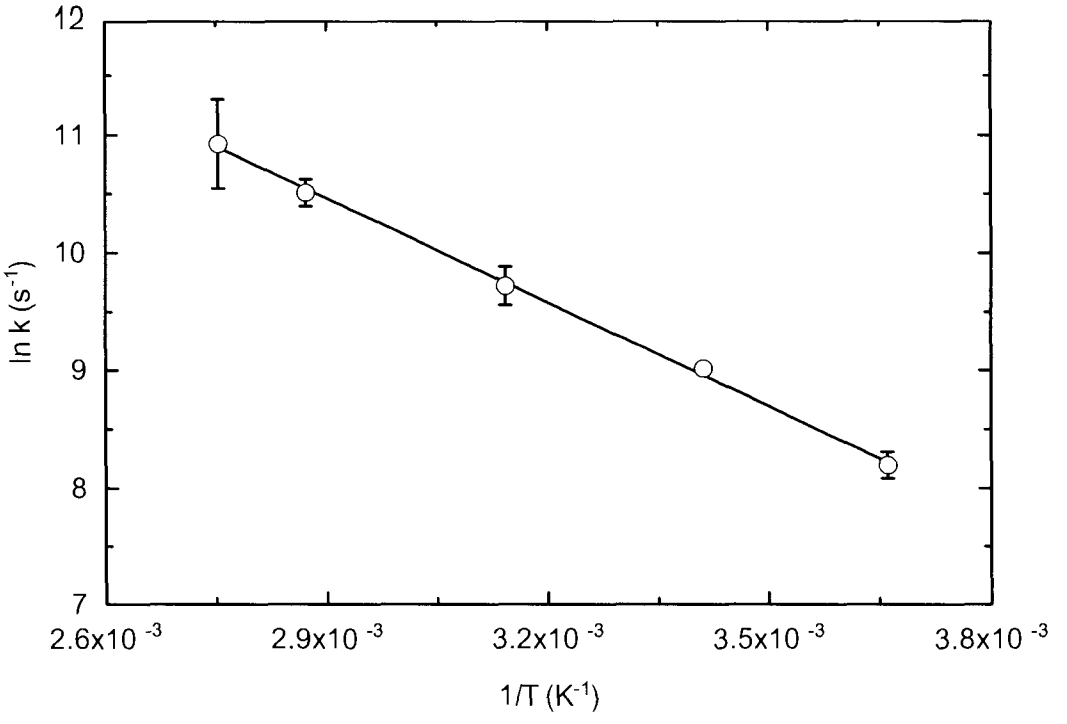

Figure 2.26. Arrhenius plot for the thermal rearrangement of **111** into **75** in dry CH_3CN using nanosecond LFP with transient UV-vis spectroscopy. Error bars are 95% confidence intervals about the mean. A regression equation of the form ln k=-2950±200×(1/T)+19.0±0.6 with a R^2=0.9993 is shown.

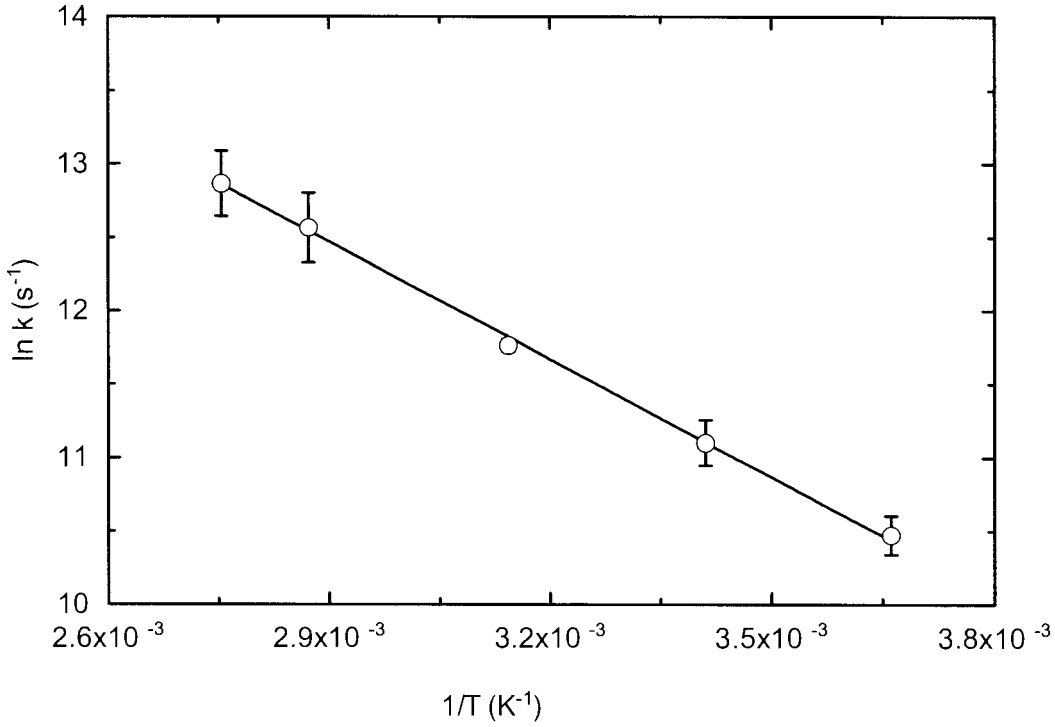

Figure 2.27. Arrhenius plot for the thermal rearrangement of **25** into **26** in dry CH_3CN using nanosecond LFP with transient UV-vis spectroscopy. Error bars are 95% confidence intervals about the mean. A regression equation of the form ln $k=-2670\pm180\times(1/T)+20.2\pm0.6$ with a $R^2=0.9993$ is shown.

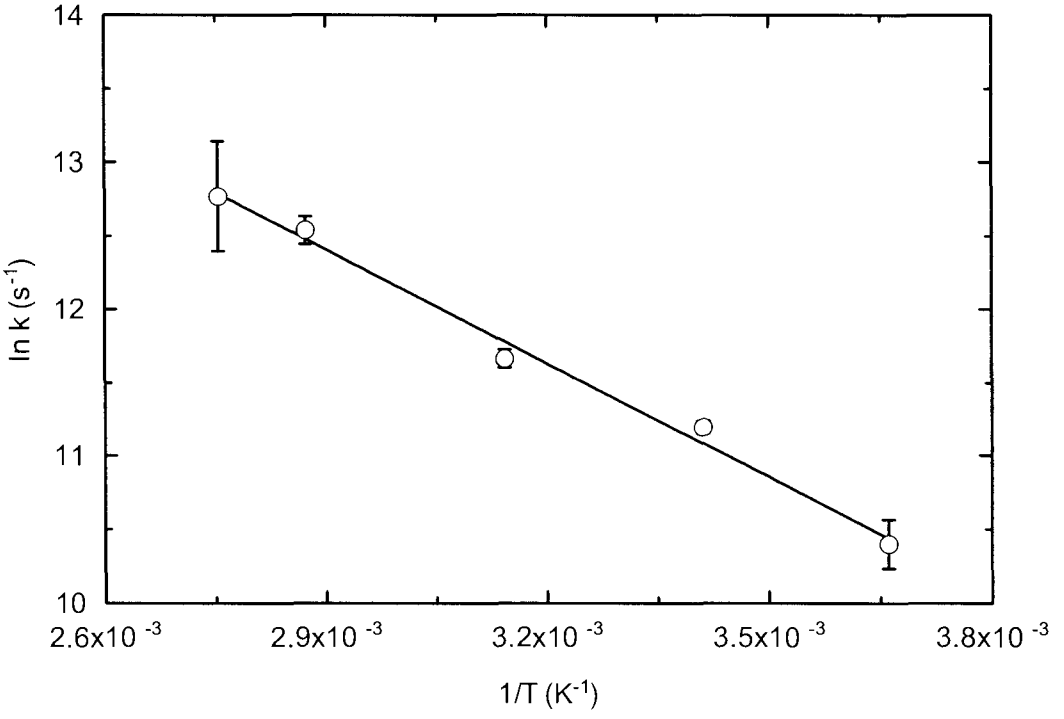

Figure 2.28. Arrhenius plot for the thermal rearrangement of **24** into **19** in dry CH_3CN using nanosecond LFP with transient UV-vis spectroscopy. Error bars are 95% confidence intervals about the mean. A regression equation of the form ln k=-2590±430×(1/T)+19.9±1.4 with a R^2=0.9959 is shown.

Table 2.11. Activation energies (E_a) and $\log_{10}$ pre-exponential factors (log A) for the rearrangements of 2-spiro-6'-cyclohexa-2',4'-dien-1'-ones **18**, **24**, **25**, and **111** into the corresponding 2,2'-biphenylquinones in CH_3CN. Error bars on E_a and log A are 95% confidence intervals about the mean. Because of the logarithmic method by which A is determined in the Arrhenius plots, conventional plus/minus error bars on A cannot be assigned.

Reaction	E_a (kJ/mol)	log A (s^{-1})
18→**16**	21.6±1.3	7.54±0.41
24→**19**	21.5±1.5	8.65±0.60
25→**26**	22.1±1.0[a]	8.78±0.25
111→**75**	24.4±1.0	8.25±0.28

Analogous to the reactivity studies on the 2,2'-biphenylquinone thermal rearrangements presented above using conventional suprasecond UV-Vis spectroscopy, the influence of solvent properties of the rate of rearrangement of 2-spiro-6'-cyclohexa-2',4'-dien-1'-ones **18**, **24**, **25**, **27**, and **111** to their corresponding 2,2'-biphenylquinones was investigated by nanosecond scale LFP. As with the UV-Vis studies of the 2,2'-biphenylquinone thermal decays, more polar organic solvents appear to stabilize the 2,2'-biphenylquinone and increase the rate of rearrangement of the 2-spiro-6'-cyclohexa-2',4'-dien-1'-ones in a similar manner for the five systems under investigation, with the greatest influence over the range of solvent dielectric constants ($\varepsilon/\varepsilon_o$; used as a surrogate for solvent polarity and obtained from ref. (*124*)) in the range from ca. 2 to 4 (Figure 2.29).

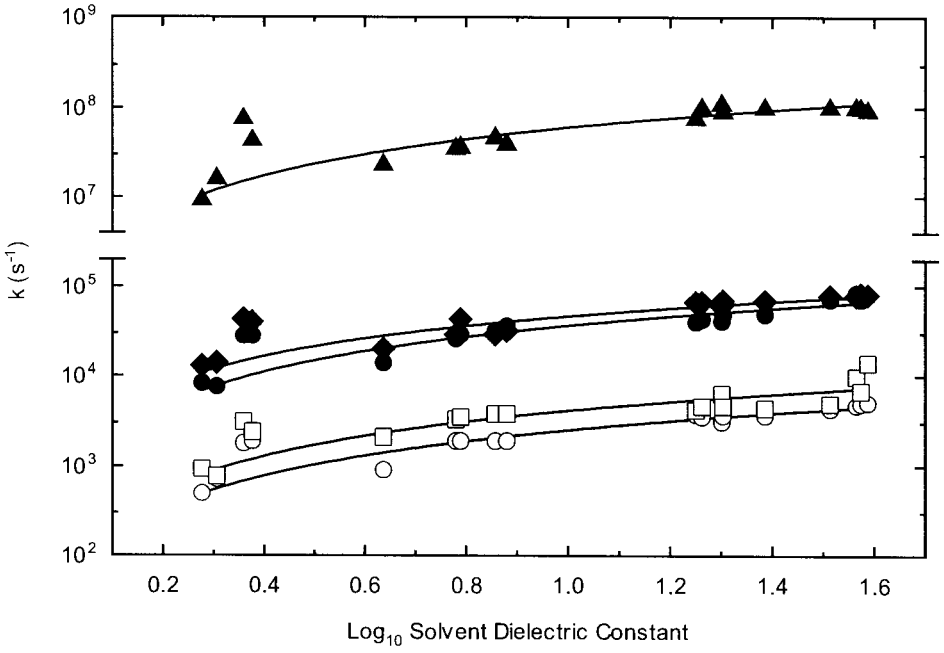

Figure 2.29. Influence of solvent dielectric constant on the rate of rearrangement of **18** (○), **24** (●), **25** (◆), **27** (▲), and **111** (□) into the corresponding 2,2'-biphenylquinones.

Of note is the apparent lack of general acid catalysis in this rearrangement (*cf.* the 2,2'-biphenylquinone thermal decay), as in the protic organic solvents, rearrangements rates do not differ from their expected $\varepsilon/\varepsilon_o$ trend. However, the two aromatic solvents in this study – benzene and toluene ($\varepsilon/\varepsilon_o$ of 2.3 and 2.4, respectively) – appear to stabilize 2,2'-biphenylquinone formation more than what would be expected based on their respective dielectric constants. This stabilization may be due to π-stacking interactions between the planar aromatic solvent and the planar conjugated 2,2'-biphenylquinone system that are unavailable with the other solvents. Consistent with the apparent absence of any general acid catalysis for these reactions in protic organic solvents, water content (on a volume basis in CH_3CN) exhibited no catalytic effect on the 2-spiro-6'-cyclohexa-

2',4'-dien-1'-one rearrangements (Figure 2.30). Rather, the steady increase in reaction rate is likely due to the increased solvent polarity with the addition of water. Assuming an additive volumetric relationship between the dielectric constants of CH_3CN ($\varepsilon/\varepsilon_o$=38) and water ($\varepsilon/\varepsilon_o$=79) seems to explain the pattern of rate constants. As well, the increasing water content studies correspond well with a hypothetical continuation of the trends observed with the aprotic and protic organic solvents, such that solvent polarity appears to be the dominant governing solvent factor on the rates of reaction. Specific acid catalysis is also absent in these rearrangements between pH values of 1 and 12, as shown by the uniformity in rate constant over this pH range (Figure 2.31).

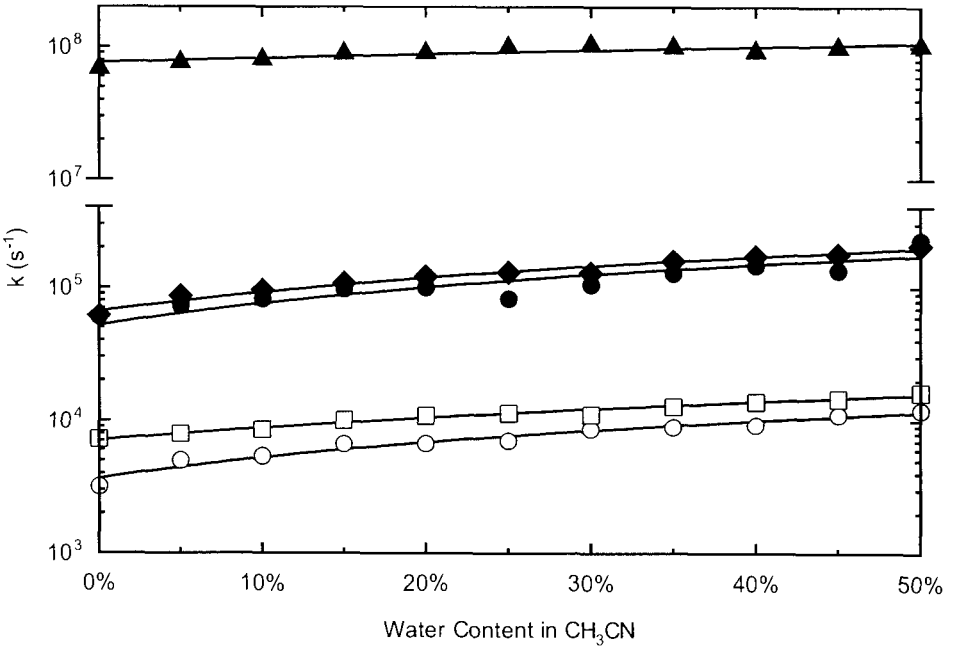

Figure 2.30. Influence of water content in CH_3CN on the rate of rearrangement of **18** (○), **24** (●), **25** (◆), **27** (▲), and **111** (□) into the corresponding 2,2'-biphenylquinones.

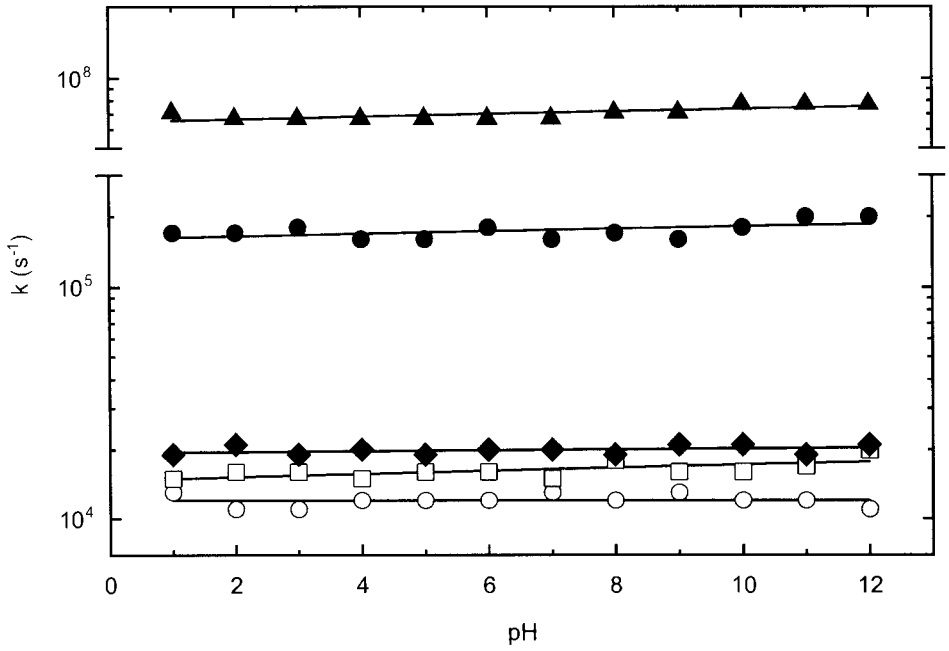

Figure 2.31. Influence of the pH of the water fraction in a 1:1 (v/v) solution of H_2O:CH_3CN on the rate of rearrangement of **18** (○), **24** (●), **25** (◆), **27** (▲), and **111** (□) into the corresponding 2,2'-biphenylquinones.

2.7 Proposed Mechanism

Based on the results discussed above, the following general photochemically initiated mechanism for the observed dibenzo[1,4]dioxin photochemistry is proposed (Scheme 2.10). Following absorption of a photon, an excited singlet state dibenzo[1,4]dioxin undergoes homolytic aryl-ether bond cleavage to generate a diradical species, which through an intramolecular *ipso* attack, gives rise to the corresponding 2-spiro-6'-cyclohexa-2',4'-dien-1'-one. Thermally allowed electrocyclic 2+2 ring opening from the 2-spiro-6'-cyclohexa-2',4'-dien-1'-one then generates the corresponding 2,2'-biphenylquinone. Following their generation, a 2,2'-biphenylquinone may be photochemically reduced via a singlet state reaction to the corresponding 2,2'-

dihydroxybiphenyl, or may react thermally via one of two pathways depending on the nature and position of substituents. 2,2'-Biphenylquinones with electron withdrawing substituents whose Hammett constants sum to greater than or equal to zero rearrange into the corresponding 1-hydroxybenzofurans, whereas 2,2'-biphenylquinones with electron donating substituents whose Hammett constants sum to less than zero rearrange into the corresponding oxepinodibenzo[2,3-b]furans.

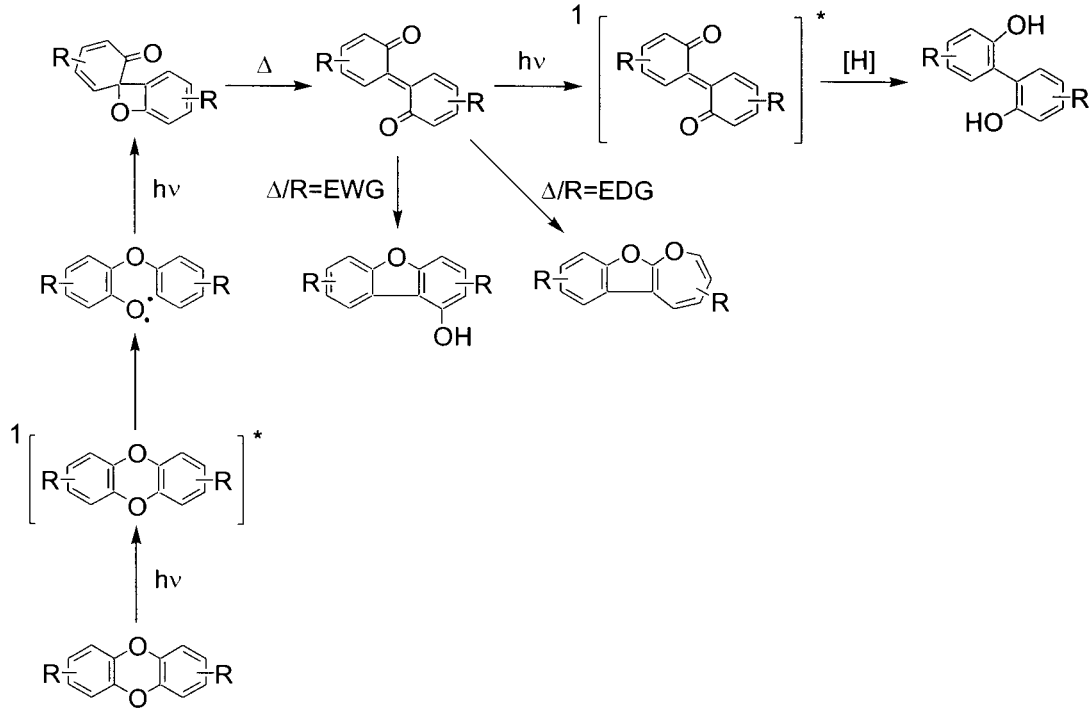

Scheme 2.10

2.8 Conclusions

Dibenzo[1,4]dioxins undergo a singlet state photochemically initiated aryl-ether bond homolysis that yields reactive 2-spiro-6'-cyclohexa-2',4'-dien-1'-one and subsequent 2,2'-biphenylquinone intermediates. Under steady-state irradiation, the 2,2'-biphenylquinones undergo excited singlet state hydrogen abstraction from the organic solvent to give corresponding 2,2'-dihydroxybiphenyls as the major isolated photoproduct, with no evidence of thermal hydrogen abstraction. Yields of the 2,2'-dihydroxybiphenyls are solvent dependent, with an increased yield and closure of the photochemical mass balance in protic solvents. In the absence of continued irradiation, 2,2'-biphenylquinones with electron donating substituents thermally rearrange to corresponding oxepino[2,3-b]benzofurans, whereas the unsubstituted 2,2'-biphenylquinone and its derivatives with electron withdrawing groups thermally rearrange to corresponding 1-hydroxydibenzofurans. Solvent polarity appears to be the dominant external influence on the rates of formation and decay of the 2,2'-biphenylquinones, with more polar solvents stabilizing the 2,2'-biphenylquinone, although general acid catalysis appears to favor more rapid 2,2'-biphenylquinone decay.

Swain-Lupton and Hammett modeling on 2,2'-biphenylquinone formation and decay, respectively, demonstrate the influence of substituent number and identity of the rates of rearrangement and facilitate predictive investigations of these processes. The results further suggest that in natural systems, 2,2'-dihydroxybiphenyls are the major primary photoproducts from dibenzo[1,4]dioxins. This finding appears to hold regardless

of the solvent environment, being either aqueous or organic in identity and polar/nonpolar or protic/aprotic in properties. Thus, both in freshwater and marine systems, as well as in more lipidic tissue such as the dermal layers which are exposed to UV radiation, 2,2'-dihydroxybiphenyl formation would be expected to dominate over other photochemical pathways such as photochemical dehalogenation. The potential endocrine disrupting tendencies of the 2,2'-dihydroxybiphenyls warrant more attention as possible major environmental degradation products of dibenzo[1,4]dioxins.

CHAPTER 3 – PHOTOCHEMISTRY OF BROMINATED DIPHENYL ETHERS

3.1 Materials

Diphenyl ethers **37**, **38**, **41**, **44**, **114**, **115**, **116**, **117**, **118**, **119**, **120**, **121**, **122**, and **123** were commercially available, as was the tetrabrominated dibenzofuran **42**. Compounds **41** and **115** were photochemical starting materials. Compounds **114** and **44** were potential photoproducts of **115**. Compounds **37**, **38**, **116**, **117**, **118**, **119**, **120**, **121**, **122**, and **123** were potential photoproducts of **41**.

3.2 Product Studies

3.2.1 Photochemistry of 115

The photochemistry of **115** was investigated in organic (CH_3CN and CH_3OH) and aqueous (1:1 (v/v) H_2O:CH_3CN) solvent systems. In dry CH_3CN, **115** (1.52×10^{-3} M; 300 nm; 0 to 60 min) underwent exclusive sequential reductive photodebromination to yield **114** as the only photoproduct in ca. 100% yield (i.e., no unaccounted mass was observed throughout the photolysis) (eq. (3.1). Under extended photolysis in dry CH_3CN, **115** was observed to undergo secondary reductive photodebromination (primary photodebromination of **114**) to give **44** (eq. (3.2). Over the course of the 60 min photolysis (aliquots removed for analysis after 0, 5, 15, 30, 45, and 60 min), a complete mass balance was maintained as measured by GC and ^{1}H NMR (100±1%), with the photochemical loss of starting material having a pseudo first-order rate constant (k) of 2.78×10^{-2} min^{-1} (Figure 3.1).

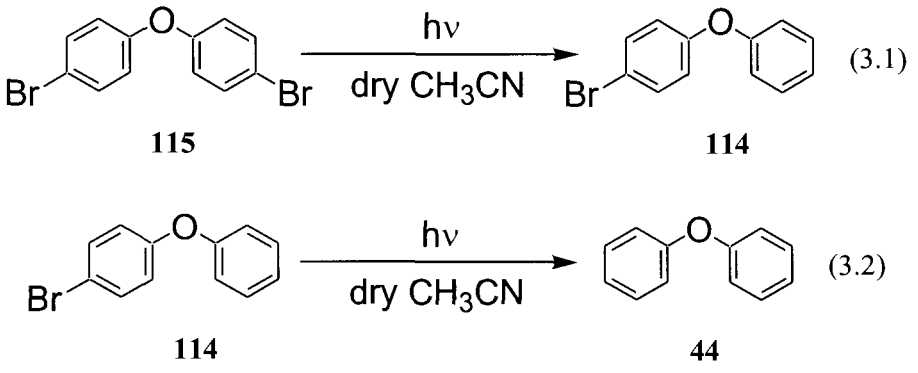

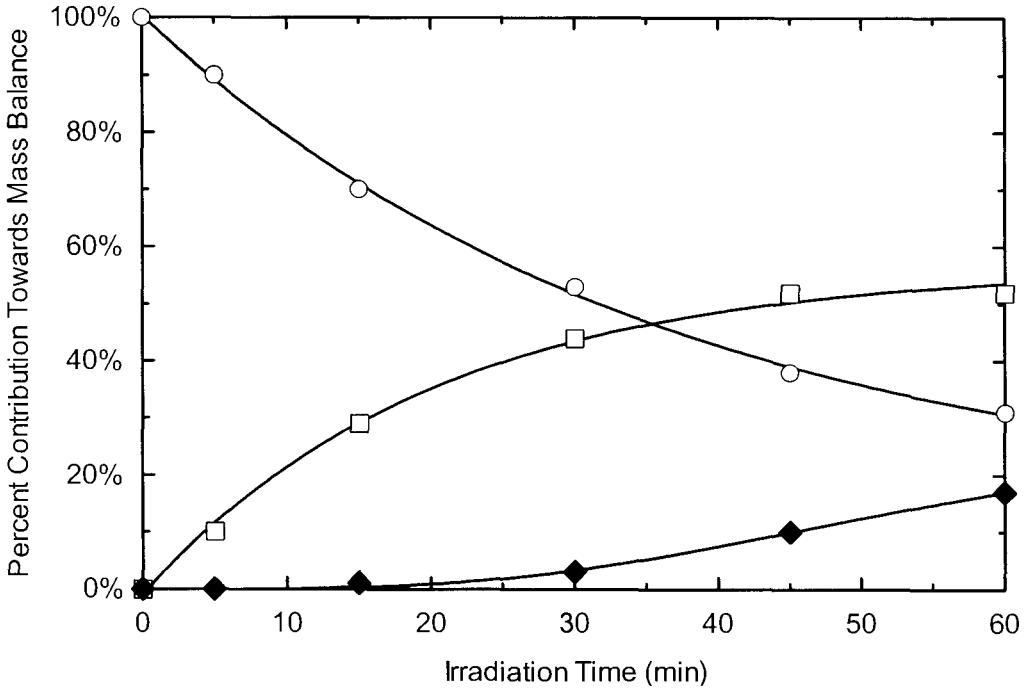

Figure 3.1. Contribution of **115** (○), **114** (□), and **44** (◆) towards the overall photochemical mass balance for **115** over a 60 min irradiation period in dry CH_3CN.

Similarly, in CH_3OH, **115** (1.52×10^{-3} M; 300 nm; 0 to 60 min) also underwent exclusive sequential reductive photodebromination to yield **114** as the only photoproduct in ca. 100% yield (i.e., no unaccounted mass was observed throughout the photolysis) (eq. (3.3). Under extended photolysis in CH_3OH, **115** was observed to undergo secondary reductive photodebromination (primary photodebromination of **114**) to give **44**

(eq. (3.4). Over the course of the 60 min photolysis (aliquots removed for analysis after 0, 5, 15, 30, 45, and 60 min), a complete mass balance was maintained as measured by GC and ^{1}H NMR (100±1%), with the photochemical loss of starting material having a pseudo first-order rate constant (k) of 3.30×10^{-2} min^{-1} (Figure 3.2).

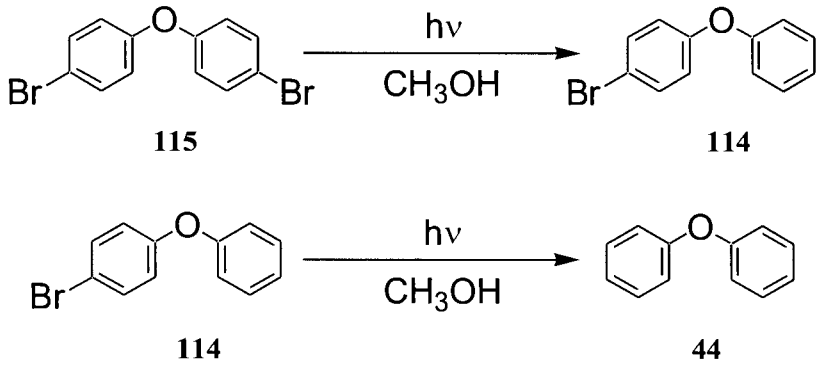

115 **114** (3.3)

114 **44** (3.4)

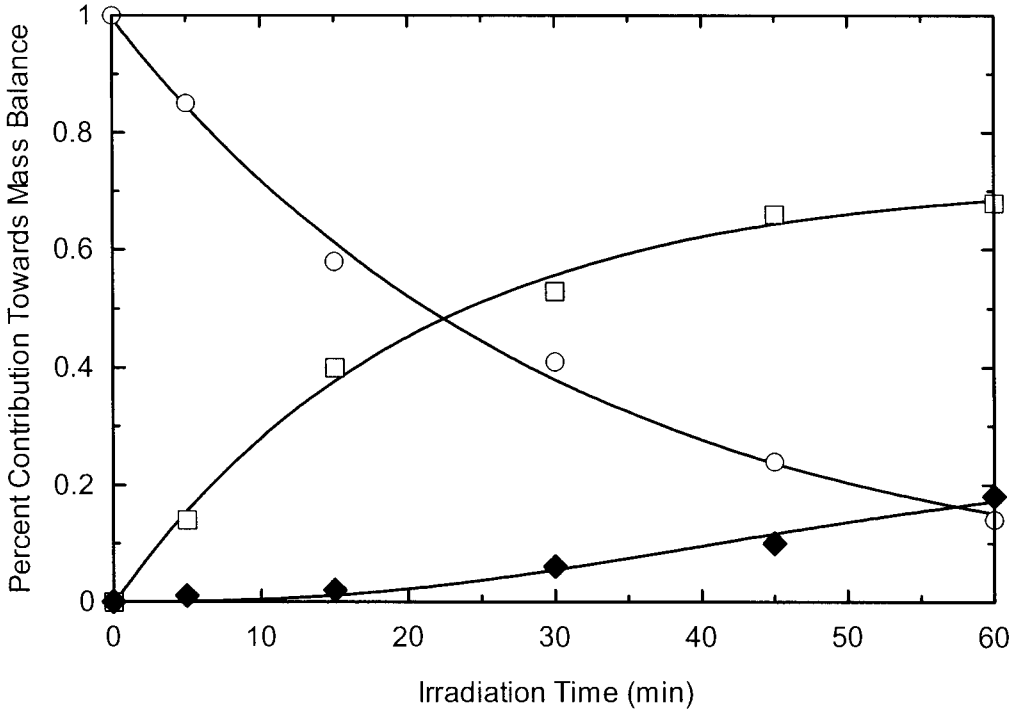

Figure 3.2. Contribution of **115** (○), **114** (□), and **44** (◆) towards the overall photochemical mass balance for **115** over a 60 min irradiation period in CH_3OH.

The higher rate constant for loss of starting material in CH_3OH versus CH_3CN, and the absence of methoxylated diphenyl ethers in the photoproduct mixture (see below) while maintaining a mass balance throughout the photolysis, is consistent with exclusive photochemically induced aryl-bromine bond homolysis followed by hydrogen abstraction from the organic solvent by the resulting aryl radical (e.g., Scheme 3.1). CH_3OH is known to be a more labile solvent than CH_3CN with regard to hydrogen atom donation (i.e., a weaker C-H bond strength on the methyl function in CH_3OH compared to the C-H bond in CH_3CN), and hence, a higher rate of photodebromination (resulting from aryl-bromine bond homolysis) is expected and was observed.

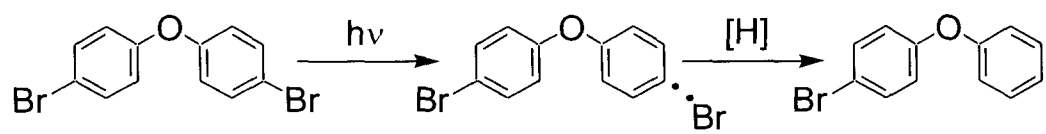

Scheme 3.1

As well, heterolytic aryl-bromine bond cleavage – if occurring – would result in the formation of an aryl cation and a bromide ion (Br^-) (e.g., Scheme 3.2). Formation of an aryl anion and a bromine cation (Br^+) would be unlikely given the high electronegativity of bromine. Such an aryl cation would likely undergo the following two processes: (1) recombination with the bromide ion to yield no net photochemistry; and (2) "trapping" by a nucleophilic solvent molecule. Thus, the weak nucleophilicity of CH_3CN would suggest that, if photochemical aryl-bromine heterolytic cleavage was the dominant mechanistic contributor to the overall photochemistry, there would be little or no conversion of starting material under prolonged photolysis (i.e., all aryl cation-bromide ion pairs would recombine following their generation as no nucleophile would be present to trap the aryl cation – this was not observed).

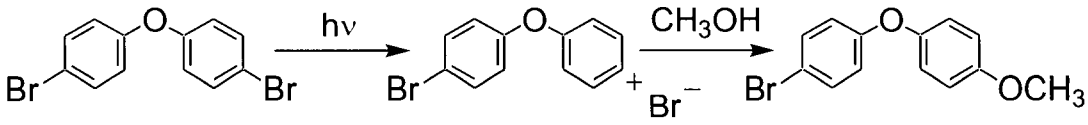

Scheme 3.2

By comparison, in CH_3OH, if photochemical aryl-bromine heterolytic cleavage was a significant mechanistic contributor to the overall photochemistry (in combination with a competing aryl-bromine bond homolysis pathway), some methoxylated diphenyl ether product would be expected to be formed as completely efficient ion-pair recombination would be unlikely (i.e., some bromide ions would statistically be required to escape the solvent cage, thus leading to trapping by the nucleophilic solvent in order to neutralize the charge separation – this was not observed). The absence of either of these pathways suggests photochemically induced aryl-bromine bond homolysis as the sole photochemical pathway for **115** and **114**.

Duplicate trials were also performed in H_2O:CH_3CN (1:1 v/v) to model the aqueous photochemical fate of **115** and to investigate any potential differences from the photochemistry in entirely organic solvents. The solubility of **115** was sufficiently low to prevent dissolution in higher concentrations of water (e.g., 2:1 H_2O:CH_3CN (v/v)) for the photochemical studies, although such higher concentrations of water would be desired as they more accurately represent some environmental conditions. In 1:1 H_2O:CH_3CN (v/v), **115** (1.52×10^{-3} M; 300 nm; 30 min) underwent exclusive sequential reductive photodebromination to yield **114** (25±1% yield) and **44** (1.2±0.2% yield), with 73±2% of unreacted starting material remaining in solution. A complete mass balance was observed after this 30 min irradiation period. Thus, reductive photodebromination is

much slower in the aqueous system compared to dry CH_3CN and CH_3OH, where only 51% and 41%, respectively, of the starting material remained after 30 min.

This result is consistent with the lack of hydrogen atom donating ability by H_2O, since the O-H bond strength in water is too great to allow efficient hydrogen abstraction by a ground state aryl radical. In addition, further evidence was provided as to the lack of a significant contribution from photochemically induced aryl-bromine bond heterolysis during the trials in 1:1 H_2O:CH_3CN (v/v). The lack of any hydroxylated diphenyls ethers, as would be expected when water traps an aryl cation (e.g., see Scheme 3.3), suggests photochemically induced aryl-bromine bond homolysis (e.g., Scheme 3.1) as the only significant pathway in this solvent system as well.

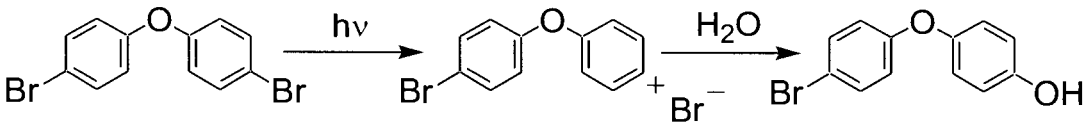

Scheme 3.3

As discussed above, no products other than strict reductive debromination were observed in any of the solvent systems. This lack of photochemically induced aryl-ether bond cleavage for either **115** or **114** is in contast to where chlorine or fluorine substituents are present on the diphenyl ether system (*132,133*) (e.g., **124** and **125**). The present observations suggests the aryl-chlorine bond strength (ca. 350-390 kJ/mol for the ground state (*134*)) in the chlorinated diphenyl ethers is of the same order as the aryl-ether bond strength. In contrast, for brominated diphenyl ethers the strength of the aryl-bromine bond (ca. 335 kJ/mol for the ground state (*134*)) must be significantly lower than

that of the aryl-ether bond such that no photochemically induced intramolecular rearrangement or aryl-ether cleavage products are observed.

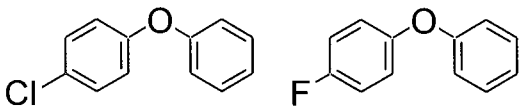

124 **156**

Previous work with the parent diphenyl ether and its substituted analogs has shown the existence of a photo-Fries type rearrangement following photochemically induced aryl-ether bond cleavage (*132,133*) (e.g., Scheme 3.4). Should this photo-Fries process have taken place with **115** (i.e., if aryl-oxygen bond homolysis was indeed operative), formation of **126** and **127** would be expected (Scheme 3.5). No chromatographic or spectroscopic evidence was obtained for a photo-Fries process resulting in the formation of brominated hydroxybiphenyls (and the continuity of the mass balance throughout the photolysis by way of photodebromination also supports the absence of this pathway). An analytical standard was also available for **127** to examine whether trace amounts were being formed. **128** and **129** would also be expected from the photochemically induced aryl-bromine bond homolysis of **115** via radical escape from the solvent cage and subsequent reduction by the organic solvent. As well, **130** would be expected from the radical coupling of two *para* brominated aryl radicals within the solvent cage. None of these three products were observed.

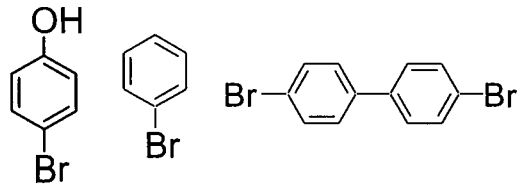

128 **129** **130**

An additional potential photolytic pathways for **115** is photochemically induced aryl-ether bond heterolysis, yielding a *para* brominated phenolate and a *para* brominated aryl cation. If in a protic organic solvent such as CH_3OH, **128** and **131** would be the expected primary photoproducts (Scheme 3.6). If in H_2O, two molecules of **128** would be expected (Scheme 3.7). The absence of any of these products suggests the aryl-ether bond heterolysis pathway was not a significant contributor to the overall photochemistry of **115**.

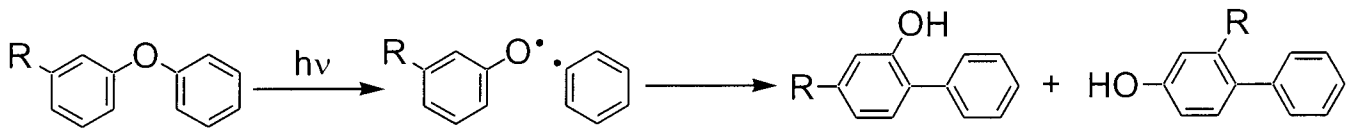

Scheme 3.4

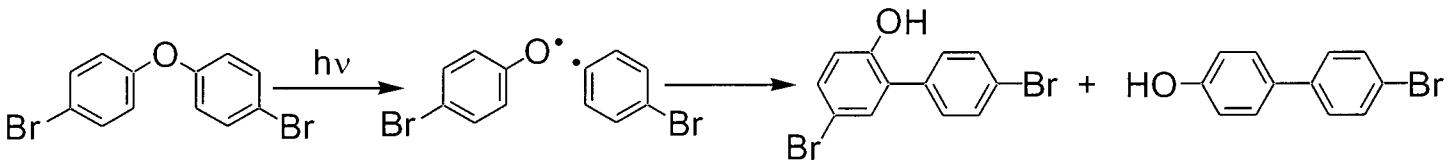

115 **126** **127**

Scheme 3.5

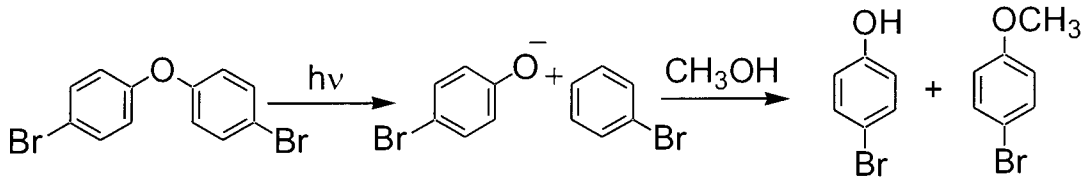

115 **128** **131**

Scheme 3.6

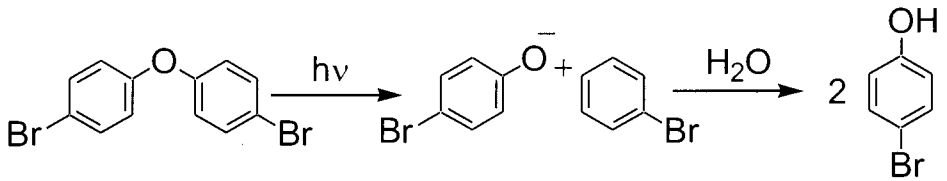

115 **128**

Scheme 3.7

3.2.2 Photochemistry of 41

3.2.2.1 Photodegradation Kinetics and Product Identification/Quantification

Because the photodegradation kinetics were unknown under the proposed irradiation conditions, separate solutions of 1.3×10^{-9} M **41** in CH_3CN were exposed to 302 nm light for 5 min intervals ranging up to a total of 60 min and analyzed by HRGC-HRMS for the presence of debromination products. Absolute quantities of the starting material and individual photoproducts, along with percent recoveries of the recovery standards and methods for correcting absolute analyte quantities to observed standard recoveries, are presented and discussed in Section 4.3.1.2.3.

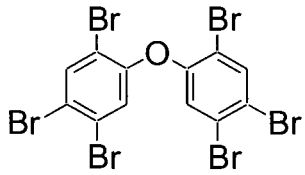

41

After 5 min irradiation, ca. 15% of the starting material remained with ca. 18% of the mass balance accounted for by the three potential pentabrominated photoproducts (ca. 14% of mass balance) and four of the potential tetra-brominated photoproducts (ca. 4% of mass balance; see below for identities) (Figure 3.3). The contributions of penta- and tetra-brominated diphenyl ethers towards the photochemical mass balance decreased exponentially over the 60 min irradiation period. Pentabrominated diphenyl ethers reached a mass balance contribution maximum of 14% after 5 min irradiation, after which their contribution declined to <0.1% after 60 min irradition. Similarly, tetrabrominated diphenyl ethers reached a mass balance contribution maximum of 2.3%

after 10 min irradiation, after which their contribution declined to <0.1% after 60 min irradition. No other brominated diphenyl ether photoproducts from mono- through tri-substituted were observed at these timescales, thus leaving ca. 65% of the photochemical mass balance unaccounted for after only 5 min irradiation, and >99% of the mass balance unaccounted for after 60 min irradiation.

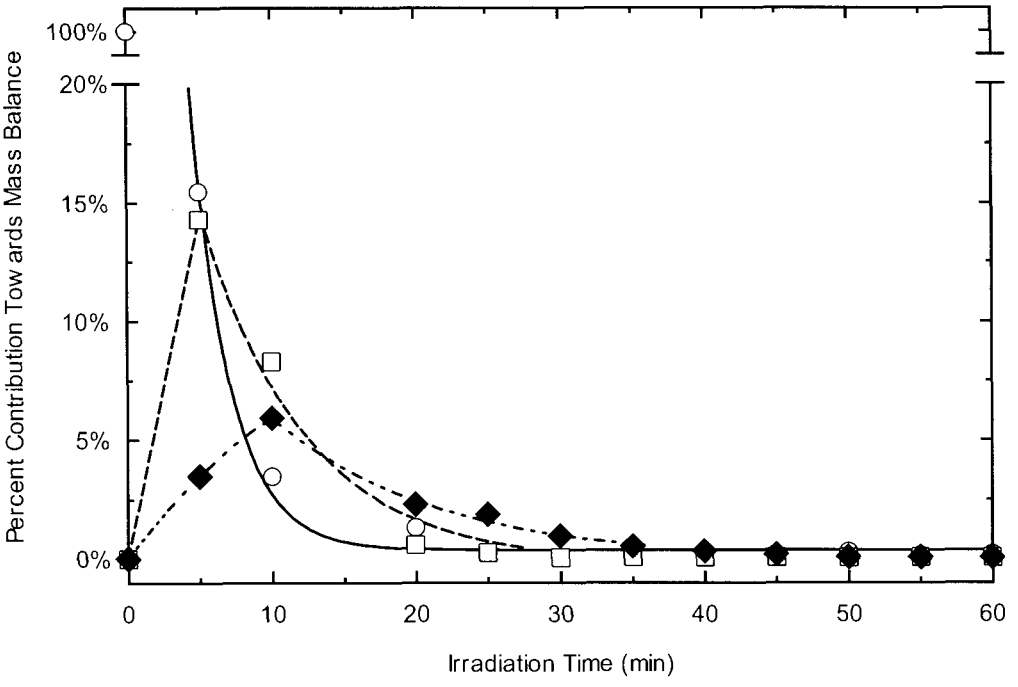

Figure 3.3. Contribution of unreacted starting material (**41**; ○, solid line), the sum of pentabrominated diphenyl ether photoproducts (□, dashed line), and the sum of tetrabrominated diphenyl ether photoproducts (◆, dash-dot-dot line) towards the overall photochemical mass balance for **41** over a 60 min irradiation period in CH_3CN.

Concentrations of the three potential primary debromination products – **38**, **121**, and **132** – were observed to reach maximum contributions towards the mass balance at 5 min of 5.7%, 4.8%, and 3.8%, respectively (Figure 3.4). Concentrations of **38**, **121**, and **132** subsequently declined under continued irradiation with first-order rate constants of

0.15 min^{-1} ($t_{1/2}$=4.6 min; R^2=0.995), 0.13 min^{-1} ($t_{1/2}$=5.3 min; R^2=0.989), and 0.14 min^{-1} ($t_{1/2}$=5.0 min; R^2=0.995), respectively. This efficient photodegradation of **41** should perhaps not be surprising, as recent reports suggest quantum yields of up to ca. 0.4-0.6 for tetra- through deca-BDEs (*81,82,135*), and other diphenyl ethers have quantum yields up to ca. 0.95 that appear to be highly solvent dependent (*136*).

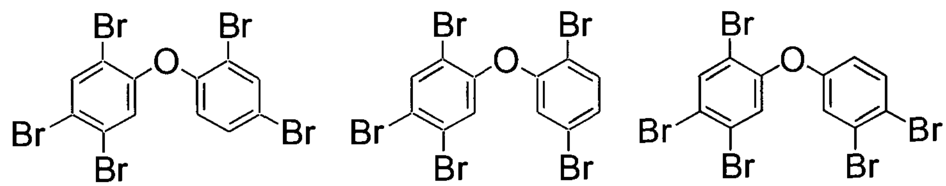

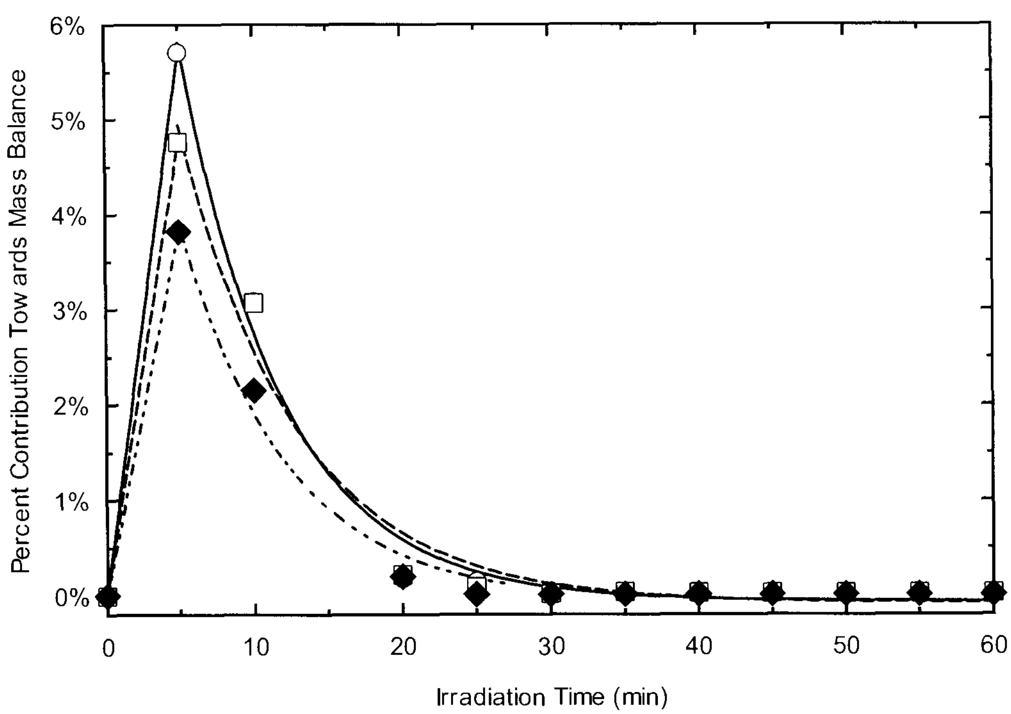

Figure 3.4. Contribution of the individual pentabrominated diphenyl ether photoproducts towards the overall photochemical mass balance for **41** over a 60 min irradiation period in dry CH_3CN: **38** (O, solid line); **121** (□, dashed line); and **132** (◆, dash-dot-dot line).

With the decay of these primary debromination products, corresponding growths in the concentrations of four secondary debromination products – **37**, **116**, **122**, and **123** – reach their maximum contributions towards the mass balance at 10 min of 1.5%, 1.1%, 1.3%, and 0.3%, respectively (Figure 3.5). Concentrations of **37**, **116**, **122**, and **123** subsequently declined under continued irradiation with first-order rate constants of 0.082 min^{-1} ($t_{1/2}$=8.5 min; R^2=0.994), 0.095 min^{-1} ($t_{1/2}$=7.3 min; R^2=0.998), 0.093 min^{-1} ($t_{1/2}$=7.5 min; R^2=0.998), and 0.091 min^{-1} ($t_{1/2}$=7.6 min; R^2=0.993), respectively. Thus, over the interval from 5 to 10 min irradiation, only ca. 40% of the reacted mass of the three pentabrominated diphenyl ether primary photoproducts could be accounted for by growth in contributions from the four tetrabrominated diphenyl ether secondary photoproducts. As noted above, no other tetrabrominated diphenyl ethers were observed in solution, and the HRGC-HRMS method had sufficient sensitivity and specificity to identify the presence and approximate quantities of any brominated diphenyl ethers for which analytical standards were not available. Indeed, both **121** and **132** were initially identified using previously published HRGC relative retention time (RRT) models (*137-139*). At the time of identification, an analytical standard was not available for **121**; subsequent purchase and analysis of this standard identified **121** as was predicted by the HRGC-RRT models.

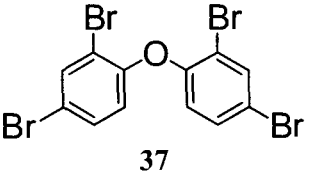

37

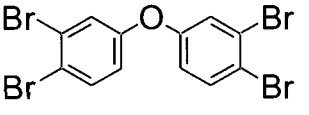

116

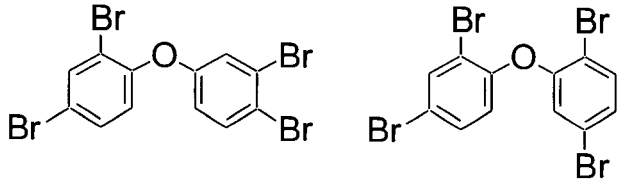

122 **123**

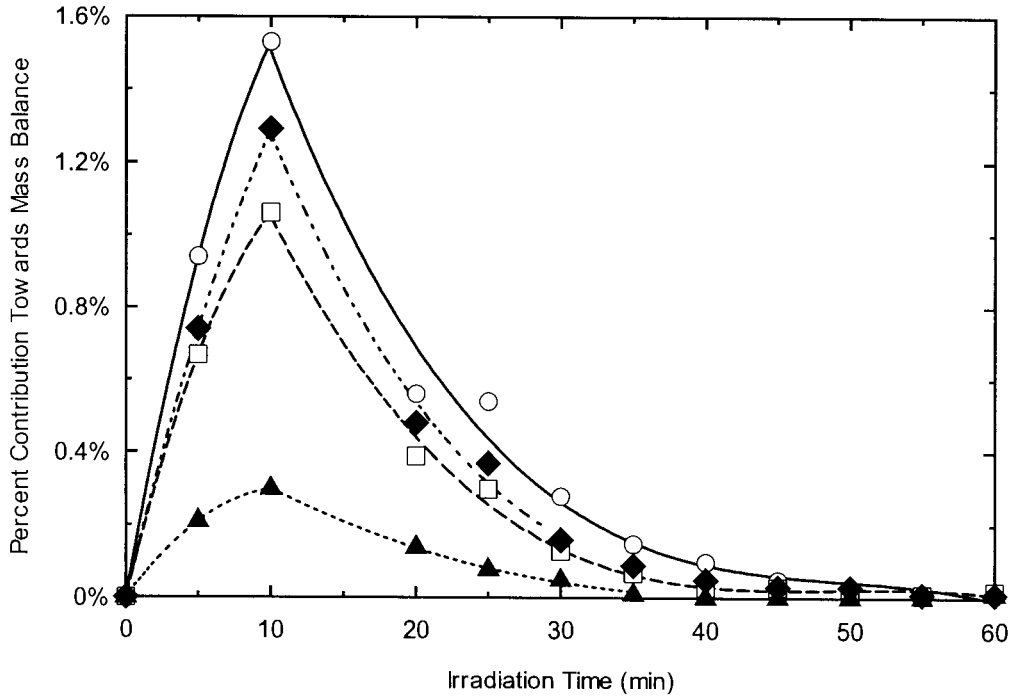

Figure 3.5. Contribution of the individual tetrabrominated diphenyl ether photoproducts towards the overall photochemical mass balance for **41** over a 60 min irradiation period in dry CH_3CN: **123** (○, solid line); **37** (□, dashed line); **122** (◆, dash-dot-dot line); and **116** (▲, dotted line).

Because of the lack of mass balance for the duration of the 60 min photolyses, significant degradation (ca. 85%) of starting material prior to the first analytical timeframe (5 min), and significant secondary photochemistry observed at these longer timescales, a suite of duplicate trials at 1 min intervals over a duration of 5 min in three solvent systems (CH_3CN, H_2O, and seawater) were performed in an attempt to capture

the primary photochemical processes of **41** and to close the mass balance. Similar difficulties in completing a photochemical mass balance for the higher brominated diphenyl ethers adsorbed on solids (i.e., sand, silica gel) and in solution have been previously reported (*80,81,84,140*). In addition, to calibrate the experimental irradiation intensity with that under solar illumination, a suite of trials in CH_3CN was exposed to natural sunlight at 3 min intervals over a duration of 15 min.

Under the four irradiation conditions, the influence of water content and solar radiation on the rate of **41** decay were evident. In CH_3CN, loss of starting material followed first order kinetics with a rate of 0.619 min^{-1} ($t_{1/2}$=1.1 min; R^2=0.998; Figure 3.6, Figure 3.7, and Figure 3.8). In H_2O, the rate of loss of **41** under the same irradiation conditions increased to 1.214 min^{-1} ($t_{1/2}$=0.57 min; R^2=0.987; Figure 3.9, Figure 3.10, and Figure 3.11). The increased reaction rate in water is also evident in the time resolved profiles for the penta- and tetra-brominated diphenyl ether debromination products. In CH_3CN, the concentrations of pentabrominated diphenyl ethers have just begun to decline and the tetrabrominated diphenyl ethers are beginning to plateau after 5 min irradiation. By contrast, in H_2O both the penta- and tetra-brominated diphenyl ether photoproducts are well into decline by 5 min irradiation.

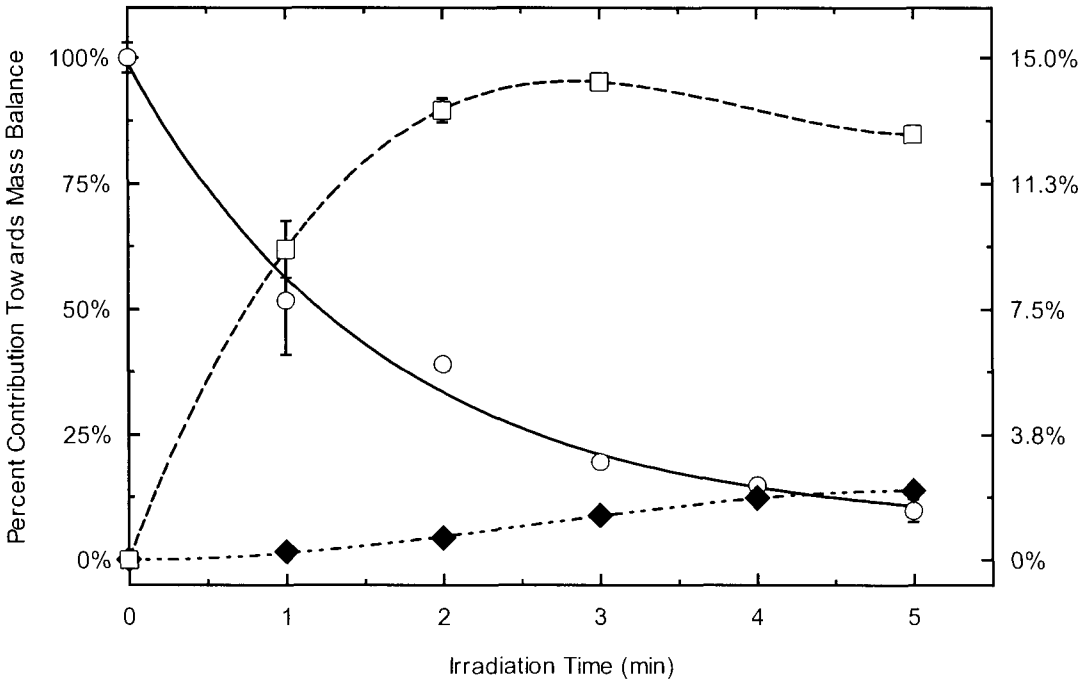

Figure 3.6. Contribution of unreacted starting material (**41**; ○, solid line), the sum of pentabrominated diphenyl ether photoproducts (□, dashed line), and the sum of tetrabrominated diphenyl ether photoproducts (◆, dash-dot-dot line) towards the overall photochemical mass balance for **41** over a 5 min irradiation period in CH_3CN. Values on left y-axis show contribution of starting material towards the mass balance. Values on right y-axis show contribution of photoproducts towards the mass balance. Error bars show the range of duplicate photolyses where available.

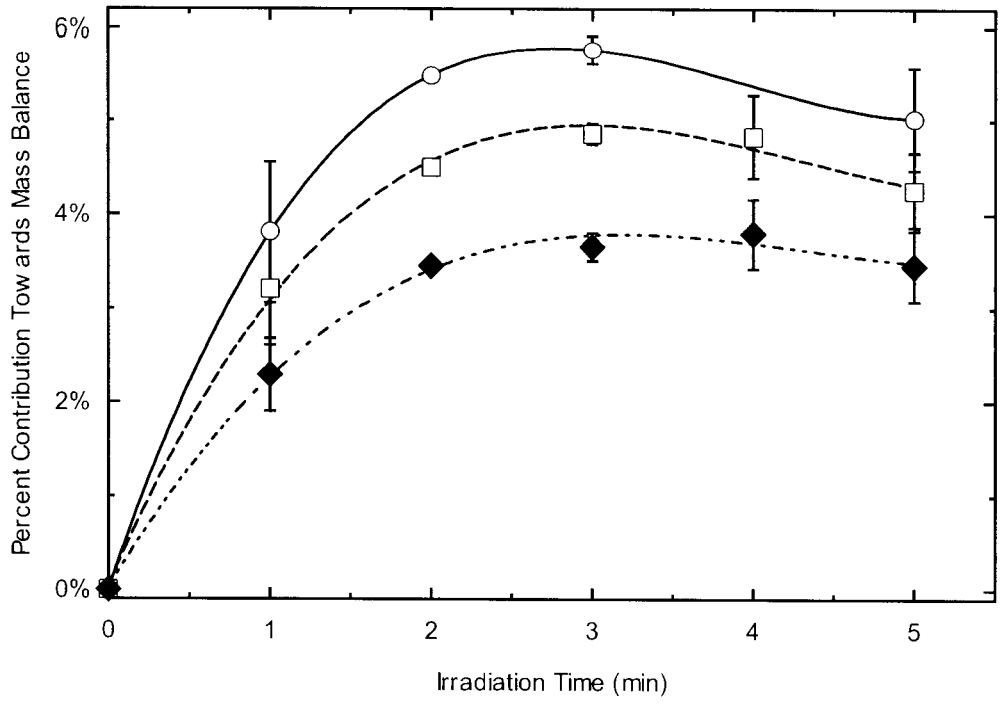

Figure 3.7. Contribution of the individual pentabrominated diphenyl ether photoproducts towards the overall photochemical mass balance for **41** over a 5 min irradiation period in CH_3CN: **38** (○, solid line); **121** (□, dashed line); and **132** (◆, dash-dot-dot line). Error bars show the range of duplicate photolyses where available.

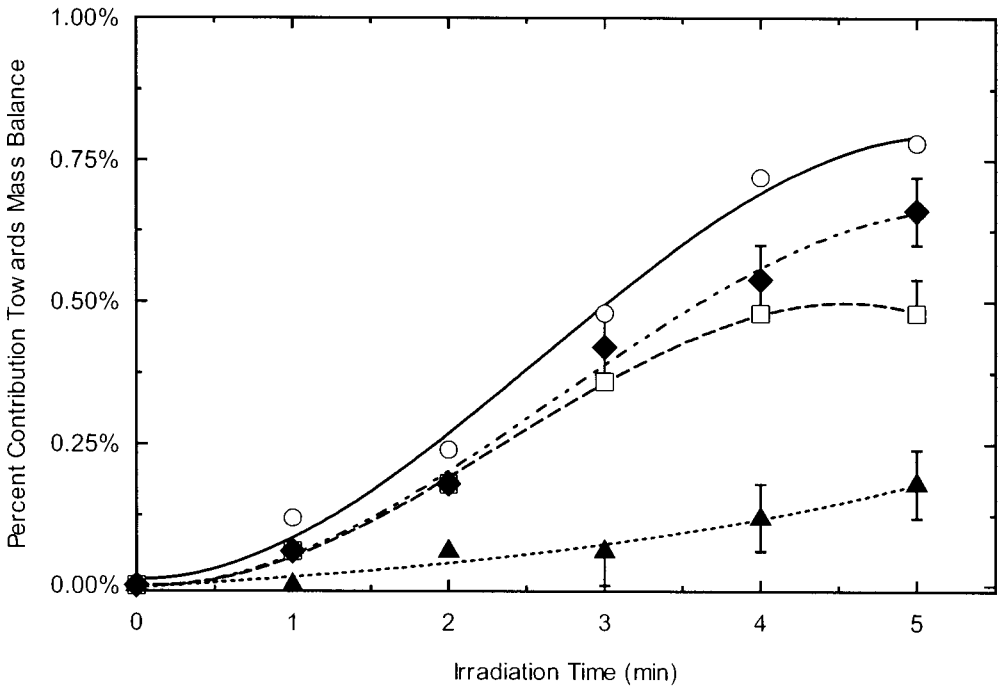

Figure 3.8. Contribution of the individual tetrabrominated diphenyl ether photoproducts towards the overall photochemical mass balance for **41** over a 60 min irradiation period in CH_3CN: **123** (○, solid line); **37** (□, dashed line); **122** (◆, dash-dot-dot line); and **116** (▲, dotted line).

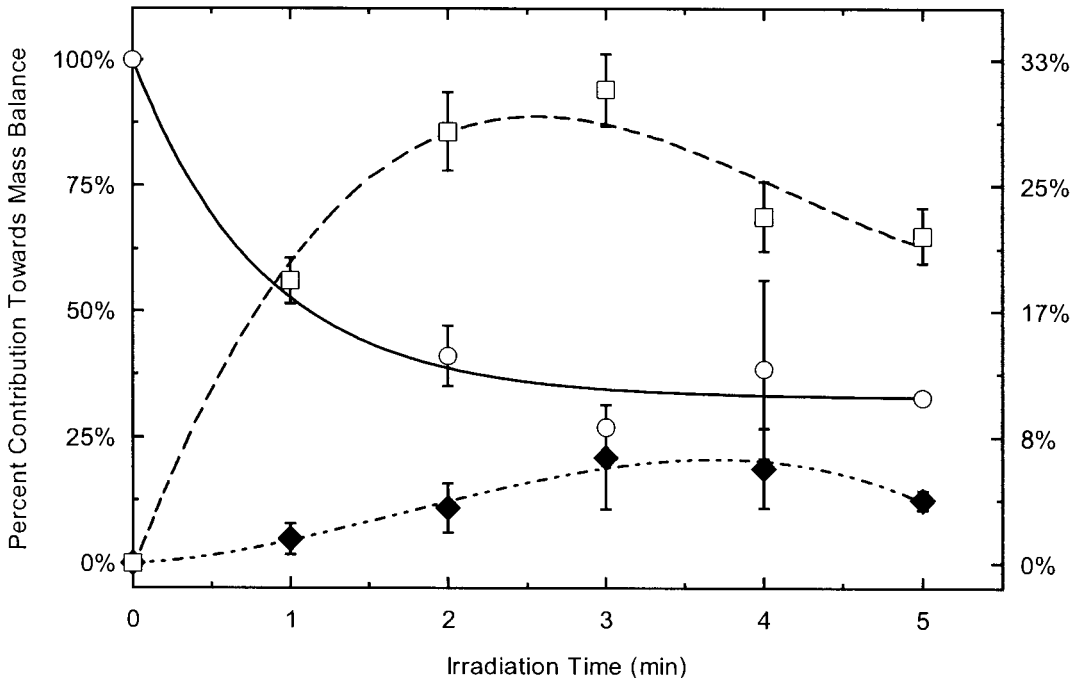

Figure 3.9. Contribution of unreacted starting material (**41**; ○, solid line), the sum of pentabrominated diphenyl ether photoproducts (□, dashed line), and the sum of tetrabrominated diphenyl ether photoproducts (◆, dash-dot-dot line) towards the overall photochemical mass balance for **41** over a 5 min irradiation period in H_2O. Values on left y-axis show contribution of starting material towards the mass balance. Values on right y-axis show contribution of photoproducts towards the mass balance. Error bars show the range of duplicate photolyses where available.

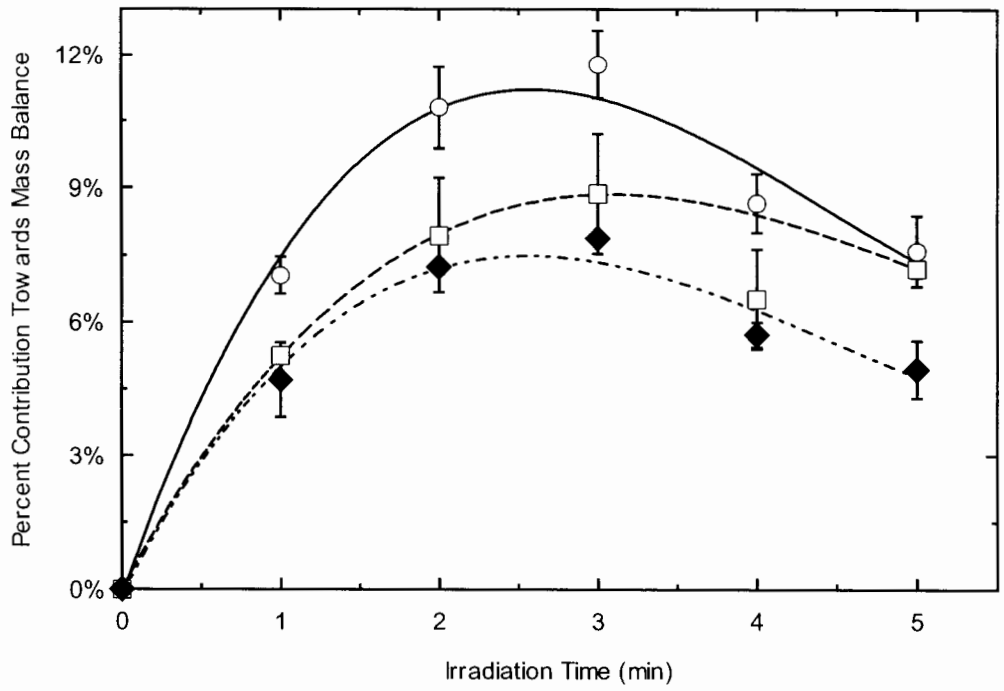

Figure 3.10. Contribution of the individual pentabrominated diphenyl ether photoproducts towards the overall photochemical mass balance for **41** over a 5 min irradiation period in H_2O: **38** (○, solid line); **121** (□, dashed line); and **132** (◆, dash-dot-dot line). Error bars show the range of duplicate photolyses where available.

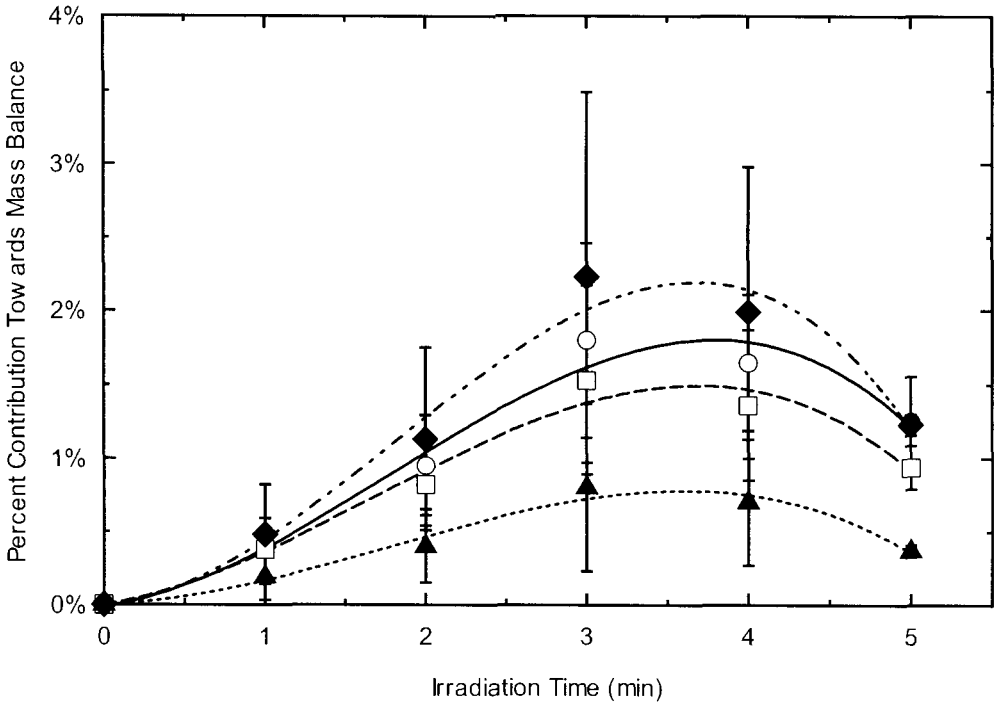

Figure 3.11. Contribution of the individual tetrabrominated diphenyl ether photoproducts towards the overall photochemical mass balance for **41** over a 60 min irradiation period in H_2O: **123** (○, solid line); **37** (□, dashed line); **122** (◆, dash-dot-dot line); and **116** (▲, dotted line).

Water appears to favor photodebromination for an as yet unidentified reason. For example, in H_2O, when ca. 60% of starting material has reacted, ca. 36% of the total mass balance (and 60% of the reacted mass balance) can be accounted for by debromination products. Conversely, in CH_3CN, debromination never accounts for more than 20% of the reacted mass balance. As well, increased water content may also be expected to favor photonucleophilic aryl-bromine substitution by water to yield hydroxylated bromodiphenylethers. The increasing contribution of the debromination pathway in H_2O – and improved mass balance – suggests this reaction is not favored, which is consistent

with the findings reported above on the aqueous photochemistry of **115** and **114** and seems to rule out heterolytic aryl-bromine bond cleavage.

In seawater, the rate of photolysis is decreased to 0.278 min^{-1} ($t_{1/2}$=2.5 min; R^2=0.997; Figure 3.12, Figure 3.13, and Figure 3.14), likely because the screening effects of dissolved and particulate organic material, and the potential binding of **41** (with its hydrophobic character as evidenced by a log K_{ow}=7.08 (*141*)) to these materials versus remaining freely dissolved in solution, both act to reduce the light exposure of starting material. However, as with the trial in H_2O, an improved mass balance is achieved in seawater, and after 1 min irradiation, ca. 95% of the total mass balance can be accounted for by starting material (ca. 80%), pentabrominated diphenyl ethers (ca. 13%), and tetrabrominated diphenyl ethers (ca. 2%). The potentially wide range of good hydrogen donating substrates in seawater (*142,143*) is a likely explanation for the preferential debromination observed in this system. Similar to that observed in distilled H_2O, concentrations of both the penta- and tetra-brominated diphenyl ether photoproducts declined after 5 min irradiation, further evidence of the increased rate of photochemical debromination in the presence of water. These results suggest that in marine systems, **41** undergoes almost exclusive and rapid photodebromination to some of the most prevalent penta- and tetra-brominated diphenyl ether congeners (e.g., **37**, **38**, **122**, and **123**) typically observed in biota, sediments, and the water column in aquatic systems (*59-62,76,144*), possibly helping to explain the environmental fate and observed congener patterns in these media.

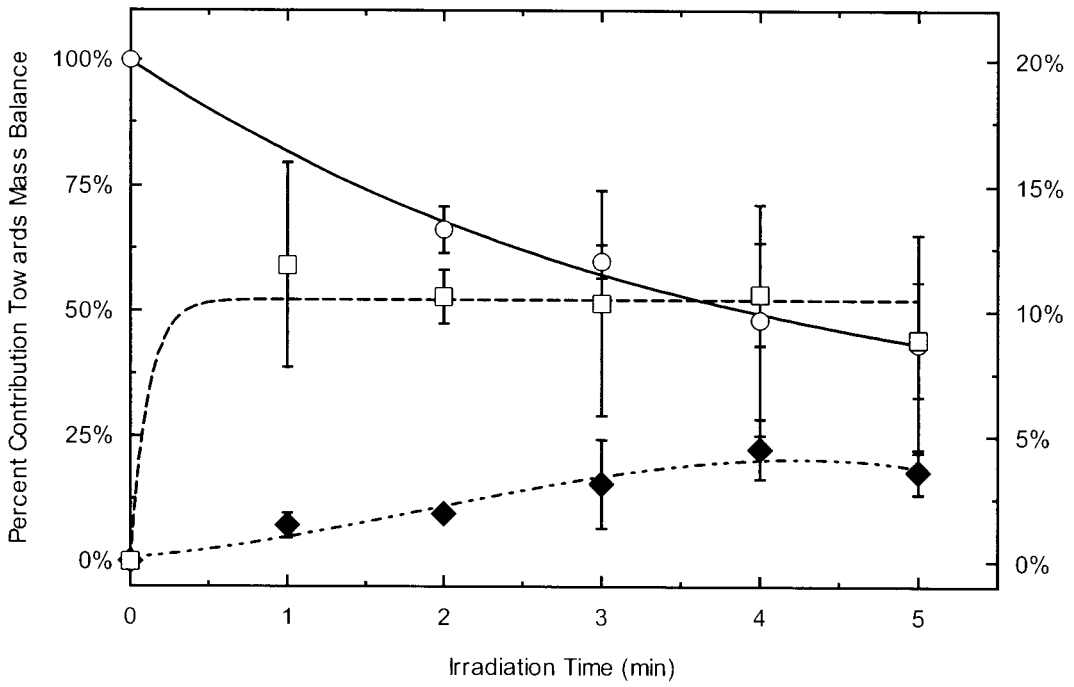

Figure 3.12. Contribution of unreacted starting material (**41**; ○, solid line), the sum of pentabrominated diphenyl ether photoproducts (□, dashed line), and the sum of tetrabrominated diphenyl ether photoproducts (◆, dash-dot-dot line) towards the overall photochemical mass balance for **41** over a 5 min irradiation period in seawater. Values on left y-axis show contribution of starting material towards the mass balance. Values on right y-axis show contribution of photoproducts towards the mass balance. Error bars show the range of duplicate photolyses where available.

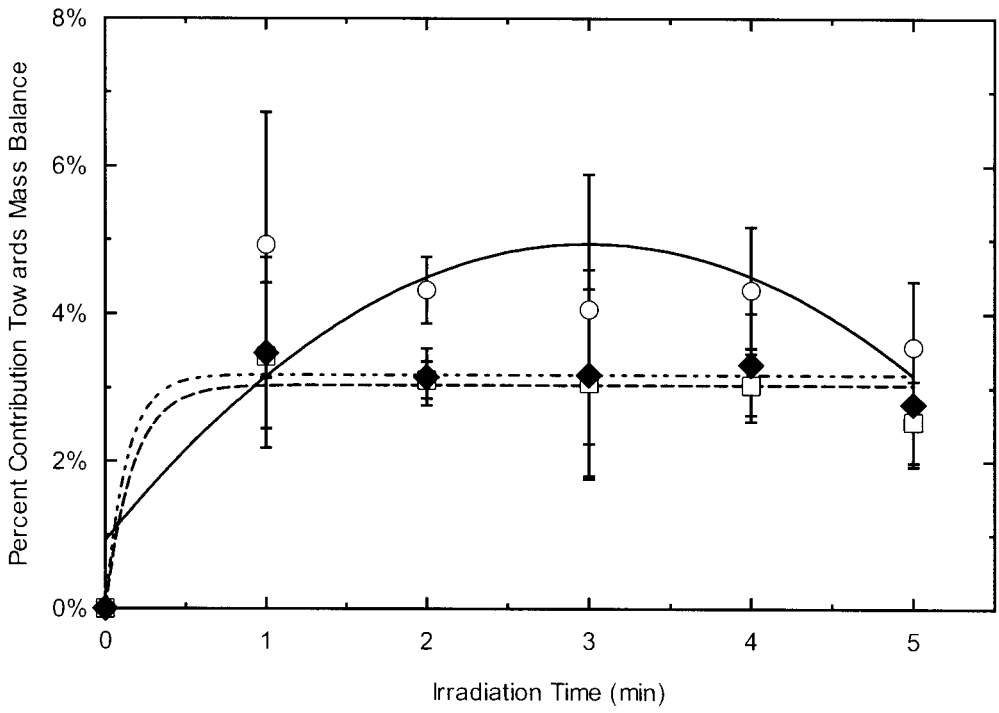

Figure 3.13. Contribution of the individual pentabrominated diphenyl ether photoproducts towards the overall photochemical mass balance for **41** over a 5 min irradiation period in seawater: **38** (○, solid line); **121** (□, dashed line); and **132** (◆, dash-dot-dot line). Error bars show the range of duplicate photolyses where available.

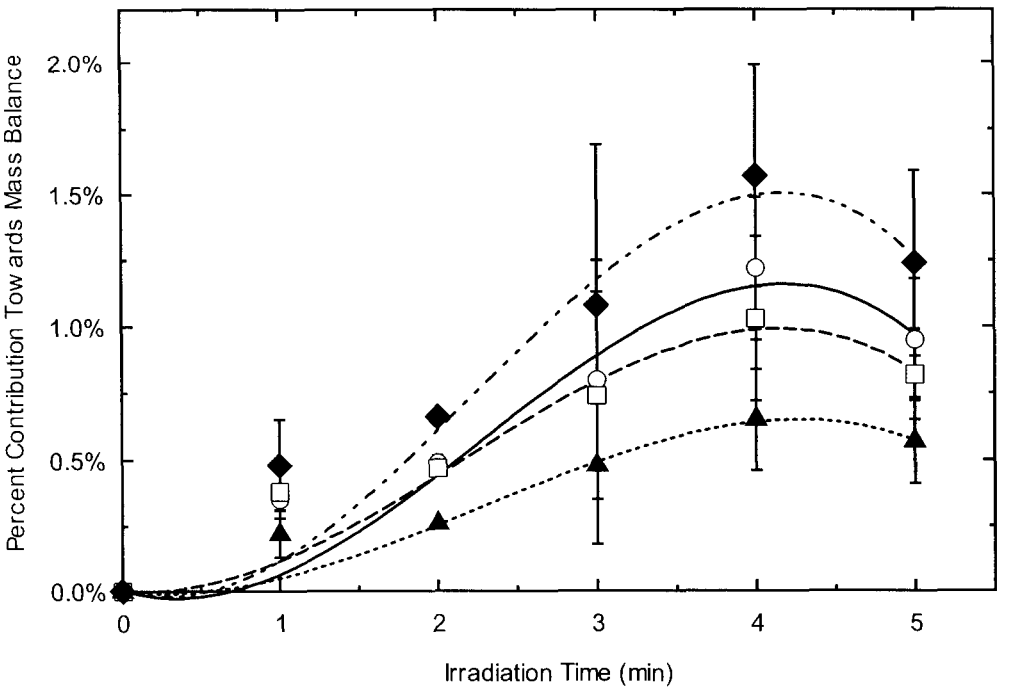

Figure 3.14. Contribution of the individual tetrabrominated diphenyl ether photoproducts towards the overall photochemical mass balance for **41** over a 60 min irradiation period in seawater: **123** (○, solid line); **37** (□, dashed line); **122** (◆, dash-dot-dot line); and 116 (▲, dotted line).

Under solar irradiation in CH_3CN, **41** decays with a rate constant of 0.790 min^{-1} ($t_{1/2}$=0.89 min; R^2=0.9997), although the mass balance for debromination products suggests a different contribution of reaction pathways than under 302 nm irradiation. Thus, while the hand-held UV lamp under which the solutions discussed above were exposed to affects photochemical reaction rates (as measured by loss of starting material) at ca. 80% the level of solar irradiation, the available solar wavelengths appear to favor non-debromination photochemical pathways. Under solar irradiation, despite the significant loss of starting material (ca. 80-85% after 3 min exposure), only ca. 0.9-1.0%

of the mass balance was observed as debromination products in the form of pentabrominated diphenyl ethers, with no evidence of subsequent tetrabrominated diphenyl ether formation.

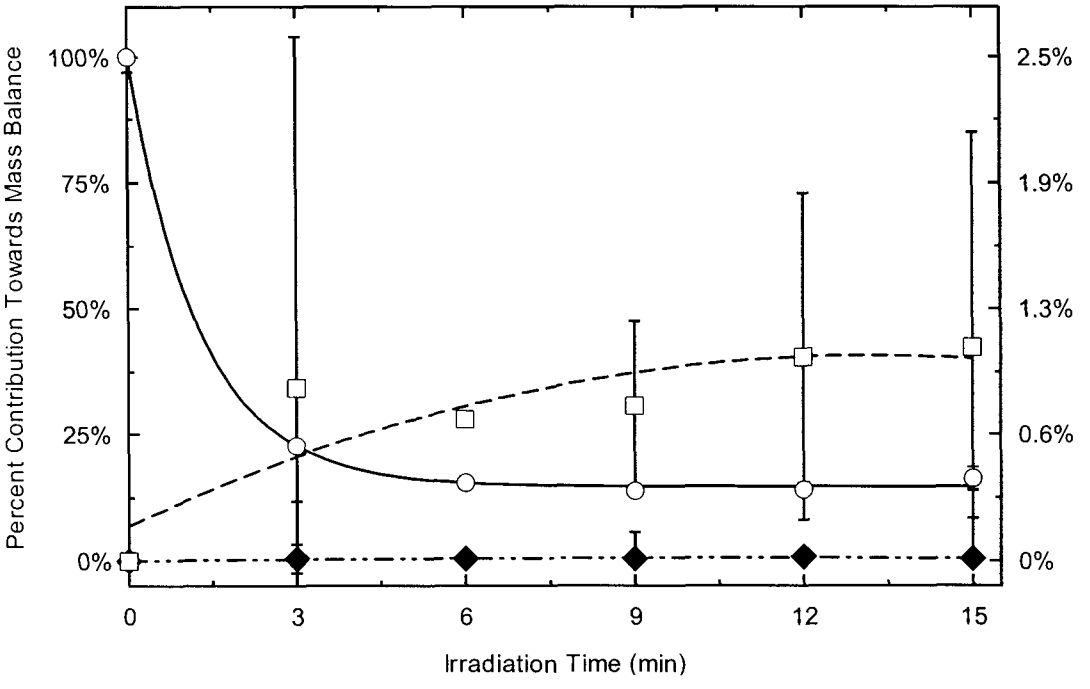

Figure 3.15. Contribution of unreacted starting material (**41**; ○, solid line), the sum of pentabrominated diphenyl ether photoproducts (□, dashed line), and the sum of tetrabrominated diphenyl ether photoproducts (◆, dash-dot-dot line) towards the overall photochemical mass balance for **41** over a 15 min irradiation period in CH_3CN under solar illumination. Values on left y-axis show contribution of starting material towards the mass balance. Values on right y-axis show contribution of photoproducts towards the mass balance. Error bars show the range of duplicate photolyses where available.

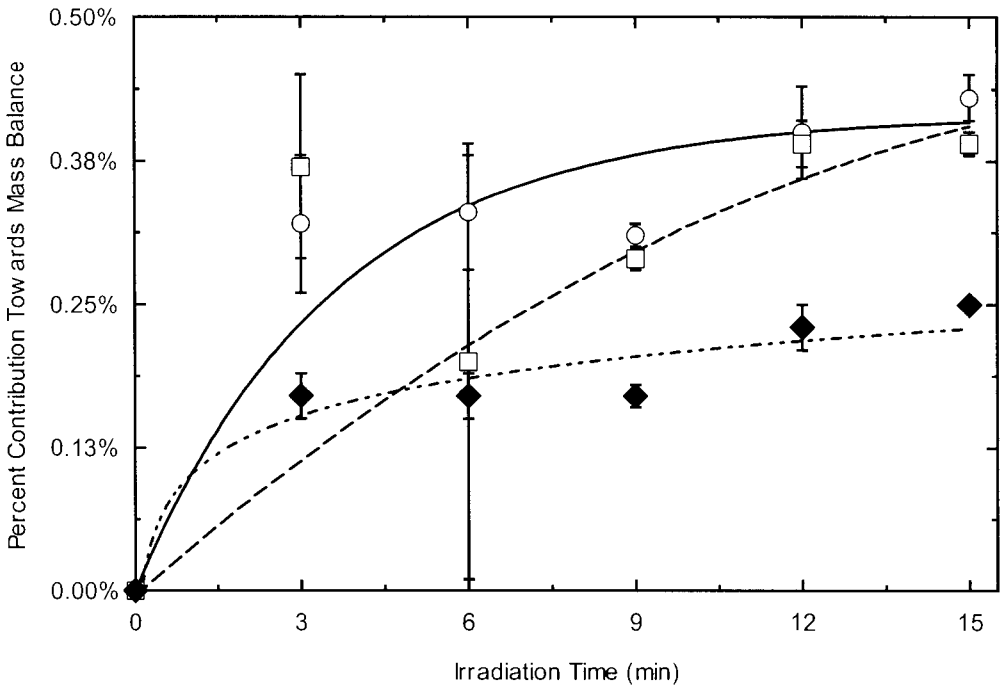

Figure 3.16. Contribution of the individual pentabrominated diphenyl ether photoproducts towards the overall photochemical mass balance for **41** over a 15 min irradiation period in CH_3CN under solar illumination: **38** (○, solid line); **121** (□, dashed line); and **132** (◆, dash-dot-dot line). Error bars show the range of duplicate photolyses where available.

3.2.2.2 Photodebromination Product Distributions.

In CH_3CN (both under 302 nm and solar irradiation), H_2O, and seawater, photodebromination of **41** results in formation of **38**, **121**, and **132**. While the relative contribution of each of these three congeners is solvent and wavelength dependent, in all cases the order of contribution is **38**>**121**>**132**. To assist in developing predictive tools for understanding the environment fate of brominated diphenyl ethers and similar halogenated aromatics, the potential for computationally modeled ground-state structural features to explain this product distribution pattern was investigated. MNDO-PM3

calculated aryl-bromine bond lengths were found to be inversely related to the observed debromination preference. For similar covalent bonds, shorter bond lengths can be used as a surrogate for higher bond strengths. With regard to **41**, the relative bond strength order was calculated to be *meta*<*para*≤*ortho*, and thus preferential debromination in the order **38**>**121**>**132** was expected and observed (Figure 3.17). Regioselective excited-state *meta* debromination could also be rationalized based on the well-known "*meta* effect" in organic photochemistry (*42*); however, this approach would not help to explain the slight preference for debromination at the *para* position versus that of the *ortho*.

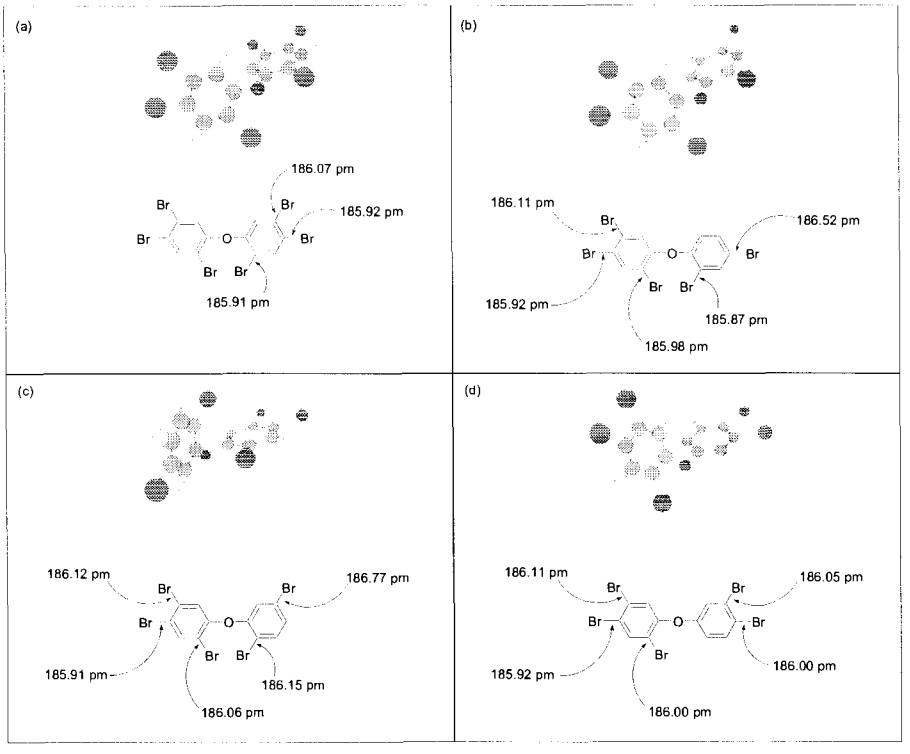

Figure 3.17. MOPAC-PM3 calculated ground-state geometries and bond lengths for (a) **41** and its major primary photodebromination products: (b) **38**, (c) **121**, and (d) **132**.

For the three primary pentabrominated photoproducts, the modeling is more complex as more than one pentabrominated diphenyl ether can subsequently produce an individual tetrabrominated diphenyl ether through a photochemical debromination process, and only four tetrabrominated diphenyl ether congeners were observed despite the possibility of forming nine (Scheme 3.8, Scheme 3.9, and Scheme 3.10).

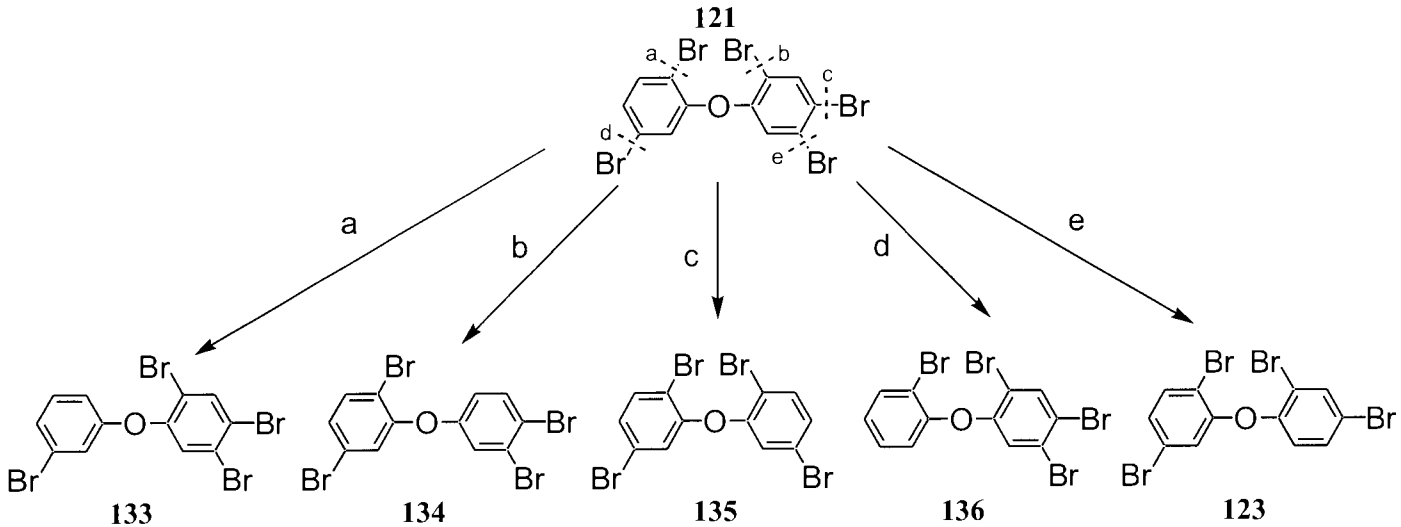

Scheme 3.8

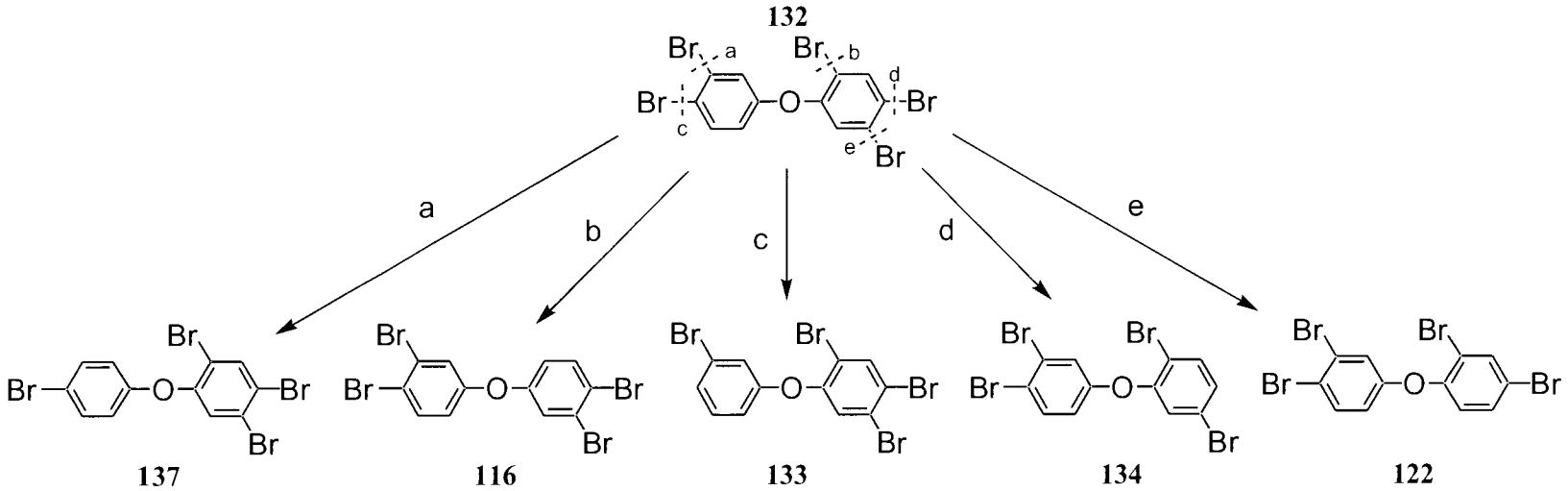

Scheme 3.9

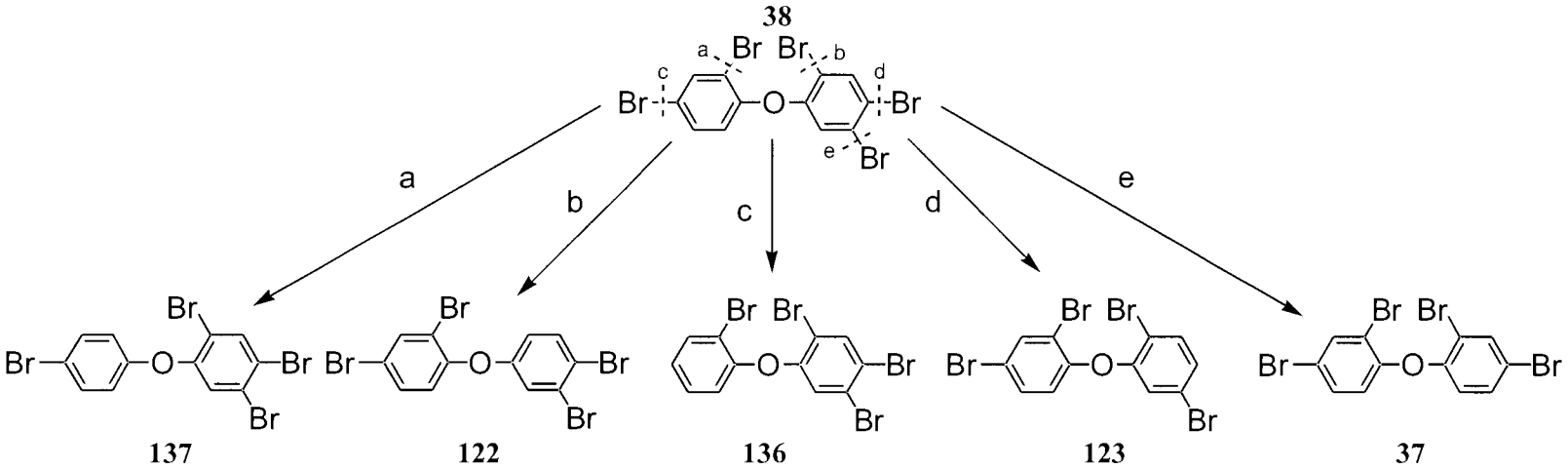

Scheme 3.10

At present, the reason these other five debromination products were not photochemically formed is not clear. In all solvents except seawater, the order of contribution is **123**>**37**≈**122**>**116**, while in seawater the order is **37**>**123**>**122**>**116**. For **38**, **121**, and **132**, the bond lengths predict debromination profiles in the following respective orders: **136**>**37**>**122**>**123**>**137**; **136**>**133**>**123**>**134**>**135**; and **122**>**137**>**116**≈**133**>**134**, respectively. Since **123** may arise from both **38** and **121**, and it is the only observed product from **121**, **123** is predicted as the major secondary debromination product. As **122** is the major predicted product from **132**, as well as a product from **38**, it is predicted as the next most abundant secondary debromination product. **37** is the major predicted product from **38**, whereas **116** is predicted to be the fourth most abundant product from **132**, and thus, we expect a relative order of **37**>**116**. This gives the predicted order of **123**>**122**>**37**>**116**, which matches the observed order in CH_3CN and H_2O.

In seawater, the assessment may need to be refined as the larger contribution of **37** over **123** from **38** may outweigh the additional **123** contribution from **121**. Since **37** is the major tetrabrominated diphenyl ether congener in environmental samples and generally dominates **123** (*59-62,71-73,76*), this debromination regioselectivity may help explain observed patterns in media where labile hydrogen atom sources are typically abundant (e.g., lipids in biota, organic matter in sediments and the water column). Although these calculations were conducted for the ground state gas-phase geometries of **41** and its primary photodebromination products, the predictive nature of these findings suggest the ground-state electronic configuration of these brominated diphenyl ethers is a

good model for the excited state.The empirical correlations offer a potential predictive tool in assessing the most likely photodegradation patterns of halogenated aromatics, and may potentially be applied to photodehalogenation of a wide range of contaminant substrates.

3.2.2.3 Photochemical Formation of Brominated Dibenzofurans and 2-Hydroxybiphenyls

In an additional attempt to complete the mass balance for the CH_3CN and H_2O systems, a 3 mL solution of 1.3×10^{-9} M **41** in freshly distilled CH_3CN was irradiated for 1 min at 302 nm and analyzed by full-scan HRGC-HRMS for potential analytes other than brominated diphenyl ethers. The investigations revealed the presence of eleven compounds for which analytical standards were not available: one pentabrominated dibenzofuran (**138**), one tetrabrominated dibenzofuran (**139**), two tribrominated dibenzofurans (**140**), three dibrominated dibenzofurans (**141**), one monobrominated dibenzofuran (**142**), and three tetrabromo-2-hydroxybiphenyls (**143**).

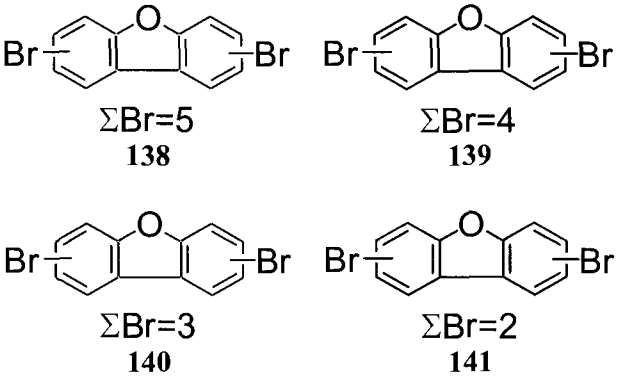

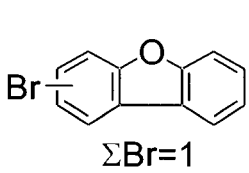

142

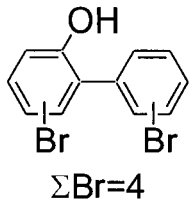

143

The brominated dibenzofuran analytes accounted for ca. 30% of the reacted mass balance. Similar results have been reported for the photodebromination products of decabromodiphenyl ether (**45**) (i.e., formation of brominated dibenzofurans from the hexabromodiphenyl ether photodebromination products of **45**) (*84*). The identity of the pentabromodibenzofuran primary photoproduct can be assigned to **144**, as no other pentabrominated dibenzofuran congeners are likely to be formed by photochemical means from **41**. With the absence of **42** for which an analytical standard was available, there appears to be no formation of the highly toxic 2,3,7,8-substituted bromodibenzofurans through either the primary or seconday photolysis of **41**.

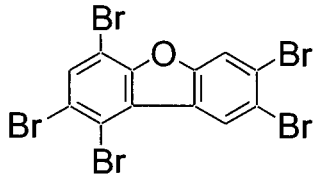

144

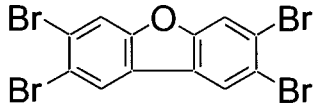

42

There have been previous reports of brominated dibenzofuran formation from hexa- through deca-brominated diphenyl ethers (*82,84*), but the identities of individual brominated dibenzofuran congeners were not provided in either study. The analogous photochemical formation of chlorinated dibenzofurans from chlorinated diphenyl ethers in ca. 10% yield was suggested to occur via the triplet state (*145*), and similar findings were also reported for hydroxychlorodiphenyl ethers (*146*). In addition, the work of

Watanabe *et al.* on decabromodiphenyl ether photochemistry in 8:1:1 hexane: benzene:acetone seems to confirm this for brominated diphenyl ethers (*84*). The heavy-atom effect (*147*) – where the efficiency of triplet state photochemical reactions is enhanced through the addition of higher molecular weight substituents – would also tend to favor the preferential photochemical formation of brominated dibenzofurans from brominated diphenyl ethers compared to the corresponding reaction for chlorinated diphenyl ethers. Thus, the ca. 30% yield of brominated dibenzofurans observed for the photolysis of **41** is consistent with a triplet state reaction providing higher yields of these products versus the chlorinated counterparts.

In addition to the brominated dibenzofuran and tetrabrominated 2-hydroxybiphenyl analytes, the same penta- and tetra-brominated diphenyl ether photoproducts as discussed above for the 0-5 min photolyses in dry CH_3CN were observed at levels approximately equal (i.e. 11% and 0.5% of the mass balance) to the 1 min duplicate photolyses for these previous trials. At this timescale, tetrabrominated 2-hydroxybiphenyls and mono- through penta-brominated dibenzofurans make up ca. 10% and 15% of the total mass balance, respectively. Together with unreacted starting material (ca. 51%) and debromination products (ca. 12%), approximately 88% of the mass balance can be accounted for (Figure 3.18). Of note is the apparent absence of the primary 2',3,4',5,5',6-2-hexabromo-2-hydroxybiphenyl product (**145**) expected from a primary photo-Fries rearrangement of **41** (Scheme 3.11), and the absence of any of its expected secondary pentabrominated 2-hydroxybiphenyl photodebromination products (**146**) that would give rise to the observed tetrabrominated 2-hydroxybiphenyls (**143**).

The absence of significant quantities of tetrabrominated diphenyl ethers (which could also photochemically rearrange to **143**) at this analytical timescale (1 min) suggests that rapid photochemically induced debromination of **145** and **146** may be the most likely source of **143**. Mono- through tri- brominated-2-hydroxybiphenyls were also not observed, although their presence may have been masked through co-elution with other analytes or impurities; these analytes could potentially account for the remaining 12% of the photochemical mass balance.

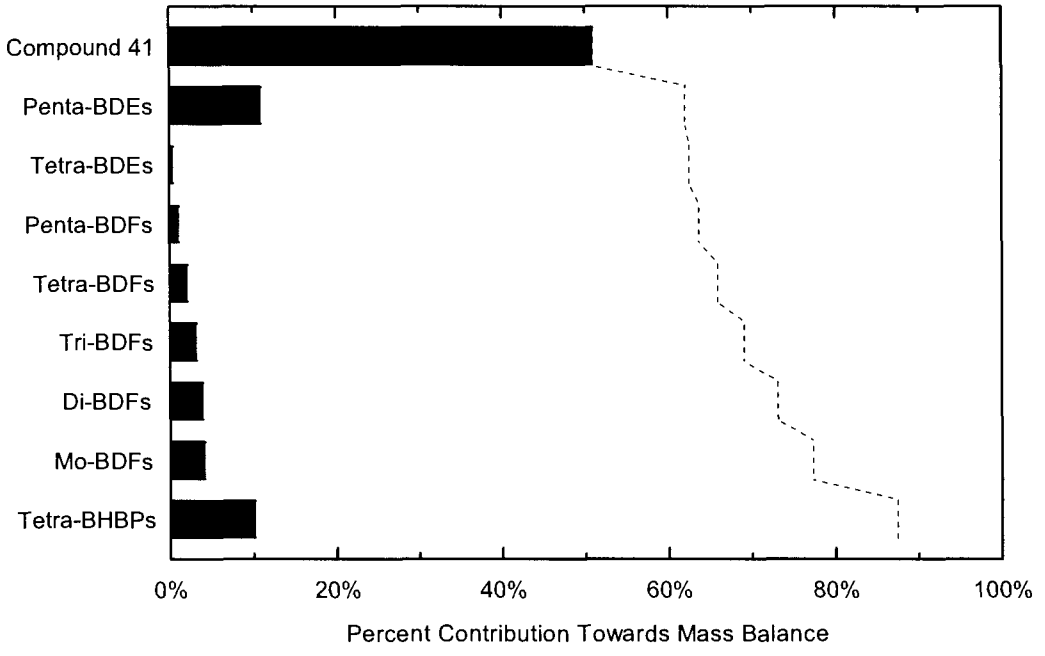

Figure 3.18. Contributions towards the photochemical mass balance of **41** after 1 min irradiation in dry CH_3CN at 302 nm by penta- and tetra-brominated diphenyl ethers (Penta- and Tetra-BDEs), penta- through tri-brominated dibenzofurans (Penta-BDFs, Tetra-BDFs, and Tri-BDFs), and tetrabrominated hydroxybiphenyls (Tetra-BHBPs)

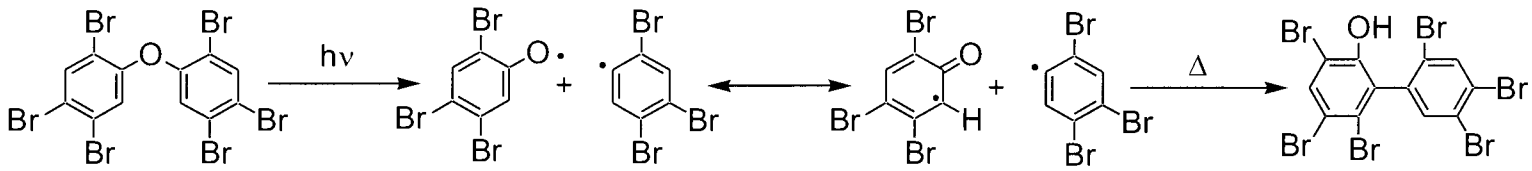

41 **145**

Scheme 3.11

That aryl-ether cleavage may be an important pathway in the photochemical fate of brominated diphenyl ethers has been previously suggested for **45**. Watanabe and Tatsukawa reported the production of tetra- and penta-bromobenzenes during the photolysis of **45**, showing that aryl-ether cleavage takes place from starting material (*84*). However, in this previous study, the use of hexane as the dominant solvent likely favors rapid hydrogen abstraction from any photogenerated phenoxyl and aryl radicals over potential reaction with dissolved oxygen (in the case of aryl radicals) or radical coupling to give hydroxylated biphenyls (as under the experimental conditions presented here). The apparent absence of brominated biphenyls and dihydroxybiphenyls from bimolecular radical coupling (from different molecules of starting material) is likely due to the low concentrations used in the present study (ca. 10^{-9} M), which would favor preferential hydrogen abstraction from either CH_3CN, impurities in the H_2O, or a variety of natural products in the seawater – as well as the reaction of dissolved oxygen with aryl radicals to yield bromophenols.

With the knowledge that brominated dibenzofurans may be formed at short time-scales through the photolysis of **41**, the samples described above that were irradiated over a 5 min period in three solvent systems (CH_3CN, H_2O, and seawater) and two light sources (302 nm and solar illumination) were reanalyzed via HRGC-HRMS in the hopes of completing the mass balances. For all samples, levels of brominated dibenzofurans were at, or near, detection limits for all potential analytes. The apparent explanation for the absence of these analytes even at the 1 min timescale in the previous CH_3CN trials is

likely due to the observed effects of water content discussed above. For the previous trials, HPLC grade CH_3CN was used without distillation, and the trace quantities of H_2O known to be present in this solvent may have resulted in more rapid kinetics than in the dry CH_3CN solvent used to first identify the presence of brominated dibenzofurans and tetrabrominated 2-hydroxybiphenyls.

The advanced debromination of brominated dibenzofurans and brominated 2-hydroxybiphenyls at the 1 min timescale in dry CH_3CN – even while primary debromination products are still increasing in concentration – suggests that only a moderate degree of enhanced photodebromination due to the presence of water would be required for these analytes to completely debrominate before the first analytical timeframe in "wet" CH_3CN (1 min irradiation). A previous report on the photochemistry of **45** suggested a similarly rapid bromodibenzofuran photodebromination pathway (*81*). In addition, brominated dibenzofurans are known to have rapid debromination kinetics with high quantum yields and greater molar extinction coefficients at wavelengths >280 nm than the corresponding homologue group of brominated diphenyl ethers (*148,149*). Furthermore, hydroxylic solvents (or their presence as cosolvents) are known to favor the photo-Fries rearrangement (*150*), suggesting that the trace amounts of water present in CH_3CN may also play an important role in defining the photoproduct distribution. Because water thus favors the photo-Fries rearrangement and appears to increase the photodebromination kinetics of brominated dibenzofurans and brominated hydroxybiphenyl, it is thus not surprising that neither brominated dibenzofurans nor brominated hydroxybiphenyls were not observed in the re-analysis of these earlier trials.

The promotion of brominated diphenyl conversion into brominated dibenzofurans and hydroxybiphenyls by water, and then the water enhancement of subsequent photodebromination for these compounds, would lead to an overall more rapid photodegration of starting material and the primary and subsequent photoproducts, making the mass balance more difficult to complete.

An additional complexity in elucidating the primary and subsequent photochemistry of **41** is the "interconnectedness" of the photochemical pathways leading to the debrominated diphenyl ether, brominated dibenzofuran, and brominated 2-hydroxybiphenyl products (Scheme 3.12). Di-*ortho* substituted di- through hexa-brominated diphenyl ethers may form the corresponding brominated dibenzofurans through loss of 2Br. As well, loss of HBr from mono-*ortho* substituted di- through hexa-brominated diphenyl ethers may also lead to production of the corresponding brominated dibenzofurans. That **144** is formed from **41**, while **42** is not, suggests that photochemical loss of HBr may be preferred over loss of 2Br. Similarly, an *ortho*-substituted brominated 2-hydroxybiphenyl may also formally lose HBr to give the corresponding brominated dibenzofuran, with these *ortho*-substituted brominated 2-hydroxybiphenyls formed via the *ortho* photo-Fries rearrangement of a corresponding brominated diphenyl ether. Of note is the lack of photochemical or thermal reversibility of these pathways. As discussed above with regard to the dibenzo[1,4]dioxin photochemistry, the dibenzofuran substructure is photochemically unreactive such that aryl-oxygen cleavage in a dibenzofuran to give a 2-hydroxybiphenyl does not appear to occur. Furthermore, it

is known that the 2-hydroxybiphenyl substructure does not undergo aryl-aryl cleavage (and subsequent rearrangement to give diphenylether) (*151*).

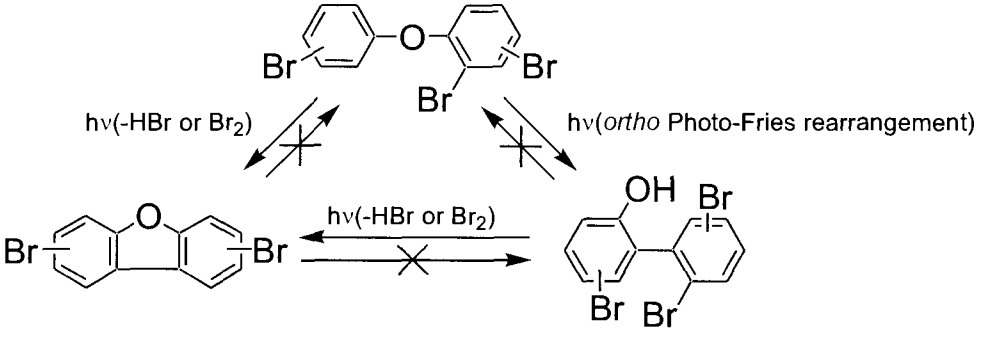

Scheme 3.12

Thus, it appears as though the pathways leading to the photochemical production of brominated dibenzofurans and brominated 2-hydroxybiphenyls from **41** involve rapid processes that occur more rapidly than photodebromination. In addition, the brominated dibenzofuran and hydroxybiphenyl pathways may account for the majority of the photochemical mass balance in poor hydrogen donating organic solvents and in aqueous systems without good hydrogen donating "impurities". However, in natural aquatic systems – perhaps with the exception of highly oligotrophic environments – the rapid water-assisted rate of photodebromination of starting material ($t_{½}$ ca. 2.5 min) and presence of labile hydrogen atom donors suggests that almost exclusive photodebromination of higher brominated diphenyl ethers such as **41** may play a significant role in their environmental fate. In aqueous systems without labile hydrogen atom donors (as approximated by a CH_3CN:H_2O solution, and in contrast to seawater), recombination of the aryl and bromine atom radicals may occur in preference to radical pair separation and hydrogen atom abstraction. This type of system may promote the

competing aryl-ether bond cleavage pathway, resulting in the formation of brominated hydroxybiphenyls (via the photo-Fries rearrangement), and may promote brominated dibenzofuran formation through the encouragement of an intramolecular hydrogen abstraction by a bromine radical.

3.3 Proposed Mechanism

The following photochemically initiated mechanism for the observed photochemistry of **115** and **114** is proposed. Following absorption of a photon by **115**, aryl-bromine bond homolysis takes place to give the *para* bromophenoxy aryl radical **147**, which subsequently abstracts a hydrogen atom from the organic solvent/cosolvent to give **114** (Scheme 3.13). Following absorption of a photon by **114**, aryl-bromine bond homolysis takes places to give the parabromophenoxy aryl radical **148**, which subsequently abstracts a hydrogen atom from the organic solvent/cosolvent to give **44** (Scheme 3.14).

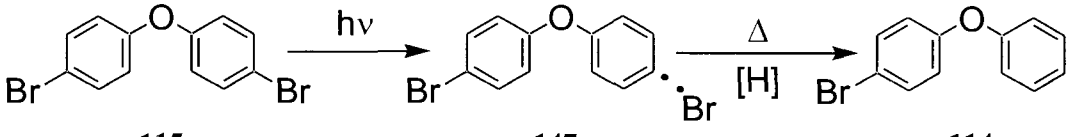

115 **147** **114**

Scheme 3.13

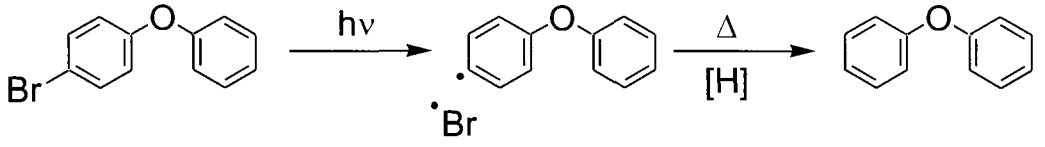

114 **148** **44**

Scheme 3.14

The following three general photochemically initiated mechanisms for the observed primary photochemistry of **41** are proposed to occur in approximately equal

yield to give the array of photoproducts shown in Scheme 3.15: (1) following absorption of a photon, **41** undergoes homolytic aryl-bromine bond cleavage at either of the brominated position to generate radicals **149**, **150**, and **151** which subsequently abstract a hydrogen atom from the organic solvent or impurities in aqueous solution to give **132**, **121**, and **38**, respectively (Scheme 3.16, Scheme 3.17, and Scheme 3.18, respectively) – subsequent photochemical debromination and/or participation in pathways (2) and/or (3) leads to complex secondary and consequent photochemistry; (2) following absorption of a photon, **41** undergoes homolytic aryl-ether bond cleavage to generate radicals **152** and **153**, which subsequently recombine in an *ortho* configuration to yield **145** (Scheme 3.19) – subsequent photochemical debromination results in the formation of mono- through tetra-brominated 2-hydroxybiphenyls; and (3) following absorption of a photon, **41** undergoes homolytic aryl-bromine bond cleavage at an *ortho* position to generate radical **149**, which subsequently attacks the *ortho* position of the hydrogenated site on the other aryl ring to yield radical **154**, after which the liberated bromine radical abstracts the *ortho* hydrogen atom on the opposite ring to give **144** (Scheme 3.20) – subsequent photochemical debromination results in the formation of mono- through tetra-brominated dibenzofurans.

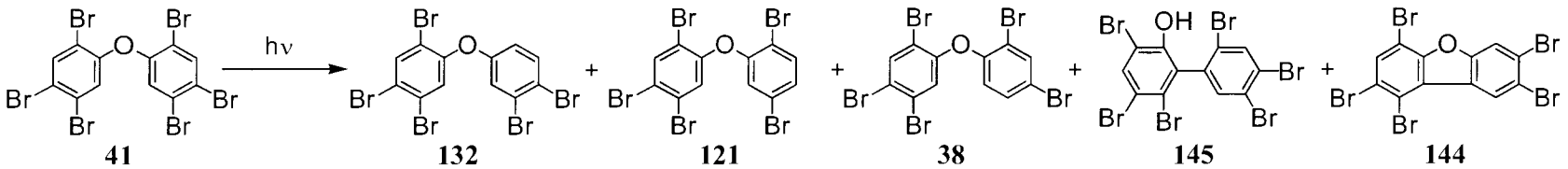

Scheme 3.15

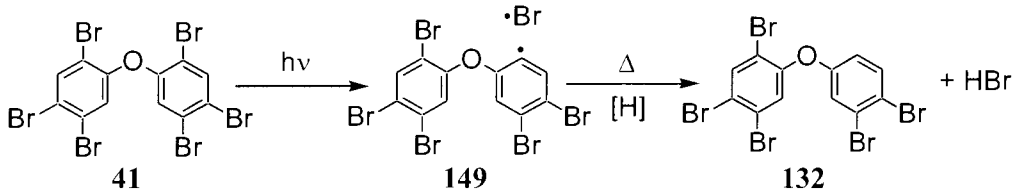

Scheme 3.16

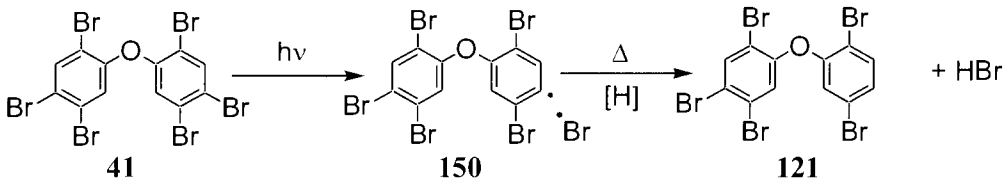

Scheme 3.17

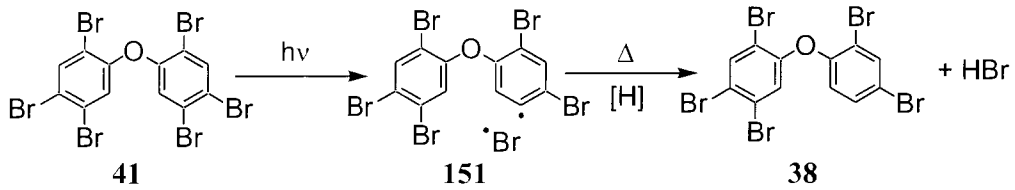

41 **151** **38**

Scheme 3.18

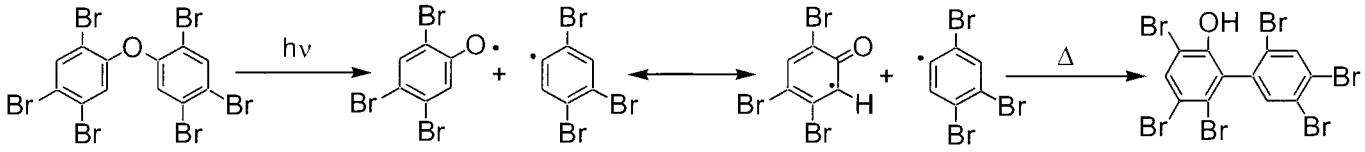

41 **152** **153** **152** **153** **145**

Scheme 3.19

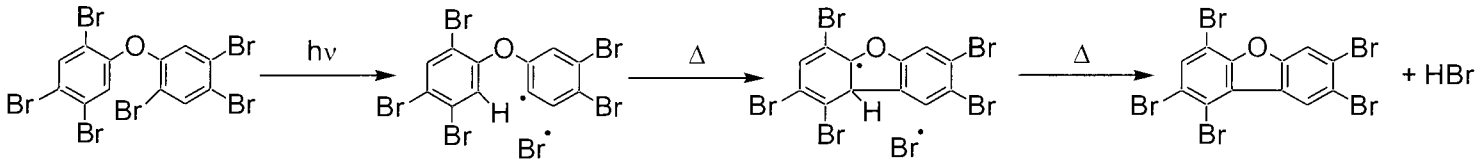

41 **149** **154** **144**

Scheme 3.20

3.4 Conclusions

These results indicate that brominated diphenyl ethers with 1 or 2 bromine substituents in the *para* position will only undergo photochemically induced aryl-bromine bond homolysis in aqueous or organic solvents, followed by hydrogen abstraction from organic solvents or similar impurities in natural aquatic systems. Mono- and di-brominated diphenyl ethers having a bromine substituent in the ortho position relative to the ether linkage may undergo an intramolecular attack to yield a brominated dibenzofuran following intial photochemical aryl bromine homolytic bond cleavage. In addition, the presence of *ortho* (and/or *meta*) bromine substituents on these lower brominated diphenyl ethers may promote photochemical aryl-ether bond cleavage that is otherwise not observed where only para bromine substituents are present. Further work is necessary in this area of study for a more complete understanding into the range of potential photochemical processes the lower brominated diphenyl ethers may participate in.

By contrast, the observed formation of brominated dibenzofurans and 2-hydroxybiphenyls from the photolysis of a model hexabrominated diphenyl ether (**41**), along with literature evidence showing similar complex reactivity for the hepta- through deca-brominated diphenyl ethers, suggests that brominated diphenyl ethers with >6 bromine substituents will undergo both photochemically induced aryl-ether and aryl-bromine bond homolysis in organic solvents. Ground state semi-empirical molecular

modeling calculations also appear to offer the potential to reliably predict the debromination photoproduct distribution of the higher brominated diphenyl ethers.

When a brominated diphenyl ether starting material has a bromine substituent in the *ortho* position relative to the ether linkage, photochemical aryl-bond homolysis can lead to the production of brominated dibenzofurans. In this regard, *ortho*-bromine bond homolysis followed by intramolecular radical abstraction during the irradiation of **41** appears to result in preferential overall loss of HBr (and formation of **144**) rather than loss of 2Br (which would yield the highly toxic 2,3,7,8-tetrabromodibenzofuran (**42**) as a photoproduct). In aqueous systems with labile hydrogen atom sources (e.g., seawater), the findings further suggest that brominated diphenyl ethers with >6 bromine substituents will dominantly undergo photochemically induced aryl-bromine bond homolysis, followed by hydrogen abstraction from organic cosolvents or compounds in natural aquatic systems. The almost exclusive and rapid photodebromination of **41** in seawater produced some of the most prevalent penta- and tetra-brominated diphenyl ether congeners (e.g., **37**, **38**, **122**, and **123**) typically observed in biota, sediments, and the water column. The results presented herehelp to explain the environmental fate (e.g., photochemical transformations to brominated hydroxybiphenyls and dibenzofurans) and observed congener patterns (via photoreduction debromination) of this contaminant class in aquatic systems.

CHAPTER 4 - EXPERIMENTAL

4.1 General

NMR spectra were recorded on either a Bruker AC 250 (250 MHz), AC 300 (300 MHz), or a Bruker AVANCE 500 (500 MHz) instrument (Bruker BioSpin Corporation) using deuterium oxide (D_2O), chloroform-*d* ($CDCl_3$), acetone-d_6 ($(CD_3)_2CO$), or acetonitrile-d_3 (CD_3CN) as solvents. Chemical shifts are reported in parts-per-million (ppm) downfield from tetramethylsilane at 0 ppm (determined from the residual solvent signal). Splitting patterns are reported as s (singlet), d (doublet), t (triplet), q (quartet), and m (multiplet). Mass spectra obtained at the University of Victoria were determined on either a Finnegan 3300 (low-resolution chemical ionization (CI)) or a Kratos Concept 1H (low-resolution (LR) or high-resolution (HR) using electron impact (EI) ionization). High-resolution gas-chromatography (HRGC) coupled to high-resolution EI mass spectrometry (HRMS) was performed at the Institute of Ocean Sciences on a Micromass VG-Autospec mass spectrometer equipped with a Hewlett Packard model 5890 series II gas chromatograph and a CTC Analytics CTCA200S autosampler. Melting points were determined on a Reichart melting point apparatus and are presented in uncorrected form. Transient UV-Vis spectra and kinetic measurements at the sub-second timescale were recorded using nanosecond laser flash photolysis (LFP) with excitation by either a Spectra-Physics GCR-12 YAG laser (λ_{ex}=266 nm) or a Lumonics EX-510 excimer laser (λ_{ex}=308 nm). Steady-state UV-Vis spectra and kinetic measurements at the supra-second timescale were recorded using a Varian Cary 50 spectrophotometer. Preparative thin layer chromatography (prep-TLC) was performed using 1000 μm silica gel plates

from Analtech and the solvent systems listed for each experiment. Analytical TLC was carried out on Machery-Nagel Polygram SIL/UV_{254} silica gel plates. In cases where samples did not readily dissolve, sonication was performed using a Bransonic 220 ultrasonic cleaner. pH measurements were taken using an Accumet Research AR25 Dual Channel pH/Ion meter.

4.2 Materials

4.2.1 Common Laboratory Reagents

HPLC grade acetonitrile (CH_3CN) was freshly distilled over calcium hydride (CaH_2) where desired. Reagent grade dichloromethane (CH_2Cl_2) was distilled over boiling chips prior to use. Spectral grades of 95% and 100% ethanol, methanol, 2-propanol, cyclohexane, and hexane were used as received. Reagent grades of anhydrous tetrahydrofuran (THF), diethyl ether, 1-propanol, 1-butanol, *t*-butanol, ethyl acetate, toluene, benzene, and chloroform ($CHCl_3$) were used as received. Sodium chloride (NaCl), magnesium sulfate ($MgSO_4$), sodium sulfate (Na_2SO_4), and methyl iodide (CH_3I) were purchased from Aldrich and used as received.

4.2.2 Commercially Available Materials

4.2.2.1 General

3-Chlorophenol (**157**), 4-chlorophenol (**158**), 3,4-dichlorophenol (**159**), 2,2'-dihydroxybiphenyl **10**, 2-phenoxyphenol (**12**) , and diphenyl ether (**44**) were purchased from Aldrich and recrystallized (or distilled if a liquid at room temperature) prior to use to obtain >99% purity as determined by GC and ^1H NMR. 1-Hydroxybenzofuran (**48**)

was available in-house as part of a previous study on dibenzo[1,4]dioxin photochemistry (*40*).

4.2.2.2 Dibenzo[1,4]Dioxin Systems

1-Monochlorodibenzo[1,4]dioxin (**46**), 2-monochlorodibenzo[1,4]dioxin (**30**), 2,3-dichlorodibenzo[1,4]dioxin (**59**), 2,7-dichlorodibenzo[1,4]dioxin (**60**), 2,8-dichlorodibenzo[1,4]dioxin (**61**), 2,3,7-trichlorodibenzo[1,4]dioxin (**62**), 2,3,7,8-tetrachlorodibenzo[1,4]dioxin (**3**), and 1,2,3,4,6,7,8,9-octachlorodibenzo[1,4]dioxin (**29**) were purchased from AccuStandard Inc. and Cambridge Isotope Laboratories and certified at >98% purity by GC-MS. No impurities were evident by mp, ^{1}H NMR ($CDCl_3$) or GC.

4.2.2.3 2,2'-Dihydroxybiphenyl Systems

4,4',5,5'-Tetrachloro-2,2'-Dihydroxybiphenyl (58). 4,4',5,5'-Tetrachloro-2,2'-dihydroxybiphenyl was obtained as a generous contribution from Drs. A. Konstantinov and N. Bunce in the Department of Chemistry and Biochemistry at the University of Guelph. Spectroscopic characterization of this compound and certification of its purity is presented elsewhere (*54*).

4.2.2.4 Diphenyl Ether Systems

4-Bromodiphenyl ether (**114**; 10 g) and 4,4'-dibromodiphenyl ether (**115**; 5 g) were purchased from Aldrich and used as received. No impurities were evident by mp, ^{1}H NMR ($CDCl_3$) or GC. Native analytical standards of 2,2',4,5'-tetrabromodiphenyl ether (**123**), 2,2',4,4'-tetrabromodiphenyl ether (**37**), 2,3',4,4'-tetrabromodiphenyl ether (**122**), 3,3',4,4'-tetrabromodiphenyl ether (**116**), 2,2',4,5,5'-pentabromodiphenyl ether

(**121**), 2,2',4,4',5-pentabromodiphenyl ether (**38**) and 2,2',4,4',5,5'-hexabromodiphenyl ether (**41**; 60 μg in 1.2 mL nonane) were purchased from Cambridge Isotope Laboratories and were used as received. ^{13}C-labelled analytical standards containing 5 μg/mL each of 2,2',4,4'-tetrabromodiphenyl ether (**37**), 2,2',4,4',5-pentabromodiphenyl ether (**38**), 2,4,4'-tribromodiphenyl ether (**118**), 2,2',4,4',5,6'-hexabromodiphenyl ether (**119**), 2,2',3,4,4',5',6-heptabromodiphenyl ether (**120**), and 2,2',4,4',5,5'-hexabromodiphenyl ether (**41**) were purchased from Wellington Laboratories and were used as received. ^{13}C-labelled analytical standards containing 100 ng/mL of 3,3',4,4'-tetrabromodiphenyl ether (**116**) and 150 ng/mL of ^{13}C-labelled 3,3',4,4',5-pentabromodiphenyl ether (**117**) were purchased from Cambridge Isotope Laboratories and were used as received. Both native and ^{13}C-labelled analytical standards of 5 μg/mL 2,3,7,8-tetrabromodibenzofuran (**42**) were purchased from Cambridge Isotope Laboratories and were used as received.

4.2.3 Synthesis

4.2.3.1 General

2-Chlorophenol (**47**), 2-bromophenol (**48**), potassium carbonate (K_2CO_3), copper powder, potassium hydroxide (KOH), 2-chloro-5-fluorophenol (**49**), 2-chloro-5-methoxyphenol (**50**), 2-chloro-4,5-dimethylphenol (**51**), 3,4-dimethoxyphenol (**53**), potassium ferricyanide ($K_3Fe(CN)_6$), sodium carbonate (Na_2CO_3), and 3,4-bismethylenedioxyphenol (**55**) were purchased from Aldrich and used as received.

4.2.3.2 Dibenzo[1,4]Dioxin Systems

Dibenzo[1,4]dioxin (9). The adapted syntheses from 2-chlorophenol (**47**) and 2-bromophenol (**48**) were based on the procedures of Tomita (*152*), Guan (*40*), and Sasaki

(*41*). 2-Chlorophenol (102.5 g; 0.79 mol), anhydrous K_2CO_3 (55 g; 0.40 mol), and copper powder (6.0 g; 9.4×10^{-2} mol) were heated under nitrogen at 170-180°C for 6 h. The tarry mixture was then further refluxed under nitrogen with 100 mL of 5 M KOH for 2 h, allowed to cool to room temperature, dissolved in CH_2Cl_2, and vacuum filtered. The resulting solution was then extracted with 0.1 M KOH (3×100 mL) and the dark CH_2Cl_2 solution filtered through a sintered glass funnel filled with 3 cm of silica gel, resulting in a yellow effluent. The crude product was obtained by evaporating the CH_2Cl_2 from the effluent. Recrystallization from ethanol/water followed by sublimation under vacuum at 160°C gave pure product (14.7 g; 0.08 mol) in 20% yield: mp 117.5-118.1°C (lit. mp 119°C (*153*)); HRMS (EI), calc. $C_{12}H_8O_2$ 184.0524, found 184.0588; LRMS (EI), *m/z*=184 (M^+), 168 (M^+-O), 155 (M^+-CHO), 139 (M^+-CHO_2), 92 (M^+-C_6H_4O). 76 (M^+-$C_6H_4O_2$); ^{1}H NMR (500 MHz, $CDCl_3$) δ 6.82 (m, AA'BB', 4 H, 2,3,7,8-H), 6.85 (m, AA'BB', 4 H, 1,4,6,9-H); ^{13}C NMR (300 MHz, $CDCl_3$) δ 116.35 (2,3,7,8-C), 123.78 (1,4,6,9-C), 142.19 (arylether-C).

2-Bromophenol (10 g, 5.8×10^{-2} mol), anhydrous K_2CO_3 (5 g; 3.6×10^{-3} mol), and copper powder (0.6 g; 9.4×10^{-3} mol) were heated under nitrogen at 170-180°C for 6 h. The tarry mixture was then further refluxed under nitrogen with 100 mL of toluene and 0.5 g (8.9×10^{-3} mol) KOH for 3 h. Hot filtration of the product solution and subsequent rotary evaporation of the toluene gave the crude product. Sublimation under vacuum at 160°C afforded **9** (1.6 g; 8.7×10^{-3} mol) as a white powder in 30% yield.

2,7-Difluorodibenzo[1,4]dioxin (20). The adapted synthesis from 2-chloro-5-fluorophenol (**49**) was based on the procedures of Tomita (*152*) and Sasaki (*41*). 2-Chloro-5-fluorophenol (5.0 g; 3.4×10^{-2} mol), anhydrous K_2CO_3 (2 g; 1.5×10^{-2} mol), and copper powder (0.25 g; 3.9×10^{-3} mol) were heated under nitrogen in a sand bath at 190-250°C for 8 h. The black solid was then refluxed under nitrogen with 25 mL of 5 M K_2CO_3 for 2 h, subsequently extracted with CH_2Cl_2, and the organic extract washed with 2 M KOH (3×100 mL). Evaporation of the CH_2Cl_2 and sublimation at 170°C gave pure product as white needles (2.1 g; 9.5×10^{-3} mol) in 56% yield: mp 174-176°C (lit. mp 174-176°C (*154*)); HRMS (EI), calc. $C_{12}H_6O_2F_2$ 220.0336, found 220.0337; LRMS (EI), *m/z*=220 (M^+); ^{1}H NMR (500 MHz, $CDCl_3$) δ 6.59 (m, ABCX, 2 H), 6.77 (m, ABCX, 1 H).. This compound is known and the mp corresponds to the literature. The observed ^{1}H NMR spectrum for **20** resembles the published ^{1}H NMR spectrum as presented in ref. (*154*).

2,7-Dimethoxydibenzo[1,4]dioxin (21). The adapted synthesis from 2-chloro-5-methoxyphenol (**50**) was based on the procedures of Tomita (*152*) and Sasaki (*41*). 2-Chloro-5-methoxyphenol (5.0 g, 2.7×10^{-2} mol), anhydrous K_2CO_3 (2 g; 1.5×10^{-2} mol), and copper powder (0.25 g; 3.9×10^{-3} mol) were heated under nitrogen in a sand bath at 190-250°C for 14 h. The black solid was then refluxed under nitrogen with 25 mL of 5 M K_2CO_3 for 2 h, subsequently extracted with CH_2Cl_2, and the organic extract washed with 2 M KOH (3×100 mL). Evaporation of the CH_2Cl_2 and recrystallization in methanol gave pure product as white needles (0.05 g; 1.6×10^{-4} mol) in 1.2% yield: mp 167-169°C; HRMS (EI), calc. $C_{14}H_{12}O_4$ 244.0735, found 244.0739; LRMS (EI), *m/z*=240 (M^+); ^{1}H

NMR (300 MHz, $(CD_3)_2CO$) δ 3.75 (s, 6 H, OCH_3), 6.48 (dd, J=3.1 Hz, 2 H, 1,6-H), 6.50 (dd, 2 H, J=8.1, 3.0 Hz, 3,8-H), 6.83 (d, J=8.1 Hz, 2 H, 4,9-H); ^{13}C NMR (300 MHz, $(CD_3)_2CO$) δ 56.0 (OCH_3), 103.1 (1,6-C), 109.3 (3,8-C), 117.3 (4,9-C), 136.2 (*p*-arylether-C), 143.4 (*m*-arylether-C), 157.2 (2,7-C).

2,3,7,8-Tetramethyldibenzo[1,4]dioxin (13). The adapted synthesis from 2-chloro-4,5-dimethylphenol (**51**) was based on the procedures of Tomita (*152*), Guan (*40*), and Sasaki (*41*). 2-Chloro-4,5-dimethylphenol (5.0 g, 3.2×10^{2} mol), anhydrous K_2CO_3 (2 g; 1.5×10^{-2} mol), and copper powder (0.25 g; 3.9×10^{3} mol) were heated under nitrogen in a sand bath at 190-250°C for 10 h. The solid material was then refluxed under nitrogen with 25 mL of 5 M K_2CO_3 for 2 h, subsequently extracted with CH_2Cl_2, and the organic extract washed with 2 M KOH (3×100 mL). Evaporation of the CH_2Cl_2 and recrystallization in methanol gave pure product as a white powder (0.21 g, 8.7×10^{-4} mol) in 5.4% yield: mp 167-169°C (lit. mp 167°C (*152*)); HRMS (EI), calc. $C_{16}H_{16}O_2$ 240.1150, found 240.1141; LRMS (CI), m/z=241 (M^++1); ^1H NMR (360 MHz, $CDCl_3$) δ 2.11 (s, 12 H, CH_3), 6.59 (s, 4 H, 1,4,6,9-H).

4.2.3.3 2,2'-Biphenylquinone Systems

4,4',5,5'-Tetramethoxy-2,2'-Biphenylquinone (52). The synthesis was based on the procedure of Adderley and Hewgill (*155*). A solution of 3,4-dimethoxyphenol (**53**; 1.0 g; 6.5×10^{-3} mol) in chloroform (150 mL) was stirred under a nitrogen atmosphere. An aqueous solution (200 mL) of potassium ferricyanide (4.4 g; 1.3×10^{-2} mol) and sodium carbonate (2.1 g; 2.0×10^{-2} mol) was added rapidly. After 5 min, the deep blue precipitate was filtered and thoroughly washed with water and cold 95% ethanol. Recrystallization

from chloroform-hexane gave pure product (0.11 g; 3.4×10^{-4} mol) in 10% yield as deep blue crystals: mp 185-186°C (lit. mp 187-188°C (*85*)); HRMS (EI), calc. $C_{16}H_{16}O_6$ 304.0947, found 304.0951; LRMS (CI), *m/z*=306 (M^++2); ^{1}H NMR (300 MHz, $CDCl_3$) δ 3.81 (s, 3 H, 5,5'-OCH_3), 3.94 (s, 3 H, 4,4'-OCH_3), 5.71 (s, 2 H, 6,6'-H), 8.26 (s, 2 H, 3,3'-H).

4,5,4'5'-Bismethylenedioxy-2,2'-Biphenylquinone (54). The synthesis was based on the procedure of Hewgill (*86*). A solution of 3,4-bismethylenedioxyphenol (**55**; 1.0 g; 7.2×10^{-3} mol) in chloroform (150 mL) was stirred under a nitrogen atmosphere. An aqueous solution (200 mL) of potassium ferricyanide (4.4 g; 1.3×10^{-2} mol) and sodium carbonate (2.1 g; 2.0×10^{-2} mol) was added rapidly. The deep purple precipitate was immediately filtered and thoroughly washed with water and cold 95% ethanol. Recrystallization from chloroform-hexane gave pure product (0.50 g; 1.8×10^{-3} mol) in 51% yield as deep blue crystals: mp 198-199°C (lit. mp 199-199.5°C (*86*)); HRMS (EI), calc. $C_{16}H_{12}O_4$ 268.0736, found 268.0725; MS (CI), *m/z*=270 (M^++2); ^{1}H NMR (300 MHz, $CDCl_3$) δ 5.88 (s, 2 H, 6,6'-H), 5.91 (s, 4 H, -OCH_2O-), 8.10 (s, 2 H, 3,3'-H).

4.3 Product Studies

4.3.1 Photochemical Product Studies

4.3.1.1 General

All preparative photolyses were carried out in a Rayonet RPR 100 photochemical reactor equipped with 16-300 nm lamps. The solutions were contained in a 150 mL quartz tube cooled to ≤15°C with tap water by means of an internal cold finger. All

solutions were sparged with argon for 15 min prior to irradiation and throughout the irradiation. Photolysis times varied from 1 to 120 min depending on the system under study. Workup of irradiated solutions in entirely organic solvents involved rotary evaporation of the solvent to give the crude photoproduct mixture. In aqueous solutions, the pH was adjusted following photolysis to ca. pH 1 with 1 M HCl, 20 mL of saturated NaCl was added, the solution was extracted with 3×100 mL of CH_2Cl_2, and the solvent removed by rotary evaporation to yield the crude photoproduct mixture. Photoproducts were separated by prep-TLC. For all dibenzo[1,4]dioxin or diphenyl ether starting materials, thermal control experiments were performed under similar conditions as outlined above, except exposure to light was prevented. No significant degradation of these starting materials was observed during these controls. Because of the known thermal reactivity of the 2,2'-biphenylquinone systems, thermal blanks were not performed for these compounds. Instead, the thermal products of this compound class were investigated and are reported below.

4.3.1.2 Results of Product Studies

4.3.1.2.1 Dibenzo[1,4]Dioxin Systems

Photolysis of 9 in CH_3CN. A 50 mg (2.7×10^{-4} mol) sample of **9** was dissolved in freshly distilled CH_3CN (100 mL) and irradiated for 60 min. Evaporation of the solvent gave the crude photoproduct mixture. The major product, 2,2'-dihydroxybiphenyl (**10**; 21 mg; 1.1×10^{-4} mol), was separated by prep-TLC (CH_2Cl_2) in 70% yield at ca. 60% conversion of starting material and compared to a sample of commercially available authentic compound. Previous work had shown **10** as the major primary photoproduct of **9** in CH_3CN (*40,41*).

Photolysis of 9 in 1:1 CH_3CN:H_2O at pH 1, 7, and 12. A 50 mg (2.7×10^{-4} mol) sample of **9** was dissolved in CH_3CN (50 mL), a 50 mL aliquot of H_2O was added (whose pH had been adjusted by the addition of either 1 M HCl or NaOH as needed), and the resulting solution irradiated for 30 min. Following workup and extraction as described above, evaporation of the residual organic solvent gave the crude photoproduct mixture. The major product, **10** (34 mg, 1.8×10^{-4} mol; 35 mg, 1.9×10^{-4} mol; and 31 mg, 1.7×10^{-4} mol), was separated by prep-TLC (CH_2Cl_2) in 70%, 74%, and 65% yields for pH 1, 7, and 12, respectively, at >95% conversion of starting material. Previous work had shown **10** as the major primary photoproduct of **9** in CH_3CN:H_2O at these pH values (*40,41*).

Photolysis of 9 in Benzene. A 50 mg (2.7×10^{-4} mol) sample of **9** was dissolved in benzene (100 mL) and irradiated for 60 min. Evaporation of the solvent gave the crude photoproduct mixture. ^{1}H NMR suggested ca. 20% conversion to **10** (33% yield), ca. 40% unreacted starting material, and 15% yield (3.7 mg; 2.4×10^{-5} mol) of biphenyl (**109**; m/z=153 [M^+-1]) which was separated by prep-TLC (1:1 CH_2Cl_2:hexane) and whose ^{1}H NMR was compared to a sample of commercially available authentic compound.

Photolysis of 9 in Cyclohexane. A 50 mg (2.7×10^{-4} mol) sample of **9** was dissolved in spectral grade cyclohexane (100 mL) and irradiated for 60 min. Evaporation of the solvent gave the crude photoproduct mixture. ^{1}H NMR suggested ca. 34% conversion to **10** (68% yield) and ca. 50% unreacted starting material.

Photolysis of 9 in Diethyl Ether. A 50 mg (2.7×10^{-4} mol) sample of **9** was dissolved in diethyl ether (100 mL) and irradiated for 60 min. Evaporation of the solvent gave the crude photoproduct mixture. ^{1}H NMR suggested ca. 31% conversion to **10** (62% yield) and ca. 50% unreacted starting material.

Photolysis of 9 in Ethyl Acetate. A 50 mg (2.7×10^{-4} mol) sample of **9** was dissolved in ethyl acetate (100 mL) and irradiated for 60 min. Evaporation of the solvent gave the crude photoproduct mixture. ^{1}H NMR suggested ca. 25% conversion to **10** (50% yield) and ca. 50% unreacted starting material.

Photolysis of 9 in Hexane. A 50 mg (2.7×10^{-4} mol) sample of **9** was dissolved in spectral grade hexane (100 mL) and irradiated for 60 min. Evaporation of the solvent gave the crude photoproduct mixture. ^{1}H NMR suggested ca. 41% conversion to **10** (81% yield) and ca. 50% unreacted starting material.

Photolysis of 9 in Toluene. A 50 mg (2.7×10^{-4} mol) sample of **9** was dissolved in toluene (100 mL) and irradiated for 60 min. Evaporation of the solvent gave the crude photoproduct mixture. ^{1}H NMR suggested ca. 23% conversion to **10** (58% yield), ca. 60% unreacted starting material, and 12% yield (5.9 mg; 3.2×10^{-5} mol) of bibenzyl (**110**; m/z=182 [M^+], 91 [M^+-C_7H_7]) which was separated by preparative TLC (1:1 CH_2Cl_2:hexane) and whose ^{1}H NMR was compared to a sample of commercially available authentic compound.

Photolysis of 9 in 1-Butanol. A 50 mg (2.7×10^{-4} mol) sample of **9** was dissolved in 1-butanol (100 mL) and irradiated for 30 min. Evaporation of the solvent gave the crude photoproduct mixture. ^{1}H NMR suggested ca. 82% conversion to **10** (91% yield) and ca. 10% unreacted starting material.

Photolysis of 9 in *t*-Butanol. A 50 mg (2.7×10^{-4} mol) sample of **9** was dissolved in *t*-butanol (100 mL) and irradiated for 30 min. Evaporation of the solvent gave the crude photoproduct mixture. ^{1}H NMR suggested ca. 65% conversion to **10** (93% yield) and ca. 30% unreacted starting material.

Photolysis of 9 in Ethanol. A 50 mg (2.7×10^{-4} mol) sample of **9** was dissolved in anhydrous ethanol (100 mL) and irradiated for 30 min. Evaporation of the solvent gave the crude photoproduct mixture. ^{1}H NMR and MS (EI) suggested ca. 70% conversion to **10** (93% yield) and ca. 25% unreacted starting material.

Photolysis of 9 in Methanol. A 50 mg (2.7×10^{-4} mol) sample of **9** was dissolved in methanol (100 mL) and irradiated for 30 min. Evaporation of the solvent gave the crude photoproduct mixture. ^{1}H NMR suggested ca. 67% conversion to **10** (96% yield) and ca. 30% unreacted starting material.

Photolysis of 9 in 2-Propanol. A 50 mg (2.7×10^{-4} mol) sample of **9** was dissolved in 2-propanol (100 mL) and irradiated for 30 min. Evaporation of the solvent gave the crude photoproduct mixture. ^{1}H NMR suggested ca. 60% conversion to **10** (92% yield) and ca. 35% unreacted starting material.

Photolysis of 13 in CH_3CN. A 50 mg (2.1×10^{-4} mol) sample of **13** was dissolved in CH_3CN (100 mL) and irradiated for 45 min. Evaporation of the solvent gave the crude photoproduct mixture. The major product, 4,4',5,5'-tetramethyl-2,2'-dihydroxybiphenyl (**14**; 19 mg; 7.9×10^{-5} mol), was separated by prep-TLC (CH_2Cl_2) in 58% yield at ca. 65% conversion of starting material: mp 150-151°C (lit. mp 150-151°C (*156*)); HRMS (EI), calc. $C_{16}H_{18}O_2$ 242.1307, found 242.1311; LRMS (CI), 243 (M^++1); ^{1}H NMR (300 MHz, $(CD_3)_2CO$) δ 2.19 (s, 6 H, 5'-CH_3), 2.20 (s, 6 H, 4'-CH_3), 5.60 (s, 2 H, 2,2'-OH,

exchangeable with D_2O), 6.76 (s, 2 H, 6,6'-H), 7.01 (s, 2 H, 5,5'-H). Previous work had shown **14** as the major primary photoproduct of **13** in CH_3CN (*40,41*).

Photolysis of 20 in CH_3CN. A 50 mg (2.3×10^{-4} mol) sample of **20** was dissolved in CH_3CN (100 mL) and irradiated for 45 min. Evaporation of the solvent gave the crude photoproduct mixture. The major product, 5,5'-difluoro-2,2'-dihydroxybiphenyl (**22**; 15 mg; 9.8×10^{-5} mol), was separated by prep-TLC (CH_2Cl_2) in 61% yield at ca. 70% conversion of starting material: mp 120°C; HRMS (EI), calc. $C_{12}H_8O_2F_2$ 222.0492, found 222.0496; LRMS (EI), 222 (M^+); ^1H NMR (500 MHz, $(CD_3)_2CO$) δ 6.99 (d, 2 H, J=8.1 Hz, 3,3'-H), 7.01 (ddd, 2 H, J=9.5, 8.1, 2.9 Hz, 4,4'-H), 7.07 (dd, 2 H, J=9.5, 2.9 Hz, 6,6'-H), 8.43 (s, 2 H, 2,2'-OH, exchangeable with D_2O); ^{13}C NMR (300 MHz, $(CD_3)_2CO$) δ 115.2 (4,4',6,6'-C), 118.2 (3,3'-C), 127.8 (1,1'-C), 150.1 (2,2'-C), 155.5 (5,5'-C). Previous work had shown **22** as the major primary photoproduct of **20** in CH_3CN (*41*).

Photolysis of 21 in CH_3CN. A 10 mg (4.1×10^{-5} mol) sample of **21** was dissolved in CH_3CN (100 mL) and irradiated for 45 min. Evaporation of the solvent gave the crude photoproduct mixture. The major product, 5,5'-dimethoxy-2,2'-dihydroxybiphenyl (**23**; 3.2 mg; 1.3×10^{-5} mol), was separated by prep-TLC (CH_2Cl_2) in 53% yield at ca. 60% conversion of starting material: mp 126°C; HRMS (EI), calc. $C_{14}H_{14}O_2$ 246.0892, found 246.0885; LRMS (EI), m/z=246 (M^+); ^1H NMR (500 MHz, $(CD_3)_2CO$) δ 6.83 (d, 2 H, J=3.0 Hz, 6,6'-H), 6.84 (dd, 2 H, J=8.0, 3.0 Hz, 4,4'-H), 6.91 (d, 2 H, J=8.0 Hz, 3,3'-H),

8.31 (s, 2 H, 2,2'-OH, exchangeable with D_2O). Previous work had shown **23** as the major primary photoproduct of **21** in CH_3CN (*41*).

Photolysis of 30 in CH_3CN. A 10 mg (4.6×10^{-5} mol) sample of **30** was dissolved in CH_3CN (100 mL) and irradiated for 20 min (2 min intervals). The reaction was followed by UV-Vis spectroscopy and allowed to continue until ca. 40% conversion of starting material (as measured by decrease in λ_{max}=299 nm). Evaporation of the solvent gave the crude photoproduct mixture. ^{1}H NMR integration analysis of the crude product showed ca. 20% conversion of starting material to 5-chloro-2,2'-dihydroxybiphenyl (**56**) and **10** (ca. 20% conversion). The major primary photoproduct, **56** (2 mg; 9×10^{-6} mol) was separated in 50% yield from **10** by prep-TLC (3:1 CH_2Cl_2:hexane v/v): HRMS (EI), calc. $C_{12}H_9O_2Cl$ 220.0291, found 220.0296; LRMS (EI), 220 (100%; M^+), 222 (37%; M^++2); ^{1}H NMR (300 MHz, $CDCl_3$) δ 6.91 (d, 1 H, *J*=8.8 Hz, 3-H), 6.94 (m, 2 H, 4',6'-H), 6.97 (dd, 1 H, *J*=8.8, 2.1 Hz, 4-H), 7.17 (d, 1 H, *J*=2.1 Hz, 6-H), 7.25 (m, 2 H, 3',5'-H), 8.36 (s, 1 H, 2'-OH, exchangeable with D_2O), 8.51 (s, 1 H, 2-OH, exchangeable with D_2O).

Photolysis of 3 in 19:1 H_2O:CH_3CN and 100% H_2O. All solvents (CH_3CN, acetone, toluene, hexane, and CH_2Cl_2) were of distilled-in-glass quality purchased from Caledon Laboratories and were used as received. NaCl and Na_2SO_4 used in sample extraction and cleanup were washed with toluene, hexane, acetone, and CH_2Cl_2 and then baked at 350°C for a minimum of 12 h before use. A similar treatment was performed on all glassware, syringes, and Teflon and stainless steel utensils; no other material types were used in order to minimize contamination. Filter papers were rinsed sequentially with toluene,

hexane, acetone, and CH_2Cl_2 and dried at 105°C. Nitrogen was ultrahigh purity grade, and deionized water was obtained from a Milli-Q water system.

Solutions of **3** (1.7 ng in 3 mL 19:1 H_2O:CH_3CN; 1.8×10^{-9} M) were irradiated at 302 nm using a 6W Ultra-Violet Products UVM-57 302 nm hand-held lamp for 0 to 60 min at 5 min intervals in separate quartz cuvettes. A single solution of **3** (1.7 ng in 3 mL H_2O; 1.8×10^{-9} M) was also irradiated for 60 min under the same experimental conditions. This entirely aqueous sample was subjected to the same workup, extraction, and analytical methods as was used for the 19:1 H_2O:CH_3CN samples described below. The UV lamp was secured 5 cm from the quartz cuvette in a perpendicular arrangement that was consistent between trials to minimize difference in incident radiation intensity. The irradiation wavelength of 302 nm is near the reported absorption maxima for **3** (304-307 nm) (*17,56,157*) in various organic solvents, although an absorption maxima in water has yet to be reported due to low solubility. Duplicate photolyses were performed at each irradiation time. Solutions were prepared by placing 25 μL of a 67.8±2.3 ng/mL (certified at 23°C) standard of **3** dissolved in 2,2,4-trimethylpentane into a quartz cuvette, evaporating the organic solvent by gentle heating under a steady stream of nitrogen, and reconstituting in either 3 mL of 19:1 H_2O:CH_3CN or 3 mL of H_2O. Three thermal blanks were also performed for each solvent system to ensure losses of **3** during the removal of 2,2,4-trimethylpentane and a subsequent 90 min nitrogen sparging period in either 19:1 H_2O:CH_3CN or 100% H_2O were negligible and that no thermal reactions were occurring. Levels of all potential photoproducts in these blanks ranged from nondetectable to 2.1%

of that found in the corresponding irradiated samples. Starting material recoveries ranged from 90-110% indicating the absence of significant thermal degradation.

Following all photolyses and thermal blanks, 1 ng of ^{13}C-labeled **3** was added to the solutions as a recovery standard. Solutions were then transferred to a separatory funnel, 3 mL of a saturated aqueous NaCl solution was added, and the solution acidified to pH 2 with 6 N HCl. The resulting aqueous fractions were extracted with 3×25 mL of CH_2Cl_2, evaporated to 3-5 mL on a rotary evaporator (gentle vacuum at 25-30°C), transferred to 10 mL glass centrifuge tubes, solvent exchanged with toluene, evaporated under nitrogen and gentle heating to a solution volume of ca. 100 μL, transferred into amber microvials with toluene, and evaporated under nitrogen to a final volume of ca. 20 μL. Internal standards (1 ng each of ^{13}C-labeled 1,2,3,4-tetrachlorodibenzo[1,4]dioxin (**155**) and 1,2,3,7,8,9-hexachlorodibenzo[1,4]dioxin (**156**)) were added immediately prior to capping the microvial for HRGC-HRMS analysis.

Photolysis extracts were analyzed by HRGC-HRMS using a Micromass VG Autospec mass spectrometer equipped with a Hewlett Packard model 5890 series II gas chromatograph at the Regional Dioxin Laboratory in the Institute of Ocean Sciences (Sidney, BC, Canada). The HRGC-HRMS analyst was Maike Fischer, who performed the injections and made the resulting datasets available for analysis, under the guidance of the facility manager, Dr. Michael Ikonomou. The GC was operated in the splitless injection mode, and the splitless injector purge valve was activated 2 min after sample injection. The volume injected was 1 μL of sample plus 0.5 μL of air. The analyses

were conducted using a 60 m J&W Scientific DB-5 fused silica capillary column (0.25 mm i.d. with 0.1 m film thickness) with ultra-high purity helium as the carrier gas at a constant head pressure of 25 psi to maintain a linear velocity of 35 cm/s. The temperature program for chlorinated dibenzo[1,4]dioxin analytes was as follows: 100°C for 2 min after injection; 20°C/min to 200°C; 1°C/min to 215°C, held for 7 min at 215°C; 4°C/min to 300°C; and held for 3 min at 300°C. The splitless injector port, direct HRGC-HRMS interface, and the HRMS ion source were maintained at 280, 290, and 290°C, respectively.

The HRMS was a sector instrument of EBE geometry coupled to the HRGC via a standard Micromass HRGC-HRMS interface. For chlorinated dibenzo[1,4]dioxin analyses, the MS was operated under positive EI conditions with the filament in the trap stabilization mode at 600 μA and an electron energy of 28-35 eV. The instrument was operated at 10,000 resolution, and data were acquired in the selected ion monitoring (SIM) mode. The M^+ and $(M + 2)^+$ ions of known relative abundance were monitored for each molecular ion cluster representing a group of isomers, as were two for each of the ^{13}C-labeled standards.

Compounds were identified only when the HRGC-HRMS data satisfied all of the following criteria: (1) two isotopes of the analyte were detected by their exact masses with the HRMS operating at 10,000 resolution during the entire chromatographic run; (2) the retention time of the analyte peak was within 3 s to the predicted time obtained from analysis of authentic compounds in the calibration standards (where available); (3) the

maxima for both characteristic isotopic peaks of an analyte coincided within 2 s; (4) the observed isotope ratio of the two ions monitored per analyte were within 15% of the theoretical isotopic ratio; and (5) the signal-to-noise ratio resulting from the peak response of the two corresponding ions was ≥3 for proper quantification of the analyte. Concentrations of analytes and their method detection limits (MDLs) were calculated by the internal standard isotope-dilution method using mean RRFs determined from calibration standard runs made before and after each batch of samples was analyzed. Recoveries of the ^{13}C-2,3,7,8-tetrachlorodibenzo[1,4]dioxin standard added immediately after photolysis ranged between 71 to 117% for all analyses. Concentrations of analytes were corrected for percent recovery of the ^{13}C-2,3,7,8-tetrachlorodibenzo[1,4]dioxin standard (^{13}C-**3**).

Absolute quantities of the 2,3,7,8-tetrachlorodibenzo[1,4]dioxin starting material (**3**) and the photodechlorination products in the photolyses extracts, along with recoveries of the ^{13}C-labeled 2,3,7,8-tetrachlorodibenzo[1,4]dioxin recovery standard (^{13}C-**3**), are presented in Table 4.1. Error bars, where shown, represent the range of duplicate analyses. Where error bars are absent, only one trial was able to be successfully analyzed. Absolute quantities of each analyte were corrected for recoveries of the corresponding internal standard. The absolute quantities of all chlorinated dibenzo[1,4]dioxins were corrected relative to the corresponding recovery of ^{13}C-**3** at each timestep. Contributions towards the overall photochemical mass balance were then calculated by dividing the corrected quantity of each analyte by its molecular mass, and then dividing the moles of

analyte observed at each timestep by the moles of starting material (**41**; 5.4×10^{-12} mol, or 1.8×10^{-9} M in 3 mL of solution).

Table 4.1. Absolute quantities (in pg; uncorrected for the recovery standard) of **3** and its mono- through tri-chlorinated photodechlorination products over the course of a 60 min irradiation period in 19:1 $CH_3CN:H_2O$ (v/v). Percent recoveries of the ^{13}C-labeled recovery standard (^{13}C-**3**) are also shown.

Time (min)	**3**	**62**	**59**	**60**	**61**	**30**	**9**	^{13}C-**3**
5	769.1±22.6	36.1±6.7	<0.2	<0.2	<0.2	<0.2	<0.2	117%
15	140.3±16.0	12.2±2.4	<0.2	<0.2	2.1±2.1	<0.2	<0.2	83%
30	68.3±6.9	<0.2	<0.2	0.2	0.3	<0.2	21.1±3.9	71%
45	269.0±48.2	<0.2	<0.2	<0.2	<0.2	<0.2	57.1±12.7	115%
60	251.4±41.4	<0.2	<0.2	1.4±2.7	1.6±2.7	<0.2	37.8±7.9	107%

To ensure no water soluble phenolic photoproducts avoided extraction and analysis, the aqueous fractions remaining after extraction with CH_2Cl_2 were nonselectively derivatized using established methyl iodide (CH_3I) based methods for the phenolic metabolites of chlorinated dibenzo[1,4]dioxins and chlorinated biphenyls (*158-160*). Solutions were then processed and analyzed by HRGC-HRMS using the instrument conditions as given above except with the following temperature program for SIM analyses: the initial column temperature was held at 80°C for 1 min after injection and increased at 10°C/min to 180°C, then at 1°C/min to 200°C, followed by a ramp of 20°C/min to 300°C, and held for 4 min. The splitless injector port, direct HRGC-HRMS interface, and the HRMS ion source were maintained at 220, 220, and 280°C, respectively. Full scans at 5,000 resolution were also performed on the derivatized samples using the following temperature program: the initial column temperature was held at 100°C for 1 min after injection and increased at 10°C/min to 180°C, then at 1°C/min to 200°C, followed by a ramp of 20°C/min to 280°C, and held for 6 min. The splitless injector port, direct HRGC-HRMS interface, and the HRMS ion source were maintained at 220, 220, and 280°C, respectively. Both SIM and full scans analyses showed no methylated photoproducts.

To help in identifying 2,2'-dihydroxybiphenyl photoproducts of **3**, a range of mono- through trichloro-2,2'-dihydroxybiphenyls (**57**, **63**, and **64**, respectively) was prepared by irradiating a 500 ng/mL solution of **58** in toluene for 1 min at 302 nm. As the percent conversion of **58** to its dechlorinated products was not known, the compounds

formed were used only to aid in photoproduct identification, and not for the purposes of quantification. To identify and quantitate non-dibenzo[1,4]dioxin photoproducts for which analytical standards were not available (all chlorinated 2-phenoxyphenols and mono- through trichloro-2,2'-dihydroxybiphenyls), sample extracts were first analyzed by HRGC-HRMS with the HRMS in full scan mode at 5,000 resolution using the following temperature program: the initial column temperature was held at 100°C for 1 min after injection and increased at 10°C/min to 180°C, then at 1°C/min to 200°C, followed by a ramp of 20°C/min to 280°C, and held for 3 min. The splitless injector port, direct HRGC-HRMS interface, and the HRMS ion source were maintained at 220, 220, and 280°C, respectively. The approximate HRGC retention times of these photoproducts were estimated using the identification criteria specified above. Where NIST/EPA/NIH library spectra were available, these were used to aid in assigning tentative retention times.

Using the estimated retention time windows from full scan analyses, SIM analyses of the M^+ and $(M + 2)^+$ ions were performed at 10,000 resolution on all extracts using the following temperature program: the initial column temperature was held at 80°C for 1 min after injection and increased at 10°C/min to 180°C, then at 1°C/min to 200°C, followed by a ramp of 20°C/min to 300°C, and held for 4 min. The splitless injector port, direct HRGC-HRMS interface, and the HRMS ion source were maintained at 220, 220, and 280°C, respectively. Compounds were identified only if they met the QA/QC criteria noted above and if their retention times were consistent with other members of the same class (e.g., dichloro analytes must elute prior to trichloro analytes

of the same compound class) and between classes (e.g., chlorinated 2-phenoxyphenols – due to their lower polarity – will elute before chlorinated 2,2'-dihydroxybiphenyls of the same homologue group). Because of the low HRMS response for analytes with absolute quantities $<0.30\times10^{-12}$ mol using SIM, sample extracts from the duplicate photolyses performed at 5, 15, 30, 45, and 60 min were subsequently combined and evaporated under nitrogen to ca. 20 μL. The combined extracts were then analyzed by HRGC-HRMS in SIM mode at 10,000 resolution using the following temperature program: the initial column temperature was held at 80°C for 1 min after injection and increased at 10°C/min to 180°C, then at 1°C/min to 200°C, followed by a ramp of 20°C/min to 300°C, and held for 4 min. The splitless injector port, direct HRGC-HRMS interface, and the HRMS ion source were maintained at 220, 220, and 280°C, respectively.

For quantitation, relative response factors (RRFs) for the chlorinated 2-phenoxyphenol series were assumed equal to their chlorinated 2,2'-dihydroxybiphenyl homologues. To estimate the RRFs of the mono- through trichloro-2,2'-dihydroxybiphenyl photoproducts, the influence of substitution pattern on the RRFs of 3-chlorophenol (**157**), 4-chlorophenol (**158**), and 3,4-dichlorophenol (**159**) models was investigated by monitoring the intensity of the M^+ and $(M + 2)^+$ ions for each compound under SIM conditions at 10,000 resolution. The number and location of chlorine substituents on the chlorophenol models was found to have only a minor effect on the RRF, resulting in estimated internal standard corrected RRFs of 1.10, 1.15, and 1.20 for **57**, **63**, and **64**, respectively, relative to **58**. While there may be some uncertainty in assigning RRFs to these compounds via chlorophenol models, it is important to note that

only **57** was a significant contributor (>25%) to the overall photochemical mass balance for **3** in 19:1 H_2O:CH_3CN. The continuity of the mass balance (92-99%) over the irradiation period suggested that the influence of such errors was minimal.

Retention times and isotopic masses used for identification and quantitation of the following potential photoproducts of **3** had available analytical standards and are not given here: **9**, **10**, **12, 30**, **58, 59**, **60**, **61,** and **62**. Thus, analytical standards were not available for the potential mono- through tri-chlorinated 2,2'-dihydroxybiphenyl photoproducts of **3** (**57**, **63**, **64**) or the potential mono- through tetra-chlorinated 2-phenoxyphenol photoproducts of **3** (**65**, **66**, **67**, **68**). Lower and upper boundaries for the retention times of the various potential individual isomers of **57**, **63**, **64** were set by the known retention times of **10** (12.25 min) and **58** (36.42 min). Following photolysis of **3**, the following chlorinated 2,2'-dihydroxybiphenyl analytes were identified and quantitated as per the QA/QC and RRF approaches described above: (1) monochloro-2,2'-dihydroxybiphenyl isomer at RT=13.58 min (*m/z* 220.0293 (100%, M^+); 220.0259 (35%, M^++2)); (2) dichloro-2,2'-dihydroxybiphenyl isomer at RT=20.16 min (*m/z* 253.9905 (100%, M^+); 255.9876 (69%, M^++2)); (3) dichloro-2,2'-dihydroxybiphenyl isomer at RT=23.42 min (*m/z* 253.9905 (100%, M^+); 255.9876 (62%, M^++2)); and (4) trichloro-2,2'-dihydroxybiphenyl isomer at RT=28.16 min (*m/z* 287.9508 (100%, M^+); 289.9483 (98%, M^++2)).

Absolute quantities of the chlorinated 2,2'-dihydroxybiphenyl photoproducts in the photolyses extracts, along with recoveries of the ^{13}C-labeled 2,3,7,8-

tetrachlorodibenzo[1,4]dioxin recovery standard (^{13}C-**3**), are presented in Table 4.2. Error bars, where shown, represent the range of duplicate analyses. Where error bars are absent, only one trial was able to be successfully analyzed. Absolute quantities of each analyte were corrected for recoveries of the corresponding internal standard. The absolute quantities of all chlorinated 2,2'-dihydroxybiphenyls were corrected relative to the corresponding recovery of ^{13}C-**3** at each timestep. Contributions towards the overall photochemical mass balance were then calculated by dividing the corrected quantity of each analyte by its molecular mass, and then dividing the moles of analyte observed at each timestep by the moles of starting material (**41**; 5.4×10^{-12} mol, or 1.8×10^{-9} M in 3 mL of solution).

Table 4.2. Absolute quantities (in pg; uncorrected for the recovery standard) of mono- through tetra-chlorinated 2,2'-dihydroxybiphenyl photoproducts of **3** over the course of a 60 min irradiation period in 19:1 $CH_3CN:H_2O$ (v/v). Percent recoveries of the ^{13}C-labeled recovery standard (^{13}C-**3**) are also shown.

Time (min)	**58**	**64**	**63** (Isomer 2)	**63** (Isomer 1)	**57**	**10**	^{13}C-**3**
5	220.7±26.5	<1	<1	24.0±6.0	394.0±31.0	44.8±6.5	117%
15	635.3±29.6	<1	<1	28.2±6.4	284.3±18.3	81.3±1.5	83%
30	67.2±13.8	<1	5.9±3.6	104.4±12.7	294.5±12.5	157.8±5.3	71%
45	<1	<1	<1	53.0±8.8	505.5±12.7	252.3±17.1	115%
60	<1	<1	6.2±2.7	34.4±8.2	240.8±28.4	416.3±14.0	107%

The retention times of the various potential individual isomers of **65**, **66**, **67**, and **68** had a lower boundary set by the known retention time of **12** (10.67 min). In addition, the chlorinated 2-phenoxyphenol analytes were expected to elute prior to their homologue equivalent 2,2'-dihydroxybiphenyls, thus giving upper RT boundaries for each of the chlorinated 2-phenoxyphenol homologues. Following photolysis of **3**, the following chlorinated 2-phenoxyphenol analytes were identified and quantitated as per the QA/QC and RRF approaches described above: (1) dichloro-2-phenoxyphenol isomer at RT=15.40 min (*m/z* 220.0293 (100%, M^+); 220.0259 (30%, M^++2)); (2) trichloro-2-phenoxyphenol isomer at RT=19.59 min (*m/z* 287.9508 (100%, M^+); 289.9483 (94%, M^++2)); and (3) 3,4,4',5-2-phenoxyphenol (**68**) at RT=19.59 min (*m/z* 321.9115 (73%, M^+); 323.9096 (100%, M^++2)). No monochlorinated 2-phenoxyphenol analytes were observed by HRGC-HRMS.

Absolute quantities of the chlorinated 2-phenoxyphenol photoproducts in the photolyses extracts, along with recoveries of the ^{13}C-labeled 2,3,7,8-tetrachlorodibenzo[1,4]dioxin recovery standard (^{13}C-**3**), are presented in Table 4.3. Error bars, where shown, represent the range of duplicate analyses. Where error bars are absent, only one trial was able to be successfully analyzed. Absolute quantities of each analyte were corrected for recoveries of the corresponding internal standard. The absolute quantities of all chlorinated 2-phenoxyphenols were corrected relative to the corresponding recovery of ^{13}C-**3** at each timestep. Contributions towards the overall

photochemical mass balance were then calculated by dividing the corrected quantity of each analyte by its molecular mass, and then dividing the moles of analyte observed at each timestep by the moles of starting material (**41**; 5.4×10^{-12} mol, or 1.8×10^{-9} M in 3 mL of solution).

Table 4.3. Absolute quantities (in pg; uncorrected for the recovery standard) of mono- through tetra-chlorinated 2-phenoxyphenol photoproducts of **3** over the course of a 60 min irradiation period in 19:1 $CH_3CN:H_2O$ (v/v). Percent recoveries of the ^{13}C-labeled recovery standard (^{13}C-**3**) are also shown.

Time (min)	**68**	**67**	**66**	**65**	**12**	^{13}C-**3**
5	109.8±19.0	<1	<1	<1	<1	117%
15	6.4±2.7	<1	6.6±4.2	<1	<1	83%
30	16.0±6.9	<1	<1	<1	63.9±6.6	71%
45	16.5±7.5	<1	<1	<1	122.1±8.6	115%
60	16.6±6.9	<1	<1	<1	164.0±8.0	107%

4.3.1.2.2 2,2'-Biphenylquinone Systems

Photolysis of 52 in CH_3CN. A 50 mg (1.6×10^{-4} mol) sample of **52** was dissolved in CH_3CN (100 mL) and irradiated for 1 min. Evaporation of the solvent gave the crude photoproduct mixture. The major photoproduct, 4,4',5,5'-tetramethoxy-2,2'-dihydroxybiphenyl (**104**; 2 mg; 6.2×10^{-6} mol), was separated by preparative TLC (CH_2Cl_2) in 3.9% yield: mp 180-181°C (lit. mp 181.5-182.5°C (*85*)); HRMS (EI), calc. $C_{16}H_{18}O_6$ 306.1103, found 306.1099; LRMS (EI), 306 (M^+); ^1H NMR (300 MHz, $CDCl_3$) δ 6.81 (s, 2 H, 6,6'-H), 6.90 (s, 2 H, 3,3'-H), 5.73 (s, 2 H, 2,2'-OH, exchangeable with D_2O).

Photolysis of 54 in CH_3CN. A 50 mg (1.8×10^{-4} mol) sample of **54** was dissolved in CH_3CN (100 mL) and irradiated for 15 min. Evaporation of the solvent gave the crude photoproduct mixture. The major photoproduct, 4,5,4',5'-bismethylenedioxy-2,2'-dihydroxybiphenyl (**105**; 10 mg; 2.3×10^{-5} mol), was separated by preparative TLC (CH_2Cl_2) in 13% yield: mp 205.5-206.5°C (lit. mp 207-207.5°C (*86*)); HRMS (EI), calc. $C_{16}H_{14}O_4$ 270.0892, found 270.0890; LRMS (EI), 274 (M^+); ^1H NMR (300 MHz, $CDCl_3$) δ 6.74 (s, 2 H, 6,6'-H), 6.84 (s, 2 H, 3,3'-H), 5.85 (s, 2 H, 2,2'-OH, exchangeable with D_2O).

4.3.1.2.3 Diphenyl Ether Systems

Photolysis of 115 in CH_3OH, CH_3CN, and 1:1 CH_3CN:H_2O. A 50 mg (2.7×10^{-4} mol) samples of **115** were dissolved in separate 100 mL solutions of CH_3OH and CH_3CN and

irradiated at 300 nm for intervals of 5, 15, 30, and 60 min total irradiation time while purging with argon. A 50 mg (2.7×10^{-4} mol) sample of **115** was also dissolved in a 100 mL solution of 1:1 CH_3CN:H_2O and irradiated at 300 nm for 30 min while purging with argon. The aqueous sample was then transferred to a separatory funnel, 100 mL of a saturated aqueous NaCl solution was added, and the solution was acidified to pH 2 to ensure that any phenolic or acidic photoproducts were captured by extraction. The acidified aqueous solution was then extracted with 3×100 mL washes of CH_2Cl_2 and concentrated to ca. 10 mL on a rotary evaporator. Direct rotoevaporation of the organic solvent to a final volume of ca. 10 mL was used when samples were irradiated in 100% CH_3OH or CH_3CN. A 1 μL aliquot of this reduced solution was then injected directly into a Hewlett Packard 5890 Series II GC with a flame ionization detector and containing a 15 m DB-5 (0.25 mm inside diameter × 0.1 μm film thickness) column from J&W Scientific. The following temperature program was used: 80°C for 2 min following injection; 10°C/min to 300°C; and held at 300°C for 20 min. No photoproducts other than 4-bromodiphenyl ether (**114**), diphenyl ether (**44**), and unreacted starting material were observed in the crude ^{1}H-NMR spectra ($CDCl_3$ as solvent). All products were identified by comparison to spectra obtained from commercially available authentic standards. The maintenance of a full mass balance (100±2%; determined via GC using hexabromobenzene as an internal standard) throughout all photolyses suggests no other products were formed in significant quantities. To ensure no ground state reactions were taking place, thermal blanks were performed by subjecting the solutions of **115** to all experimental procedures except irradiation. No significant conversion of the starting material (<0.01%) was observed during these blanks as measured by GC.

Photolysis of 41 in CH_3CN, H_2O, and Seawater. Solutions of 1.3×10^{-9} M **41** in HPLC grade CH_3CN (Caledon Laboratories), Milli-Q grade distilled/deionized H_2O, and unfiltered seawater (taken at 1 m depth ca. 5 m from shoreline at the Institute of Ocean Sciences [Patricia Bay, Sidney, BC, Canada] on June 11, 2002) were prepared by dissolving 2.5 ng of **41** in 3 mL of solvent. These concentrations are ca. 20-fold lower than the reported water solubility limit of 2.6×10^{-8} M for **41** (*141*). Solutions were not degassed prior to, or during, photolysis and were expected to contain an equilibrium quantity of dissolved oxygen. Samples were irradiated in 3 mL quartz cuvettes open to the atmosphere and placed 5 cm from a hand-held 6 W 302 nm 38 cm×8.1cm×6.4cm UV lamp (Ultra-Violet Products UVM-57) mounted horizontally in a secure placement. With the exception of the exploratory 0-60 min trials (at 5 min intervals), all samples were run in duplicate at each time interval. To compare the relative effects of the hand-held lamp versus solar irradiation, duplicate solutions of 1.3×10^{-9} M **41** in CH_3CN in a 3 mL quartz cuvette were also exposed to solar irradiation for periods of 0, 3, 6, 9, 12, and 15 min between 1:30-3:00 pm on June 11, 2002, a clear day with an air temperature of 22°C.

Following photolysis, all samples were spiked with 25 μL each of the following commercial recovery standards prior to workup: (1) MBDE-MXA from Wellington Laboratories containing 5 μg/mL each of ^{13}C-labelled 2,2',4,4'-tetrabromodiphenyl ether (**37**), 2,2',4,4',5,5'-pentabromodiphenyl ether (**38**), and **41**; and (2) ^{13}C-labeled **42**. Because HPLC grade CH_3CN contains trace amounts of water, the 100 μL aliquots removed for analysis from this solvent were filtered through a Pasteur pipette containing

a 0.2 cm layer of $MgSO_4$ filter over a 0.2 cm layer of hexane-rinsed Kimwipes. The $MgSO_4$ was subsequently rinsed with 3×250 μL of pesticide grade distilled-in-glass toluene, the extract combined with the 100 μL aliquots of the dried CH_3CN, and the final solution reduced in volume to ca. 25 μL under gentle heating and a stream of nitrogen, and subsequently transferred to an amber glass microvial. The 100 μL aliquots removed for analysis from H_2O and seawater samples were extracted with 3×250 μL of pesticide grade distilled-in-glass toluene (Caledon Laboratories), reduced in volume to ca. 25 μL under gentle heating and a stream of nitrogen, and subsequently transferred to an amber glass microvial where 10 μL each of the following commercial internal standards were added: EO-5101 from Cambridge Isotope Laboratories containing 100 ng/mL of ^{13}C-labelled 3,3',4,4'-tetrabromodiphenyl ether (**116**) and 150 ng/mL of ^{13}C-labelled 3,3',4,4',5-pentabromodiphenyl ether (**117**); and MBDE-MXB from Wellington Laboratories containing 5 μg/mL each of ^{13}C-labelled 2,4,4'-tribromodiphenyl ether (**118**), 2,2',4,4',5,6'-hexabromodiphenyl ether (**119**), and 2,2',3,4,4',5',6-heptabromodiphenyl ether (**120**). Microvials were capped immediately after addition of the recovery standard and stored at -20°C in preparation for analysis by HRGC-HRMS.

Analyses were performed by HRGC-HRMS using a Micromass Ultima HRMS equipped with an Agilent 6890 HRGC. For all analyses, the HRGC was operated in the splitless injection mode, and the splitless injector purge valve was activated 2 min after sample injection. The volume injected was 1 μL of sample plus 0.5 μL of air. The HRMS was operated under positive EI conditions with the filament in the trap stabilization mode at 600 μA, an electron energy of 35 eV, and perfluorokerosene used as

the calibrant. For brominated diphenyl ether and brominated dibenzofuran analyses (see below), the instrument operated at 10,000 resolution, data were acquired in the SIM mode, and the two most abundant isotopic peaks were monitored for each molecular ion cluster. Analytes were identified only when the HRGC-HRMS data satisfied all of the following criteria: (1) two isotopes of the analyte were detected by their exact masses with the HRMS operating at 10,000 resolution during the entire chromatographic run; (2) the retention time of the analyte peak was within 3 s of the predicted time obtained from analysis of authentic compounds in the calibration standards (where available); (3) the maxima for both characteristic isotopic peaks of an analyte coincided within 2 s; (4) the observed isotope ratio of the two ions monitored per analyte were within 15% of the theoretical isotopic ratio; and (5) the signal-to-noise ratio resulting from the peak response of the two corresponding ions was ≥ 3 for proper quantification of the analyte. Concentrations of brominated diphenyl ethers and brominated dibenzofurans and their method detection limits (MDLs) were calculated by the internal standard isotope-dilution method using mean RRFs determined from calibration standard runs made before and after each batch of samples was analyzed. Recoveries of individual internal standards were between 40-120% for all analyses. Concentrations of analytes were corrected for percent recovery of the internal standards.

Analyses for brominated diphenyl ether photoproducts and unreacted starting material were performed using a standard 15 m DB5-HT column (0.25 mm I.D.×0.1 μm film thickness) from J&W Scientific with ultra-high purity helium as the carrier gas. The temperature program used under constant pressure (42 kPa) was as follows: hold at

100°C for 1 min; 2°C/min to 140°C; 4°C/min to 220°C; 8 °C/min to 330°C; and hold 1.2 min. The splitless injector port, direct HRGC-HRMS interface, and the HRMS ion source were maintained at 300°C, 260°C, and 300°C, respectively. Analytical standards were available for identification and quantitation of the following congeners: 2,2',4,5'-tetrabromodiphenyl ether (**123**); 2,2',4,4'-tetrabromodiphenyl ether (**37**); 2,3',4,4'-tetrabromodiphenyl ether (**122**); 3,3',4,4'-tetrabromodiphenyl ether (**116**); 2,2',4,5,5'-pentabromodiphenyl ether (**121**); 2,2',4,4',5-pentabromodiphenyl ether (**38**); and 2,2',4,4',5,5'-hexabromodiphenyl ether (**41**). Note that an analytical standard was not available for **132**, but that this is the only other primary photodebromination product of **41** other than **38** and **121**. Thus, **132** was identified as the remaining pentabrominated diphenyl ether peak for which an analytical standard was not available. The RRF of **132** was assumed to be equal to the average of the RRFs of **38** and **121**. A suite of 41 individual mono- through deca-brominated diphenyl ether analytical standards was available, but only congeners representing potential primary or secondary photodebromination products of **41** are listed above.

Absolute quantities of the brominated diphenyl ether starting material (**41**) and the photodebromination products in the photolyses extracts, along with recoveries of the ^{13}C-labeled tetra-, penta-, and hexa-brominated diphenyl ether recovery standards, are presented in the following tables: (1) a 60 min irradiation period (302 nm) in 100% CH_3CN at 5 min intervals (Table 4.4); (2) a 5 min irradiation period (302 nm) in 100% CH_3CN at 1 min intervals (Table 4.5); (3) a 5 min irradiation period (302 nm) in 100% H_2O at 1 min intervals (Table 4.6); a 5 min irradiation period (302 nm) in seawater at 1

min intervals (Table 4.7); and (5) a 15 min irradiation period (solar irradiation) in 100% CH_3CN at 3 min intervals (Table 4.8). Error bars, where shown, represent the range of duplicate analyses. Where error bars are absent, only one trial was able to be successfully analyzed. Where no sample at a given timeframe was able to be successfully analyzed, a "n/a" appears in the cell. Absolute quantities of each analyte were corrected for recoveries of the corresponding internal standard. The absolute quantities of **41** were corrected relative to the corresponding recovery of ^{13}C-**41** at each timestep. The absolute quantities of **38**, **121**, and **132** were corrected relative to the corresponding recovery of ^{13}C-**38** at each timestep. The absolute quantities of **123**, **37**, **122**, and **116** were corrected relative to the corresponding recovery of ^{13}C-**37** at each timestep. Contributions towards the overall photochemical mass balance were then calculated by dividing the corrected quantity of each analyte by its molecular mass, and then dividing the moles of analyte observed at each timestep by the moles of starting material (**41**; 3.9×10^{-12} mol, or 1.3×10^{-9} M in 3 mL of solution).

Table 4.4. Absolute quantities (in pg; uncorrected for recovery standards) of **41** and its penta- and tetra-brominated photodebromination products over the course of a 60 min irradiation period in 100% CH_3CN. Percent recoveries of the three ^{13}C-labeled recovery standards are also shown.

Time (min)	**41**	**38**	**121**	**132**	**123**	**37**	**122**	**116**	^{13}C-**41**	^{13}C-**38**	^{13}C-**37**
5	339.6	128.6	107.2	86.0	15.7	11.2	12.4	3.5	87%	102%	88%
10	76.0	53.8	53.6	37.5	24.7	17.1	20.8	4.8	87%	79%	85%
20	27.1	3.7	4.6	4.2	10.9	7.6	9.3	2.7	81%	94%	103%
25	7.3	3.0	1.8	0.2	7.6	4.2	5.2	1.1	100%	90%	74%
30	0.0	0.3	0.3	0.1	4.1	1.9	2.3	0.7	85%	59%	76%
35	6.0	0.5	1.0	0.2	1.7	0.8	1.0	0.1	79%	111%	59%
40	2.9	0.4	0.6	0.2	1.7	0.5	0.9	0.0	117%	96%	92%
45	2.1	0.2	0.3	0.1	0.5	0.3	0.3	0.0	76%	43%	58%
50	5.4	0.2	0.3	0.1	0.5	0.2	0.5	0.0	72%	42%	93%
55	1.9	0.5	0.8	0.3	0.2	0.2	0.2	0.0	50%	117%	99%
60	2.5	0.3	0.4	0.1	0.2	0.4	0.2	0.2	50%	65%	100%

Table 4.5. Absolute quantities (in pg; uncorrected for recovery standards) of **41** and its penta- and tetra-brominated photodebromination products over the course of a 5 min irradiation period in 100% CH_3CN. Percent recoveries of the three ^{13}C-labeled recovery standards are also shown.

Time (min)	**41**	**38**	**121**	**132**	**123**	**37**	**122**	**116**	^{13}C-**41**	^{13}C-**38**	^{13}C-**37**
1	904.1±190.6	38.3±7.5	32.3±6.0	23.0±3.9	1.3	0.6	0.6	<0.1	70%	46%	57%
2	623.6	119.8	98.4	75.4	4.5	3.4	3.4	1.1	64%	99%	98%
3	270.4±12.7	128.7±3.6	108.4±2.5	81.4±3.3	7.2±0.2	5.4±0.9	6.3±0.9	0.9	55%	101%	79%
4	383.8±34.2	n/a	85.5±7.8	67.1±6.5	9.3±0.1	6.2±0.8	7.0±0.8	1.5±0.8	103%	80%	68%
5	285.0±64.5	50.6±5.5	42.9±4.0	34.7±3.7	11.1±0.1	6.8±0.9	9.4±0.9	2.6±0.9	115%	46%	75%

Table 4.6. Absolute quantities (in pg; uncorrected for recovery standards) of **41** and its penta- and tetra-brominated photodebromination products over the course of a 5 min irradiation period in 100% H_2O. Percent recoveries of the three ^{13}C-labeled recovery standards are also shown.

Time (min)	**41**	**38**	**121**	**132**	**123**	**37**	**122**	**116**	^{13}C-**41**	^{13}C-**38**	^{13}C-**37**
1	n/a	138.7±8.3	103.3±2.8	92.5±16.5	6.9±3.8	6.9±3.8	8.8±6.2	3.5±2.9	111%	89%	96%
2	1169.3±172.7	209.8±17.9	154.2±24.7	140.6±3.1	17.6±6.3	15.2±5.2	21.0±11.5	7.4±4.6	114%	88%	98%
3	300.1±6.9	167.9±10.8	126.5±19.0	112.4±1.1	35.4±13.0	30.1±12.6	43.8±24.8	15.7±11.2	44%	65%	104%
4	734.0±337.7	81.6±6.1	61.4±10.5	53.9±2.6	37.2±10.4	30.6±11.5	44.8±22.3	15.8±9.7	76%	43%	119%
5	768.9	178.6±18.6	169.4±4.9	116.1±15.3	22.3±5.5	16.8±2.7	22.0±1.3	6.6±0.7	94%	107%	94%

Table 4.7. Absolute quantities (in pg; uncorrected for recovery standards) of **41** and its penta- and tetra-brominated photodebromination products over the course of a 5 min irradiation period in seawater. Percent recoveries of the three ^{13}C-labeled recovery standards are also shown.

Time (min)	**41**	**38**	**121**	**132**	**123**	**37**	**122**	**116**	^{13}C-**41**	^{13}C-**38**	^{13}C-**37**
1	n/a	76.3±27.7	53.1±15.3	53.7±20.0	3.8±1.4	4.1±1.1	5.2±1.8	2.4±1.0	63%	70%	57%
2	942.9±65.9	62.5±6.5	45.0±3.6	45.6±5.6	11.0±0.7	10.6	14.9	5.9±0.2	57%	66%	119%
3	1571.3±85.2	72.9±32.9	55.1±22.8	57.1±25.5	9.4±5.3	8.7±4.6	12.7±7.2	5.6±3.5	104%	82%	62%
4	588.5±281.8	99.9±19.7	70.3±11.6	76.8±16.0	24.9±5.5	21.0±6.3	32.0±8.6	13.2±3.9	49%	105%	108%
5	1004.2±502.9	60.3±14.9	43.1±9.5	47.1±14.4	19.0±4.6	16.4±3.4	24.8±7.0	11.4±3.2	92%	77%	106%

Table 4.8. Absolute quantities (in pg; uncorrected for recovery standards) of **41** and its pentabrominated photodebromination products over the course of a 15 min irradiation period in 100% CH_3CN under solar irradiation. Note that no tetrabrominated diphenyl ethers photoproducts were detected over the irradiation period. Percent recoveries of the three ^{13}C-labeled recovery standards are also shown.

Time (min)	**41**	**38**	**121**	**132**	^{13}C-**41**	^{13}C-**38**	^{13}C-**37**
3	471.7±227.2	7.0±1.3	8.0±1.7	3.7±0.4	83%	99%	43%
6	227.2	4.0±0.6	2.4±2.3	2.1±0.2	59%	55%	42%
9	292.4±19.5	7.9±0.3	7.4±0.3	4.3±0.3	84%	115%	73%
12	351.1±33.0	7.6±0.8	7.4±0.4	4.3±0.4	100%	86%	95%
15	480.3±66.0	8.8±0.4	8.0±0.2	5.1	118%	93%	42%

Analyses for brominated dibenzofuran photoproducts were performed using a 15 m DB5HT column (0.25 mm I.D.×0.10 μm film thickness) from J&W Scientific with ultra-high purity helium as the carrier gas. The temperature program used under constant pressure (36 kPa) was as follows: hold at 100°C for 2 min; 20°C/min to 200°C; and 4°C/min to 314°C. The splitless injector port, direct HRGC-HRMS interface, and the HRMS ion source were maintained at 282°C, 260°C, and 300°C, respectively. An analytical standard was available for the following potential primary photoproduct: 2,3,7,8-tetrabromodibenzofuran (**42**). Quantities of mono- through penta-brominated dibenzofurans were below the method detection limits of ca. 0.5-1 pg over the course of the photolyses in 100% CH_3CN (both 302 nm and solar irradiation], 100% H_2O, and seawater. A 3 mL solution of 1.3×10^{-9} M **41** in freshly distilled CH_3CN was also irradiated for 1 min at 302 nm and analyzed for brominated dibenzofurans. Absolute quantities of the mono- through penta-brominated photoproducts are given in Table 4.9. The absolute quantities of these analytes were corrected relative to the corresponding recovery of ^{13}C-**42**. Contributions towards the overall photochemical mass balance were then calculated by dividing the corrected quantity of each analyte by its molecular mass, and then dividing the moles of analyte observed by the moles of starting material (**41**; 3.9×10^{-12} mol, or 1.3×10^{-9} M in 3 mL of solution).

Table 4.9. Absolute quantities (in pg; uncorrected for recovery standard) of the brominated dibenzofuran photoproducts following a 1 min irradiation period (302 nm) of **41** in 100% dry CH_3CN. The percent recovery of the ^{13}C-**42** recovery standard was 72%.

Analyte	Quantity (pg)
138	19.0
139	29.3
140 (Isomer 1)	20.1
140 (Isomer 2)	16.7
141 (Isomer 1)	10.5
141 (Isomer 2)	8.2
141 (Isomer 3)	17.9
142	29.1

A 3 mL solution of 1.3×10^{-9} M **41** in freshly distilled CH_3CN was irradiated for 1 min at 302 nm and analyzed by full-scan HRGC-HRMS for potential analytes other than brominated diphenyl ethers. Full scan analyses to look for photoproducts without an available standard were performed on the using a standard 30 m DB5 column (0.25 mm I.D.×0.25 μm film thickness) from J&W Scientific with ultra-high purity helium as the carrier gas. The temperature program used under constant flow conditions (1 mL/min) was as follows: hold at 100°C for 2 min; 4°C/min to 300°C; and hold 3 min. The splitless injector port, direct HRGC-HRMS interface, and the HRMS ion source were maintained at 300°C, 270°C, and 250°C, respectively. The HRGC-HRMS was operated at unit resolution over the mass range from *m/z* 50-725. The following three unknown photoproducts were observed with relative molecular ion cluster areas of 1.1:1.8:1.0 and

were tentatively assigned as tetrabrominated 2-hydroxybiphenyls since their elution times were significantly greater (ca. 10 min) than the corresponding RT windows for tetrabrominated diphenyl ethers and tetrabrominated dibenzofurans: RT=46.91 min, *m/z*=481.8846 (17%, M^+), 483.8240 (74%, M^++2), 485.8463 (100%, M^++4), 487.8409 (64%, M^++6), 489.9061 (15%, M^++8), 324.0544 (41%, M^+-2Br), 326.0583 (74%, M^++2-2Br), 328.0367 (40%, M^++4-2Br); RT=47.67 min, *m/z*=481.8374 (23%, M^+), 483.8112 (77%, M^++2), 485.8483 (100%, [M^++4), 487.8556 (69%, M^++6), 489.9176 (20%, M^++8), 324.1168 (49%, M^+-2Br), 326.0527 (91%, M^++2-2Br), 328.0646 (46%, M^++4-2Br); RT=48.70 min, *m/z*=481.8516 (11%, M^+), 483.8405 (63%, M^++2), 485.8309 (100%, M^++4), 487.8014 (63%, M^++6), 489.8161 (17%, M^++8).

The quantities of these analytes were estimated by assuming an RRF of 0.5 for the intensity of the molecular ion cluster compared to that of **42**, equal to the observed RRF between a tetrachlorinated dihydroxybiphenyl and 2,3,7,8-tetrachlorodibenzo[1,4]dioxin as described above. The estimated absolute quantities of the three tetrabrominated 2-hydroxybiphenyl analytes were as follows: (1) RT=46.91 min, 39.2 pg; (2) RT=47.67 min, 64.2 pg; and (3) RT=48.70 min, 35.7 pg. The absolute quantities of these analytes were corrected relative to the corresponding recovery of ^{13}C-**42**. Contributions towards the overall photochemical mass balance were then calculated by dividing the corrected quantity of each analyte by its molecular mass, and then dividing the moles of analyte observed by the moles of starting material (**41**; 3.9×10^{-12} mol, or 1.3×10^{-9} M in 3 mL of solution).

4.3.2 Thermal Product Studies

Thermolysis of 16 in CH_3CN. A 6×10^{-4} M solution of **9** in 3 mL CH_3CN was placed in a 10 mm×10 mm i.d. 3 mL quartz cuvette and sparged with argon for 15 min. The cell was then placed in a Rayonet RPR 100 photochemical reactor with 16-300 nm lamps for 15 s. Following irradiation, a 100 μL aliquot of the solution was injected into a Varian 230 ProStar LC with a model 310 ProStar UV detector monitoring at 280 nm and 520 nm and a Varian Microsorb Phenyl-MV 150 mm long×4.6 mm i.d. column eluting HPLC grade CH_3CN (Caledon Laboratories) at 2 mL/min. Each LC run took 2.5 min to complete, at which time a new aliquot of the solution described above was injected. Three injections could be completed over a 8 min period before the decay of **16** (having a RT=1.780 min) reduced the absorbance at 520 nm below the instrumental detection limit. The pseudo first-order decay rate constant of **16** as measured by normalized absorbance area using fluorene as the internal standard was comparable with that observed by the UV-visible spectroscopy studies described below ($7.12\pm0.61\times10^{-3}$ by LC-UV vs. $8.87\pm0.21\times10^{-3}$ s^{-1} by conventional UV). In addition to **16**, two other compounds were evident in the chromatograms. Comparison with the RTs of authentic standards identified these as **10** (RT=1.280 min) and **11** (RT=1.470 min). The concentration of **10** did not change during the time-resolved LC trials, whereas the concentration of **11** had a growth rate ($7.72\pm0.42\times10^{-3}$ s^{-1}) comparable to the decay of **16**.

Thermolysis of 52 in CH_3CN. A 50 mg (1.6×10^{-4} mol) sample of **52** was dissolved in CH_3CN (100 mL) and allowed to stand in the dark at 20°C for 24 h. Removal of the solvent by rotary evaporation yielded the major thermal product, 3,3',4,4'-

tetramethoxyoxepino[2,3-b]benzofuran (**94**; 32 mg; 1.1×10^{-4} mol), which was separated by prep-TLC (CH_2Cl_2) in 32% yield: mp 143-145°C (lit. mp 144-145 (*85*)); HRMS (EI), calc. $C_{16}H_{16}O_6$ 304.0947, found 304.0949; LRMS (EI), 304 (M^+); ^1H NMR (300 MHz, $CDCl_3$) δ 5.36 (s, 1 H, 2'-H), 5.62 (s, 1 H, 5'-H), 6.84 (s, 1 H, 2-H), 6.91 (s, 1 H, 5-H). The rate constant for the thermal decay of **52** in CH_3CN was determined by preparing a 6×10^{-4} M solution and immediately placing it in a 10 mm×10 mm i.d. 3 mL quartz cuvette and monitoring the decay at 520 nm using single-wavelength kinetic data acquired at 0.1 s intervals.

4.4 UV-Vis Studies

Solutions (6×10^{-5} M) of **52**, **16**, **75**, **26**, **28**, and **19** were placed in 10 mm × 10 mm i.d. 3 mL quartz cuvettes and sparged with nitrogen or oxygen for 15 min. Replicate trials were performed for each starting material under separate nitrogen and oxygen purging. The cells were then sealed from the atmosphere and placed in a UV-Vis spectrometer which acquired spectra over the range from 190-900 nm at 2 nm intervals every 30 s for 60 min. To determine rate constants for decays of photogenerated 2,2'-biphenylquinones, the experimental setup described above was used with the exception that single-wavelength kinetic data at the individual compound λ_{max} in the range from 500-700 nm for the 2,2'-biphenylquinones was acquired at 0.1 s intervals. Kinetic parameters were determined using either Kaleidagraph 3.08 (Synergy Software) or KyPlot v. 2.0 b.15 (Department of Biochemistry and Biophysics, Tokyo Medical and Dental University).

4.5 Laser Flash Photolysis

All LFP studies were carried out at the University of Victoria LFP facility with excitation achieved by either a Spectra-Physics GCR-11 YAG laser (λ_{ex}=266) or a GSI Lumonics EX-510 excimer laser (λ_{ex}=308 nm). In order to avoid multiple photon processes, the laser pulse energies were adjusted to <25 mJ/pulse through the use of neutral density filters in the case of the excimer laser, or by attenuation of power for the YAG laser. The monitoring beam utilized was either a pulsed 150 W lamp (Oriel model 66057 housing, Spectra-Physics; XBO150W-1 lamp, OSRAM GmbH; LPS-220 power supply, Photon Technology International) or a 75 W lamp (model A1010 housing, Photon Technology International; 75XE xenon short arc lamp, USHIO Inc.; LPS-220 power supply, Photon Technology International) for lifetimes up to 5 μs and a custom lamp (custom housing; XBO150W-1 lamp, OSRAM GmbH; 28302a starter and power supply, HANOVIA) for lifetimes >5 μs. In all cases, the monitoring lamp and detection equipment were angled at 90° to the laser beam. The light intensity at each wavelength was determined by a monochromator (CVI Digikrom 240; CVI Laser LLC) and photomultiplier tube (PMT; model R446, Hamamatsu Photonics). The PMT signal was sent to a baseline compensation unit that holds the value of the background intensity from the xenon lamp after the lamp pulse immediately prior to firing the laser. The signal received upon triggering the laser was recorded by a TDS 520 digital oscilloscope (Tektronix, Inc.) and sent to a desktop computer for processing. Transient signals were corrected for baseline slope when the 150 W Oriel or 75 W PTI lamps were used and the timescale of interest was >5 μs/division. Instrumental control and data processing and analysis was carried out via custom software written in Labview 5.01 (National

Instruments Corporation) on a MacIntosh G3 personal computer (Apple Inc.). For all samples, P_0 values were maintained in the range from –0.20 to –0.25 V by the software program, which adjusted the PMT voltage and monochromator slit width recursively.

In a typical experiment, a solution with an optical density (OD) of ≤0.3 was prepared in a given solvent system using a modified graduated cylinder attached to a flow cell (7 mm × 7 mm quartz) from a stock solution of the desired compound in dry CH_3CN according to eq. (4.1,

$$V = \frac{0.3 \cdot s \cdot x}{A \cdot \left(3 + \frac{s}{1000}\right)} \cdot \frac{10}{7} \qquad (4.1)$$

where V is the spiking volume in μL required for an OD of 0.3 in x mL of solution, s is the spiking volume in μL used to give an absorbance of ca. 0.3 in a 3 mL cuvette, A is the absorbance from a spike of size S in a 3 mL cuvette, x is the volume of solvent required in the LFP flow cell (typically 60-100 mL), and 10/7 is a factor to account for the differing pathlengths in the cuvette (10 mm) and flow (7 mm) cells. Solutions were then sparged with either oxygen or nitrogen for a minimum of 10 min prior to irradiation and continuously during the experiment. The flow cell system was utilized to provide fresh solution for each laser pulse to avoid secondary excitation of excited states or primary photoproducts. The flow rate was adjusted so two transient spectra and the required decay/growth traces at desired wavelengths could be obtained from a single solution.

Transient decay/growth were recorded as a time resolved collection of 500 individual points in a given time scale at a desired wavelength. The kinetic parameters for a particular transient signal were determined using either Kaleidagraph 3.08 (Synergy Software) or KyPlot v. 2.0 b.15 (Department of Biochemistry and Biophysics, Tokyo Medical and Dental University). The absorption spectra of the transients were collected in a similar fashion, with transient growth/decay recorded at individual wavelengths and 10 or 20 nm intervals over the range of interest. At each wavelength, the transient signal was divided into four time windows and the average ΔOD from each window plotted versus the average time. Four points were obtained for each wavelength to provide a time-resolved absorption spectrum for the transient of interest.

Static cell experiments were also performed to examined the influence of solvent identity, pH, water content, and temperature on the rate of transient growth/decay. For these experiments, 3 mL of the desired solvent system and sufficient starting material to give an absorbance of ca. 0.3 at the excitation wavelength was added to an individual 7 mm $\times$ 7 mm quartz cuvette, sealed with a rubber septum, and purged with either oxygen or nitrogen for a minimum of 10 min prior to irradiation. Static cell samples were exposed to <20 laser pulses to avoid secondary photochemistry and a build-up of photoproducts and long-lived transients.

Acknowledgements

Special thanks are extended to Dr. Michael Ikonomou and Ms. Maike Fischer of the Regional Dioxin Laboratory at the Institute of Ocean Sciences, as well as the support of Fisheries and Oceans Canada. Dr. Ikonomou manages the Regional Dioxin Laboratory and generously donated instrumental time, analytical expertise, materials and supplies, and staff assistance to facilitate studies into the photochemistry of 2,3,7,8-tetrachlorodibenzo[1,4]dioxin and 2,2',4,4',5,5'-hexabromodiphenyl ether. Ms. Fischer kindly performed all instrumental injections using HRGC-HRMS on these two materials at the Regional Dioxin Laboratory. Dr. MacMurray Whale (formerly of the Department of Mechanical Engineering at the University of Victoria) was a key collaborator whose financial support, intellectual guidance, and mentorship allowed photochemical studies on 4-monobromodiphenyl ether and 4,4'-dibromodiphenyl ether. Pioneering synthetic work and photochemical studies on dibenzo[1,4]dioxins were performed by Mr. Ryan Sasaski (formerly of the Department of Chemistry at the University of Victoria), on which the current work investigating the photochemistry of these compounds is built and whose friendship is deeply valued. Drs. Alexandre Konstantinov and Nigel Bunce generously donated a sample of 4,4',5,5'-tetrachloro-2,2'-dihydroxybiphenyl as a key component towards elucidating the photochemistry of 2,3,7,8-tetrachlorodibenzo[1,4]dioxin. The financial support of the Natural Sciences and Engineering Research Council (NSERC) of Canada in the form of a post-graduate scholarship and supplement to S. Rayne, and research grants to Dr. P. Wan, is gratefully acknowledged. This work would also not have been possible without the support and

encouragement of all members of the Department of Chemistry at the University of Victoria, and especially my supervisor, Dr. Peter Wan.

References

(1) Hays, S. M.; Aylward, L. L. *Regul. Toxicol. Pharm.* 37, **2003**, 202.

(2) Alcock, R. E.; Jones, K. C. *Environ. Sci. Technol.* 30, **1996**, 3133.

(3) Hites, R. A. *Acc. Chem. Res.* 23, **1990**, 194.

(4) Landers, J. P.; Bunce, N. J. *Biochem. J.* 276, **1991**, 273.

(5) Staples, J. E.; Murante, F. G.; Fiore, N. C.; Gasiewicz, T. A.; Silverstone, A. E. *J. Immunol.* 160, **1998**, 3844.

(6) Alcock, R. E.; Jones, K. C. *Environ. Sci. Technol.* 30, **1996**, 3133.

(7) Rappe, C.; Andersson, R.; Bergqvist, P. A.; Brohede, C.; Hansson, M.; Kjeller, L. O.; Lindstrom, G.; Marklund, S.; Nygren, M.; Swanson, S. E.; Tysklind, M.; Wiberg, K. *Chemosphere* 16, **1987**, 1603.

(8) Devault, D.; Dunn, W.; Bergqvist, P. A.; Wiberg, K.; Rappe, C. *Environ. Toxicol. Chem.* 8, **1989**, 1013.

(9) Rappe, C.; Andersson, R.; Bergqvist, P. A.; Brohede, C.; Hansson, M.; Kjeller, L. O.; Lindstrom, G.; Marklund, S.; Nygren, M.; Swanson, S. E.; Tysklind, M.; Wiberg, K. *Waste Mgmt. Res.* 5, **1987**, 225.

(10) Lohmann, R.; Jones, K. C. *Sci. Total Environ.* 219, **1998**, 53.

(11) Baker, J. I.; Hites, R. A. *Environ. Sci. Technol.* 34, **2000**, 2879.

(12) Brzuzy, L. P.; Hites, R. A. *Environ. Sci. Technol.* 30, **1996**, 1797.

(13) Fiedler, H.; Hutzinger, O.; Timms, C. W. *Toxicol. Environ. Chem.* 29, **1990**, 157.

(14) Bumb, R. R.; Crummett, W. B.; Cutie, S. S.; Gledhill, J. R.; Hummel, R. H.; Kagel, R. O.; Lamparski, L. L.; Luoma, E. V.; Miller, D. L.; Nestrick, T. J.; Shadoff, L. A.; Stehl, R. H.; Woods, J. S. *Science* 210, **1980**, 385.

(15) Plimmer, J. R. *Residue Rev.* 33, **1971**, 47.

(16) Plimmer, J. R.; Klingebiel, U. I.; Crosby, D. G.; Wong, A. S. *Adv. Chem. Ser.* 120, **1973**, 44.

(17) Crosby, D. G.; Wong, A. S.; Plimmer, J. R.; Woolson, E. A. *Science* 173, **1971**, 748.

(18) Plimmer, J. R.; Klingebiel, U. I. *Science* 174, **1971**, 407.

(19) Lamparski, L. L.; Stehl, R. H.; Johnson, R. L. *Environ. Sci. Technol.* 14, **1980**, 196.

(20) Stehl, R. H.; Papenfuss, R. R.; Bredeweg, R. A.; Roberts, R. W. *Adv. Chem. Ser.* 120, **1973**, 119.

(21) Buser, H.-R. *J. Chromatogr.* 129, **1976**, 303.

(22) Kearney, P. C.; Isensee, A. R.; Helling, C. S.; Woolson, E. A.; Plimmer, J. R. *Adv. Chem. Ser.* 120, **1973**, 105.

(23) Nestrick, T. J.; Lamparski, L. L.; Townsend, D. I. *Anal. Chem.* 52, **1980**, 1865.

(24) Buser, H.-R. *Chemosphere* 8, **1979**, 251.

(25) Kim, M. K.; O'Keefe, P. W. *Chemosphere* 41, **2000**, 793.

(26) Hung, L. S.; Ingram, L. L. *Bull. Environ. Contam. Toxicol.* 44, **1989**, 380.

(27) Konstantinov, A.; Bunce, N. J. *J. Photochem. Photobiol. A.* 94, **1996**, 27.

(28) Isosaari, P.; Tuhkanen, T.; Vartiainen, T. *Environ. Sci. Poll. Res.* 11, **2004**, 181.

(29) Wiberg, K.; Rappe, C.; Haglund, P. *Chemosphere* 24, **1992**, 1431.

(30) Hagenmaier, H.; She, J.; Benz, T.; Dawidowsky, N.; Dusterhoft, L.; Lindig, C. *Chemosphere* 25, **1992**, 1457.

(31) Jay, K.; Stieglitz, L. *Chemosphere* 35, **1997**, 1227.

(32) Tong, H. Y.; Monson, S. J.; Gross, M. L.; Huang, L. Q. *Anal. Chem.* 63, **1991**, 2697.

(33) Sidhu, S. S.; Maqsud, L.; Dellinger, B.; Mascolo, G. *Combust. Flame* 100, **1995**, 11.

(34) Mennear, J. H.; Lee, C. C. *Environ.Health Perspect.* 102, **1994**, 265.

(35) Hornung, M. W.; Zabel, E. W.; Peterson, R. E. *Toxicol. Appl. Pharm.* 140, **1996**, 227.

(36) Schwarzenbach, R. P.; Gschwend, P. M.; Imboden, D. M. *Environmental Organic Chemistry*. John Wiley and Sons: New York, NY, USA, 1993.

(37) Huang, C.-G.; Beveridge, K. A.; Wan, P. *J. Amer. Chem. Soc.* 113, **1991**, 7676.

(38) Huang, C.-G.; Shukla, D.; Wan, P. *J. Org. Chem.* 56, **1991**, 5437.

(39) Masse, R.; Pelletier, B. *Chemosphere* 16, **1987**, 7.

(40) Guan, B.; Wan, P. *J. Photochem. Photobiol. A.* 80, **1994**, 199.

(41) Sasaki, R. R. *Photochemistry of Dibenzo[p]dioxins*. M.Sc. Thesis. Department of Chemistry, University of Victoria:Victoria, BC, Canada, 2002.

(42) Zimmerman, H. E. *J. Amer. Chem. Soc.* 117, **1995**, 8988.

(43) Choudhry, G. G.; Webster, G. R. B. *Chemosphere* 14, **1985**, 893.

(44) Choudhry, G. G.; Webster, G. R. B. *Chemosphere* 14, **1985**, 9.

(45) Choudhry, G. G.; Webster, G. R. B. *J. Agr. Food Chem.* 37, **1989**, 254.

(46) Friesen, K. J.; Muir, D. C. G.; Webster, G. R. B. *Environ. Sci. Technol.* 24, **1990**, 1739.

(47) Dung, M. H.; Okeefe, P. W. *Environ. Sci. Technol.* 28, **1994**, 549.

(48) Friesen, K. J.; Foga, M. M.; Loewen, M. D. *Environ. Sci. Technol.* 30, **1996**, 2504.

(49) Chen, J. W.; Quan, X.; Peijnenburg, W. J. G. M.; Yang, F. L. *Chemosphere* 43, **2001**, 235.

(50) Chen, J. W.; Quan, X.; Schramm, K. W.; Kettrup, A.; Yang, F. L. *Chemosphere* 45, **2001**, 151.

(51) Konstantinov, A.; Bunce, N. J. *J. Photochem. Photobiol. A.* 94, **1996**, 27.

(52) Buser, H. R. *J. Chromatogr.* 129, **1976**, 303.

(53) Koshioka, M.; Yamada, T.; Kanazawa, J.; Murai, T. *Chemosphere* 19, **1989**, 681.

(54) Konstantinov, A. D.; Johnston, A. M.; Cox, B. J.; Petrulis, J. R.; Orzechowski, M. T.; Bunce, N. J.; Tashiro, C. H. M.; Chittim, B. G. *Environ. Sci. Technol.* 34, **2000**, 143.

(55) Colombini, M. P.; DiFrancesco, F.; Fuoco, R. *Microchem. J.* 54, **1996**, 331.

(56) Dulin, D.; Drossman, H.; Mill, T. *Environ. Sci. Technol.* 20, **1986**, 72.

(57) Mamantov, A. *Environ. Sci. Technol.* 18, **1984**, 808.

(58) Mamantov, A. *Chemosphere* 14, **1985**, 897.

(59) Darnerud, P. O.; Eriksen, G. S.; Johannesson, T.; Larsen, P. B.; Viluksela, M. *Environ. Health Perspect.* 109, **2001**, 49.

(60) Rahman, F.; Langford, K. H.; Scrimshaw, M. D.; Lester, J. N. *Sci. Total Environ.* 275, **2001**, 1.

(61) de Boer, J. In *The Handbook of Environmental Chemistry. Part K: New Types of Persistent Halogenated Compounds*; Paasivirta, J., Ed.; Springer-Verlag: Berlin, Germany, 2000; Vol. 3, p. 62.

(62) Hites, R. A. *Environ. Sci. Technol.* 38, **2004**, 945.

(63) Renner, R. *Environ. Sci. Technol.* 34, **2000**, 223A.

(64) Pelley, J.; Renner, R.; Burke, M. *Environ. Sci. Technol.* 37(21), **2003**, 387A.

(65) Betts, K. S. *Environ. Sci. Technol.* 35, **2001**, 274A.

(66) Renner, R.; Cooney, C. M. *Environ. Sci. Technol.* 38, **2004**, 14A.

(67) Christen, K.; Petkewich, R. *Environ. Sci. Technol.* 37, **2003**, 13A.

(68) World Health Organization. *Environmental Health Criteria 162: Brominated Diphenyl Ethers*. AB Firmatrych: Geneva, Switzerland, 1994.

(69) Environment International. *Special Issue on "The State-of-Science and Trends of BFRs in the Environment"* 29, **2003**, 663.

(70) Chemosphere. *Special Issue on "Brominated Flame Retardants in the Environment"* 46, **2002**, 579.

(71) Ikonomou, M. G.; Rayne, S.; Fischer, M.; Fernandez, M. P.; Cretney, W. *Chemosphere* 46, **2002**, 649.

(72) Ikonomou, M. G.; Rayne, S.; Addison, R. F. *Environ. Sci. Technol.* 36, **2002**, 1886.

(73) Rayne, S.; Ikonomou, M. G.; Antcliffe, B. *Environ. Sci. Technol.* 37, **2003**, 2847.

(74) Pijnenburg, A. M. C. M.; Everts, J. W.; de Boer, J.; Boon, J. P. *Rev. Environ. Contam. Toxicol.* 141, **1995**, 1.

(75) Hooper, K.; McDonald, T. A. *Environ. Health Perspect.* 108, **2000**, 387.

(76) Rayne, S.; Ikonomou, M. G. *Environ. Toxicol. Chem.* 21, **2002**, 2292.

(77) Ebert, J.; Bahadir, M. *Environ. Int.* 29, **2003**, 711.

(78) Weber, R.; Kuch, B. *Environ. Int.* 29, **2003**, 699.

(79) Pollard, R.; Wan, P. *Org. Prep. Proc. Int.* 25, **1993**, 1.

(80) Soderstrom, G.; Sellstrom, U.; de Wit, C. A.; Tysklind, M. *Environ. Sci. Technol.* 38, **2004**, 127.

(81) Eriksson, J.; Green, N.; Marsh, G.; Bergman, A. *Environ. Sci. Technol.* 38, **2004**, 3119.

(82) Raloff, J. *Science News* 163, **2003**, 334.

(83) Hua, I.; Kang, N.; Jafvert, C. T.; Fabrega-Duque, J. R. *Environ. Toxicol. Chem.* 22, **2003**, 798.

(84) Watanabe, I.; Tatsukawa, R. *Bull. Environ. Contam. Toxicol.* 39, **1987**, 953.

(85) Adderly, C. J. R.; Hewgill, F. R. *J. Chem. Soc. (C)* **1968**, 1434.

(86) Hewgill, F. R. *Tetrahedron* 34, **1978**, 1595.

(87) Kieatiwong, S.; Nguyen, L. V.; Hebert, V. R.; Hackett, M.; Miller, G. C.; Miille, M. J.; Mitzel, R. *Environ. Sci. Technol.* 24, **1990**, 1575.

(88) Dougherty, E. J.; Mcpeters, A. L.; Overcash, M. R. *Chemosphere* 23, **1991**, 589.

(89) Makino, M.; Kamiya, M.; Matsushita, H. *Chemosphere* 24, **1992**, 291.

(90) Makino, M.; Kamiya, M.; Matsushita, H. *Environ. Int.* 19, **1993**, 203.

(91) Freeman, P. K.; Srinivasa, R. *J. Agric. Food Chem.* 31, **1983**, 775.

(92) Ritterbusch, J.; Vogt, R.; Lorenz, W.; Bahadir, M.; Hopf, H. *Chemosphere* 29, **1994**, 457.

(93) Epling, G. A.; Qiu, Q. W.; Kumar, A. *Chemosphere* 18, **1989**, 329.

(94) Kutz, F. W.; Barnes, D. G.; Bretthauer, E. W.; Bottimore, D. P.; Greim, H. *Toxicol. Environ. Chem.* 26, **1990**, 99.

(95) Hovander, L.; Malmberg, T.; Athanasiadou, M.; Athanassiadis, L.; Rahm, S.; Bergman, A.; Wehler, E. K. *Arch. Environ. Contam. Toxicol.* 42, **2002**, 105.

(96) Bergman, A.; Klassonwehler, E.; Kuroki, H. *Environ. Health Perspect.* 102, **1994**, 464.

(97) Brouwer, A.; Klassonwehler, E.; Bokdam, M.; Morse, D. C.; Traag, W. A. *Chemosphere* 20, **1990**, 1257.

(98) Brouwer, A.; Vandenberg, K. J. *Toxicol. Appl. Pharmacol.* 85, **1986**, 301.

(99) Korach, K. S.; Sarver, P.; Chae, K.; Mclachlan, J. A.; Mckinney, J. D. *Mol. Pharmacol.* 33, **1988**, 120.

(100) Toppari, J.; Larsen, J. C.; Christiansen, P.; Giwercman, A.; Grandjean, P.; Guillette, L. J.; Jegou, B.; Jensen, T. K.; Jouannet, P.; Keiding, N.; Leffers, H.; McLachlan, J. A.; Meyer, O.; Muller, J.; RajpertDeMeyts, E.; Scheike, T.; Sharpe, R.; Sumpter, J.; Skakkebaek, N. E. *Environ. Health Perspect.* 104, **1996**, 741.

(101) Brouwer, A.; Morse, D. C.; Lans, M. C.; Schuur, A. G.; Murk, A. J.; Klasson-Wehler, E.; Bergman, A.; Visser, T. J. *Toxicol. Ind. Health* 14, **1998**, 59.

(102) Schuur, A. G.; Legger, F. F.; van Meeteren, M. E.; Moonen, M. J. H.; Van Leeuwen-Bol, I.; Bergman, A.; Visser, T. J.; Brouwer, A. *Chem. Res. Toxicol.* 11, **1998**, 1075.

(103) Onodera, S.; Takahashi, M.; Ogawa, M.; Suzuki, S. *Jpn. J. Tox. Env. Health* 41, **1995**, 212.

(104) Hamilton, S. J.; Cleveland, L.; Smith, L. M.; Lebo, J. A.; Mayer, F. L. *Environ. Toxicol. Chem.* 5, **1986**, 543.

(105) Choi, J.; Choi, W.; Mhin, B. J. *Environ. Sci. Technol.* 38, **2004**, 2082.

(106) Lowry, T. H.; Richardson, K. S. *Mechanism and Theory in Organic Chemistry.* Harper & Row: New York, NY, USA, 1987.

(107) Atkins, P. W. *Physical Chemistry.* Freeman: New York, NY, USA, 1998.

(108) Hewgill, F. R.; Hewitt, D. G. *J. Chem. Soc. (C)* **1967**, 723.

(109) Bourdon, J.; Calvin, M. *J. Org. Chem.* 22, **1957**, 101.

(110) Detroit, W. J.; Hart, H. *J. Amer. Chem. Soc.* 74, **1952**, 5215.

(111) Woodward, R. B. *J. Am. Chem. Soc.* 63, **1941**, 1123.

(112) Woodward, R. B. *J. Amer. Chem. Soc.* 64, **1942**, 76.

(113) Hay, A. S. *J. Org. Chem.* 36, **1971**, 218.

(114) Hageman, H. J.; Huysmans, W. G. B. *Chem. Comm.* **1969**, 837.

(115) Schneider, H. P.; Winter, W.; Rieker, A. *J. Chem. Res. (S)* **1978**, 336.

(116) Meier, H.; Schneider, H. P.; Rieker, A.; Hitchcock, P. B. *Agnew. Chem., Int. Ed. Engl.* 17, **1978**, 121.

(117) Hewgill, F. R.; Howie, G. B. *Aust. J. Chem.* 31, **1978**, 1061.

(118) Hewgill, F. R.; La Greca, B.; Legge, F.; Roga, P. E. *J. Chem. Soc. Perk. Trans. 1* **1983**, 131.

(119) Burnstein, S. H.; Ringold, H. J. *J. Amer. Chem. Soc.* 86, **1964**, 4952.

(120) Lewis, E. S.; Perry, J. M.; Grinstein, R. H. *J. Amer. Chem. Soc.* 92, **1970**, 899.

(121) Bacon, R. G. R.; Stewart, O. J. *Chem. Comm.* **1967**, 977.

(122) Altwicker, E. R. *Chem. Rev.* 67, **1967**, 475.

(123) Becker, H.-D. *J. Org. Chem.* 29, **1964**, 3078.

(124) Lide, D. R. *CRC Handbook of Chemistry and Physics, 84th Ed.* CRC Press: Cleveland, OH, USA, 2003-2004.

(125) Hay, A. S. *Tetrahedron Lett.* 47, **1965**, 4241.

(126) Tsuruya, S.; Yonezawa, T. *J. Org. Chem.* 39, **1974**, 2438.

(127) Bruce, J. M.; Chaudhry, A.-u.-h. *J. Chem. Soc. Perk. Trans. 1* **1974**, 295.

(128) Joschek, H. I.; Miller, S. I. *J. Amer. Chem. Soc.* 88, **1966**, 3273.

(129) Pochon, A.; Vaughan, P. P.; Gan, D.; Vath, P.; Blough, N. V.; Falvey, D. E. *J. Phys. Chem. A.* 106, **2002**, 2889.

(130) Gorner, H. *J. Phys. Chem. A.* 107, **2003**, 11587.

(131) Becker, H.-D.; Gustafsson, K. *Tetrahedron Lett.* 52, **1976**, 4883.

(132) Pollard, R.; Wan, P. *Org. Prep. Proc. Int.* 25, **1993**, 1.

(133) Haga, N.; Takayanagi, H. *J. Org. Chem.* 61, **1996**, 735.

(134) Bunce, N. J. In *CRC Handbook of Organic Photochemistry and Photobiology*; Song, P.-S., Ed.; CRC Press: Boca Raton, 1995; p 1181.

(135) Palm, W.-U.; Sossinka, W.; Ruck, W.; Zetzsch, C. *Environ. Toxicol. Chem.* **2005**, In Press.

(136) Scrano, L.; Bufo, S. A.; D'Auria, M.; Emmelin, C. *J. Photochem. Photobiol. A.* 129, **1999**, 65.

(137) Rayne, S.; Ikonomou, M. G. *Anal. Chem.* 75, **2003**, 1049.

(138) Rayne, S.; Ikonomou, M. G. *J. Chromatogr. A.* 1016, **2003**, 235.

(139) Ikonomou, M. G.; Rayne, S. *Anal. Chem.* 74, **2002**, 5263.

(140) Norris, J. M.; Ehrmantraut, J. W.; Gibbons, C. L.; Kociba, R. J.; Schwetz, B. A.; Rose, J. Q.; Humiston, C. G.; Jewett, G. L.; Crummett, W. B.; Gehring, P. J.; Tirsell, J. B.; Brosier, J. S. *Appl. Polym. Symp.* 22, **1973**, 195.

(141) Wania, F.; Dugani, C. B. *Environ. Toxicol. Chem.* 22, **2003**, 1252.

(142) Larson, R. A.; Weber, E. J. *Reaction Mechanisms in Environmental Organic Chemistry*. Lewis Publishers: Boca Raton, 1994.

(143) Schwarzenbach, R. P.; Gschwend, P. M.; Imboden, D. M. *Environmental Organic Chemistry*. Wiley: Hoboken, NJ, USA, 2003.

(144) Stapleton, H. M.; Baker, J. E. "Comparing the temporal trends, partitioning and biomagnification of PBDEs and PCBs in Lake Michigan". *The 3rd Annual Workshop on Brominated Flame Retardants in the Environment*: Burlington, ON, Canada, p. 22.

(145) Choudhry, G. G.; Sundstrom, G.; Ruzo, L. O.; Hutzinger, O. *J. Agric. Food Chem.* 25, **1977**, 1371.

(146) Freeman, P. K.; Srinivasa, R. *J. Agric. Food Chem.* 31, **1983**, 775.

(147) Turro, N. J. *Modern Molecular Photochemistry*. University Science Books: Sausalito, CA, USA, 1991.

(148) Watanabe, I.; Kawano, M.; Tatsukawa, R. *Organohalogen Compd.* 19, **1994**, 235.

(149) Lenoir, D.; Schramm, K.-W.; Hutzinger, O.; Schedel, G. *Chemosphere* 22, **1991**, 821.

(150) Ogata, Y.; Takagi, K.; Ishino, I. *Tetrahedron* 26, **1970**, 2703.

(151) Lukeman, M.; Wan, P. *J. Amer. Chem. Soc.* 124, **2002**, 9458.

(152) Tomita, M. *J. Pharm. Soc. Jpn.* 52, **1932**, 49.

(153) Gilman, H.; Dietrich, J. J. *J. Amer. Chem. Soc.* 79, **1957**, 1439.

(154) Haffer, U.; Rotard, W.; Mailahn, W. *Chemosphere* 29, **1994**, 1803.

(155) Adderley, C. J. R.; Hewgill, F. R. *J. Chem. Soc. (C)* **1968**, 1434.

(156) Anderson, A.; Nonhebel, D. C.; Pauson, P. L. *J. Chem. Res. (S)* **1977**, 243.

(157) Podoll, R. T.; Jaber, H. M.; Mill, T. *Environ. Sci. Technol.* 20, **1986**, 490.

(158) Tulp, M. T. M.; Olie, K.; Hutzinger, O. *Biomed. Mass Spectrom.* 4, **1977**, 310.

(159) Tulp, M. T. M.; Olie, K.; Hutzinger, O. *Biomed. Mass Spectrom.* 5, **1978**, 224.

(160) Rozemeijer, M. J. C.; Olie, K.; deVoogt, P. *J. Chromatogr. A.* 761, **1997**, 219.

Vita

Surname: Rayne **Given Name:** Sierra

Place of Birth: Peace River, Alberta, Canada

Educational Institutions Attended:

Okanagan University College	1994-2000
University of Saskatchewan	1995
University of Victoria	2000-2005

Degrees and Diplomas Awarded:

Diploma in Water Quality Technology	1999
B.Sc. Chemistry, Okanagan University College	2000

Honours and Awards:

2002 The Edward Bassett Family Scholarship, University of Victoria

2002 Chemical Institute of Canada Environment Division Poster Presentation Award, 85th Canadian Society for Chemistry Conference

2001 Natural Sciences and Engineering Research Council (NSERC) Department of Fisheries and Oceans (DFO) Supplement

2001 President's Research Scholarship, University of Victoria

2000 Natural Sciences and Engineering Research Council (NSERC) Postgraduate Scholarship

2000 Dean's List, Faculty of Science, Okanagan University College

1999 Dean's List, Faculty of Science, Okanagan University College

1999 Natural Sciences and Engineering Research Council (NSERC) Undergraduate Student Research Award

1998 Pushor Mitchell Lawyers Award, Okanagan University College

1998 British Columbia Water and Wastewater Association Award, Okanagan University College

Publications:

Rayne, S., Ikonomou, M.G. (200x) Polybrominated Diphenyl Ethers in an Advanced Wastewater Treatment Plant: Part 1. Concentrations, Patterns, and Influence of Treatment Processes. *Journal of Environmental Engineering and Science*. In Press.

Rayne, S., Ikonomou, M.G. (200x) Polybrominated Diphenyl Ethers in an Advanced Wastewater Treatment Plant: Part 2. Potential Effects on a Unique Aquatic System. *Journal of Environmental Engineering and Science*. In Press.

Rayne, S. (200x) Using Exterior Building Surface Films to Assess Human Exposure and Health Risks from PCDD/Fs in New York City, USA, after the World Trade Center Attacks. *Journal of Hazardous Materials*. In Press.

Rayne, S., Carey, S., Forest, K. (200x) Evidence for Tin Inhibition of Biological Phosphorus Removal at a Municipal Wastewater Treatment Plant. *Journal of*

Environmental Science and Health, Part A-Toxic/Hazardous Substances & Environmental Engineering. 40(3), 535-548.

Rayne, S., Ikonomou, M.G., Butt, C.M., Diamond, M.L., Truong, J. (200x) Polychlorinated Dioxins and Furans (PCDD/Fs) from the World Trade Center Attacks in Exterior Window Films from Lower Manhattan in New York City, USA. *Environmental Science and Technology*. 39(7), 1995-2003.

Rayne, S., Ikonomou, M.G., Ellis, G.M., Barrett-Lennard, L.G., Ross, P. (2004) PBDEs, PBBs, and PCNs in Three Communities of Free Ranging Killer Whales (*Orcinus orca*) from the Northeastern Pacific Ocean. *Environmental Science and Technology*, 38(16), 4293-4299.

Rayne, S., Henderson, G.S. (2004) Airborne Thermal Infrared Remote Sensing of Stream and Riparian Temperatures in the Nicola River Watershed, British Columbia, Canada. *Journal of Environmental Hydrology*, 12(14), 1-11.

Butt, C.M., Rayne, S., Ikonomou, M.G., Diamond, M.L., Truong, J. (2003) Butt, C.M., Rayne, S., Ikonomou, M.G., Diamond, M.L., Truong, J. (2003) Polychlorinated Dioxins and Furans (PCDD/F) in Organic Window Films after September 11th. *Organohalogen Compounds*, 63, 320-323.

Rayne, S., Ikonomou, M.G. (2003) Predicting Gas Chromatographic Retention Times for the 209 Polybrominated Diphenyl Ether Congeners. *Journal of Chromatography A*, 1016(2), 235-248.

Rayne, S., Ikonomou, M.G., Antcliffe, B. (2003) Rapidly Increasing Polybrominated Diphenyl Ether Concentrations in the Columbia River System from 1992 to 2000. *Environmental Science and Technology*, 37(13), 2847-2854.

Rayne, S., Ikonomou, M.G. (2003) Development of a Multiple Class High-Resolution Gas Chromatographic Relative Retention Time Model for Halogenated Environmental Contaminants. *Analytical Chemistry*, 75(5), 1049-1057.

Rayne, S., Ikonomou, M.G., Whale, M.D. (2003) Photochemical and Anaerobic Microbial Degradation of 4,4'-Dibromodiphenyl Ether. *Water Research*, 37(3), 551-560.

Ikonomou, M.G. and Rayne, S. (2002) Investigating the Chromatographic and Ionization Properties of Mono- through Hexa-Brominated Diphenyl Ethers using GC-HRMS with MAB and EI Ionization. *Analytical Chemistry*, 74(20), 5263-5272.

Rayne, S., Ikonomou, M.G. (2002) Reconstructing Source PBDE Congener Patterns from Semipermeable Membrane Devices in the Fraser River, British Columbia, Canada: Comparison to Commercial Mixtures. *Environmental Toxicology and Chemistry*, 21(11), 2292-2300.

Rayne, S., Wan, P., Ikonomou, M.G., Konstantinov, A.D. (2002) Photochemical Mass Balance of 2,3,7,8-TeCDD in Aqueous Solution under UV Light shows Formation of Chlorinated Dihydroxybiphenyls, Phenoxyphenols, and Dechlorination Products. *Environmental Science and Technology*, 36(9), 1995-2002.

Ikonomou, M.G., Rayne, S., Addison, R.F. (2002) Exponential Increases of the Brominated Flame Retardants, Polybrominated Diphenyl Ethers, in the Canadian Arctic from 1981 to 2000. *Environmental Science and Technology*, 36(9), 1886-1892.

Ikonomou, M.G., Rayne, S., Fischer, M., Fernandez, M.P., Cretney, W. (2002) Occurrence and Congener Profiles of Polybrominated Diphenyl Ethers (PBDEs) in Environmental Samples from Coastal British Columbia, Canada. *Chemosphere*, 46(5), 649-663.

Conference Presentations and Invited Lectures:

Butt, C.M., Rayne, S., Ikonomou, M.G., Diamond, M.L., Truong, J. (2003) Polychlorinated Dioxins and Furans (PCDD/F) in Organic Window Films after September 11th. Oral Presentation in a Special Session on "Post-9/11 Environmental Impacts from Dioxins and Related Compounds" at the *23rd International Symposium on Halogenated Organic and Persistent Organic Pollutants: Dioxin 2003*. Boston, MA, USA, August 24-29, 2003.

Rayne, S., Sasaki, R.R., Wan, P. (2003) Photochemical Rearrangement of Dibenzo-*p*-Dioxins Proceeds Through Reactive 2,2'-Diphenylquinone Intermediates. Poster presentation at the *39th IUPAC Congress and 86th Conference of The Canadian Society for Chemistry*. Ottawa, ON, Canada. August 10-15, 2003.

Rayne, S., Wan, P., Ikonomou, M.G., Konstantinov, A. (2002) Photochemical Mass Balance of 2,3,7,8-TeCDD in Aqueous Solution under UV Light shows Formation of Chlorinated Dihydroxybiphenyls, Phenoxyphenols, and Dechlorination Products. Oral presentation at the *85th Canadian Society for Chemistry Conference*. University of British Columbia, Vancouver, BC, Canada. June 1-5, 2002.

Rayne, S., Ikonomou, M.G. (2002) Investigating the Chromatographic and Ionization Properties of Polybrominated Diphenyl Ethers using GC-HRMS with MAB and EI Ionization. Oral presentation at the *85th Canadian Society for Chemistry Conference*. University of British Columbia, Vancouver, BC, Canada. June 1-5, 2002.

Rayne, S., Ikonomou, M.G., Addison, R.F. (2002) Exponential Increases of the Brominated Flame Retardants, Polybrominated Diphenyl Ethers, in the Canadian Arctic from 1981 to 2000. Poster presentation at the *85th Canadian Society for Chemistry Conference*. University of British Columbia, Vancouver, BC, Canada. June 1-5, 2002.

Ikonomou, M.G., Fischer, M., Rayne, S., Fernandez, M.P., Antcliffe, B., Addison, R.F. (2001) PBDEs on the rise: As reflected by aquatic species from British Columbia and the Arctic. Oral Presentation at the *3rd Annual Workshop on Brominated Flame Retardants in the Environment*. Canada Centre for Inland Waters, Burlington, ON, Canada. August 23-24, 2001.

Rayne, S. (2003) *Using Octanol-Air Partition Coefficients to Reconstruct Atmospheric Concentrations of PCDD/Fs in Lower Manhattan Following the World Trade Center Attacks*. Department of Chemistry, Malaspina University College, Nanaimo, BC, Canada. September 9, 2003.

Rayne, S. (2002) *Using Semi-Permeable Membrane Devices (SPMDs) and Equilibrium-Based Partitioning Models to Reconstruct Source Patterns of Polybrominated Diphenyl Ether Flame Retardants*. Department of Chemistry, Malaspina University College, Nanaimo, BC, Canada. November 5, 2002.

Rayne, S. (2002) *Polybrominated Diphenyl Ether Flame Retardants in the Canadian Arctic. Exponentially Increasing Concentrations over the Past Two Decades*. Department of Chemistry, Malaspina University College, Nanaimo, BC, Canada. November 5, 2002.